

# **Novel Battery Chemistries Using Electrically Conducting Polymers Synthesised from Deep Eutectic Solvents and Aqueous Solutions**

Thesis submitted for the degree of  
Doctor of Philosophy  
at the University of Leicester

By

**Hani Khalil Ismail**

Department of Chemistry  
University of Leicester

May 2017



UNIVERSITY OF  
**LEICESTER**

## **Abstract**

### **Novel Battery Chemistries Using Electrically Conducting Polymers Synthesised from Deep Eutectic Solvents and Aqueous Solutions**

**Hani Khalil Ismail**

**University of Leicester 2017**

Here we describe the fabrication and testing of novel cells using a conducting polymer membrane, Zn metal anode and a deep eutectic solvent electrolyte.

Several different polyaniline-modified electrodes have been formed in various deep eutectic solvents (DESs) and aqueous media using cyclic voltammetry, and subsequently characterised using the electrochemical quartz crystal microbalance (EQCM). The morphologies of the obtained polymers have also been characterised using scanning electron microscopy (SEM), atomic force microscopy (AFM) and 3D optical microscopy. The more compact and dense polyaniline (PANI) films were achieved in DESs, while the films produced from aqueous media exhibited open structures of increased porosities. EQCM showed that the motion of mobile species between films and electrolyte during redox cycling, via the related change in mass, is different in DESs compared to aqueous media; a contributory factor is the higher viscosity and ionic nature of the latter. The electrochemical stabilities and capacitances of these polymers were studied after incorporation of graphite (GR) particles or metal oxides. Graphite particles improved the power and energy densities, as well as the stability of polymers, compared with their 'pure' counterparts.

The capacity retention of the ternary nanocomposites (PANI/MoO<sub>2</sub>/GR electrode grown from Oxaline) was 87 %, whereas the lowest retention was found for pure PANI was 13 % after 300 charge–discharge cycles. The PANI composite has been successfully used as a cathode, with Zn metal as anode, in wet batteries (aqueous salt/DES electrolyte). The battery suffered from a low coulombic efficiency of only 51 % in DES at room temperature, whereas at 50°C the efficiency was 97 %. At 50°C and a current density of 0.0625 mA cm<sup>-2</sup>, the battery showed an energy density of 104 Wh kg<sup>-1</sup> at a power density of 75 W kg<sup>-1</sup>, and a capacity of 344 mA hg<sup>-1</sup> for discharge at 0.09 mC cm<sup>-2</sup>. This suggests the polymer/graphite systems would be more suitable for a power source and battery applications than those using only the pure polymer.

# Publications

## A- Papers

Fundamental aspects of electrochemically controlled wetting of nanoscale composite materials. Accepted in Faraday Discussions 2017

## B- Conferences

### (1) Talk

- 1- H. K. Ismail, K. S. Ryder, and A. P. Abbott, Novel Battery Chemistries Using Electrically Conducting Polymers Synthesized from Deep Eutectic, 25<sup>th</sup> May 2015, *Midlands Electrochemistry Group Meeting (MEG) 2016*, Department Of Chemistry, George Porter Building, University of Leicester, Leicester, LE1 7RU.
- 2- H. K. Ismail, Karl S. Ryder, Andrew P. Abbott, Novel Battery Chemistries Using Electrically Conducting Polymers Synthesized from Deep Eutectic, Leicester University for the 21st meeting of the ELECTROCHEM conference series, 17th-19th August 2016, Stamford Court, Manor Rd, Leicester LE2 2LH

### (2) Poster

- 1- H. K. Ismail, K. S. Ryder, and A. P. Abbott Electrically conducting polymers synthesised from Deep Eutectic Solvents / aqueous solution, Department Of Chemistry Postgraduate Research. Day, 14th April 2015, University of Leicester, Leicester.
- 2- H. K. Ismail, K. S. Ryder, and A. P. Abbott Electrically conducting polymers synthesised from Deep Eutectic Solvents / aqueous solution, 22<sup>nd</sup> June 2015, WMG International Digital Laboratory University of Warwick Coventry, University of Warwick, Coventry.
- 3- H. K. Ismail, K. S. Ryder, and A. P. Abbott, Electrically conducting polymers synthesised from Deep Eutectic Solvents / aqueous solution, Durham University for the 21<sup>st</sup> meeting of the ELECTROCHEM conference series, 13<sup>th</sup>-15<sup>th</sup> September 2015, The Mountjoy Centre, Maple Wing, Stockton Road, Durham ,DH1 3LE.

## Statement

The work explained in this thesis for the degree of Ph.D. entitled “Novel Battery Chemistries Using Electrically Conducting Polymers Synthesized from Deep Eutectic Solvents and Aqueous Solutions” was carried out by the author in the Department of Chemistry at the University of Leicester between March 2013 and January 2017.

In this thesis, the work recorded was original except where acknowledged or referenced. None of the work has been submitted for another degree at this or any other university.

Signed .....

Date.....

## Acknowledgments

I would like to express my gratitude and appreciation to my first supervisor, Prof Karl Ryder, for his guidance and encouragement to me throughout my PhD. I also thank my second supervisor, Prof. Robert Hillman for the great help and invaluable advice. Many thanks go to Prof. Andrew P. Abbott, for his insightful suggestions and ideas during the group meeting to improve my work.

I am thankful to all my colleagues in the Materials Centre Group for their help and support during my studies, particularly when I ran into difficulties. A special thank you to Dr. Andrew Ballantyne, Dr Alex Goddard, Dr. Rachel Sapstead, and Dr. Christopher Zaleski, who taught me many of techniques used in this thesis like EQCM, CV, IR, AFM and TGA; I am also thankful to technician Graham, who taught me SEM. A great thanks to Prof. Peter Foot (Kingston University London) for measuring the conductivity of our polymers. My acknowledgements to Dr. Mark Watkins and Dr. Rachel Sapstead for proof reading a great deal of this thesis. I would also like to thank my close friends Azhar Al-Murshedi, Dr. Jamil Juma, Jalil Kareem, Hassan Al-Esary, Mohammad Q. Mohammad, Idrees Qadir, Ahmed Al-Bassam, Sahar Alabdullah, Asuman Unal and Salih Cihangir for their individual contributions and academically to my experiences.

I would also like to acknowledge support of the Human Capacity Development Program (HCDP) in the Iraqi Kurdistan Regional Government for a scholarship and funding this research.

My immeasurable appreciation for my parents, who made me what I am today. Unlimited thanks for all your prayers, sacrifices and love is unmatched and priceless for you. I am very grateful to all my brothers and my sisters, who have heled and supported me throughout all my life. Thank you for everything.

Special thanks goes to my dear wife for being a perfect homemaker, successful manager, her patience, and being a lovely mother to her children. A good wife makes a good husband, many thanks to a wonderful wife like you. Finally, thank you so much to my dear daughter (Noora) and sons (Ali and Murtatha) for listening to me, you are so special to me and I am so proud and so blessed that I have a daughter and sons like you.

## **Dedication**

I would like to dedicate this thesis to:

*My dearest mother*, who has spared no effort in my upbringing and orientation.

*My dearest father*, who strives to comfort and well-being, which he gave everything to push me in the way of success.

*My brothers and sisters*, whose love flows in my veins, and my heart always remembers them.

*My lovely wife*, for her support, encouragement and attention to my children.

*My children*; flowers and fruits of my life.

**Hani Khalil Ismail**

**Leicester, 2017**

## Thesis contents

Abstract.....	i
Publications.....	ii
Statement.....	iii
Acknowledgements.....	iv
Dedication.....	v
Thesis contents.....	vi

### Chapter 1: Introduction

1.1	Overview.....	2
1.2	Polymer-modified Electrodes.....	2
1.2.1	Redox Polymer.....	4
1.2.2	Conducting Polymers.....	5
1.3	Polyaniline.....	7
1.3.1	Mechanism of Electropolymerisation of Aniline.....	8
1.3.2	Optical Properties and Chemical Structures of Polyaniline.....	10
1.4	Applications of Polymers Modified Electrodes.....	12
1.4.1	Polymer Capacitors and Supercapacitors.....	12
1.4.2	Batteries.....	14
1.5	Electrodeposition from Ionic Liquid.....	17
1.5.1	Ionic Liquids.....	17
1.5.2	Deep Eutectic Solvents.....	19
1.6	Aim of Project.....	22
1.7	References.....	25

### Chapter 2: General Theory of Methodology

2.1	Introduction.....	32
2.2	Concepts of Electrochemistry.....	32
2.2.1	Mass Transport.....	32
2.3	Electrochemical Techniques.....	35

2.3.1	Cyclic Voltammetry.....	35
2.3.2	Impedance Analysis.....	39
2.4	Non-Electrochemical Techniques.....	41
2.4.1	The Crystal Impedance Technique.....	41
2.4.2	Electrochemical Quartz Crystal Microbalance.....	47
2.5	Surface Imaging Techniques.....	49
2.5.1	Scanning Electron Microscopy.....	49
2.5.2	Atomic Force Microscopy.....	50
2.6	Spectroscopic Techniques.....	52
2.6.1	Infrared Spectroscopy.....	52
2.4	References.....	53

### **Chapter 3: Experimental**

3.1	Introduction.....	58
3.2	Materials.....	58
3.2.1	Chemicals and Reagents.....	58
3.2.2	Deep Eutectic Solvents Formulations.....	59
3.3	Instrumentations.....	61
3.3.1	Electrochemical Techniques.....	61
3.3.1.1	Cyclic Voltammetry.....	61
3.3.1.2	Electrochemical Quartz Crystal Microbalance.....	62
3.3.2	Non-Electrochemical techniques.....	64
3.3.2.1	Surface Characterization Techniques.....	64
3.3.2.2	Physical Properties for DESs.....	65
3.3.2.3	Four-Probe Conductivity Measurements.....	66
3.3.2.4	Thermo-Gravimetric Analysis.....	66
3.3.2.5	Spectroscopic Techniques.....	66
3.4	Procedure.....	67
3.4.1	Polyaniline Deposition using CV.....	67
3.4.1.1	Polyaniline Film Deposition from Aqueous Solutions.....	67
3.4.1.2	PANI Film Deposition from DESs.....	67
3.4.1.3	Preparation of PANI- MoO <sub>2</sub> and/or GR Modified Electrode.....	67

3.4.1.4	Electrochemical Impedance Spectroscopy.....	68
3.4.1.5	Charge and Discharge Batteries.....	68
3.4.2	Polyaniline Deposition Using EQCM.....	70
3.4.2.1	PANI Film Deposition from Aqueous Solution.....	70
3.4.2.2	PANI Film Deposition from DESs.....	71
3.5	References.....	72

#### **Chapter 4: Characterisation of the Behaviour of Polyaniline (grown from aqueous electrolytes) in Aqueous Solutions and Deep Eutectic Solvents using EQCM**

4.1	Overview.....	75
4.2	Objective.....	76
4.3	Results and Discussion.....	77
4.3.1	Film preparation from H <sub>2</sub> SO <sub>4</sub> /H <sub>2</sub> O (thick film).....	77
4.3.2	Effect of different acids/anions electrolytes on the growth of polyaniline.	81
4.3.3	Effect of background/DES electrolytes on PANI stability and reversibility	83
4.3.4	Effect of different anions on PANI films stability at constant thickness...	86
4.3.5	Morphology and topography of the polymer films.....	89
4.3.6	Selection of polymer for further studies.....	93
4.3.7	Characterisation the behaviour of PANI using EQCM technique.....	93
4.3.8	Conclusion.....	115
4.4	References.....	118

#### **Chapter 5: Electrochemical Synthesis of Polyaniline from Choline-Based Type (III) Deep Eutectic Solvents and Characterisation of the Properties of Conducting Polymers using EQCM.**

5.1	Overview.....	122
5.2	Objective.....	123
5.3	Results and discussion.....	124
5.3.1	Viscosity and conductivity measurements of DESs.....	124
5.3.2	Film preparation.....	129
5.3.3	Growth of PANI in Ethaline.....	130
5.3.4	Effect of dopant ions on electrochemical polymerisation of aniline.....	132

5.3.5	Effect of different DES electrolytes on the growth of aniline.....	134
5.3.6	Effect of various electrolytes on PANI stability and reversibility.....	136
5.3.7	Morphology and topography of the polymer films.....	140
5.3.8	Selection of polymer for further study.....	145
5.3.9	EQCM investigations of ions and solvents regarding polyaniline film.....	145
5.3.10	Conclusion.....	164
5.4	References.....	166

## **Chapter 6: Synthesis, Characterisation and Electrochemical Supercapacitor Properties of MoO<sub>2</sub>-Graphite-Polyaniline Composite Electrodes.**

6.1	Overview.....	171
6.2	Background .....	173
6.2.1	Carbon composite.....	173
6.2.2	Metal oxides composite.....	175
6.3	Objective.....	175
6.4	Results and discussion.....	176
6.4.1	Stability and capacitance of PANI film during redox peaks.....	176
6.4.2	Effect of MoO <sub>2</sub> particles on stability and capacitance.....	178
6.4.3	Effect of GR particles on stability and capacitance.....	183
6.4.4	Effect of GR particles and MoO <sub>2</sub> on stability and capacitance.....	187
6.4.5	Capacitance retention.....	192
6.4.6	Effect of scan rates on the CVs and capacitance of PANI.....	194
6.4.7	Conductivity Measurements.....	196
6.4.8	Electrochemical impedance spectroscopy study.....	198
6.4.9	Spectroscopy studies.....	203
6.4.10	Thermogravimetric analysis of polyaniline composite.....	207
6.4.11	Morphology and topography of the polymer films.....	210
6.4.12	Conclusion.....	215
6.5	References.....	217

## **Chapter 7: Novel Battery Based on Zinc and Polyaniline/Metal Oxide/Graphite Composite as a Cathode.**

7.1	Overview.....	223
7.2	Commercial Zinc Batteries.....	224
7.3	Zinc-Polymer Battery Concept.....	224
7.4	Objective.....	225
7.5	Results and discussion.....	226
7.5.1	Effect of polymer composite.....	226
7.5.2	Effect of electrolyte composite.....	229
7.5.3	Effect of current density.....	230
7.5.4	Effect of electrolyte temperature.....	233
7.5.5	Specific energy and specific power .....	235
7.5.6	CR2025 Coin cell assembly.....	237
7.5.7	Conclusion.....	240
7.6	References.....	242

## **Chapter 8: General Conclusions and Future Work**

8.1	General Conclusions.....	246
8.2	Future work.....	249
8.3	References.....	250

<b>Chapter 9: Appendix.....</b>	<b>251</b>
---------------------------------	------------

## Nomenclature

Abbreviations	Full names and unit
<i>A</i>	Electrode area (cm <sup>2</sup> )
AFM	Anomic Force Microscopy
CPs	Conducting Polymers
<i>C</i> <sub>∞</sub>	Concentration in bulk of solution (mol dm <sup>-3</sup> )
<i>C</i> <sub>Ox</sub>	Concentration of oxidised species (mol dm <sup>-3</sup> )
<i>C</i> <sub>Red</sub>	Concentration of reduced species (mol dm <sup>-3</sup> )
<i>C</i> <sub>s</sub>	Specific Capacitance (F g <sup>-1</sup> )
CV	Cyclic Voltammetry
CE	Counter Electrode
<i>C</i> <sub>dl</sub>	Capacitance of double layer
ChCl	Choline Chloride
<i>D</i>	Diffusion coefficient (cm <sup>2</sup> s <sup>-1</sup> )
EB	Emeraldine Base
ES	Emeraldine Salt
DES	Deep Eutectic Solvent
<i>E</i>	Potential / Voltage
<i>E</i> <sup>o</sup>	Standard electrode potential (V)
<i>E</i> <sub>a</sub>	Activation energy for viscous flow (J)
<i>E</i> <sub>pc</sub>	Cathodic peak potential (V)
<i>E</i> <sub>pa</sub>	Anodic peak potential (V)
<i>E</i> <sub>g</sub>	Energy gap
EIS	Electrochemical Impedance Spectroscopy
EQCM	Electrochemical Quartz Crystal Microbalance
EDLC <sub>s</sub>	Electrical Double Layer Capacitors
EDX	Energy Dispersive X-ray
<i>E</i> <sub>η</sub>	The activation energy of viscous movement
<i>F</i>	Faraday constant (96 485 C mol <sup>-1</sup> )
FTIR	Fourier Transform Infrared Spectroscopy
<i>f</i>	Frequency (Hz)

$f^0$	Fundamental frequency of a QCM (Hz)
$f_s$	Resonant Frequency (Hz)
$\Delta f_q$	The observed resonant frequency change
$h_q$	Quartz thickness (m)
$\lambda$	Wavelength (m)
$\lambda_q$	Acoustic wavelength (m)
$\gamma$	Shear rate ( $s^{-1}$ )
HBD	Hydrogen Bond Donor
HCS	Hybrid Capacitors
ILs	Ionic Liquids
$i$	Current (A)
$i_{pc}$	Cathodic peak current (A)
$i_{pa}$	Anodic peak current (A)
$i_p$	Peak Current
LB	Leucoemeraldine Base
$m$	Mass (g)
$\Delta m$	Mass change
$m_q$	Mass of the quartz crystal ( $g\ cm^{-3}$ )
$n$	Number of electrons
MoO <sub>2</sub>	Molybdenum dioxide
$\eta$	Viscosity of the liquid (Pa)
OCV	Open circuit voltage
Ox	Oxidised form of the electroactive sites
PANI	Polyaniline
PA	Polyacetylene
PTh	Polythiophene
PEDOT	Polyethylene dioxythiophene
PPy	Polypyrrole
PPP	Polyparaphenylene
PB	Pernigraniline Base
PG	Propylene glycol
P <sub>s</sub> C <sub>s</sub>	Pseudo Capacitors

$\rho_q$	Density of quartz (2.65 g cm <sup>-3</sup> )
$\rho_L$	Density of the liquid (g cm <sup>-3</sup> )
Q	Charge (C)
QCM	Quartz Crystal Microbalance
SEM	Scanning Electron Microscope
R	Gas constant (J mol <sup>-1</sup> K <sup>-1</sup> )
R <sub>s</sub>	Resistance of solution
R <sub>ct</sub>	Resistance of charge transfer
RV	Rotational Viscometer
RE	Reference Electrode
Red	Reduced form of the electroactive sites
RTILs	Room-Temperature Ionic Liquids
$\sigma$	Conductivity of polymer
<i>t</i>	Time (s)
<i>T</i>	Temperature
TSM	Thickness shear mode
TGA	Thermo Gravimetric Analysis
$\Gamma$	Surface coverage of the polymer (mol cm <sup>-2</sup> )
<i>v<sub>q</sub></i>	Wave velocity (3.34 x 10 <sup>5</sup> cm s <sup>-1</sup> )
<i>v</i>	Scan rate (mV s <sup>-1</sup> )
<i>Z</i>	Impedance
<i>Z''</i>	Imaginary components of the impedance
<i>Z'</i>	Real components of the impedance
<i>Z<sub>w</sub></i>	Warburg impedance
WE	Working Electrode
$\omega$	Angular frequency (radians/s)
Y	Admittance

# Chapter 1: Introduction

## Contents

<b>1.1</b>	<b>Overview</b> .....	<b>2</b>
<b>1.2</b>	<b>Polymer-modified Electrodes</b> .....	<b>2</b>
1.2.1	Redox Polymer .....	4
1.2.2	Conducting Polymers .....	5
<b>1.3</b>	<b>Polyaniline</b> .....	<b>7</b>
1.3.1	Mechanism of Electropolymerisation of Aniline .....	8
1.3.2	Optical Properties and Chemical Structures of Polyaniline .....	10
<b>1.4</b>	<b>Applications of Polymers Modified Electrodes</b> .....	<b>12</b>
1.4.1	Polymer Capacitors and Supercapacitors .....	12
1.4.2	Batteries .....	14
<b>1.5</b>	<b>Electrodeposition from Ionic Liquid</b> .....	<b>17</b>
1.5.1	Ionic Liquids.....	17
1.5.2	Deep Eutectic Solvents.....	19
<b>1.6</b>	<b>Aim of Project</b> .....	<b>22</b>
<b>1.7</b>	<b>References</b> .....	<b>25</b>

## 1.1 Overview

Polymeric substances have historically been employed as insulators for metallic conductors and find use in many areas of the electronic industry.<sup>1</sup> However, the attention given to polymers as highly conductive organic materials began with the discovery, in 1977, with the doping of polyacetylene (PA). Shirakawa, MacDiarmid and Heeger discovered that polyacetylene becomes more conductive when exposed to iodine vapour. They concluded that a significant increase in conductivity occurs in these materials as a result of doping with anions (i.e. anion doping as consequence of removal of electrons, with the conductivity arising from the generation of mobile charge caused by this removal) and also due to the resonance forms of the polymer having delocalised electrons on each double bond. They received the Nobel Prize for chemistry in 2000 due to this discovery.<sup>2-4</sup> Further experimentation revealed polymers with conjugated  $\pi$ -electrons, which have been extensively studied due to their transition from insulator to conductor, caused by changes in their chemical and physical properties.<sup>5</sup> The developments in this field have led to a renewed interest in many optical and electronic applications for such polymers, including photovoltaic, conducting textiles,<sup>4</sup> supercapacitors,<sup>6</sup> electrochromic display devices,<sup>7</sup> energy storage in battery devices,<sup>8,9</sup> electrocatalysis,<sup>10,11</sup> biosensors and gas sensors,<sup>12,13</sup> and corrosion protection.<sup>14</sup> Due to a number of applications and topics of interest regarding conducting polymers, electrochemists have shown increasing interest in these fields, focussing on the mechanism of polymer growth via chemical/electrochemical methods, which starts with the formation of oligomers, then nucleation and growth, finally ending with the formation of polymeric substances.<sup>15</sup> They have also modified polymer electrodes with different materials, such as carbonaceous materials and metal oxides, to enhance their conductivity and improve their electrochemical stability.<sup>16-19</sup> In addition, electrochemists have studied charge propagation and the quantity of solvents that followed ion transfer through polymer chains via Electrochemical Quartz Crystal Microbalance (EQCM) methods to understand the mechanisms involved in doping/dedoping reactions.<sup>20,21</sup>

## 1.2 Polymer-modified Electrodes

The first studies of polymer-modified electrodes were reported by Merz and Bard on poly(vinylferrocene),<sup>22</sup> while Miller and van de Mark reported their work on poly(4-

nitrostyrene).<sup>23</sup> Since these reports, surface modification of electrodes with polymeric materials has attracted a great deal of interest regarding the use of different materials. Generally speaking, these modifications can be synthesised via chemical or electrochemical methods. In the chemical method, preparation of the polymer and derivatives can be controlled and manipulated by changing the conditions of the experiment, such as the concentration of monomer, the initiator, the reaction temperature, and other factors. The resultant material may be of lower quality compared to electrochemically modified electrodes because it contains a number of impurities and, therefore, needs to be purified.<sup>24, 25</sup> Electrochemically modified electrodes are produced by coating the electrode surface with a thin film of material via oxidation of monomers such as pyrrole, thiophene, aniline, or their derivatives, via an electropolymerisation process at the electrode/electrolyte interface.<sup>26</sup> The reaction in polymer-modified electrodes offers a large reactive surface area with thin films due to its natural three-dimensional morphology and porosity compared to the unmodified electrode. Hence, a greater number of species can ingress/egress the bulk of the coated polymer compared to monolayer-modified species, which represent only two-dimensional interfaces (see **Figure 1.1**).<sup>27, 28</sup> Moreover, modified electrodes can have a much longer lifetime across a range of oxidation states than monolayer films due to films being chemically more stable and including multiple monolayers of redox sites.<sup>27</sup>

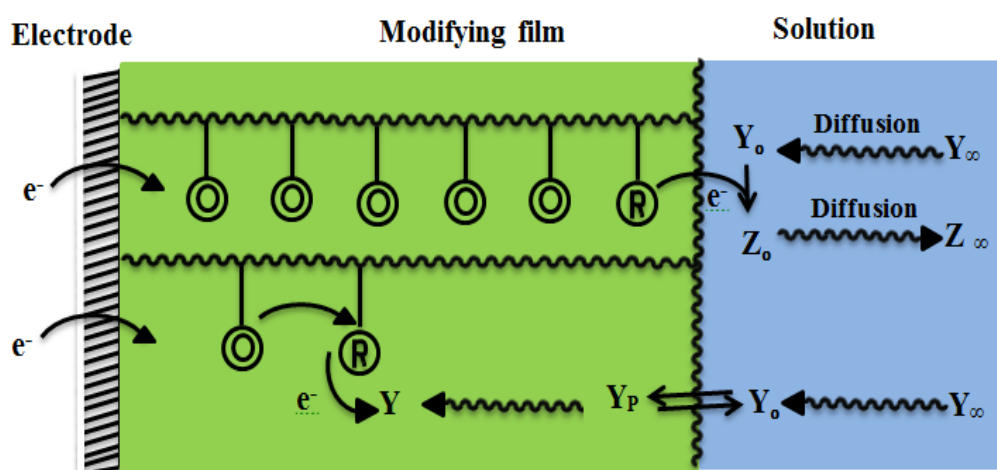


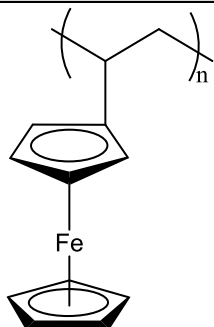
**Figure 1.1:** Schematic of the operation of a polymer-modified electrode. At the polymer/ electrode interface, there is an electron exchange due to potential perturbation and at the film/solution interface, ion and solvent transfer occurs due to electroneutrality and activity constraints.  $Y$  and  $Z$  represent electroactive species undergoing reduction/oxidation the subscript “p” denotes species diffusing in the bulk of the polymer.<sup>29</sup>

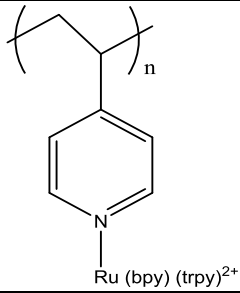
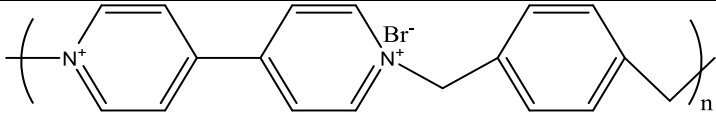
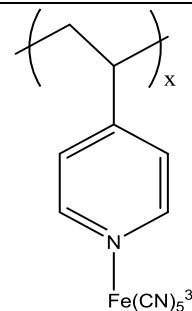
Generally, the features of modified polymeric materials depend on their structures and (electro) chemical properties, which can be classified as being one of three types: redox polymers, conjugated polymers (conducting polymers), and ion-exchange and co-ordination polymers.<sup>27, 30, 31</sup> Redox and conducting polymers are considered to be of particular importance because both have an electroactive product, where transport of electrons can take place between localized/delocalized redox sites via discrete redox centres covalently linked to the chemical structure of the polymer or within the polymer chains, respectively. However, whilst ion-exchange and co-ordination polymers are not electroactive due to containing electrostatically bound redox centres such as Poly(Styrene Sulfonate) (PSS) and Poly(4-Vinylpyridine) (PVP). Therefore, they can merge electroactive guest molecules,<sup>27</sup> so we will concentrate on electron-conducting polymers herein.

### 1.2.1 Redox Polymer

Redox polymers have localised redox sites and hence oxidation or reduction processes can occur at these same sites. In this case, electron transport takes place by an electron hopping mechanism<sup>32, 33</sup> or self-exchange<sup>34</sup> between neighbouring redox sites within the polymer. Because electron transport to/from the redox centre is slow, the conductivity of such a system is relatively low compared to a conducting polymer.<sup>35</sup> Some models of redox polymers are presented in **Table 1.1**.

**Table 1.1:** models of redox polymer structures.

Name	Structure
Poly(vinylferrocene) <sup>36</sup> -38	 <p>The diagram shows a ferrocene molecule consisting of two cyclopentadienyl rings sandwiching an iron (Fe) atom. One of the rings is connected to a polymer chain, represented by a zigzag line with a subscript 'n' in parentheses, indicating the repeating unit of the polymer.</p>

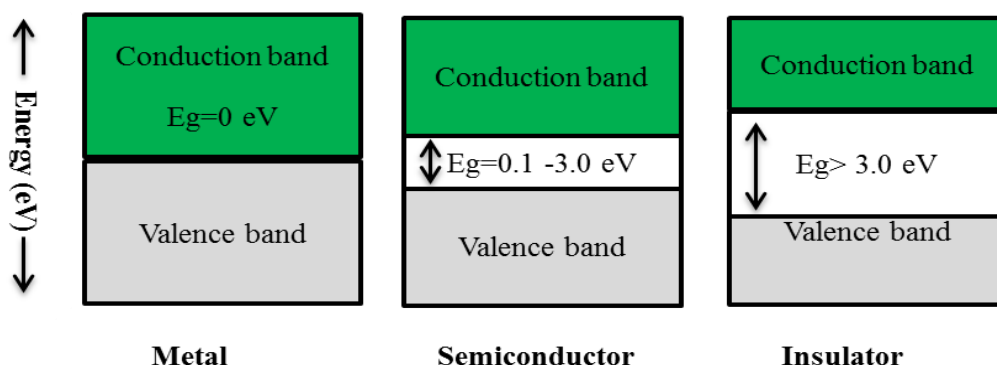
Poly(pyridyl) ruthenium(II) complex <sup>39, 40</sup>	
Poly(viologen) <sup>41, 42</sup>	
Poly(pyridyl) iron(II) complex <sup>43, 44</sup>	

### 1.2.2 Conducting Polymers

Conducting Polymer (CP) systems are different to redox polymers due to their conjugated backbone; by comparison, the backbone of redox polymers is unsaturated, and conduction relies on the motion of delocalized electrons occurs through conjugated systems. They are organic substances such as polypyrrole, polythiophene and polyaniline that have conjugated  $\pi$ -electron systems in their backbone. These materials, in addition to the basic elements of carbon and hydrogen, also contain heteroatoms like nitrogen, sulphur and oxygen.<sup>3, 45</sup> The conduction phenomena in CPs can be explained through band theory, in terms of the energy gap ( $E_g$ ) between the conduction and valence bands. In a metal,  $E_g = 0$  eV, which means there is no band gap due to the conduction and valence bands overlapping; as a result, the free transition of electrons can readily occupy the conduction band and giving a high electronic conductivity.

Semiconductors have an energy gap of between 0.1 - 3.0 eV, which is larger than metals and lower than insulators ( $E_g > 3.0$  eV). Therefore, electrons can transfer from their atoms (valence band) to a higher energy level in the conduction band by jumping due to thermal or photochemical excitation. On the other hand, insulator materials are non-electrical conductors because their electron cannot jump between bands, as shown in **Figure 1.2**.<sup>46</sup> Typically, conduction occurs in the oxidised or “doped” polymer as a

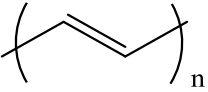
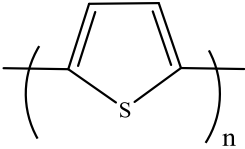
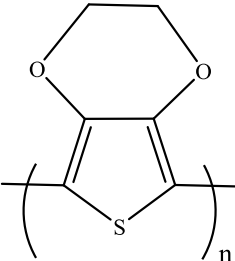
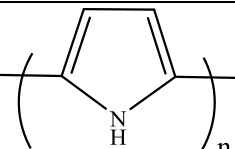
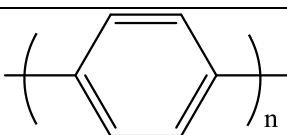
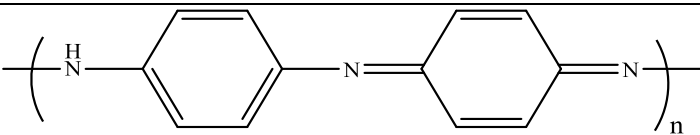
consequence of the conjugated system, allowing for a large degree of delocalisation in overlapping  $\pi$ -orbitals, while in the undoped state the conjugated polymers are insulating.<sup>4, 47</sup> In the doping process, the polymer gains a positive charge due to an electron being removed from its backbone. To maintain electroneutrality and thermodynamic activity constraints, an ion and/or neutral species from the bathing electrolyte transfers across the polymer; these species do not react with the polymer, but connect with the redox sites.<sup>20, 48, 49</sup> The characterisation of electroactive polymers relies on their redox behaviour, which is affected by different factors; for example, the type of electrolyte, the reaction temperature, the acidity of the solution and the precipitation time (i.e. the timescale of the experiment, which is itself entirely dependent on the scan rate and number of cycles).<sup>50</sup> A detailed study related to kinetic and thermodynamic issues on mobile species transfer during the redox process will be discussed in chapters 4 and 5.



**Figure 1.2:** Energy gap diagrams for conductors, semiconductors and insulators.<sup>46</sup>

Polyaniline is of great interest as a conducting polymer because of its interesting chemical/electrochemical structure. We focus on this polymer as the main subject of this thesis, as well as the electrochemical methods used in its preparation. **Table 1.2** shows some examples of common conducting polymers.

**Table 1.2:** Chemical structures of some common conjugated polymers.

Name	Structure
Polyacetylene (PA) <sup>51</sup>	
Polythiophene (PTh) <sup>52, 53</sup>	
Polyethylenedioxythiophene (PEDOT) <sup>54, 55</sup>	
Polypyrrole (PPy) <sup>56, 57</sup>	
Polyparaphenylene (PPP) <sup>58, 59</sup>	
Polyaniline (PANI) <sup>20, 56</sup>	

### 1.3 Polyaniline

Polyaniline (PANI) is probably the most famous of the electroconducting polymers. It can be synthesised by either chemical or electrochemical processes. It was initially prepared around 180 years ago by Rounge, who, in 1834, explored why the colour of the polymer can change from dark green to black depending on the conditions of the solution used.<sup>60</sup> Following this, Perkin, in 1856, supported Rounge's finding that PANI can be produced as a black precipitate.<sup>61</sup> Moreover, Letheby, in 1862, investigated this interesting feature of polyaniline through the electrolysis of aniline sulphate.<sup>62</sup> These changes in colour have been extensively employed in different industries such as

printing and dyeing.<sup>60</sup> Since then, a considerable number of investigations have been undertaken to improve the conductivity of this material due to the fact that PANI has a number of favourable properties: it can be prepared easily; it has good redox reversibility; it has high chemical stability to its environment; and it has high capacitive and superior electrical conductivity properties.<sup>63, 64</sup> The unique properties of this polymer led to its investigation for use in various applications, as given in section 1.1.

Recently, many methods and techniques have been used to prepare PANI from aniline; for example, chemical polymerisation,<sup>65</sup> electrochemical polymerisation,<sup>66</sup> enzyme-catalysed polymerisation,<sup>67</sup> vapour-phase deposition,<sup>68</sup> photopolymerisation<sup>69</sup> and electron acceptor polymerisation.<sup>70</sup> However, among these methods, synthesis of polyaniline by electrochemical deposition is greatly preferred. The significance of the use of this particular synthetic route is because it is inexpensive, and allows for easy preparation in a short time because the film is deposited directly on the electrode surface. It is also easy to control desirable characteristics, for example electrical and morphological properties, and the thickness of film, which can be achieved by controlling the conditions of growth such as the electrolyte bath, scan number, scan rate and applied voltage.<sup>71</sup>

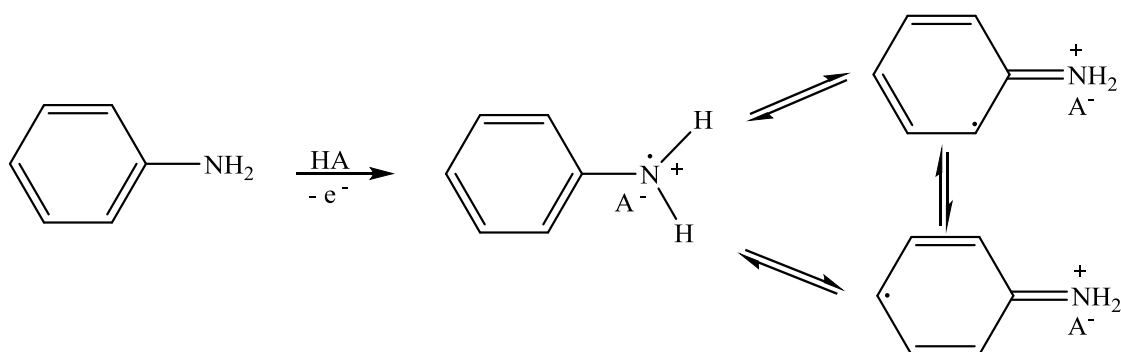
### **1.3.1 Mechanism of Electropolymerisation of Aniline**

In many previous studies, the type of mechanical interactions arising in the electrochemical polymerisation of aniline in aqueous solution have been suggested, as presented in **Figure 1.3**. Initially, the free radical cation of aniline is formed due to removal of an electron from the monomer upon oxidation on the electrode surface via an acidic electrolyte. In this step, the anilinium cation is formed, which exists in three resonance forms. In the second step, two such radicals couple in a 'head to tail' manner (the N- and para- radical cations are formed), and in this process two protons will be promptly eliminated to produce the dimer species. This dimer returns to its neutral state by a re-aromatisation process, producing an intermediate called *p*-aminodiphenylamine. In the third step, further oxidation at the anode occurs due to chain propagation, which occurs as a result of the anilinium radical-cation reacting with the radical of the oligomer. Finally, the presence of acid in the electrolyte leads to the formation of a counter-anion to balance the charge which migrates into the polymer, producing PANI/HA (step 4). It was found that electropolymerisation of aniline is most

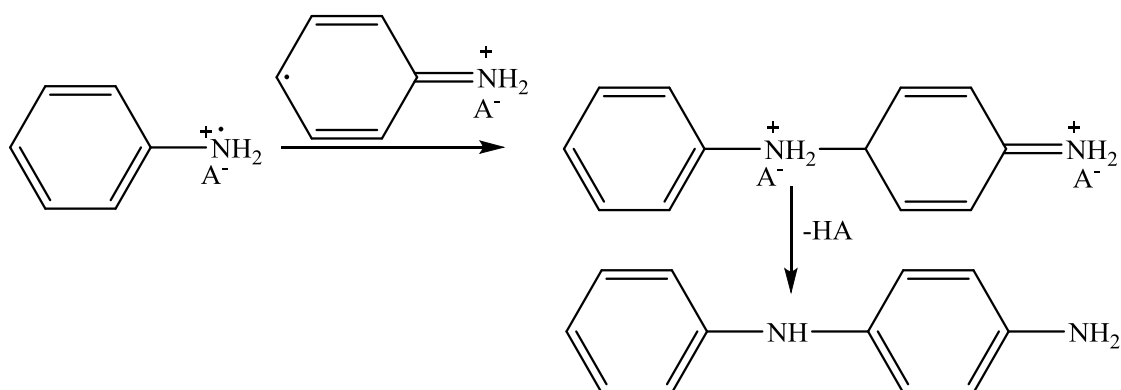
likely to be an autocatalytic reaction. This means the larger the amount of polymer on the electrode surface, the higher the rate of polymer formation.

Generally, many factors have an impact on the electrochemical growth of PANI such as the composition of the solution, the deposition methodology, the nature of the doping anion, the electrode compound, the temperature of the electrolyte, and the pH and viscosity of the solvent.<sup>72, 73</sup> Previous studies have shown that the polymerisation of aniline at  $\text{pH} > 4$  results in the formation of a polymer with less conjugation and lower conductivity, whereas the doped emeraldine salt form is highly conductive when generated in acidic media of  $\text{pH} \leq 2$ .<sup>74, 75</sup> There are several electrochemical techniques used to deposit the monomer such as potentiostatic, potentiodynamic or galvanostatic techniques.<sup>76</sup>

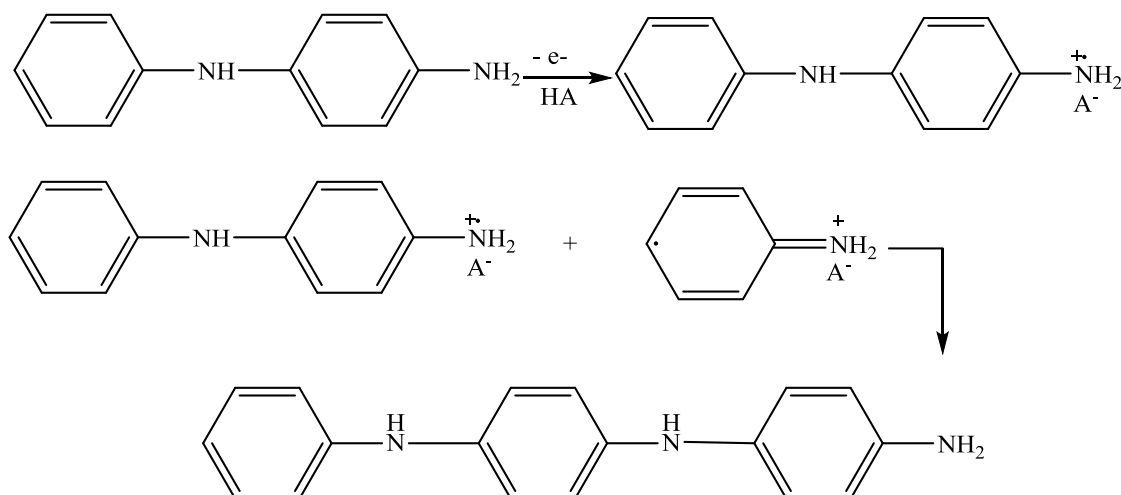
Step 1: Oxidation of monomer



Step 2: Radical coupling and re-aromatisation



Step 3: Chain propagation



Step 4: Oxidation and doping of the polymer

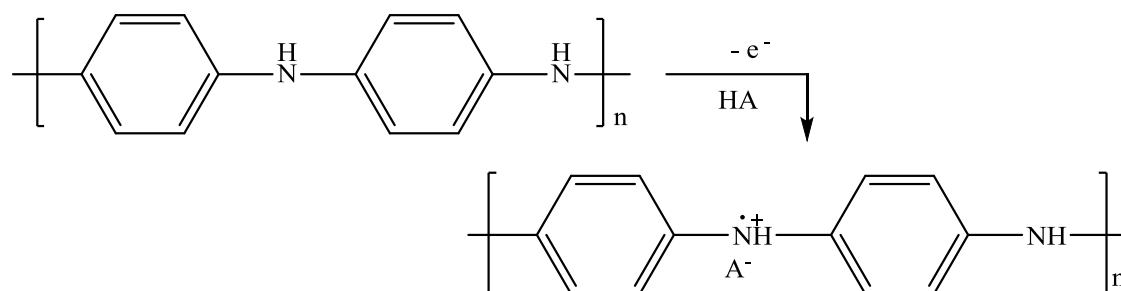


**Figure.1.3:** Mechanism of electropolymerisation of aniline.<sup>73</sup>

### 1.3.2 Optical Properties and Chemical Structures of Polyaniline

The polyaniline chain has various chemical forms, which can be attributed to switching between oxidation states. As a result, it is not only the chemical structure that changes but also its optical properties and conductivity. Four main types of structure can exist in polyaniline, as illustrated in scheme 1.4. These types can be classified as base or salt, and are:

- 1- **Leucoemeraldine Base (LB)** which is an electrically non-conducting state due to its unconjugated backbone. In addition, this kind is a completely reduced state and it has a yellow or light green colour.
- 2- **Emeraldine base (EB)** which is an intermediate form and a partially oxidised state. It has a blue colour and is an insulator.

3- **Emeraldine salt (ES)** which is the protonated form of EB and is a half-oxidised state. Indeed, the most important property of this form is that it is characterised by good conductivity, and it has a green colour.

4- **Pernigraniline base (PB)** is the fully oxidised form. This form normally has a purple or violet colour, and its considered to be an insulating state because no protons are localised on the imine (=N-) sites to cause charge transfer between quinoid rings.<sup>64,77</sup>

It is possible to switch between these states by electrochemical methods such as cyclic voltammetry, as seen in **Figure 1.4a**.

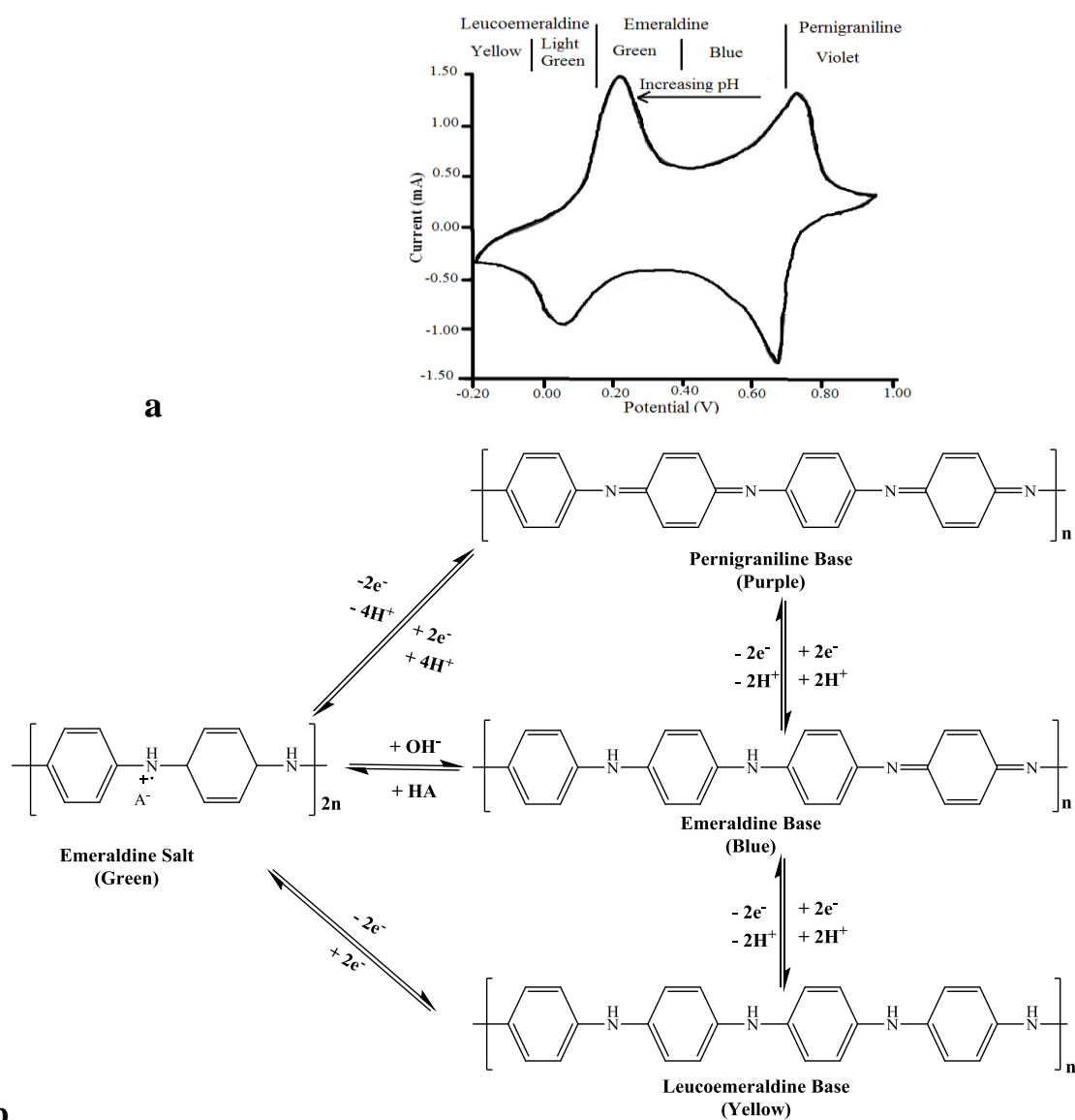


**Figure.1.4:** a) Colour changes take place with the change in the potential for PANI deposited on a glassy carbon electrode from 1 M  $\text{HCl}_{(aq)}$  at  $50 \text{ mV s}^{-1}$  by cyclic voltammogram<sup>73</sup> and b) structural changes between different redox states.<sup>78</sup>

## 1.4 Applications of Polymers Modified Electrodes

Due to their significant physical and chemical properties, as well as their potential applications, polymer-modified electrodes have been the subject of considerable attention in recent years. Consequently, the wide range of applications in different fields (as mentioned in section 1.1) is becoming of interest in the field of conducting ( $\pi$ -conjugated) polymers. It is well known that the majority of these applications are based on the redox reaction of the conducting polymer transported by the insertion/expulsion of charge following the variation in the composition and structural properties of the polymer materials. Among the many applications for conducting polymers this project focuses on two, which are supercapacitance and battery applications. The following sections will briefly highlight key concepts of both these applications.

### 1.4.1 Polymer Capacitors and Supercapacitors

The term electrochemical capacitors refers to the amount of energy and power (see equations 1.2 and 1.3) in a device which depends on the charge storage in the electrical double layer (EDL) or redox capacitor using carbonaceous electrodes or carbonaceous electrodes catalysed with metal oxides.<sup>79</sup> They have two parallel conductive plates, which are isolated by an ionic electrolyte, and are charged as a result of applying a potential difference across the electrodes. This process leads to the transferral of the positive and negative charges toward the surfaces of the electrodes of reverse polarity, respectively, as shown in **Figure 1.5** (left panel). After charging, the capacitor works as voltage source for a limited time as measured by its capacitance ( $C_s$ ), which is represented as the electric charge of an individual electrode over the potential difference (V) between them, as shown in equation 1.1:<sup>80, 81</sup>

$$C_s = \frac{Q}{V} \quad 1.1$$

where  $C_s$  is the capacitance measured in Farads ( $F$ ) from the total charge/discharge. In this system, the energy ( $E$ ) is expressed either in terms of “*specific energy*” (the amount of energy stored is given in mass  $Wh\ kg^{-1}$ ) or “*energy density*” (the amount of energy stored is given in volume  $Wh\ l^{-1}$ ), which is attributed to the charge at each electrode and the potential difference ( $V$ ), according to equation 1.2.<sup>81</sup>

$$E = \frac{1}{2} C_s V^2 \quad 1.2$$

Power ( $P$ ) is described by “specific power” ( $W\text{ kg}^{-1}$ ) or “power density” ( $W\text{ l}^{-1}$ ), which is attributed to the ability of cell to deliver power per unite mass or unite volume, respectively, as shown in equation 1.3.<sup>81</sup>

$$P = \frac{E}{t} \quad 1.3$$

In 1975, Becker obtained the first patent on capacitors, which depended on using carbon material with a high surface area. Since then, many researchers have shown an increased interest in electrochemical capacitors for energy storage applications, up to the 1980s.<sup>82, 83</sup> Based on this knowledge, there are now many types of capacitors, such as electrolytic, electrochemical and non-electrolytic capacitors. Electrochemical capacitors are subdivided into Electric Double Layer Capacitors (EDLCs), Pseudocapacitors (PsCs), and Hybrid Capacitors (HCs). The energy storage and mechanism of the electric charger can vary fundamentally between EDLCs and PsCs, with the latter having a higher capacitance. This is due to the fact that pseudocapacitors are based on a redox reaction in which fast Faradic charge transfer is achieved between the electrode and solution, while the magnitude of capacitance in EDLCs is generated from the accumulation of electrons, or ionic charge, which is separated from the electrode/solution interface. Hence, its action is based on an electrostatic mechanism (non-Faradaic) and no chemical reaction is involved. This, in turn, is strongly dependent on the large surface area of the electrode and its porosity. The substances are utilised for PsCs are conducting polymers and metal oxides, while EDLCs are formed from carbon materials.<sup>80, 84</sup>

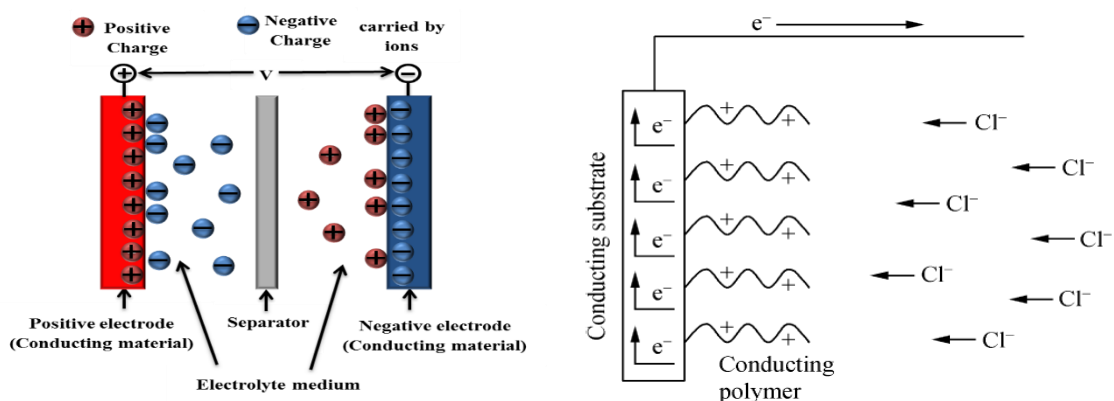


**Figure 1.5:** Left panel represents an electric double-layer supercapacitor<sup>85</sup> while the right panel indicates the pseudocapacitance in a conducting polymer.<sup>19</sup>

### 1.4.2 Batteries

A battery is an electrochemical device that has the ability to produce electrical energy from chemical energy via redox reactions. The first study of an electrochemical battery was carried out by Alessandro Volta in 1800. After that, various studies have been undertaken in recent years in order to improve battery science and technology for energy storage systems. Today, batteries are an important part of our life because a wide range of technologies and industrial processes are dependent on an electrical energy source. They successfully provide electrical energy to portable electronic tools such as phones, laptops, and digital cameras. In addition, providing high energy density in batteries opens the route for renewable energy sources to be developed for ecological alternative power sources, such as solar and wind energy, and low-emission transportation, such as hybrid and electric vehicles. However, the main problem with these applications is the economy of their use.<sup>86,87</sup> Generally, batteries are composed of three/four compounds, as shown in **Figure 1.6** (left panel):

**Anode:** also known as the negative electrode of the cell, which produces electrons for the circuit through oxidative chemical reactions.

**Cathode:** also known as the positive electrode of the cell, which acquires electrons from the circuit during reductive chemical reactions.

**Separator:** the physical barrier (semi-permeable membrane) between the cathode and anode that allows ions to flow between the two electrodes, and electrically isolates the battery system.

**Electrolyte:** supplies a source of dopants between the positive and negative electrodes during the redox reactions in the cell.

Defined by their principles of operation, there are two main types of battery, as follows:

- 1- Primary (Non-rechargeable) Batteries: produced in a charged state and can be employed until the constituent compounds reach their equilibrium concentrations and hence cannot be recharged again, at which point the battery (cell) has to be discarded.
- 2- Secondary (Rechargeable) Batteries: produced in a discharged state and can be charged and discharged multiple times. In order to recharge the battery (cell), an

electrical current is provided to the discharged cell to reverse the cell reaction and re-form the reactant (non-equilibrium concentrations of compounds).<sup>88, 89</sup>

Additionally, the amount of energy stored in the battery (i.e. the charge storage capability) can be defined as the specific energy ( $Wh\ kg^{-1}$ ) or energy density ( $Wh\ l^{-1}$ ). The power indicates the ability of the cell to deliver power per unit mass ( $W\ kg^{-1}$ ) or volume ( $W\ l^{-1}$ ) (i.e. it is time dependent). The performance of various batteries are compared in terms of energy storage and power, which can easily be characterised by plotting specific power as a function of specific energy in a so-called Ragone plot, as presented in **Figure 1.6** (right panel).

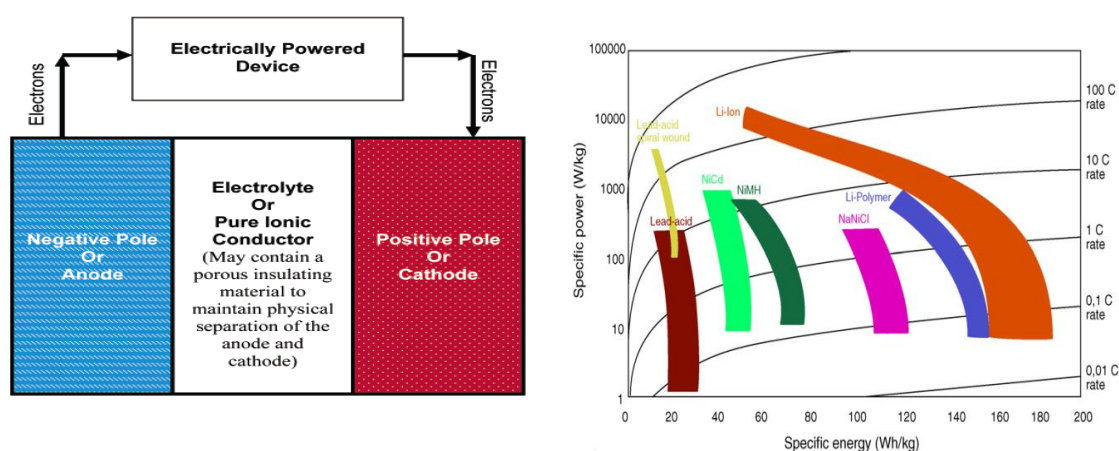


**Figure 1.6:** Left panel: a block diagram of a battery cell (images from Winter and Brodd).<sup>88</sup> Right panel: Ragone plot of different energy storage devices (images from Van den Bossche)<sup>90</sup>

The important qualities required of useful in the batteries are: <sup>88, 91, 92</sup>

- High energy and power densities.
- Cyclability (i.e. number of cycles).
- Ability to operate over a wide temperature range (i.e. can be used in hot/cold climates).
- Cheap manufacturing costs compared to other sources, such as petrol/diesel powered vehicles.
- Safety: manufacture does not require toxic substances.

There are many common commercial battery systems, whose energies and storage capabilities depend on the materials used for their manufacture, such as:

**Lead Acid (Pb-Acid):** includes a lead dioxide cathode (positive electrode), a lead anode (negative electrode) and a sulphuric acid electrolyte. The materials are inexpensive and it performs reliably. However, this system is limited by loss of capacity, and safety issues due to corrosion of the anode (Pb) and active substances being detached owing to normal mechanical bumping.

**Nickel–Cadmium battery:** consists of cadmium for the anode (negative electrode), nickel hydroxide for cathode (positive electrode), and the electrolyte is made of a mixture of KOH and  $\text{Li}(\text{OH})_2$ . A key issue in this battery are the associated safety concerns due to the toxicity of the nickel cadmium (nicad). This fact was the main goal in the improvement of other rechargeable systems.

**Nickel Metal Hydride (NiMH):** based on a nickel oxyhydroxide cathode and a metal hydride anode in a basic, aqueous sodium or potassium hydroxide electrolyte. The advantages of this system are high electrochemical capacity, low self-discharge rates, safety and good environmental compatibility. The main disadvantages of this technology are those of poor charge retention and the costs of manufacture, which are more expensive than NiCd.

**Lithium Ion (Li-Ion) battery:** the cathode is made of a metal oxide intercalated with lithium metal, such as  $\text{LiMn}_2\text{O}_4$  or  $\text{LiCoO}_2$ , with a lithiated carbon anode in an organic electrolyte containing a lithium-based salt. This system has the advantage of using lighter weight materials compared to other technologies. It also has the advantage of a high open-circuit voltage (OCV). However, the main drawbacks of Li-Ion batteries are those of high costs, and the use of a non-aqueous electrolyte that can increase the internal resistance of the battery, causing flammability.

**Zinc polymer battery:** is an alternative energy source, which consists of polymeric materials such as PANI as the cathode and zinc metal as the anode. The advantages of such a battery are that it can use aqueous and non-aqueous electrolytes, is inexpensive, non-toxic, lightweight relative to most metals, and its materials are abundant.<sup>89, 90, 93-95</sup> Our focus is on the concept of Zinc-Polymer battery systems, however, which will be addressed in chapter 7 of this thesis.

## **1.5 Electrodeposition from Ionic Liquid**

In recent years, the electrodeposition of conducting polymers has been utilised extensively in ionic liquids to improve the sustainability of certain properties of organic semiconductors, particularly regarding conductivity durability, thermal stability and morphology.<sup>64</sup> Thus, these electrolytes have been extensively investigated in various fields as alternatives to conventional solvents in electrochemical industries; for example, electroplating, catalysis, electronics, sensors, biosensors, and so forth.<sup>64</sup> In the following sections, we will define Ionic Liquids (ILs), why they have become significant in recent the past decades and how they contribute to industrial processes. Moreover, we will remind ourselves of a number of advantages of ILs, which have almost certainly impacted a wide range of evolving industries.

### **1.5.1 Ionic Liquids**

Ionic liquids (ILs) are salt compounds, which are in the liquid state at a temperature of less than 100°C.<sup>96</sup> These liquids are composed of particular ions, such as cations and anions. They are conducting in that they permit the measurement of charge through the liquid.<sup>97</sup> Recent studies have shown that ionic liquids have significant value because they have various unique properties, such as being non-flammable, non-volatile, and having high conductivities and high themostabilities. As a result, they are employed and developed in a wide range of industrial applications; for example, synthesis of organic reagents, extraction, solvents, electrodeposition and catalysis.<sup>98</sup> Wassercheid and Welton have highlighted the fact that ionic liquids at room temperature have extremely low vapour pressures and non-volatile characteristics. As a consequence, they cannot evaporate into the atmosphere, as opposed to traditional solvents. This particular feature of ILs is likely to become increasingly important as it allows us to decrease levels of pollutant emission into the atmosphere during industrial processes. However, there are some important handicaps one encounters when using them, such as their expensive preparation and possible toxicity. They can cause environmental problems because some types of IL can dissolve in water, and they have poor biodegrading properties, such as is seen with [C<sub>10</sub>MIM][BF<sub>4</sub>] ILs.<sup>99</sup>

The physical characteristics of ionic liquids have a profound influence on their sustainability for numerous applications compared to molecular solvents.<sup>98, 100</sup> Freemantle<sup>97</sup> explains that ILs at room temperature are generally salts, and consist of long-chain alkyl groups with nitrogen-rich and phosphorus-rich groups including organic cations. For example, imidazolium ILs have been the dedicated subject of many research groups' investigations, especially 1-alkyl-3-methylimidazolium cations. The low melting point of ILs is attributed to the low symmetry of their ions, which prevents the system from solidification, as well as allowing for easy charge dispersion, which allows the entropy of the system to increase.<sup>98, 101</sup> The most common chemical structures of cations in ionic liquids are shown in **Figure 1.7**. In addition, there are some ILs which contain common anions, for example, halides such as bromide (Br<sup>-</sup>), chlorides (Cl<sup>-</sup>), hexafluorophosphates [PF<sub>6</sub>]<sup>-</sup>, nitrates [NO<sub>3</sub>]<sup>-</sup>, tetrafluoroborate [BF<sub>4</sub>]<sup>-</sup>, chloroaluminates [Al<sub>2</sub>Cl<sub>4</sub>]<sup>-</sup> and [Al<sub>2</sub>Cl<sub>7</sub>]<sup>-</sup>, and alkyl sulphates [RSO<sub>4</sub>]<sup>-</sup> such as ethyl sulphate [C<sub>2</sub>H<sub>5</sub>SO<sub>4</sub>]<sup>-</sup>.<sup>97</sup>

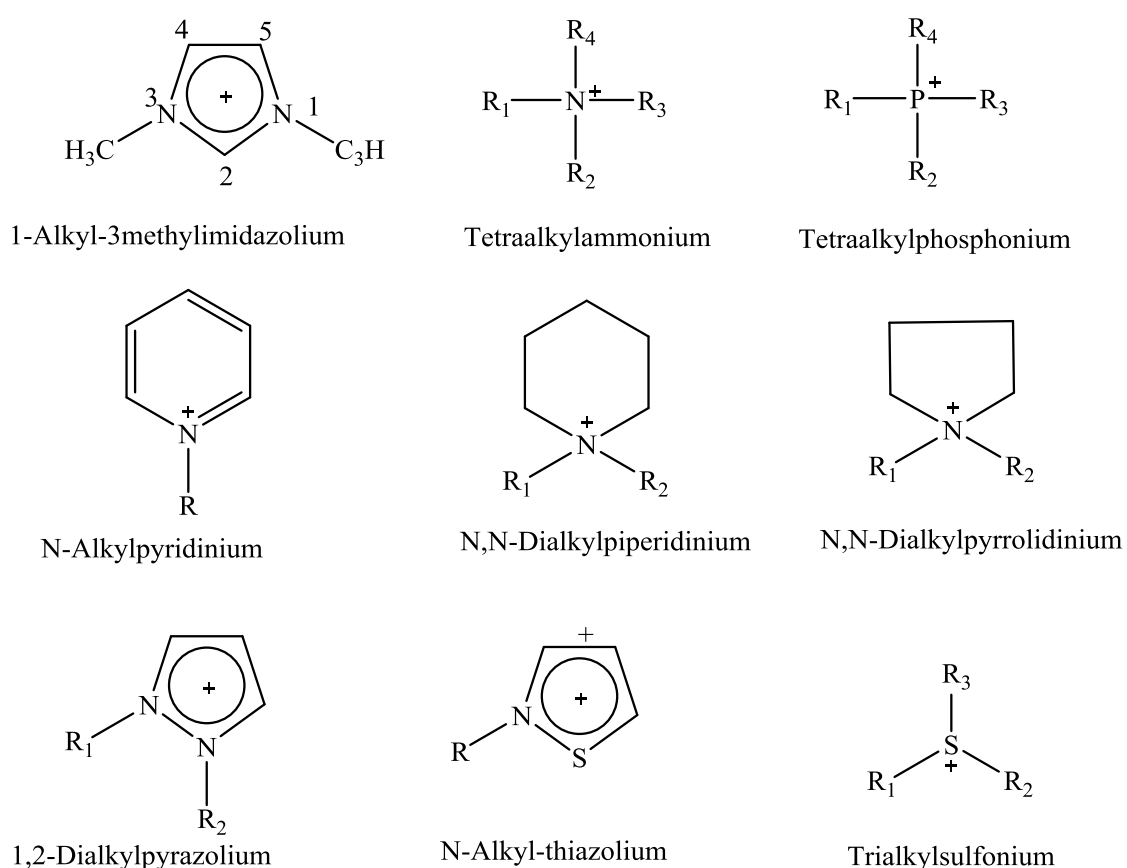


**Figure.1.7:** Various types of IL cations (the R in each structure represents an alkyl group).<sup>97</sup>

Other important properties of ILs have been examined, such as solubility and miscibility. Both ionic and covalent compounds can dissolve in ILs. In other words, ILs have a high ability to dissolve a huge number of metal salts; for instance, Seddon mentions that Kerogen can be dissolved in ILs, while Kerogen, a fossilised organic material present in sedimentary rock, was found to be insoluble in ILs and all known solvents except hydrofluoric acid.<sup>97</sup>

Another characteristic of ionic liquids is that they can have high decomposition temperatures. This means that these solvents can be used across a wide range of temperatures whilst remaining in the liquid phase and with limited degradation. The main reason for the high temperatures stability of ILs is that they have extremely low vapour pressure; for instance, the melting point of 1-alkyl-3-methylimidazolium is -70 to -90°C, while, IL boiling points can range from 250 to 450 °C.<sup>97, 98</sup> Physical features, such as density and viscosity, are important for some salts, such as [C<sub>2</sub>mim] AlCl<sub>4</sub>, when considering the sustainability of an ionic liquid for a potential application.<sup>102</sup>

Regarding current potential applications, one of the most significant of those is that they can be used as non-traditional solvents to manufacture conducting polymer. For example, 1-butyl-3-methyl imidazolium hexafluorophosphate [C<sub>4</sub>mim PF<sub>6</sub>] ILs can be utilised as solvents for electropolymerisation of aniline at room temperature on a platinum substrate using cyclic voltammetry. Consequently, many applications may be achieved as a result of the electrochemical polymerisation of certain organic semiconductors such as polyaniline, polypyrrols and polythiophenes in ILs.<sup>78</sup> Further information regarding the properties and applications of ionic liquids can be found in reviews by Plechkova and Seddon,<sup>103</sup> Hallett and Welton<sup>104</sup> and Marsh.<sup>105</sup>

### **1.5.2 Deep Eutectic Solvents**

The interest in employing ionic liquids across a range of applications has been limited in industrial use because of their expensive synthesis and the fact they have only one type of detaching species (cation or anion) in their structure. Abbott *et al.*<sup>106</sup> found, in 2003, a related, and alternative, type of solvents called “Deep-Eutectic Solvents” (DESs) which are commonly known as a novel class of IL because the two (DESs and ILs) have similar physical characteristics. However, the application fields are clearly varied for both due to the fact that they have different chemical properties.<sup>107, 108</sup> DESs are cationic and anionic compounds, which are combined together by hydrogen bonding

interactions to produce a component eutectic mixture, such as urea and choline chloride (high melting point), which can be combined to produce Reline. After combination of its compounds, the new compound (Reline) has a melting point that is lower than its two individual components. Simply put, a range of eutectic mixtures can be formed from a range of quaternary ammonium salts mixed with metal salts or Hydrogen Bond Donors (HBDs), as shown in **Figure 1.8**.<sup>108</sup>

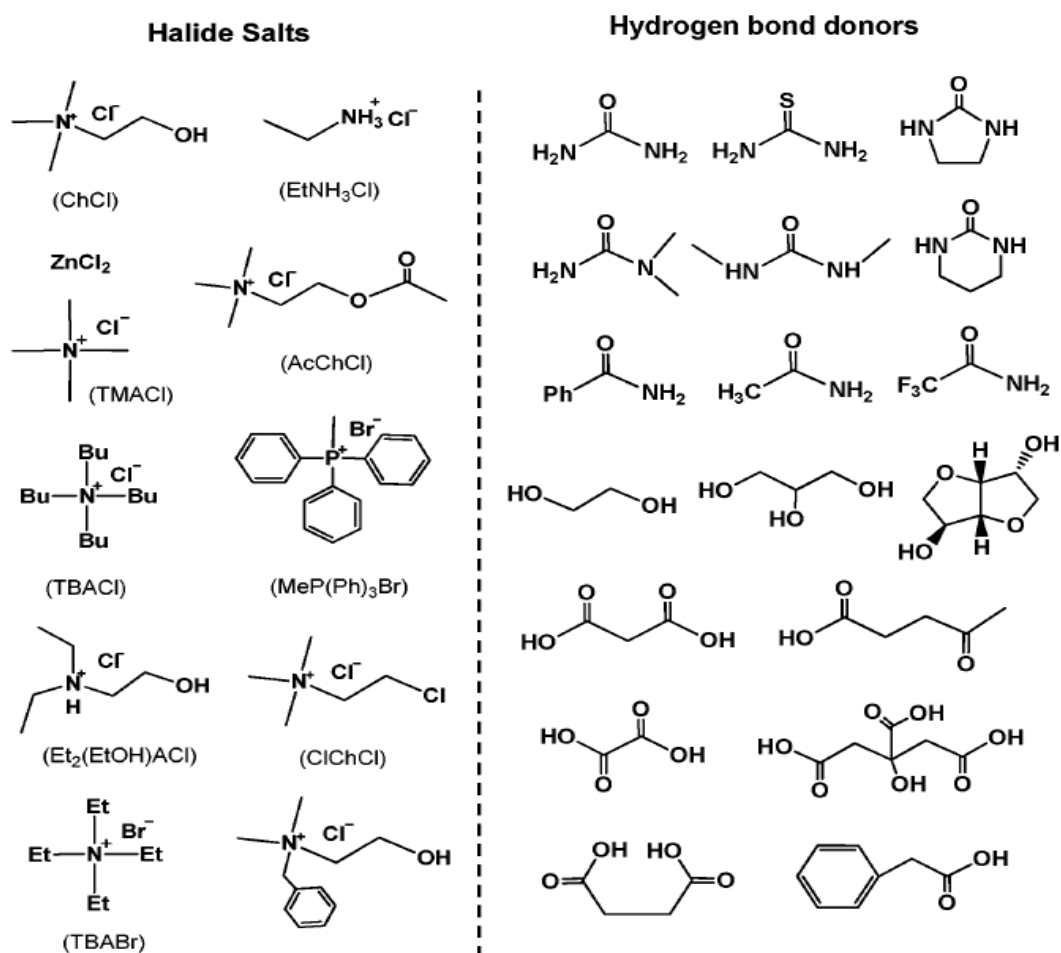


**Figure 1.8:** Some structures of hydrogen bond donors and halide salts employed for DES preparation.<sup>108</sup>

The freezing point of non-interacting compounds converts linearly with mole fraction, “whereas large negative deviations can occur when the components interact strongly with each other”<sup>4</sup>, as can be seen in the schematic in **Figure 1.9**.

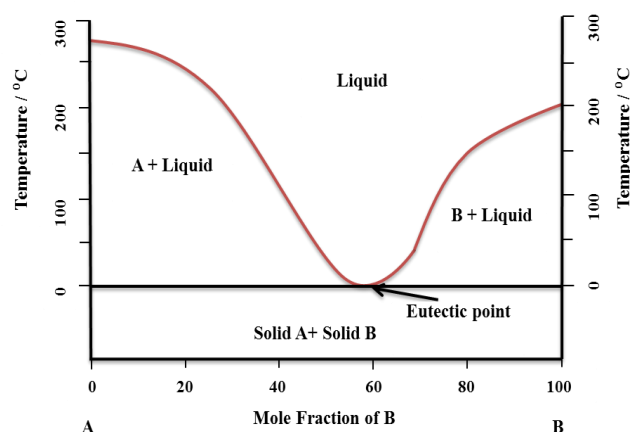


**Figure 1.9:** Schematic representation of a eutectic point on a two component phase diagram.<sup>4</sup>

Usually, the eutectic point represents the lowest freezing point of the various mole fractions, which can be recognised due to the extensive depression in freezing point of the mixed materials. DESs have large non-symmetric ions, which also encourage a decreasing lattice energy, and thus the depression of the melting point of resultant product. In addition, the charge dissipation between the halide ion and the hydrogen-donor moiety during the formation of hydrogen bonds is responsible for the reduction in the melting point and lattice energy of the mixture when compared to the melting points of the independent components.<sup>109</sup> Furthermore, the interaction between the components is contingent on the size of the anions which has an effect on melting point.<sup>4</sup> The generalised chemical formula that can be used to represent DESs can be expressed as  $\text{Cat}^+\text{X}^-z\text{Y}$ , and is dependent on the complexity of mixture used in its formation, where  $\text{Cat}^+$  is any cation and X is a Lewis base, commonly a halide anion. Generally, they are divided into four types, as presented in **Table 1.3**.<sup>107, 110</sup>

**Type 1.3:** Types of DESs and their general formula

Types	General formula	Terms
Type I	$\text{Cat}^+\text{X}^- + z\text{MCl}_x$	M = Zn, Sn, Fe, Al, Ga
Type II	$\text{Cat}^+\text{X}^- + z\text{MCl}_x \cdot y\text{H}_2\text{O}$	M = Cr, Co, Cu, Ni, Fe
Type III	$\text{Cat}^+\text{X}^- + z\text{RZ}$	Z = -CONH <sub>2</sub> , COOH, OH
Type IV	$\text{MCl}_x + z\text{RZ}$	M = Zn, Al Z = OH, CONH <sub>2</sub>

These solvents are being increasingly studied due to a wide range of advantages in their physical characteristics.<sup>111</sup> Firstly, they are cheap and easy to prepare, as well as being safe to use as solvents in a wide range of industrial areas. Moreover, they can dissolve a wide range of solutes and show exceptional solubility towards metal oxides.<sup>112</sup> Additionally, they have other characteristics, such as low vapour pressures, high ionic conductivity,<sup>113</sup> biodegradability, low toxicity<sup>108</sup> and insensitivity to water.<sup>112</sup> Owing to the physical characteristics mentioned above, DESs have become important components in a range of applications over recent years; for example, metal recycling and electrodeposition, biochemistry, separation, extraction solvents, electropolishing and polymer synthesis.<sup>114-116</sup>

## **1.6 Aim of Project**

The general objective of this project is to study the properties of conducting polymers in new electrolytes (DESs) in order to understand how conducting polymers behave in such electrolyte and thus their use as non-toxic electrolytes in battery applications (energy storage). This includes an investigation into whether DESs are more appropriate electrolytes than organic and aqueous solvents with regards to their applications in batteries and as supercapacitance devices.

One half of a battery involves metal stripping and metal deposition; DESs are very good at controlling metal stripping and deposition (chemical reversibility), especially for zinc (Zn is a cheap, lightweight, environmentally acceptable and abundant metal) and inhibiting electrochemical hydrogen evolution on the zinc electrode due to having a wider potential window than aqueous solutions (though less than ILs). In addition, DESs reduce zinc dendritic growth during charge-discharge cycling. The other half of battery is that of a conducting polymer, for which we chose the polymer PANI because it is cheap, lightweight and available, though we do not know how this conducting polymer behaves in DESs. Therefore, the motivation of this work is to understand the electrochemistry, ion transfer and solvent transfer (neutral species) processes of this polymer in DES for use in energy storage applications.

**The first objective** will include the electrodeposition of aniline on a platinum substrate employing an acidic medium as the background electrolyte. An attempt to understand the electrochemical behaviour of the film deposited in novel electrolytes (DES) and acidic media will be made using an electrochemical quartz crystal microbalance (EQCM).

**The second objective** is to electrodeposit aniline on a platinum substrate employing a DES (type III) as the background electrolyte, and then monitoring the mass change and electrochemical behaviour of the film deposited in the DES electrolytes and acidic media using EQCM. Comparison will then be made with polymer-modified electrodes formed using aqueous solutions. In this study, different parameters (film thickness, timescale, number of scans, temperature) will be varied in order to analyse the ion transfer dynamics of PANI films during the charging/discharging of films in DESs and aqueous electrolytes. The two objectives above can help answer the following question as to whether the behaviour of PANI is the same in DES and aqueous solutions, or otherwise. If not, then the second question will consider whether the differences are due to the properties and composition of the film or the behaviour of the monomer-free electrolytes.

**The third objective** is to use PANI in a supercapacitor application by the incorporation of a PANI film into graphite and/or metal oxides particles in both electrolytes (DES and aqueous solutions) to improve the capacitance, stability, morphology (more porous surface), impedance behaviour, mechanical and thermostability of the PANI modified electrode, as controlled by experimental variables.

**The final objective** is to use PANI modified with graphite and a metal oxide in a rechargeable battery application (modified PANI represents the cathode and zinc metal the anode) in both systems (DES and aqueous). Further details regarding the objectives of each study can be found at the outset of each chapter. **Figure 1.10** summarises the overall methodology of the research.

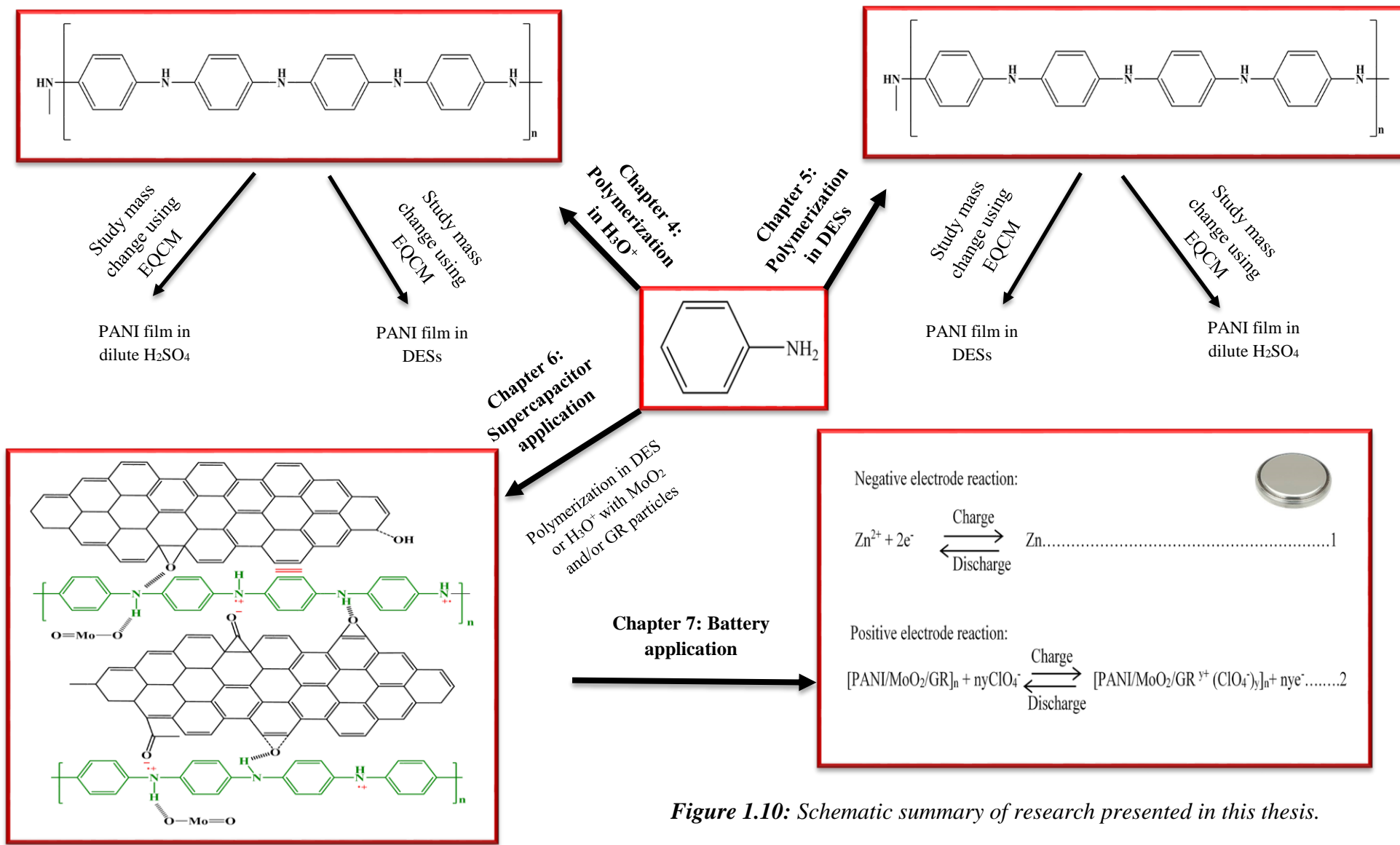


Figure 1.10: Schematic summary of research presented in this thesis.

## 1.7 References

1. A. Elschner, S. Kirchmeyer, W. Lovenich, U. Merker and K. Reuter, *PEDOT: Principles and Applications of an Intrinsically Conductive Polymer*, CRC Press, 2010.
2. C. K. Chiang, C. Fincher Jr, Y. W. Park, A. J. Heeger, H. Shirakawa, E. J. Louis, S. C. Gau and A. G. MacDiarmid, *Physical Review Letters*, 1977, **39**, 1098.
3. P. Chandrasekhar, *Conducting Polymers, Fundamentals and Applications: A Practical Approach*, Springer US, 2013.
4. F. Endres, D. MacFarlane and A. Abbott, *Electrodeposition from Ionic Liquids*, Wiley, 2008.
5. J. M. Margolis, *Conductive Polymers and Plastics*, Springer Science & Business Media, 2012.
6. T. C. Girija and M. V. Sangaranarayanan, *Synthetic Metals*, 2006, **156**, 244-250.
7. T. Kobayashi, H. Yoneyama and H. Tamura, *Journal of Electroanalytical Chemistry and Interfacial Electrochemistry*, 1984, **177**, 281-291.
8. A. Kitani, M. Kaya and K. Sasaki, *Journal of the Electrochemical Society*, 1986, **133**, 1069-1073.
9. R. Holze and Y. Wu, *Electrochimica Acta*, 2014, **122**, 93-107.
10. M. P. Gustafson, K. Matsumoto, D. R. MacFarlane and B. Winther-Jensen, *Electrochimica Acta*, 2014, **122**, 166-172.
11. Y. Yang, M. h. Diao, M. m. Gao, X. f. Sun, X. w. Liu, G. h. Zhang, Z. Qi and S. g. Wang, *Electrochimica Acta*, 2014, **132**, 496-503.
12. X. Yin, J. Ding, S. Zhang and J. Kong, *Biosensors and Bioelectronics*, 2006, **21**, 2184-2187.
13. H. Bai and G. Shi, *Sensors*, 2007, **7**, 267-307.
14. D. Sazou and D. Kosseoglou, *Electrochimica Acta*, 2006, **51**, 2503-2511.
15. J. Heinze, B. A. Frontana-Urbe and S. Ludwigs, *Chemical Reviews*, 2010, **110**, 4724-4771.
16. K. Zhang, L. L. Zhang, X. S. Zhao and J. Wu, *Chemistry of Materials*, 2010, **22**, 1392-1401.
17. G. Wang, Q. Tang, H. Bao, X. Li and G. Wang, *Journal of Power Sources*, 2013, **241**, 231-238.

18. Z. Wang, J. Yuan, M. Li, D. Han, Y. Zhang, Y. Shen, L. Niu and A. Ivaska, *Journal of Electroanalytical Chemistry*, 2007, **599**, 121-126.
19. C. Peng, S. Zhang, D. Jewell and G. Z. Chen, *Progress in Natural Science*, 2008, **18**, 777-788.
20. A. R. Hillman and M. A. Mohamoud, *Electrochimica Acta*, 2006, **51**, 6018-6024.
21. L. Lizarraga, E. M. Andrade and F. V. Molina, *Electrochimica Acta*, 2007, **53**, 538-548.
22. A. Merz and A. J. Bard, *Journal of the American Chemical Society*, 1978, **100**, 3222-3223.
23. M. R. Van de Mark and L. L. Miller, *Journal of the American Chemical Society*, 1978, **100**, 3223-3225.
24. T. Yamamoto, T. Maruyama, Z.-H. Zhou, T. Ito, T. Fukuda, Y. Yoneda, F. Begum, T. Ikeda and S. Sasaki, *Journal of the American Chemical Society*, 1994, **116**, 4832-4845.
25. A. Jackson, PhD Theses, University of Leicester, 2001.
26. T. A. Skotheim, *Handbook of Conducting Polymers, Second Edition*, Marcel Dekker, New York, 1998.
27. R. W. Murray, *Molecular Design of Electrode Surfaces*, Wiley-Interscience, New York, 1992.
28. A. R. Hillman and R. Linford, *Electrochemical Science and Technology of Polymers, Elsevier, London*, 1987, **1**, pp. 103–291.
29. A. M. Mohamoud, *PhD Theses, University of Leicester*, 2007.
30. M. M. Walczak, C. Chung, S. M. Stole, C. A. Widrig and M. D. Porter, *Journal of the American Chemical Society*, 1991, **113**, 2370-2378.
31. A. Ulman, *Chemical Reviews*, 1996, **96**, 1533-1554.
32. F. C. Anson, D. N. Blauch, J. M. Saveant and C. F. Shu, *Journal of the American Chemical Society*, 1991, **113**, 1922-1932.
33. A. Akhoury, L. Bromberg and T. A. Hatton, *The Journal of Physical Chemistry B*, 2012, **117**, 333-342.
34. J. Facci and R. W. Murray, *The Journal of Physical Chemistry*, 1981, **85**, 2870-2873.
35. M. S. Freund and B. A. Deore, *Self-Doped Conducting Polymers*, John Wiley & Sons Ltd, 2007.
36. J. B. Flanagan, S. Margel, A. J. Bard and F. C. Anson, *Journal of the American Chemical Society*, 1978, **100**, 4248-4253.

37. A. R. Hillman, D. C. Loveday and S. Bruckenstein, *Langmuir*, 1991, **7**, 191-194.
38. I. Jureviciute, S. Bruckenstein and A. R. Hillman, *Journal of Electroanalytical Chemistry*, 2000, **488**, 73-81.
39. S.-J. Lu, J.-Y. Luo, S.-B. Ji, N.-X. Li, H. Li and W.-S. Li, *Electrochimica Acta*, 2014, **136**, 130-137.
40. A. M. Lapides, D. L. Ashford, K. Hanson, D. A. Torelli, J. L. Templeton and T. J. Meyer, *Journal of the American Chemical Society*, 2013, **135**, 15450-15458.
41. R. Sydam, M. Deepa, S. M. Shivaprasad and A. K. Srivastava, *Solar Energy Materials and Solar Cells*, 2015, **132**, 148-161.
42. A. R. Hillman and E. F. Mallen, *Journal of Electroanalytical Chemistry and Interfacial Electrochemistry*, 1991, **309**, 159-171.
43. J. E. Monat and J. K. McCusker, *Journal of the American Chemical Society*, 2000, **122**, 4092-4097.
44. G. J. Britovsek, M. Bruce, V. C. Gibson, B. S. Kimberley, P. J. Maddox, S. Mastroianni, S. J. McTavish, C. Redshaw, G. A. Solan and S. Strömberg, *Journal of the American Chemical Society*, 1999, **121**, 8728-8740.
45. G. Inzelt, *Conducting Polymers: A New Era in Electrochemistry*, Springer-Verlag Berlin Heidelberg, 2008.
46. K. M. Molapo, P. M. Ndangili, R. F. Ajayi, G. Mbambisa, S. M. Mailu, N. Njomo, M. Masikini, P. Baker and E. I. Iwuoha, *International Journal of Electrochemical Science*, 2012, **7**, 11859-11875.
47. J. Roncali, R. Garreau and M. Lemaire, *Journal of Electroanalytical Chemistry and Interfacial Electrochemistry*, 1990, **278**, 373-378.
48. A. R. Hillman, M. A. Mohamoud and S. Bruckenstein, *Electroanalysis*, 2005, **17**, 1421-1432.
49. S. Bruckenstein, I. Jureviciute and A. R. Hillman, *Journal of the Electrochemical Society*, 2003, **150**, E285-E291.
50. D. D. Borole, U. R. Kapadi, P. P. Kumbhar and D. G. Hundiwale, *Materials Letters*, 2002, **56**, 685-691.
51. K. Nishio, M. Fujimoto, N. Yoshinaga, N. Furukawa, O. Ando, H. Ono and T. Suzuki, *Journal of Power Sources*, 1991, **34**, 153-160.
52. Y. Kim, S. Cook, S. M. Tuladhar, S. A. Choulis, J. Nelson, J. R. Durrant, D. D. Bradley, M. Giles, I. McCulloch and C.-S. Ha, *Nature Materials*, 2006, **5**, 197-203.
53. J. Roncali, *Chemical Reviews*, 1992, **92**, 711-738.

54. B. Sankaran and J. R. Reynolds, *Macromolecules*, 1997, **30**, 2582-2588.
55. T. Bashir, *Conjugated Polymer-Based Conductive Fibers for Smart Textile Applications*, Chalmers University of Technology, 2013.
56. N. V. Blinova, J. Stejskal, M. Trchová, J. Prokeš and M. Omastová, *European Polymer Journal*, 2007, **43**, 2331-2341.
57. J. Thiéblemont, J. Gabelle and M. Planche, *Synthetic Metals*, 1994, **66**, 243-247.
58. F. Schlütter, T. Nishiuchi, V. Enkelmann and K. Müllen, *Polymer Chemistry*, 2013, **4**, 2963-2967.
59. M. Banerjee, R. Shukla and R. Rathore, *Journal of the American Chemical Society*, 2009, **131**, 1780-1786.
60. G. Ćirić-Marjanović, *Synthetic Metals*, 2013, **177**, 1-47.
61. O. Meth-Cohn and M. Smith, *Journal of the Chemical Society, Perkin Transactions 1*, 1994, 5-7.
62. H. Letheby, *Journal of the Chemical Society*, 1862, **15**, 161-163.
63. P. M. Fernandes, J. M. Campiña, C. M. Pereira and F. Silva, *Journal of the Electrochemical Society*, 2012, **159**, G97-G105.
64. P. M. V. Fernandes, J. M. Campiña, N. M. Pereira, C. M. Pereira and F. Silva, *Journal of Applied Electrochemistry*, 2012, **42**, 997-1003.
65. K. Lee, S. Cho, S. H. Park, A. Heeger, C.-W. Lee and S.-H. Lee, *Nature*, 2006, **441**, 65-68.
66. J. Li, L. Liu, P. Wang and J. Zheng, *Electrochimica Acta*, 2014, **121**, 369-375.
67. Z. Gao, S. Rafea and L. H. Lim, *Advanced Materials*, 2007, **19**, 602-606.
68. J.-Y. Kim, J.-H. Lee and S.-J. Kwon, *Synthetic Metals*, 2007, **157**, 336-342.
69. Y. Kim, S. Fukai and N. Kobayashi, *Synthetic Metals*, 2001, **119**, 337-338.
70. S.-J. Su and N. Kuramoto, *Macromolecules*, 2001, **34**, 7249-7256.
71. A. Baba, M.-K. Park, R. C. Advincula and W. Knoll, *Langmuir*, 2002, **18**, 4648-4652.
72. N. Gospodinova and L. Terlemezyan, *Progress in Polymer Science*, 1998, **23**, 1443-1484.
73. G. G. Wallace, P. R. Teasdale, G. M. Spinks and L. A. P. Kane-Maguire, *Conductive Electroactive Polymers: Intelligent Polymer Systems, Third Edition*, CRC Press, 2008.
74. N. Gospodinova, P. Mokreva and L. Terlemezyan, *Polymer*, 1993, **34**, 2438-2439.
75. L. Duic and Z. Mandic, *Journal of Electroanalytical Chemistry*, 1992, **335**, 207-221.

76. S.-J. Choi and S.-M. Park, *Journal of the Electrochemical Society*, 2002, **149**, E26-E34.
77. J. Stejskal, P. Kratochvil and A. D. Jenkins, *Elsevier Science Ltd*, 1996, **37**, 367.
78. P. C. Innis, J. Mazurkiewicz, T. Nguyen, G. G. Wallace and D. MacFarlane, *Current Applied Physics*, 2004, **4**, 389-393.
79. T. A. Skotheim and J. Reynolds, *Conjugated Polymers: Theory, Synthesis, Properties, and Characterization*, CRC Press, 2006.
80. F. Beguin and E. Frackowiak, *Supercapacitors: Materials, Systems and Applications*, Wiley-VCH Verlag GmbH & Co., 2013.
81. A. Virya and K. Lian, *Electrochemistry Communications*, 2017, **74**, 33-37.
82. R. Kötz and M. Carlen, *Electrochimica Acta*, 2000, **45**, 2483-2498.
83. V. S. Bagotsky, A. M. Skundin and Y. M. Volkovich, *Electrochemical Power Sources: Batteries, Fuel Cells, and Supercapacitors*, Wiley, 2015.
84. K. S. Ryu, K. M. Kim, N.-G. Park, Y. J. Park and S. H. Chang, *Journal of Power Sources*, 2002, **103**, 305-309.
85. A. Yu, V. Chabot and J. Zhang, *Electrochemical Supercapacitors for Energy Storage and Delivery: Fundamentals and Applications*, CRC Press Taylor & Francis, 2013.
86. C. A. Vincent and B. Scrosati, *Modern Batteries: An Introduction to Electrochemical Power Sources*, Elsevier Science, 1997.
87. M. R. Palacin, *Chemical Society Reviews*, 2009, **38**, 2565-2575.
88. M. Winter and R. J. Brodd, *Chemical Reviews*, 2004, **104**, 4245-4270.
89. M. Silberberg, *Chemistry: The Molecular Nature of Matter and Change*, McGraw-Hill Companies, Incorporated, 2008.
90. P. Van den Bossche, F. Vergels, J. Van Mierlo, J. Matheys and W. Van Autenboer, *Journal of Power Sources*, 2006, **162**, 913-919.
91. H. A. Kiehne, *Battery Technology Handbook*, Taylor & Francis, 2003.
92. F. Beck and P. Ruetschi, *Electrochimica Acta*, 2000, **45**, 2467-2482.
93. C. H. Hamann, A. Hamnett and W. Vielstich, *Electrochemistry*, Wiley, 2007.
94. J. Larminie and J. Lowry, *Electric Vehicle Technology Explained*, Wiley, 2012.
95. A. M. Bernardes, D. C. R. Espinosa and J. A. S. Tenório, *Journal of Power Sources*, 2004, **130**, 291-298.
96. A. P. Abbott, K. S. Ryder and U. König, *Transactions of the Institute of Metal Finishing*, 2008, **86**, 196-204.

97. M. Freemantle, *An Introduction to Ionic Liquids*, Royal Society of Chemistry, Cambridge, UK, 2010.
98. S. Keskin, D. Kayrak-Talay, U. Akman and Ö. Hortaçsu, *The Journal of Supercritical Fluids*, 2007, **43**, 150-180.
99. P. Wasserscheid and T. Welton, *Ionic Liquids in Synthesis*, Wiley, 2008.
100. J. Zhang and A. M. Bond, *Analyst*, 2005, **130**, 1132-1147.
101. M. Deetlefs, K. R. Seddon and M. Shara, *Physical Chemistry Chemical Physics*, 2006, **8**, 642-649.
102. R. Renner, *Environmental Science & Technology*, 2001, **35**, 410A-413A.
103. N. V. Plechkova and K. R. Seddon, *Chemical Society Reviews*, 2008, **37**, 123-150.
104. J. P. Hallett and T. Welton, *Chemical Reviews*, 2011, **111**, 3508-3576.
105. K. Marsh, J. Boxall and R. Lichtenthaler, *Fluid Phase Equilibria*, 2004, **219**, 93-98.
106. A. P. Abbott, G. Capper, D. L. Davies, R. K. Rasheed and V. Tambyrajah, *Chemical Communications*, 2003, 70-71.
107. E. L. Smith, A. P. Abbott and K. S. Ryder, *Chemical Reviews*, 2014, **114**, 11060-11082.
108. Q. Zhang, K. De Oliveira Vigier, S. Royer and F. Jerome, *Chemical Society Review*, 2012, **41**, 7108-7146.
109. A. P. Abbott, G. Capper, D. L. Davies, H. L. Munro, R. K. Rasheed and V. Tambyrajah, *Chemical Communications*, 2001, 2010-2011.
110. A. P. Abbott, J. C. Barron, K. S. Ryder and D. Wilson, *Chem. Eur. J.*, 2007, **13**, 6495-6501.
111. M. Francisco, A. van den Bruinhorst and M. C. Kroon, *Angewandte Chemie*, 2013, **52**, 3074-3085.
112. A. P. Abbott, D. Boothby, G. Capper, D. L. Davies and R. K. Rasheed, *American Chemical Society*, 2004, **129**, 9142-9147.
113. A. P. Abbott, G. Capper, D. L. Davies and R. Rasheed, *Inorganic Chemistry*, 2004, **43**, 3447-3452.
114. K. E. ttaib, *PhD Theses, University of Leicester*, 2011
115. A. Paiva, R. Craveiro, I. Aroso, M. Martins, R. L. Reis and A. R. C. Duarte, *ACS Sustainable Chemistry & Engineering*, 2014, **2**, 1063-1071.
116. S. L. Perkins, P. Painter and C. M. Colina, *The Journal Physical Chemistry B*, 2013, **117**, 10250-10260.

## Chapter 2: General Theory of Methodology

### Contents

<b>2.1</b>	<b>Introduction.....</b>	<b>32</b>
<b>2.2</b>	<b>Concepts of Electrochemistry .....</b>	<b>32</b>
2.2.1	Mass Transport .....	32
<b>2.3</b>	<b>Electrochemical Techniques .....</b>	<b>35</b>
2.3.1	Cyclic Voltammetry .....	35
2.3.2	Impedance Analysis.....	39
<b>2.4</b>	<b>Non-Electrochemical Techniques.....</b>	<b>41</b>
2.4.1	The Crystal Impedance Technique.....	41
2.4.2	Electrochemical Quartz Crystal Microbalance.....	47
<b>2.5</b>	<b>Surface Imaging Techniques.....</b>	<b>49</b>
2.5.1	Scanning Electron Microscopy.....	49
2.5.2	Atomic Force Microscopy .....	50
<b>2.6</b>	<b>Spectroscopic Techniques .....</b>	<b>52</b>
2.6.1	Infrared Spectroscopy.....	52
<b>2.4</b>	<b>References.....</b>	<b>53</b>

## 2.1 Introduction

This chapter will explain in detail the principles and general theory behind the electrochemical techniques that have been used. This involves the fundamentals of cyclic voltammetry, the electrochemical quartz crystal microbalance that was used for the deposition of polymer films, and identification of the mass transport and charge transfer processes through the film during the redox process. In addition, surface techniques that were used to characterise the morphology of the polymer film will be also reported.

## 2.2 Concepts of Electrochemistry

Electrochemistry deals with the formation of electrical charge resulting from redox reactions between electrodes and reactant molecules present in the electrolyte when an electrical current/potential is applied.<sup>1</sup> In general, the redox process in electrochemical reactions at the electrode surface can be represented by the following reaction:



where *Ox* and *Red* indicate the oxidised and reduced forms of the electroactive sites in the film, respectively. By applying a potential to a conductive modified electrode, the current value can be identified using the kinetics of the reaction (2.1). Many interfaces occur in polymer-modified electrodes, such as the electron transfer interface between the electrode and polymer, ion/solvent transport across the interface between the polymer and electrolyte, and the rate of charge transfer at the interface of the polymer film.<sup>2</sup>

### 2.2.1 Mass Transport

Overall, in conventional electrodes, there are three steps describing the exchange of mobile species between the electrode and bulk solution during the oxidation and reduction process, as shown in **Figure 2.1**. The initial step includes the reactant molecule being conveyed from the bulk solution to the electrode surface. The second step involves the exchange of electrons that occurs on the electrode surface, leading to the production of reaction products, while in the third step the products are detached from the electrode surface. All these processes (steps 1 and 3) are called “mass transport” and are essential for an electrochemical reaction to proceed. Basically, the

rate of an electrochemical reaction is dependent on the slowest step, either the mass transport (steps 1 and 3) or the kinetics of electron exchange (step 2). With regard to fast electron transfer, the electrochemical reaction can be fast, mass transport is the rate limiting. However, when the rate of electron transfer is slow, the electrochemical reaction is also slow. Here, the study of electron kinetics becomes far more significant than the observation of mass transport in order to explain our data successfully. There are three processes that explain the transportation of the mobile species from bulk solution to the electrode surface, depending on experimental conditions.<sup>1,3</sup>

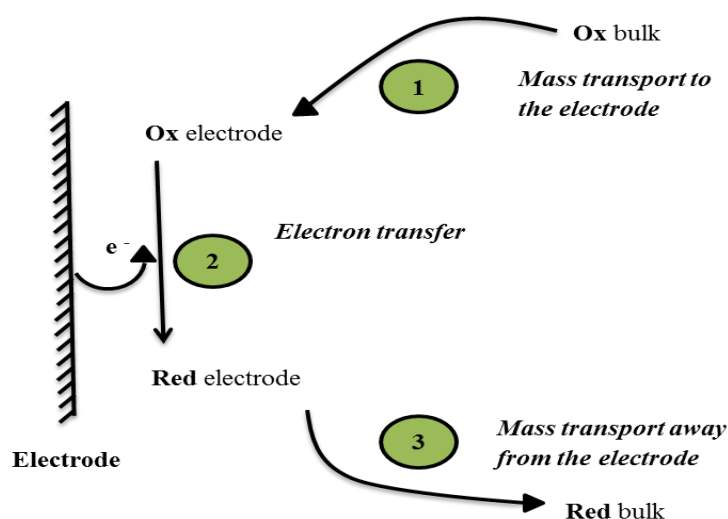


**Figure 2.1:** Redox conversion occurs during electrochemical reactions, explaining electron transfer and mass transport.<sup>4</sup>

### 2.2.1.1 Diffusion

The motion of a chemical species (ions or molecules) occurs spontaneously because of a concentration gradient. The species is transported from a region of high concentration to one of low concentration until the species becomes evenly distributed throughout the system. Indeed, the speed of transport in this process can be quantified by employing Fick's general laws (first and/or second) or the Cottrell equation by relying on a specific electrochemical technique. Fick's first law describes that the rate of diffusion is proportional to the concentration gradient at a certain region, as shown in equation 2.2.

$$j = -D_B \frac{\partial[B]}{\partial x} \quad 2.2$$

where  $j$  is the number of moles of the diffusional flux for a species  $B$  per unit time,  $D_B$  is the diffusion coefficient ( $\text{cm}^2 \text{s}^{-1}$ ) and  $[B]$  is the concentration of  $B$  ( $\text{mol cm}^{-3}$ ).

Fick's second law (equation 2.3) shows how the concentration of electroactive substances changes with time.<sup>1</sup>

$$\frac{\partial[B]}{\partial x} = D_B \frac{\partial^2[B]}{\partial x^2} \quad 2.3$$

In the case of the Cottrell equation, the diffusion can be expressed as shown in equation 2.4, which describes that the current response is directly proportional to time.

$$i(t) = \frac{nFAD^{1/2}C_\infty}{(\pi t)^{1/2}} \quad 2.4$$

where  $i$  is current in Amperes,  $n$  is the number of electrons,  $F$  is Faraday constant ( $96485 \text{ C mol}^{-1}$ ),  $A$  is area of the electrode in  $\text{cm}^2$ ,  $C_\infty$  is the concentration of the analyte,  $D$  is the diffusion coefficient for species in  $\text{cm}^2 \text{s}^{-1}$  and  $t$  is time in seconds.<sup>5,6</sup>

### 2.2.1.2 Migration

In migration, ions move through a solution due to the influence of an electric field (a gradient of electrical potential), at a rate supported by the concentration of the background electrolyte. This process generally occurs in the vicinity of the electrode/electrolyte interface and is enhanced as the electrode potential increases, as well as by increases in ionic conductivity. In most electrochemical reactions, the migration process can be affected by using a large excess of a particular size of ion, ionic charge and the viscosity of the electrolyte.

### 2.2.1.3 Convection

Convection involves the movement of species from the solution or electrode by a mechanical act or by hydrodynamic transport. Usually, there are two types of convection. The first is called natural convection, where chemical species are transported under the influence of thermal and/or density variations to or from an electrode. The second is called forced convection, and this can be caused by mechanical stirring of solution, shaking the vessel or rotating the electrode. Over a short

experimental timescale and/or where the vessel is unstirred, the influence of convection is very small, so can generally be ignored.<sup>1-3,5</sup>

## **2.3 Electrochemical Techniques**

Electrochemical techniques are a popular method for characterising conducting polymers electrodeposited in various media. These techniques are useful for studying the growth and decay mechanisms of films during electropolymerisation, as well as interfacial properties of electrodes/films and films/solutions when probing a system.<sup>7,8</sup> There are a number of important methods utilised for characterising electroactive polymers, such as galvanostatic or potentiostatic, and these are used in combination with other techniques such as the Quartz Crystal Microbalance (QCM). In the following sections, the basic principles of the techniques used for polymer deposition and characterisation will be described in greater detail.

### **2.3.1 Cyclic Voltammetry**

Cyclic Voltammetry (CV) is considered one of the most important methods in the study and description of redox processes, and gives both qualitative and quantitative information. This technique can give substantial information on the redox potentials of electroactive materials and on surface species. Basically, the technique relies on recording the current ( $I$  – units Amperes) with the potential ( $E$  – units Volts) of the working electrode, giving information in the form of a “voltammogram”, which studies the relationship between potential versus current. A standard electrochemical cell involves three electrodes immersed in an electrolyte. Firstly, the Working Electrode (WE) is the place in which the redox process occurs. Secondly, the Counter Electrode (CE) is used to supply the second dipole in order to allow the current to pass between the WE and CE, as well as to confirm that no current passes through the final electrode, the Reference Electrode (RE), which acts to govern the potential applied.<sup>9</sup>

In cyclic voltammetry, a triangular waveform is linearly constructed by applying an electrode potential with respect to time, as shown in **Figure 2.2a**. Usually, the plot occurs during the switching potentials, where the working electrode potential sweeps

between two limits, from  $E1$  to  $E2$ ; the scan direction of working electrode potential is then reversed to the starting point,  $E1$ . Furthermore, the currents of the oxidation and reduction peaks are measured in the potentiostat as a result of the applied potential between the WE and CE.<sup>5</sup> Depending upon the required results, a single, full cycle or multiple cycles can be employed. Thus the scan rate ( $V s^{-1}$ ) controls the experimental timescale.<sup>10-12</sup> The driving force for electrochemical reactions can be supplied from the potential (equation 2.5).

$$\Delta G = -nFE \quad 2.5$$

The characterisation of the electrochemical responses in a cyclic voltammogram can be identified depending on the system (i.e. reversible, irreversible and quasi-reversible). **Figure 2.2b** illustrates a cyclic voltammogram for a reversible system. In the beginning, no current is developed due to applied potential insufficient to induce electron transfer. At  $E = -0.1$  V, current starts to develop, which arises from the oxidation reaction at the electrode (faradaic current). Then, the scan is rapidly increased in current until the oxidant concentration gets smaller and smaller, ultimately causing the peak maximum. Following that, mass transfer to the electrode from the electrolyte is relatively same in comparison with the rate of consumption, and here the current response in the voltammogram is controlled by diffusion (concentration gradient). Analogous behaviour in the opposite direction occurred due to reduced species (*Red*) at the electrode surface. In general, many parameters affect the current and the kinetics of the electrode reaction, such as:

- 1- The speed of electron transfer across the electrode surface
- 2- The rate of mass transport across the electrode/solution interface
- 3- The kinetic type of the chemical reaction (homogenous/ heterogeneous rate constant)
- 4- The nature of the interaction on the surface, for example electrodeposition, adsorption, or desorption<sup>9, 13</sup>

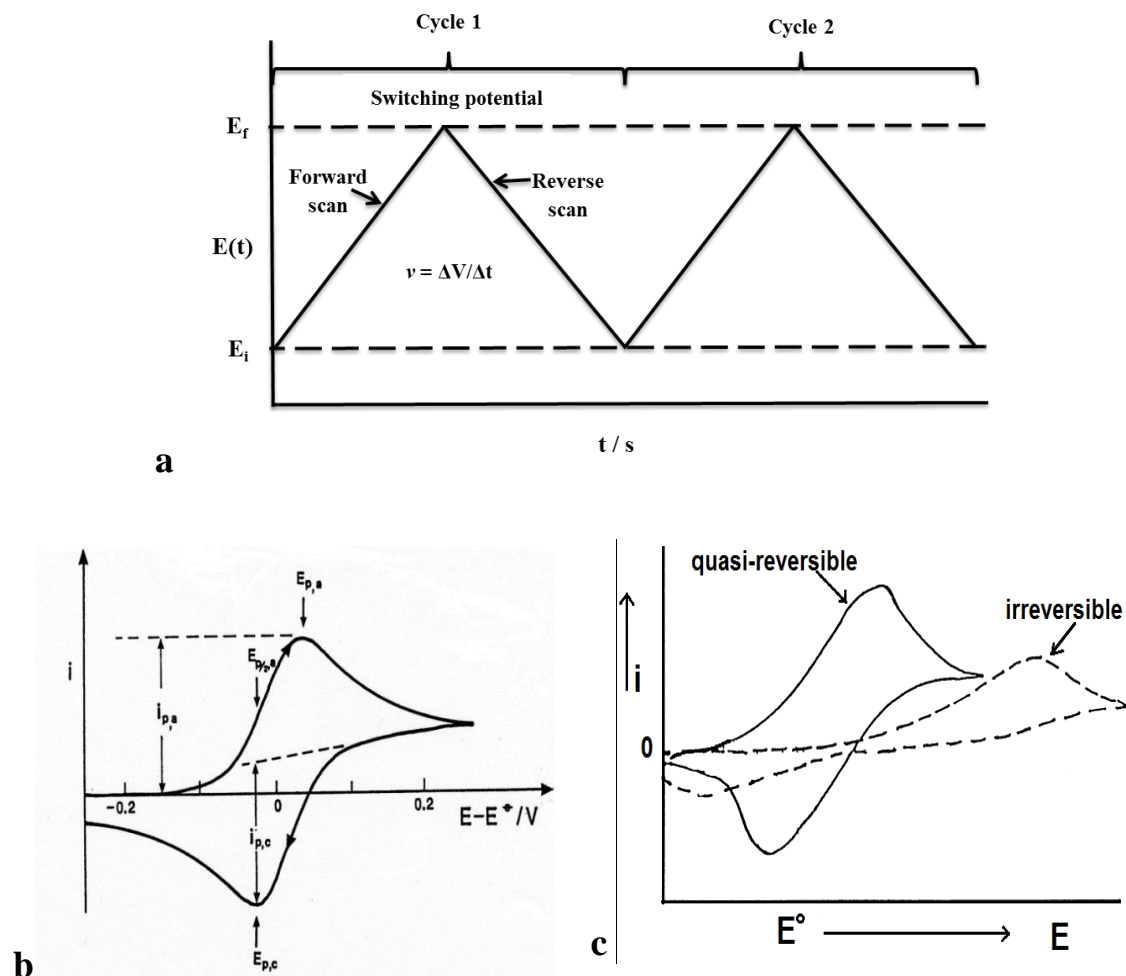


**Figure 2.2:** Schematic illustrating CV curves. a) potential against time in a CV experiment; b) cyclic voltammogram for a reversible reaction (diffusion mechanism); c) the behaviour of the voltammogram for irreversible and quasi-reversible systems.<sup>5</sup>

In reversible systems (diffusion controlled), the current peak increases directly with increasing concentration, and thus is proportional to the square root of the scan rate ( $i_p \propto v^{1/2}$ ). The ratio of the redox couple peak currents is unity ( $-i_{p,c}/i_{p,a} = 1$ ), as illustrated in **Figure 2.2b**. The quantity of peak current for the reversible reaction (at 25 °C) can be determined by employing the Randles-Sevcik equation:<sup>5, 14</sup>

$$i_p = 2.69 * 10^5 n^{3/2} A C D^{1/2} v^{1/2} \quad 2.6$$

where  $n$  is the number of electrons,  $A$  is the area of substrate (in  $\text{cm}^2$ ),  $D$  is the diffusion coefficient of the redox species (in  $\text{cm}^2 \text{s}^{-1}$ ),  $C$  is the concentration of the redox species in solution (in  $\text{mol cm}^{-3}$ ), and  $v$  is the scan rate (experimental timescale). The position

of the potential voltage for the redox process,  $E^\circ$ , between the oxidation and reduction current peaks is:

$$E^\circ = \frac{E_{p,a} + E_{p,c}}{2} \quad 2.7$$

whereas the separation between the peak potentials,  $\Delta E_p$ , is given by:

$$\Delta E_p = E_{p,a} - E_{p,c} = \frac{0.059}{n} V \quad 2.8$$

Furthermore, the peak potential for the forward and reverse scans is not dependent on scan rate, while the quantities of the peak currents for both scans rely on the sweep rate. The electrochemical reversible systems are governed by the diffusional control mechanism in the case of the rate of electron transfer being faster than mass transport of the redox species, as well as the redox system maintaining equilibrium during the potential scan. The concentration of the reactants and the resultants at the electrode surface can be calculated using the Nernst equation:

$$E = E^\circ + \frac{RT}{nF} \ln \frac{[Ox]^\circ}{[Red]^\circ} \quad 2.9$$

where  $E^\circ$  is standard electrode potential,  $[Ox]^\circ$  and  $[Red]^\circ$  are the formal concentrations of oxidised and reduced materials, respectively,  $n$  is the number of electrons for the electroactive species in redox reaction, and  $F$  is the Faraday Constant.<sup>3</sup>

In the irreversible system, the Nernst equation cannot be used due to the rate of the electron transfer reaction being slow relative to the mass transport reaction (in other words, there is not enough time for mass transport to maintain a rate compatible with the electrode dynamics). The peak current  $i_p$  (equation 2.10) remains proportional to concentration of species in the bulk and the square root of the scan rate ( $i_p \propto v^{1/2}$ ). However, peak potential shift becomes large with increasing scan rate (hysteresis).

$$i_p = 2.99 \times 10^5 n (\alpha n_a)^{\frac{1}{2}} A C D^{\frac{1}{2}} v^{\frac{1}{2}} \quad 2.10$$

In the CV, the redox-active species is in solution, whereas it's fixed to the electrode surface. The integral of the current under the peak as a function of the time is used to determine the total charge passed, which represents to the amount of electroactive species formed. From the charge value, the surface coverage ( $\Gamma$ ) of the polymer (or

deposited product) can be determined by the application of Faraday's law,<sup>5, 15</sup> via equation (2.11):

$$\Gamma = \frac{Q}{nFA} \quad 2.11$$

where  $Q$  is the quantity of charge passed through the redox reaction and  $A$  is the electrode area.

There is another type of electrochemical reaction, termed quasi-reversible, which was identified and described for the first time by Matsuda and Ayabe.<sup>16</sup> In this system, the current is governed by the rate of electron transfer and mass transport, which is reversible for slow scan rates, and shows irreversible behaviour in the case of fast scan rates.<sup>5</sup> **Figure 2.2c** shows the behaviour of the irreversible and quasi-reversible electrochemical systems discussed above.

### **2.3.2 Impedance Analysis**

Electrochemical Impedance Spectroscopy (EIS) is a significant technique used to elucidate the electrical properties of materials.<sup>17</sup> This technique is based on the application of a sinusoidal voltage of small amplitude (~5 mV) to the cell at various frequencies. This process leads to recording the AC current response and the result of impedance ( $Z$ ) and phase angle data are supplied. Measurement of the ratio of AC voltage to AC current gives a frequency-dependent impedance.<sup>18, 19</sup> The timeframe of the experiment can be controlled by choosing a range of frequencies of sinusoidal perturbation, and hence the electrochemical and physical properties can be varied by controlling the angular frequency,  $\omega$  (radians/s) of the system. Using EIS allows analysis of the mechanisms by which the electrode surface deals with contributions from kinetic, diffusion, double layer, homogenous/heterogeneous reactions, the polymer/electrode interface and the polymer/solution interface. Thus, the redox couple concentrations at the surface during the  $E_{ac}$  perturbation to an electrochemical system can be maintained by applying a certain  $E_{dc}$  in EIS. As a result of the characterisations above, a wide range of important applications becomes available, in particular studies such as the rate of charge transfer and mass transport processes obtained in conducting polymer/metal, corrosion, the interactions between liquid and liquid, membranes, conductivity, ionic solids and solid electrolytes.<sup>6, 20, 21</sup>

EIS measurements can be performed by lock-in amplifiers or frequency response analysers. In this technique, resistors can be connected with capacitors as parallel or series models. The data obtained for electrochemical processes at the electrode surface are characterised by Randle's equivalent circuit<sup>1, 22</sup> (**Figure 2.3a**), which arises from amplitude change and/or phase shift. Consequently, useful information can be acquired from EIS, such as the resistance of the solution,  $R_s$ , the resistance to charge transfer,  $R_{ct}$ , double layer capacitance,  $C_{dl}$ , angular frequency,  $\omega$ , and the Warburg impedance,  $Z_w$ . These parameters can be evaluated via two well-known formats: the Nyquist plot and Bode plot. The Nyquist plot requires plotting imaginary components of the impedance ( $Z''$ ) versus the real components of the impedance ( $Z'$ ), whilst, the Bode plot is found as the plot of  $|Z|$  vs.  $\log \omega$ . These components can be mathematically represented through the following equations:<sup>18</sup>

$$Z' = R_s + \frac{R_{ct}}{1 + \omega^2 R_{ct}^2 C_{dl}^2} \quad 2.12$$

and

$$Z'' = \frac{R_{ct}^2 C_{dl} \omega}{1 + \omega^2 R_{ct}^2 C_{dl}^2} \quad 2.13$$

From **Figure 2.3b**, the resistance of the solution can be found at higher frequency values when  $Z''$  is zero, whilst the resistance to charge transfer ( $R_{ct}$ ) can be calculated from the diameter of the semicircle produced by exciting from high frequency to low frequency ranges. The maximum value of  $Z''$  that can be used to determine the capacitance of the double layer ( $C_{dl}$ ) is shown in equation 2.14.

$$C_{dl} = \frac{1}{\omega_{max} R_{ct}} \quad 2.14$$

The diffusional feature of the system in the very low frequency range can be evaluated from the slope (straight line) of the Warburg impedance ( $Z_w$ ), which occurs due to mass transport (i.e. diffusion control) of species.

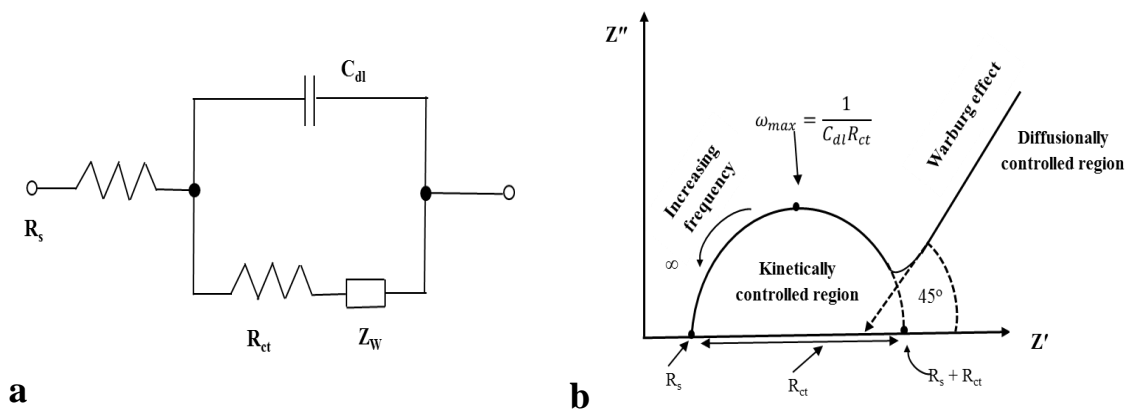


**Figure 2.3:** a) The Randle's circuit; and b) typical Nyquist plot.

## 2.4 Non-Electrochemical Techniques

### 2.4.1 The Crystal Impedance Technique

The Thickness Shear Mode (TSM) resonator, also called a quartz crystal microbalance, represents one of the most important tools used to investigate gravimetric sensors and/or the physical properties of a material.<sup>23-27</sup> This technique is based on piezoelectric resonators that operate in an electric field.<sup>28</sup> It is crucial to understand the basic concepts of this technique to further understand some of the aims considered in this project.

#### 2.4.1.1 Piezoelectric Quartz Crystal

The origin of the word piezoelectric is *piezein* which comes from the Greek, meaning “to press”. It was discovered by Jacques and Pierre Curie in 1880 and, as a result, the production of an electrical potential in materials when a mechanical stress is applied to the quartz crystal surface is named the “direct piezoelectric effect”.<sup>29</sup> Production of charge in a crystal when a mechanical stress is applied is attributed to a shift of dipoles as a consequence of displacement of atoms.<sup>30</sup> By contrast, applying an electrical potential to one of the faces of the crystal creates a corresponding mechanical distortion, in an effect known as the “converse piezoelectric effect”,<sup>31</sup> as shown in **Figure 2.4**. The piezoelectric effect is only found in acentric forms of asymmetric arrangements of atoms in crystalline materials.

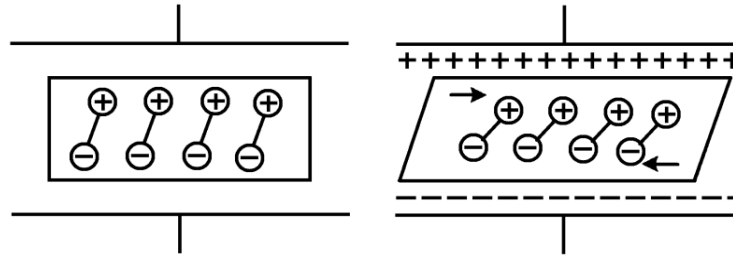


**Figure 2.4:** Schematic illustration the converse piezoelectric influence.

Based on the cutting angle, which relies on the crystallographic axis of a single crystal, there are many models of crystals that have been produced to show piezoelectric behaviour, such as quartz, tourmaline, barium/lead titanate, rochelle salts and lead zirconate. Among these models, *AT*-cut quartz, with the a cleavage angle of  $35^{\circ}15'$ , is the most common and significant material employed to date because of its low cost, high stability over a range of frequencies, its abundance and zero temperature coefficient.<sup>30</sup> In this project, we use a quartz crystal as an electrochemical microbalance, and in the following sections the fundamentals of this technique will be reported.

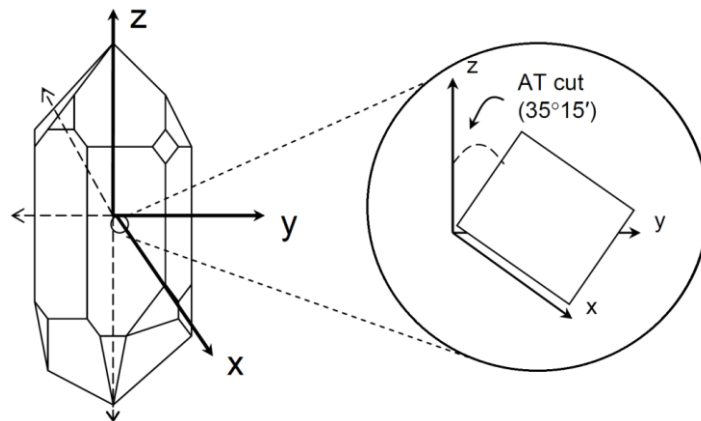


**Figure 2.5:** Schematic diagram showing the *AT*-cut  $\alpha$ -quartz crystal.<sup>4</sup>

#### 2.4.1.2 Quartz Crystal Microbalance

The Quartz Crystal Microbalance (QCM) is a frequency control tool, which relies on the piezoelectric characterisation of the *AT*-cut  $\alpha$ -quartz crystal. This technique involves an oscillator circuit and a crystal, where the piezoelectric crystal consists of two metal electrodes placed on opposite sides of a thin disc of crystal wafer, as shown in **Figure 2.6**. The mechanical vibrations of the quartz crystal are attributed to TSM resonators, which are characterised by resonant frequency and amplitude responses. Mechanical

oscillations are generated within the crystal lattice due to the fact that an alternating potential is applied, leading to a shear distortion of the crystal due to its piezoelectric properties. The thickness-shear mode and cut of the quartz shape are sensitive to deposited mass, which affects the crystal's fundamental vibrational frequency. The most commonly employed crystals used in QCM experiments have fundamental frequencies of 5 and 10 MHz (for *AT*-cut crystals).

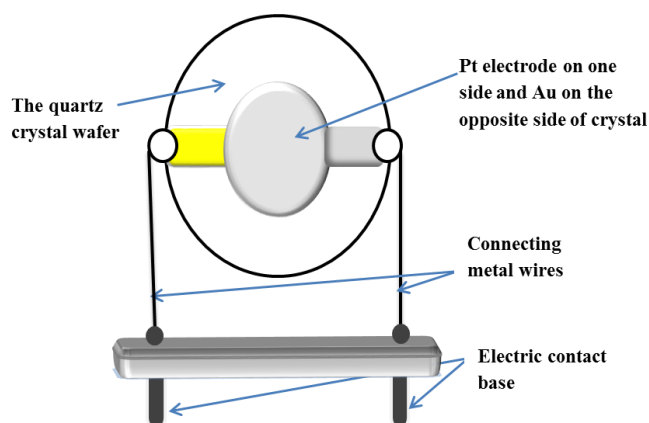


**Figure 2.6:** The quartz crystal thickness-shear mode resonator consists of a platinum electrode on one side and a gold electrode on the other side of the quartz crystal.

The excitation of the crystal resonance by application of an alternating voltage in contact with the electrolyte leads to an interaction where the resonator oscillates with the medium. As a consequence, the resulting mechanical properties will be transformed into electrical characteristics of the resonator.<sup>32</sup> The deposition of species can be characterised by monitoring the resonant frequency of a quartz crystal oscillator. The decrease/increase of the resonant frequency depends on the addition/subtraction of mass, and this process involves the shifting of the fundamental resonant frequency from its original value due to a quantitative effect (i.e. mass deposited).

#### **2.4.1.3 Sauerbrey Equation**

The relationship between mass and frequency response was first investigated by Lord Rayleigh in 1945, who found that the mass change is inversely proportional to its change in resonant frequency changes, as found through the change in fundamental vibrational frequency of quartz.<sup>33</sup> However, the true relationship between the quantitative mass and the resonant frequency was given by Sauerbrey in 1959.<sup>34</sup> The resonant frequency ( $f$ ) of a crystal is a standing wave, which is constituted within the

crystal. The thickness of the acoustic wave in quartz crystal is affected by acoustic wavelength, as can be seen from equation 2.15 and **Figure 2.7**.

$$h_q = \frac{\lambda_q}{2} \quad 2.15$$

Here,  $h_q$  is the quartz thickness and  $\lambda_q$  is the acoustic wavelength. The shear wave velocity,  $v$ , can be described via the frequency,  $f$ , as given in equation 2.16:

$$v = f\lambda \quad 2.16$$

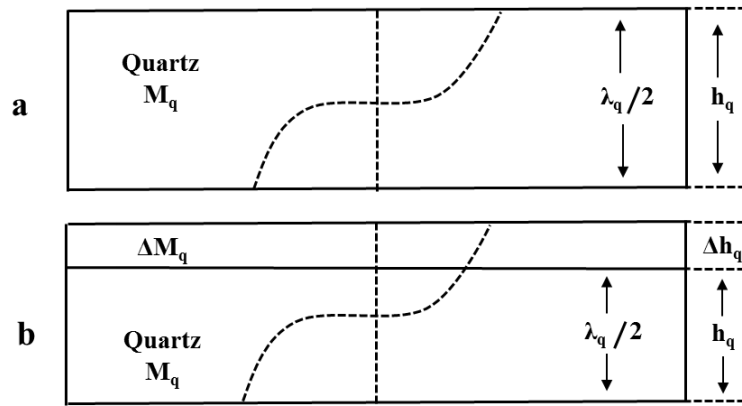


**Figure 2.7:** Schematic representation of a thickness shear mode resonator. a) The thickness of the quartz plate,  $h_q$ , is related to acoustic wavelength,  $\lambda_q$ ; b) an increase in the thickness of the quartz,  $\Delta h_q$ , results in an increase in the wavelength,  $\Delta \lambda_q$ .

The wave velocity ( $v_q$ ) of an oscillating quartz crystal can be obtained by substituting equation 2.15 into 2.16 to give equation 2.17.

$$f_q = \frac{v_q}{2h_q} \quad 2.17$$

The thickness of the quartz crystal is increased as a result of the addition/ deposition of mass on the crystal surface, which in turn results in an increase in wavelength, and hence the resonant frequency reduces (frequency change,  $\Delta f$ ), as shown in **Figure 2.7**.

Mathematically, this relationship can be defined by the following equation:

$$\frac{\Delta f_q}{f_q} = -\frac{\Delta M_q}{M_q} \quad 2.18$$

where  $\Delta M_q$  and  $M_q$  are the increase in mass of the quartz crystal due to deposition and the original mass of the quartz crystal, respectively. The negative sign represents the reverse directions of change between the mass (thickness) and frequency changes. Assuming that the mass deposition is evenly distributed across the quartz crystal, equation (2.18) can be converted into equation (2.19) using areal mass density, with a corresponding mass per unit area:

$$\frac{\Delta f_q}{f_q} = -\frac{m_f}{m_q} \quad 2.19$$

where  $m_f$  and  $m_q$  are the areal mass density of the homogenous mass deposition on the crystal and the mass of the quartz crystal, respectively. The areal mass density is equivalent to the density ( $\rho_q$ ) and thickness ( $h_q$ ) of the added mass/quartz crystal.

$$m_q = h_q \rho_q \quad 2.20$$

Substituting equation 2.17 into equation 2.20 produces equation 2.21:

$$m_q = \frac{v_q \rho_q}{2f_q} \quad 2.21$$

By combining equation 2.21 and equation 2.19 one can write the following:

$$m_f = -\Delta f_q \frac{v_q \rho_q}{2f_q^2} \quad 2.22$$

Equation 2.22 can be described in a more general form, equation 2.23, according to Sauerbrey assumption that any tiny, rigid, homogeneously distributed mass deposition on the surface of a quartz crystal may be treated as a change in the crystal mass itself:

$$\Delta m = -\Delta f_q \frac{v_q \rho_q}{2f_q^2} \quad 2.23$$

where  $\rho_q$  is  $2.65 \text{ g cm}^{-3}$  and  $v_q$  is  $3.34 \times 10^5 \text{ cm s}^{-1}$  and are, respectively, the density and shear wave velocity within the quartz crystal,  $\Delta f_q$  is the observed resonant frequency change,  $f_q$  is the fundamental resonant frequency, and  $\Delta m$  is the change of surface mass density.<sup>35, 36</sup> The coefficient between the change of the resonant frequency ( $\Delta f$ ) and the change of mass of the surface layer ( $\Delta m$ ) (within  $\pm 2 \%$ ) for a 10 MHz *AT*-cut quartz

crystal shows that a 1 Hz change corresponds to a mass change of ca. 1.1 ng for the crystal used in the work presented in this thesis.<sup>37</sup>

#### 2.4.1.4 The Viscosity – Frequency Relationship

Initially, the QCM was utilised as a gravimetric device to determine the mass of materials in vacuum or gaseous systems. However, a number of investigations in the early 1980's observed that the QCM could also be used for liquid materials such as liquid chromatography<sup>38</sup> and the characterisation of organic liquids.<sup>39</sup> **Figure 2.8** shows one face of an AT-cut crystal when immersed in liquid.

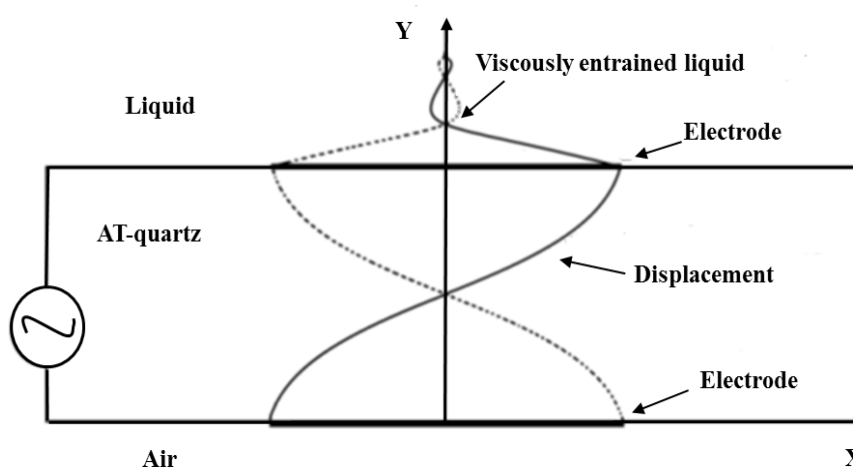


**Figure 2.8:** Vibrations of an At-cut quartz crystal when an alternating electric field is applied.

When a quartz crystal electrode contacts a liquid, the operation of QCM is unlike that in air because the resonator material will be viscous and it is the effective mass coupling of a viscously entrained layer to the crystal that causes the frequency shift and damping of the crystal. Basically, the physical properties of liquids such as viscosity<sup>24, 40</sup> and density<sup>25</sup> can be determined by QCM as functions of the decrease of the resonant frequency of the crystal during its oscillation when contacting the liquid. In this case, the Sauerbrey equation has to be modified, as achieved by Kanazawa and Gordon<sup>41</sup> in 1985 to allow detection of a sensitive mass in the liquid environment, given in equation (2.24):

$$\Delta f = f_0^{3/2} \left[ \frac{\eta_L \rho_L}{\pi \mu_q \rho_q} \right]^{1/2} \quad 2.24$$

where  $\eta_L$  and  $\rho_L$  are the viscosity and density of the fluid, respectively.  $\mu_q$  and  $\rho_q$  are the shear modulus and density of quartz, with values of  $2.947 \times 10^{11} \text{ g cm}^{-1} \text{ s}^{-2}$  and  $2.65 \text{ g cm}^{-3}$ , respectively.

#### **2.4.2 Electrochemical Quartz Crystal Microbalance**

QCM enables the *in situ* measurement of mass changes of films deposited on the electrode surface, as well as the “fluid” and viscoelastic properties of polymer films. This technique can be connected with versatile electrochemical techniques, which are generally referred to as Electrochemical Quartz Crystal Microbalance (EQCM) techniques; for example, cyclic voltammetry, potentiostatic, galvanostatic, chronoamperometry, and so forth. These techniques can detect very small changes in mass and density with high accuracy, even changes at the surface of an electrified interface as small as 1ng. Therefore, in this case, it is termed an Electrochemical Quartz Crystal Nanobalance (EQCN).<sup>15</sup> The outcome of the use of this technique is that of various data such as potential, current, and charge at the surface of working electrode, which are analysed simultaneously with the acquisition of frequency and resistance variations. In these investigations, the working electrode is one of the two crystal surfaces which has to be presented to the liquid medium in order to deposit the conductive polymer film on it. Here, the change in the resonant frequency (a reduction) does not only rely on the increased mass of material that is precipitated on the surface of crystal electrode but, also, on the density and viscosity of the contacting fluid.<sup>41-44</sup>

The EQCM technique is widely using for polymer-modified electrodes as an *in situ* interfacial probe to monitor gravimetric and/or viscoelastic changes of the surface-attached species during redox switching. This is dependent on the properties of species deposited on the crystal electrode, and the composition and viscosity of the bathing electrolyte. The resonance frequency of the quartz crystal is reduced due to increased mass on the crystal surface, and vice versa.<sup>27, 42, 45</sup> As a result, the ionic and the solvent composition can be determined for thin polymer films through the associated mass changes altering the resonant frequency ( $\Delta f$ ) of the quartz crystal. Such changes can also be identified *in situ*, e.g., the amount of charge exchange, the ingress/egress of counter ions, the species/solvent transfer required to maintain electroneutral conditions during the doping/dedoping process of the polymer/solution interface.<sup>46-48</sup>

### 2.4.2.1 Crystal Admittance Analysis

In order to study the composition of the polymer film (the quantity and the movement of ions /solvent during the redox process) using EQCM as gravimetric analysis (i.e. whether the Sauerbrey equation is applicable), the film deposited on the surface of the electrode should be rigid. Crystal impedance analysis is an important technique employed to characterise the rigid and non-rigid (viscoelastic behaviour) of polymer films during their deposition on crystal electrodes or redox cycling in monomer-free electrolyte.<sup>30, 49-51</sup> This includes measuring the admittance of the polymer (which is the inverse of the impedance response under an applied voltage,  $Y = I/V$ ) as a function of frequency.

**Figure 2.9** describes the three peaks of the admittance spectra for rigid films (spectrum b) and non-rigid films (spectrum c) deposited on electrode surfaces. When the frequency of a loaded crystal is only shifted to the frequency of the original quartz crystal (unloaded crystal, spectrum a) without damping in the admittance peak (see peak b in **Figure 2.9**), the behaviour of the film is considered rigid (termed “acoustically thin”). In this case, gravimetric measurements for the polymer deposited by EQCM can be achieved using the Sauerbrey equation to determine the amount of mass change. However, if EQCM shows a shift to lower frequency when it is correlated with deposited mass and there is damping in the admittance peak (see peak c in **Figure 2.9**), the polymer behaves as a non-rigid material (termed “acoustically thick”), and here the Sauerbrey equation cannot be employed for gravimetric analysis due to energy dissipation. Furthermore, the large decline in the height of the peak admittance and broadening in width with frequency shift is not only related to the film deposited on the electrode surface, but also gives an indication as to its viscoelastic properties.<sup>49, 52</sup> Therefore, crystal impedance analysis is used to distinguish between rigid and viscoelastic behaviour of polymer films. Further information regarding this subject can be found in the literature.<sup>23, 53-55</sup>

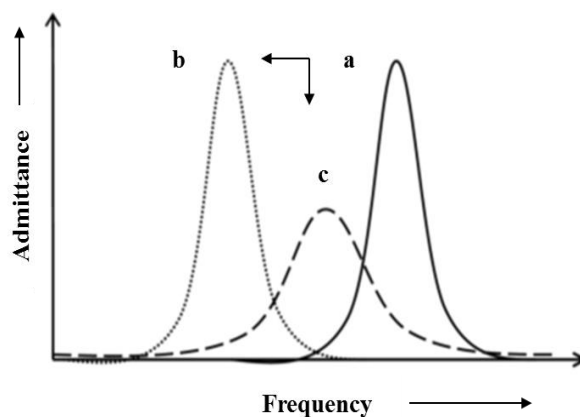


**Figure 2.9:** Schematic illustration of the admittance – frequency spectra for a) original crystal (unloaded), the bare crystal; b) thin, or rigid, mass deposition; c) thick, or non-rigid, mass deposition.

## 2.5 Surface Imaging Techniques

Imaging probe techniques are surface characterisation tools used to study morphological and topographic features of metals and polymer materials. They provide useful information through images of surfaces that help to understand mechanisms of growth, structural changes, thickness, and roughness of electroactive polymers with synthetic conditions.<sup>56-59</sup> Two important techniques are used in this project for the characterisation surface of polymer-modified electrodes: scanning electron microscopy and atomic force microscopy.

### 2.5.1 Scanning Electron Microscopy

Scanning Electron Microscopy (SEM) is one of the most important techniques used to characterise the surface morphology of polymer-modified electrodes, on the basis that this technique can examine and analyse high-resolution images of bulk models of an electrode surface carried out in high vacuum. This is based on a beam of electrons passing into the surface and interacting with the surface atoms. As a result, secondary electrons, backscattered electrons and photons are created. Thereafter, the SEM is tool able to produce information about the specimen such as quantitative data regarding the presence of individual elements, morphology, and crystalline composition.<sup>15, 60</sup>

In a typical SEM, a beam of electrons is produced by the electron gun, which are accelerated to energies between 0.1 and 30 keV (100 - 30000 electron volts). Spot sizes of the electron beam less than 10 nm across are obtained via a series of condenser lenses. The electron beam is deflected in a raster pattern in two directions (along the  $x$

and y axes) due to electron beam being passed through scanning coils. The secondary electrons, which are of low energy, are emitted off from the surface due to the electron beam interaction with any given spot on the model. After that, the secondary electrons move to the detector which, counts the number of electron interactions that is then recorded to produce an image on the computer screen. A scanning electron microscope schematic is depicted in **Figure 2.10**. SEM needs a vacuum to producing images to prevent the spread of electrons from the sample due to air particles. In addition, the materials used should to be conductive to prevent the assemblage of electrons on the surface.<sup>61, 62</sup>

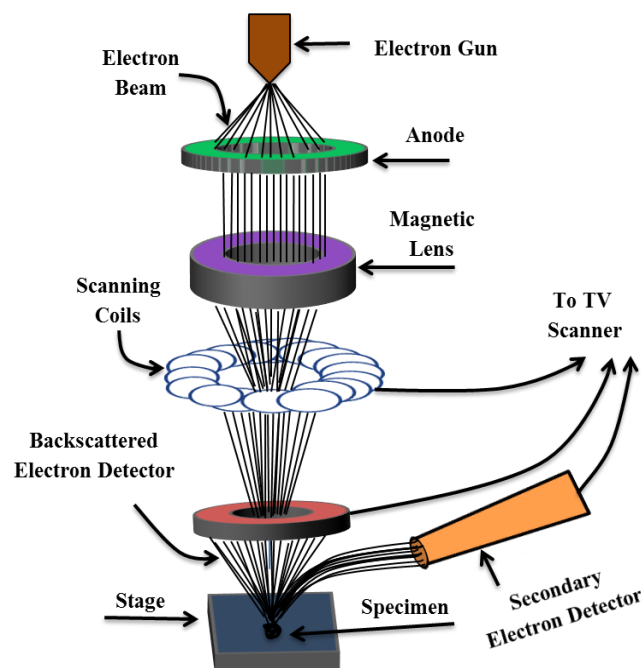


**Figure 2.10:** Schematic representation of SEM.

### 2.5.2 Atomic Force Microscopy

Atomic Force Microscopy (AFM) is a technique employed to characterise the surface of materials that depends on a very sharp probe, scanned a few nm from the sample surface to acquire three-dimensional high resolution surface maps. The probe is a tip located at one end of a cantilever, which crosses to the sample and is monitored using the deflection of a laser beam. The reflected beam is emitted towards a photodiode when it falls on the back surface of cantilever, as shown in **Figure 2.11**. In AFM, the surface image of the sample is produced as a plot of tip deflection verses lateral position. When the probe is much closer to the surface, during up and down scans, its

position is maintained by repulsive inter-atomic forces that force the tip away from the surface to avoid any risk of damaging the tip. However, it should be noted that attractive forces can occur due to van der Waals interactions when the separation between the tip and surface is a large (i.e. a few Ångstroms).<sup>62, 63</sup>

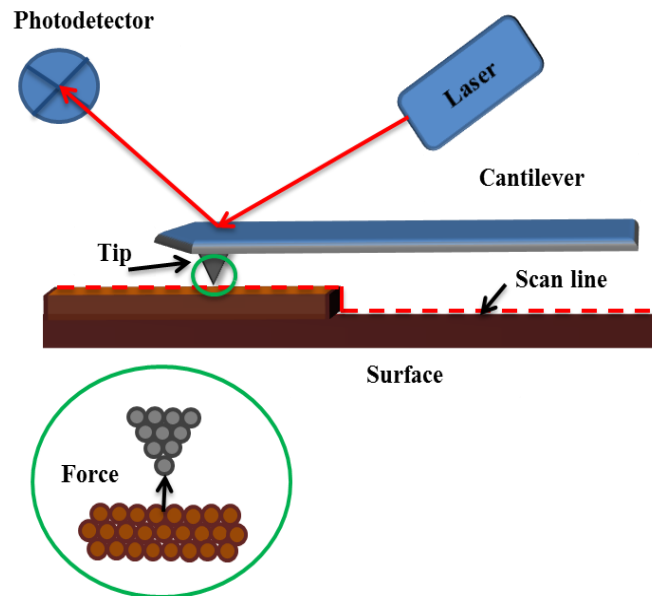


**Figure 2.11:** Schematic representation of AFM.

In this technique, there are three common operating modes that can be utilised.<sup>62-64</sup>

- 1- **Contact mode:** the tip is probed in the repulsive interaction regime due to its very close contact with the surface. The cantilever is deflected as result of the force of the interaction between the tip and the sample being measured, and hence information on the sample properties is obtained. Due to the fact of dragging the tip, which probes across the surface by strong lateral forces, this mode can be destructive.
- 2- **Non-contact mode:** a small distance is maintained between the tip and the sample during probing, so this is a non-destructive mode. As a result of this increased separation, attractive van der Waals forces occur between the tip and the sample. Only a small oscillation occurs in this mode due to the weak forces formed in comparison to those employed in contact mode, but its magnitude is nevertheless sufficient to detect the changes in separation between the tip and sample.
- 3- **Tapping mode:** oscillations resulting from the cantilever are caused by an external driver signal. As a result, attractive and repulsive interaction forces are

intermittently obtained as the tip probes across the sample surface. Because of changes in the cantilever vibration (frequency and phase), information on the sample properties are acquired. This mode is less destructive due to the short contact time between the sample and tip, and this leads to a dramatic reduction in the lateral and vertical forces. This mode gives high resolution topographic imaging and it is particularly suitable for soft samples, such as polymers.

## **2.6 Spectroscopic Techniques**

Spectroscopic techniques are used to gain information about structural changes in the polymer-modified electrode through identification at the atomic and molecular level as a response to electrochemical effects. The most widely used techniques for this purpose are Ultraviolet–visible (UV/Vis) absorbance and Infrared (IR) spectroscopies. The significance of the IR spectroscopy employed to analyse the structural properties of the polymer-modified electrodes in this thesis will be highlighted in the following section.

### **2.6.1 Infrared Spectroscopy**

Infrared spectroscopy is a powerful technique used to characterise the vibrational motions of molecular bonds in pure organic and inorganic compounds. This includes molecules absorbing incident infrared radiation. As a result, the vibrational modes of the target species are excited and absorb some of the incident radiation; as molecular vibrations occur at different, unique frequencies, reported in IR spectroscopy in wavenumbers ( $\text{cm}^{-1}$ ), the observed infrared bands can be used to identify the functional groups present within the target compound. This process is attributed to a changing dipole moment with respect to the field of the incident radiation, and the vibrational energy levels of the species are then transferred from the low energy levels (ground state) to high energy levels (excited state). There are various modes of bonds which may be generated from IR frequencies, such as stretching, bending or wagging of individual bonds. Fourier Transform Infrared Spectroscopy (FTIR) is a variation of the infrared technique that converts the raw frequency versus absorbance data through the mathematical process of a Fourier transform.<sup>65, 66</sup> Therefore FTIR can give specific information on the structure of polymer chains, molecular orientation, and identity at electrode surfaces, as well as explore vibrational motions, which depend on the nature of the redox species that exist in the conducting polymer films.<sup>67-69</sup>

## 2.4 References

1. A. C. Fisher, *Electrode Dynamics*, Oxford University Press, 1996.
2. F. Scholz, *Electroanalytical Methods: Guide to Experiments and Applications*, Springer Berlin Heidelberg, 2010.
3. A. J. Bard and L. R. Faulkner, *Electrochemical Methods: Fundamentals and Applications*, John Wiley & Sons, 2000.
4. A. M. Mohamoud, *PhD Theses, University of Leicester*, 2007.
5. J. Wang, *Analytical Electrochemistry*, Wiley-VCH, 2001.
6. C. M. A. Brett and A. M. O. Brett, *Electrochemistry: Principles, Methods, and Applications*, Oxford University Press, 1993.
7. R. W. Murray, *Molecular Design of Electrode Surfaces*, Wiley-Interscience, New York, 1992.
8. A. R. Hillman and R. Linford, *Electrochemical Science and Technology of Polymers*, Elsevier, London, 1987, **1**, pp. 103–291.
9. R. G. Compton and C. E. Banks, *Understanding Voltammetry*, Imperial College Press, 2011.
10. J. Agrisuelas, C. Gabrielli, J. J. García-Jareño, H. Perrot and F. Vicente, *Electrochimica Acta*, 2014, **125**, 83-93.
11. E. Sefer, H. Bilgili, B. Gultekin, M. Tonga and S. Koyuncu, *Dyes and Pigments*, 2015, **113**, 121-128.
12. M. Ertas, R. M. Walczak, R. K. Das, A. G. Rinzler and J. R. Reynolds, *Chemistry of Materials*, 2012, **24**, 433-443.
13. P. T. Kissinger, *Journal of Chemical Education*, 1983, **60**, 702-706.
14. D. A. Skoog, D. M. West, F. J. Holler and S. R. Crouch, *Fundamentals of Analytical Chemistry*, Thompson Brooks/Cole, 2004.
15. G. Inzelt, *Conducting Polymers: A New Era in Electrochemistry*, Springer-Verlag Berlin Heidelberg, 2008.
16. H. Matsuda and Y. Ayabe, *Zeitschrift für Elektrochemie, Berichte der Bunsengesellschaft für physikalische Chemie*, 1955, **59**, 494-503.
17. E. Barsoukov and J. R. Macdonald, *Impedance Spectroscopy: Theory, Experiment, and Applications*, John Wiley & Sons, 2005.
18. E. P. Randviir and C. E. Banks, *Analytical Methods*, 2013, **5**, 1098.

19. E. Gileadi, *Physical Electrochemistry*, Wiley-VCH Verlag GmbH & Co. KGaA, 2011.
20. S.-M. Park and J.-S. Yoo, *Analytical Chemistry*, 2003, **75**, 455 A-461 A.
21. M. D. Levi, Y. Gofer, D. Aurbach and A. Berlin, *Electrochimica Acta*, 2004, **49**, 433-444.
22. J. E. B. Randles, *Transactions of the Faraday Society*, 1948, **44**, 322-327.
23. A. R. Hillman, A. Jackson and S. J. Martin, *Analytical Chemistry*, 2001, **73**, 540-549.
24. G. McHale, C. Hardacre, R. Ge, N. Doy, R. W. Allen, J. M. MacInnes, M. R. Bown and M. I. Newton, *Analytical Chemistry*, 2008, **80**, 5806-5811.
25. F. Herrmann, D. Hahn and S. Büttgenbach, *Sensors and Actuators A: Physical*, 1999, **78**, 99-107.
26. L. Daikhin, E. Gileadi, V. Tsionsky, M. Urbakh and G. Zilberman, *Electrochimica Acta*, 2000, **45**, 3615-3621.
27. A. R. Hillman, *Journal of Solid State Electrochemistry*, 2011, **15**, 1647-1660.
28. R. Lucklum and P. Hauptmann, *Electrochimica Acta*, 2000, **45**, 3907-3916.
29. J. Curie and P. Curie, *Comptes Rendus*, 1880, **91**, 294-295.
30. D. A. Buttry and M. D. Ward, *Chemical Reviews*, 1992, **92**, 1355-1379.
31. J. Curie and P. Curie, *Comptes-rendus de l'Académie des Sciences*, 1881, **93**, 1137-1140.
32. H. L. Bandey, A. R. Hillman, M. J. Brown and S. J. Martin, *Faraday Discussions*, 1997, **107**, 105-121.
33. J. W. S. B. Rayleigh and R. B. Lindsay, *The Theory of Sound*, Dover, 1945.
34. G. Sauerbrey, *Zeitschrift für Physik*, 1959, **155**, 206-222.
35. C. Lu and A. W. Czanderna, *Applications of Piezoelectric Quartz Crystal Microbalances*, Elsevier Science, 1984.
36. D. S. Ballantine, R. M. White, S. J. Martin, A. J. Ricco, E. T. Zellers, G. C. Frye, H. Wohltjen, M. Levy and R. Stern, *Acoustic Wave Sensors: Theory, Design, & Physico-Chemical Applications*, Elsevier Science, 1997.
37. M. Skompska and A. Tarajko-Wazny, *Electrochimica Acta*, 2011, **56**, 3494-3499.
38. P. L. Konash and G. J. Bastiaans, *Analytical Chemistry*, 1980, **52**, 1929-1931.
39. T. Nomura and M. Okuhara, *Analytica Chimica Acta*, 1982, **142**, 281-284.

40. N. Doy, G. McHale, M. Newton, C. Hardacre, R. Ge, J. MacInnes, D. Kuvshinov and R. Allen, *Biomicrofluidics*, 2010, **4**, 014107.
41. K. K. Kanazawa and J. G. Gordon, *Analytica Chimica Acta*, 1985, **175**, 99-105.
42. S. Bruckenstein and M. Shay, *Electrochimica Acta*, 1985, **30**, 1295-1300.
43. G. Hayward and G. Chu, *Analytica Chimica Acta*, 1994, **288**, 179-185.
44. S. Kurosawa, H. Kitajima, Y. Ogawa, M. Muratsugu, E. Nemoto and N. Kamo, *Analytica Chimica Acta*, 1993, **274**, 209-217.
45. C. Reed, K. K. Kanazawa and J. Kaufman, *Journal of Applied Physics*, 1990, **68**, 1993-2001.
46. A. R. Hillman and E. F. Mallen, *Journal of Electroanalytical Chemistry and Interfacial Electrochemistry*, 1991, **309**, 159-171.
47. A. R. Hillman and M. A. Mohamoud, *Electrochimica Acta*, 2006, **51**, 6018-6024.
48. I. Efimov, A. Ispas and A. Bund, *Electrochimica Acta*, 2014, **122**, 16-20.
49. H. L. Bandey, S. J. Martin, R. W. Cernosek and A. R. Hillman, *Analytical Chemistry*, 1999, **71**, 2205-2214.
50. M. J. Brown, A. R. Hillman, S. J. Martin, R. W. Cernosek and H. L. Bandey, *Journal of Materials Chemistry*, 2000, **10**, 115-126.
51. S. J. Martin, V. E. Granstaff and G. C. Frye, *Analytical Chemistry*, 1991, **63**, 2272-2281.
52. V. T. Gruia, A. Ispas, M. Wilke, I. Efimov and A. Bund, *Electrochimica Acta*, 2014, **118**, 88-91.
53. A. R. Hillman, *Solid State Ionics*, 1997, **94**, 151-160.
54. L. Daikhin, S. Sigalov, M. D. Levi, G. Salitra and D. Aurbach, *Analytical Chemistry*, 2011, **83**, 9614-9621.
55. A. Bund and G. Schwitzgebel, *Electrochimica Acta*, 2000, **45**, 3703-3710.
56. E. Detsri and S. T. Dubas, *Journal of Applied Polymer Science*, 2013, **128**, 558-565.
57. M. F. Suárez and R. G. Compton, *Journal of Electroanalytical Chemistry*, 1999, **462**, 211-221.
58. J. S. Mondschein, A. Kowalski, J. D. Kehlbeck, M. E. Hagerman and R. Cortez, *Materials Letters*, 2014, **131**, 262-265.
59. L. Zhang, Y. Long, Z. Chen and M. Wan, *Advanced Functional Materials*, 2004, **14**, 693-698.

60. D. H. Krinsley, K. Pye, S. Boggs and N. K. Tovey, *Backscattered Scanning Electron Microscopy and Image Analysis of Sediments and Sedimentary Rocks*, Cambridge University Press, 2005.
61. J. Goldstein, D. E. Newbury, D. C. Joy, C. E. Lyman, P. Echlin, E. Lifshin, L. Sawyer and J. R. Michael, *Scanning Electron Microscopy and X-ray Microanalysis: Third Edition*, Springer US, 2013.
62. D. A. Skoog, F. J. Holler and S. R. Crouch, *Principles of Instrumental Analysis*, Thomson Brooks/Cole, 2007.
63. G. Attard and C. Barnes, *Surfaces (Oxford Chemistry Primers). First Edition en anglais*, Oxford University Press, New York, 1998.
64. G. J. Vancso and H. Schönherr, *Scanning Force Microscopy of Polymers*, Springer Berlin Heidelberg, 2010.
65. P. R. Griffiths and J. A. De Haseth, *Fourier Transform Infrared Spectrometry*, John Wiley & Sons, 2007.
66. D. C. Harris, *Quantitative Chemical Analysis*, W. H. Freeman and Compay, New York, 2007.
67. R. Deka, M. M. Bora, M. Upadhyaya and D. K. Kakati, *Journal of Applied Polymer Science*, 2015, **132**, 41600.
68. S. S. Patil, K. V. Harpale, S. P. Koiry, K. R. Patil, D. K. Aswal and M. A. More, *Journal of Applied Polymer Science*, 2015, **132**, 41401.
69. S. Cetiner, F. Kalaoglu, H. Karakas and A. S. Sarac, *Polymer Composites*, 2011, **32**, 546-557.

## Chapter 3: Experimental

### Contents

<b>3.1</b>	<b>Introduction.....</b>	<b>58</b>
<b>3.2</b>	<b>Materials .....</b>	<b>58</b>
3.2.1	Chemicals and Reagents .....	58
3.2.2	Deep Eutectic Solvents Formulations .....	59
<b>3.3</b>	<b>Instrumentations.....</b>	<b>61</b>
3.3.1	Electrochemical Techniques.....	61
3.3.1.1	Cyclic Voltammetry .....	61
3.3.1.2	Electrochemical Quartz Crystal Microbalance .....	62
3.3.2	Non-Electrochemical Techniques .....	64
3.3.2.1	Surface Characterisation Techniques .....	64
3.3.2.2	Physical Properties for DESs .....	65
3.3.2.3	Four-Probe Conductivity Measurements .....	66
3.3.2.4	Thermo-Gravimetric Analysis .....	66
3.3.2.5	Spectroscopic Techniques .....	66
<b>3.4</b>	<b>Procedure.....</b>	<b>67</b>
3.4.1	Polyaniline Deposition using CV .....	67
3.4.1.1	Polyaniline Film Deposition from Aqueous Solutions .....	67
3.4.1.2	PANI Film Deposition from DESs .....	67
3.4.1.3	Preparation of PANI- MoO <sub>2</sub> and/or GR Modified Electrode .....	67
3.4.1.4	Electrochemical Impedance Spectroscopy.....	68
3.4.1.5	Charge and Discharge Batteries .....	68
3.4.2	Polyaniline Deposition Using EQCM .....	70
3.4.2.1	PANI Film Deposition from Aqueous Solution.....	70
3.4.2.2	PANI Film Deposition from DESs .....	71
<b>3.5</b>	<b>References.....</b>	<b>72</b>

### 3.1 Introduction

This chapter includes an explanation of the materials and electrochemical techniques used throughout this thesis, as well as the detailed procedures used to gain the results reported in chapters four to seven.

### 3.2 Materials

#### 3.2.1 Chemicals and Reagents

All materials and reagents used in this study are shown in **Table 3.1** with respective purities and their sources. The aniline monomer was kept in a cold room (4°C) when not being used.

*Table 3.1: List of chemicals and their specifications.*

Chemicals	Source	Purity
Aniline	Sigma-Aldrich	≥ 99.5 %
Potassium chloride	Fisher Scientific	99 %
Sulphuric acid	Fisher chemical	> 95 %
Nitric acid	Fisher chemical	97 %
Hydrochloric acid	Fisher chemical	37 %
Perchloric acid	Fisher chemical	60 %
Choline chloride(ChCl)	Sigma-Aldrich	≥ 98 %
Ethylene glycol (EG)	Sigma-Aldrich	99 %
1, 2-propylene glycol (PG)	Reagent	99 %
Oxalic acid. dihydrate (Oxa)	Sigma-Aldrich	≥ 98 %
Glycerol (Gly)	Fisher chemical	98 %
Urea	Sigma-Aldrich	99.9 %
Malonic acid	Acros Organics	99 %
Graphite (GR)	Alfa Aesar	99 %
Molybdenum dioxide (IV) [MoO <sub>2</sub> ]	Sigma-Aldrich	99 %

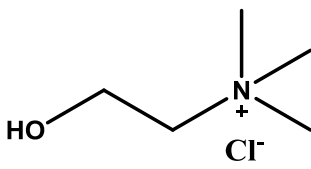
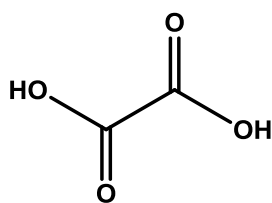
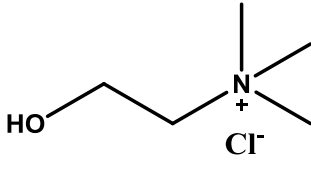
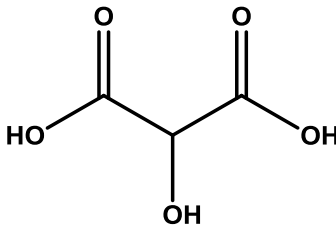
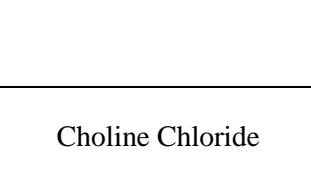
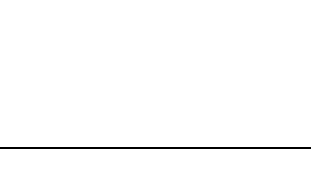
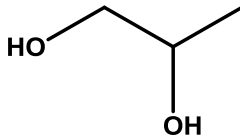
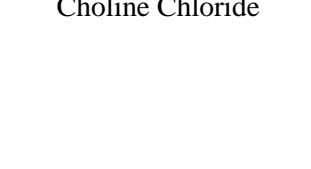
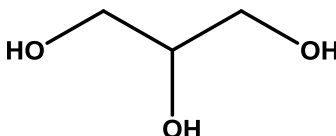
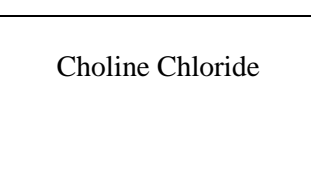
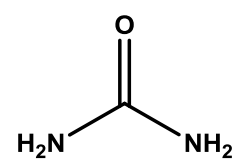
Ammonium chloride [NH <sub>4</sub> Cl]	Sigma-Aldrich	99.5 %
Ammonium perchlorate [NH <sub>4</sub> ClO <sub>4</sub> ]	Sigma-Aldrich	99.5 %
Ammonium nitrate [NH <sub>4</sub> NO <sub>3</sub> ]	BDH	98 %
Ammonium sulphate [(NH <sub>4</sub> ) <sub>2</sub> SO <sub>4</sub> ], ACS reagent	Sigma-Aldrich	≥ 99 %
Zinc chloride [ZnCl <sub>2</sub> ], reagent grade	Sigma-Aldrich	≥ 99 %
Zinc perchlorate hexahydrate [Zn(ClO <sub>4</sub> ) <sub>2</sub> .6H <sub>2</sub> O]	Sigma-Aldrich	≥ 98 %
Zinc nitrate hexahydrate [Zn(NO <sub>3</sub> ) <sub>2</sub> .6H <sub>2</sub> O]	Alfa Aesar	99 %
Zinc sulphate monohydrate [Zn(SO <sub>4</sub> ) <sub>2</sub> .H <sub>2</sub> O]	Sigma-Aldrich	≥ 99.9 %

### 3.2.2 Deep Eutectic Solvents Formulations

Deep Eutectic Solvents (DESs), type III, were prepared by mixing two components, the first being a quaternary ammonium salt and the other a hydrogen-bond donor (HBD).<sup>1</sup> As an example, Ethaline 200 was prepared by mixing choline chloride (quaternary ammonium salt) and ethylene glycol (HBD) in a 1:2 molar ratio, respectively. The mixture was stirred in a beaker and heated on the hot plate at c.a. 80°C, for 2 - 3 hours until a homogeneous and colourless liquid was formed.<sup>2,3</sup> A similar procedure was used for Propaline and Glyceline production; however, instead of the ethylene glycol used for Ethaline, other HBD structures were mixed with choline chloride in various molar ratios, as given in **Table 3.2**.

For the preparation of Reline, choline chloride and urea in a 1:2 molar ratio were mixed. The mixture was stirred in a beaker and placed in an oven at 50°C, with stirring every hour (~4 times), and then left in the oven for 24 hours until a clear liquid was achieved. A similar procedure was used for the preparation of Maline and Oxaline, except the molar ratio of the Maline mixture was 1:1 (ChCl: malonic acid); for Oxaline a 1:1 (ChCl: oxalic acid) mixture was also used. After preparation of the DESs, they were subsequently stored in sealed containers in an oven at 50°C for later use. **Table 3.2** shows the names of DESs (type III) and the ions forming each DES with the appropriate molar ratios.

**Table 3.2:** Names of DESs with their ions formed and molar ratio

DES	Components		Molar ratio Ch Cl: HBD
	Quaternary ammonium salt	Hydrogen Bond Donor (HBD)	
Oxaline 100	Choline Chloride 	Oxalic acid dihydrate 	1:1
Maline 100	Choline Chloride 	Malonic acid 	1:1
Ethaline 200	Choline Chloride 	Ethylene glycol 	1:2
Propaline 200	Choline Chloride 	1,2-Propylene glycol 	1:2
Glyceline 200	Choline Chloride 	Glycerol 	1:2
Reline 200	Choline Chloride 	Urea 	1:2

### 3.3 Instrumentations

#### 3.3.1 Electrochemical Techniques

##### 3.3.1.1 Cyclic Voltammetry

Cyclic Voltammetry (CV) studies were carried out using an Autolab PGSTAT12 potentiostat (Ecochemie, Holland) controlled with GPES2 software. All electrochemical experiments were carried out using the standard three electrodes (working, counter and reference) immersed in the required background electrolyte at room temperature ( $25 \pm 2^\circ\text{C}$ ), as shown in **Figure 3.1**. Brief information about the electrodes used in CV experiments is reported below.

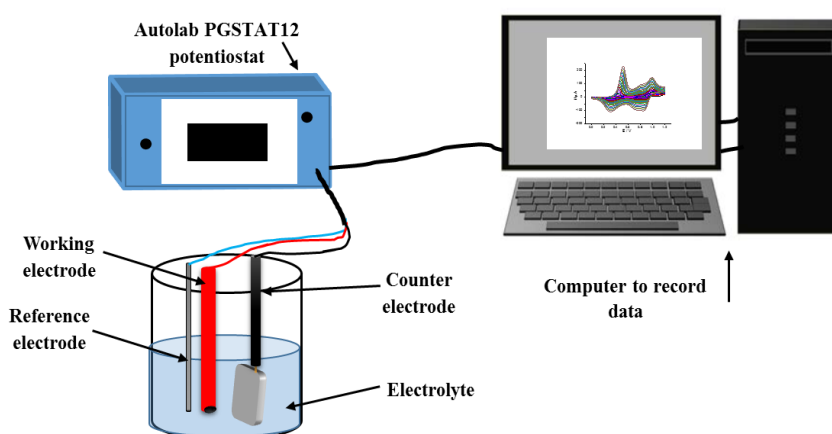


*Figure 3.1: CV experimental set-up to record redox process for PANI films.*

The electrodes used in the CV experiments were a platinum electrode 1.0 mm (0.04 in) dia., Premion, 99.997 % (metal basis) from Alfa Aesar, which is home-made and was used as the working electrode (WE) in all electrochemical experiments in this thesis. A counter electrode (CE), which is home-made from a platinum sheet 1.0 mm (0.004 in) thick, Premion, 99.997 % (metal basis) from Alfa Aesar having surface area  $1 \text{ cm}^2$ . The surface area of the CE is larger than all WE, and is used to provide surplus electroactive area and prevent the limitation of the current reaction by the CE electrode.<sup>4</sup> Two types of reference electrode were used in the electrochemical experiments in this thesis. The first reference electrode (RE), was Ag/AgCl a home-made electrode consisting of an Ag wire (0.5 mm diameter, 99 % from Alfa Aesar), immersed in a saturated potassium chloride electrolyte in a glass body with a porous Vycor glass frit on the bottom of the body. It is known that the interaction of an Ag/AgCl RE takes place between the Ag(s) and AgCl salt.<sup>5</sup> In DES experiments, a silver wire (0.5 mm diameter, 99 % from Alfa

Aesar) was directly immersed into DES electrolytes and used as a pseudo-reference electrode. In most studies of Room-Temperature Ionic Liquids (RTILs), quasi-REs or pseudo-REs made from Ag or Pt wires<sup>6, 7</sup> are used as the RE by immersing in the RTIL.<sup>8</sup> The pseudo-RE used in RTIL is likely to maintain the potential of the redox peaks during electrochemical measurements.<sup>9</sup> It is well known that DESs have a high concentration of Cl<sup>-</sup> ions (3.8 M Cl<sup>-</sup> in Ethaline). Therefore, Cl<sup>-</sup> ions can surround the Ag immersed into the DESs. As a result, the interaction between the Ag and AgCl for Ag wire pseudo-RE seems to be similar to the Ag/AgCl RE in aqueous solution.

### **3.3.1.2 Electrochemical Quartz Crystal Microbalance**

In the Electrochemical Quartz Crystal Microbalance (EQCM) experiments, two network analysers were used to record the electrochemical and gravimetric results. The first was a Hewlett Packard (HP) 8751A 5Hz – 500 MHz network analyser conducted with an Autolab III potentiostat, which was used for growth of the PANI film. The importance of the HP device is that it includes an admittance spectrum, which supplies information about the film behaviour, whether is a rigid (acoustically thin) or non-rigid material (acoustically thick).<sup>10-12</sup> One admittance spectrum for the quartz crystal impedance was recorded every 4 seconds, in reflectance mode. The raw spectral data required a separate fitting program (Lorentzian-fitted admittance spectra) to extract frequency (which gives information about polymer mass), peak intensity, and peak shape.

The second instrument used for gravimetric experiments was a Gamry Instruments eQCM 10M conducted with a Gamry Instruments Reference 600 potentiostat. The electrochemical and gravimetric data were obtained automatically in this equipment, which does not demand a separate fitting program like the HP instrument. The Gamry eQCM instrument was used to study the ion exchange of the films in electrolyte (monomer free) during the redox reactions, after the films were obtained by Hewlett Packard network analysis (EQCM), and confirmed the validity of the Sauerbrey equation for gravimetric analysis through appropriate admittance-frequency spectra.<sup>13</sup> In the EQCM studies, the electrochemical cells used were home-made, as shown in **Figure 3.2**.

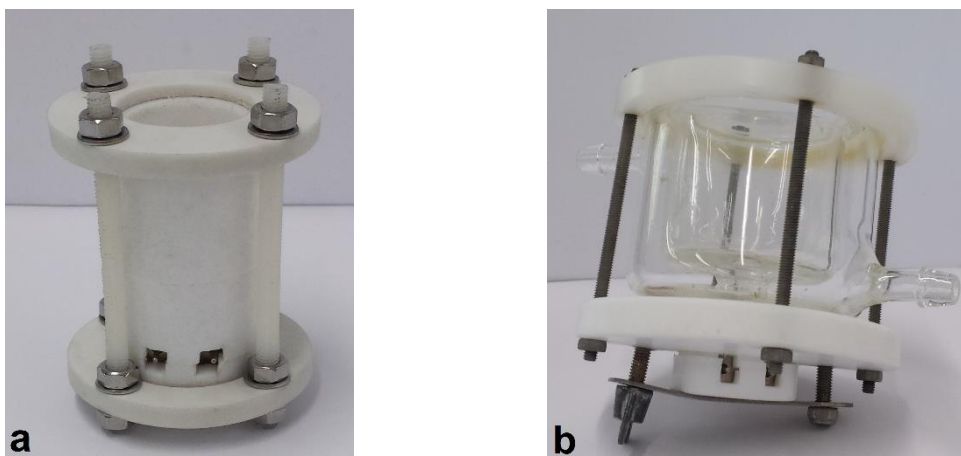


**Figure 3.2:** Home-made EQCM cells designed from Teflon, used for electrochemical experiments in this study. a) The cell used for experiments at room temperature, and b) the cell used for experiments at 50°C.

Three-electrode electrochemical cells were used in EQCM experiments (RE, CE and WE), which were placed close to each other whilst running experiments, and then connected to the EQCM (including a network analyser and the potentiostat), as shown in **Figure 3.3a**. Here, the WE was a 10 MHz *AT*-cut quartz crystal (coated with Pt on one side and Au on the other), which was supplied by International Crystal Manufacturing Co. Ltd., Oklahoma City, USA, mounted. The electrochemical and piezoelectric active area for the WE were 0.23 cm<sup>2</sup> and 0.21 cm<sup>2</sup>, respectively. The Pt quartz crystals were used as polished in all EQCM experiments in order to avoid the effects of surface roughness in unpolished quartz crystals, which cause mass trapping in the surface electrode.<sup>14</sup> The quartz crystal was mounted on the Teflon plate using screws to tighten the cell to prevent the solution leaking from the cell, which would cause loss of oscillation of the quartz crystal.<sup>15</sup> The Pt surface was placed in contact with the solution in order to deposit the PANI film on it, as shown in **Figure 3.3c**.

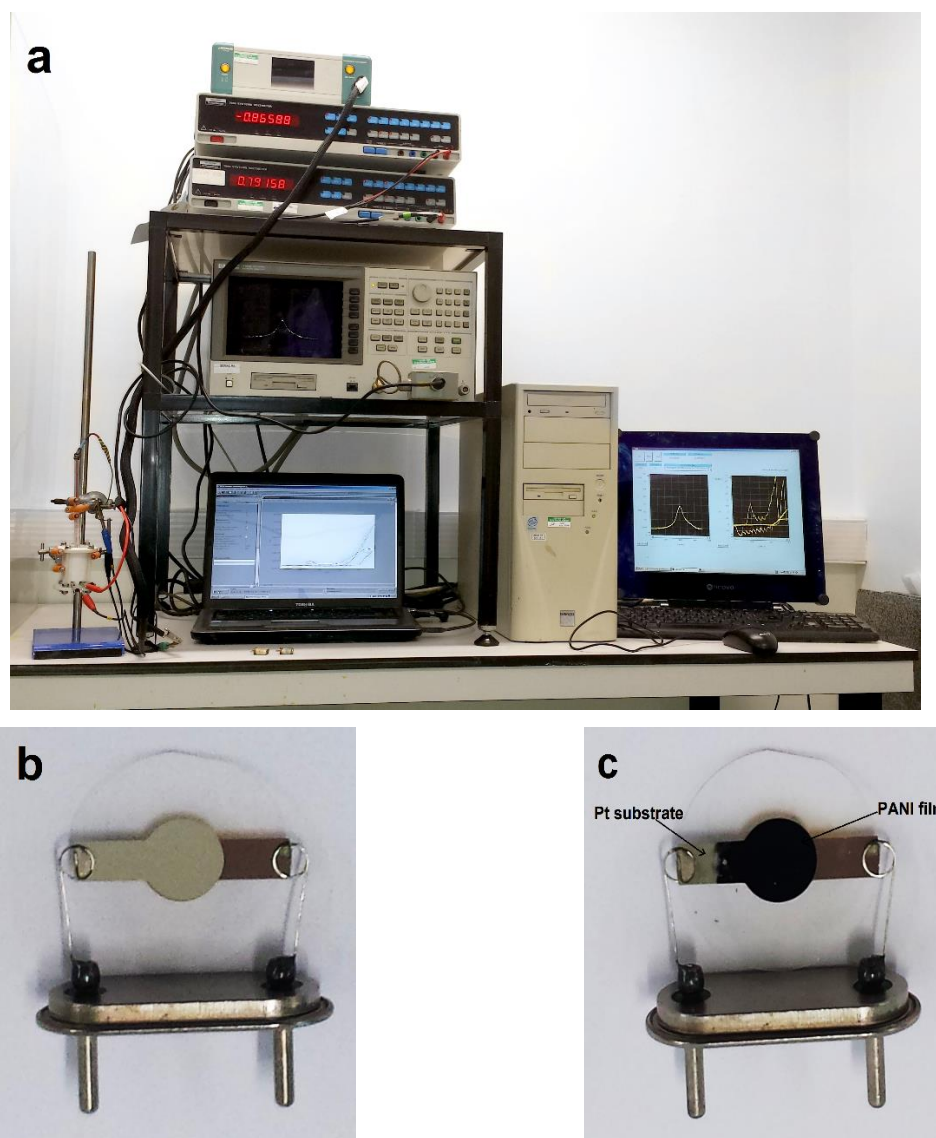


**Figure 3.3:** *a) EQCM experimental set-up. Pt crystal (10 MHz AT-cut polished) used as the working electrode in EQCM experiments, b) before PANI deposition, and c) after PANI was deposited.*

### 3.3.2 Non-Electrochemical Techniques

#### 3.3.2.1 Surface Characterisation Techniques

##### 3.3.2.1.1 Scanning Electron Microscopy and Energy Dispersive X-ray

The surface morphology of the deposited PANI electrodes was investigated in this thesis by a FEI SIRION SEM scanning electron microscope, which was carried out under vacuum (10<sup>-5</sup> Pa). Energy Dispersive X-ray spectroscopy (EDX) was used to characterise the elements that presented in the deposited PANI compositions by

bombardment of electrons on the required sample, using a Phillips XL30 ESEM instrument with an accelerating voltage of 5 keV.

#### **3.3.2.1.2 Atomic Force Microscopy**

The AFM employed in this study used a Digital Instruments, Dimension™ 3100 Microscope Controller. This was coupled to a Nanoscope® Scanning Probe Microscope Controller. The instrument was controlled through Nanoscope ® software. The tips used were provided by Veeco (model: RTESP, part: MPP-11100-10). The image/scan size was 20  $\mu\text{m}^2$  with a scan rate of 0.5 Hz.

#### **3.3.2.1.3 Zeta-20 Optical Profiler**

The Zeta-20 Optical Microscope was used to measure the thickness of the polymer. It is a completely integrated microscope based on a system that provides 3D imaging and metrology capability in a tiny, strong and cost-effective package. The instrument, based on proprietary technology, enables imaging of surfaces with very high roughness, and very low reflectivities.

### **3.3.2.2 Physical Properties for DESs**

#### **3.3.2.2.1 Viscosity Measurements**

The viscosity of all (pure and with 1 M H<sub>2</sub>SO<sub>4</sub>) DESs used in this thesis were measured as function of temperature using a Rotational Viscometer (RV) (Brookfield DV-II+ Pro) fitted with a thermostated jacket. The rotation of the spindle in each electrolyte was 100 rpm over a range of temperatures (25 - 80°C), which was controlled using a thermocouple. The accuracy of this method is relied on the size and shape of the spindles, torque percentage, and temperature.<sup>16</sup>

#### **3.3.2.2.2 Conductivity Measurements**

A Jenway 4510 conductivity meter was used to measure the conductivity of the DESs/1 M H<sub>2</sub>SO<sub>4</sub> DESs as function of temperature. The procedure included immersing the probe of the conductivity meter in a hot electrolyte (> 80°C) and the average of conductivity (two readings) was taken every five degrees (i.e. 80, 75, 70.....25°C).

### **3.3.2.3 Four-Probe Conductivity Measurements**

The sample discs (13 mm diameter) were placed in a PTFE cell to make four-probe measurements using uniformly-spaced, spring-loaded, silver-coated copper electrodes at the periphery. Sample thicknesses were determined by means of a digital micrometre. A Keithley 195 current source and a Keithley 197 electrometer were used to make the electrical measurements under computer control.

The van der Pauw equation was used to calculate the conductivity of the samples, as follows:

$$\sigma = \frac{\ln 2}{\pi R d} \quad 3.1$$

where  $\sigma$  is the conductivity of the sample,  $R$  is the gradient of the voltage vs. current graph and  $d$  is thickness of the disc.

### **3.3.2.4 Thermo-Gravimetric Analysis**

The thermal stability and mass change as a function of the temperature for polymer powders were characterised by Thermo-Gravimetric Analysis (TGA) using a Mettler Toledo 44 TGA/DSC 1 STARe machine. The weight of each sample used was between 15 – 20 mg in open aluminium pans. The STARe system software was utilised to obtain the percentage of the mass change from the raw data analysis, which was then transferred to, and re-plotted, using the Origin graphing<sup>17</sup> program.

### **3.3.2.5 Spectroscopic Techniques**

#### **3.3.2.5.1 Fourier Transformation Infrared Spectroscopy**

Polymer samples were mixed with potassium bromide (KBr) powder, and pressed to form a transparent disk using a standard 13 mm disc compressor (30 ton press, C-300, Research and Industrial Instruments Company, London, England). Spectra were obtained using a Perkin Elmer Spotlight 400 FTIR imaging system. The KBr spectrum was taken as the background model before recording the spectrum of any conducting polymer samples. The absorption peaks of the samples were measured in the region between  $4000 \text{ cm}^{-1}$  –  $700 \text{ cm}^{-1}$ .

## **3.4 Procedure**

### **3.4.1 Polyaniline Deposition using CV**

#### **3.4.1.1 Polyaniline Film Deposition from Aqueous Solutions**

Firstly, the deposition of polyaniline (PANI) films were carried out electrochemically in different acidic solutions using CV. The films were grown from 0.2 M aniline in 1 M HA (HA = H<sub>2</sub>SO<sub>4</sub>, HCl, HNO<sub>3</sub> and HClO<sub>4</sub>) with a potential range of -0.16 V to 0.96 V vs. Ag/AgCl RE at a scan rate of 100 mV s<sup>-1</sup> for 20 scans. After film deposition, each film was immersed in different monomer-free solutions, namely the same background electrolyte, then Ethaline, and then returned to the initial electrolyte at a scan rate of 100 mV s<sup>-1</sup> for 20 scans.

#### **3.4.1.2 PANI Film Deposition from DESs**

PANI films were electrically polymerised from 0.8 M aniline in 1 M H<sub>2</sub>SO<sub>4</sub> DESs (type III) over the potential range of 0.0 to 1.2 V at a scan rate of 100 mV s<sup>-1</sup> for 20 scans. The background electrolyte consisted of 1 M H<sub>2</sub>SO<sub>4</sub> in Ethaline, Propaline, Glyceline and Reline, except for the Maline and Oxaline electrolytes. After growth, each film was cycled in different monomer-free solutions as follows: in the same background electrolyte, 0.5 M H<sub>2</sub>SO<sub>4</sub>, and then returned to the initial electrolyte at a scan rate of 100 mV s<sup>-1</sup> for 20 scans. Prior to transferring the PANI films into the required solution, the films were washed with deionised water several times then rinsed with the solution it was to be cycled in. For DESs, a hot (50°C) DES was used in order to abstract aqueous solution that presented between the voids in the PANI films, and all experiments were performed at 25 ± 2°C.

#### **3.4.1.3 Preparation of PANI- MoO<sub>2</sub> and/or GR Modified Electrode**

The PANI/GR, PANI/MoO<sub>2</sub> and PANI/MoO<sub>2</sub>/GR-modified electrodes were prepared from aqueous and Oxaline electrolytes through a stepwise method. In the case of Oxaline being used as the background electrolyte, firstly, a thin layer of PANI was deposited on a Pt electrode (0.55 cm<sup>2</sup>) from 0.2 M aniline in Oxaline, in which the potential range was between 0.0 to 1.2 V at a scan rate of 5 mV s<sup>-1</sup> for 5 scans, using the cell described in **Figure 3.2a**. Secondly, the deposition solution was removed from the cell, and then about 3 mg of MoO<sub>2</sub>, GR or GR+MoO<sub>2</sub> (3:1) particles were dispersed on

the PANI surface. The modified electrodes were then put in an oven at 50°C for 24 h. In the third step, PANI was again electrodeposited onto the PANI-modified electrode using the same deposition solution and scan rate, except the potential window was between -0.2 and 1.3 V versus Ag wire for 10 cycles.

The same strategy described above was used for PANI-modified electrodes prepared from 0.2 M aniline in 1 M H<sub>2</sub>SO<sub>4</sub> aqueous solution, but the potential window was between -0.25 and 0.8 V versus Ag/AgCl. In terms of cycle number, PANI film was deposited for one cycle in the first step and for 5 cycles in the third step (i.e. after adding particles) at a scan rate of 5 mV s<sup>-1</sup>. After polymerisation, each PANI-modified electrode was cycled in different monomer-free solutions as follows: in Ethaline, 0.5 M H<sub>2</sub>SO<sub>4</sub>, and Ethaline, respectively, if the polymer was grown from Oxaline, whereas in the case of polymers grown from 1 M H<sub>2</sub>SO<sub>4</sub> aqueous solution cycled in 0.5 M H<sub>2</sub>SO<sub>4</sub>, Ethaline and 0.5 M H<sub>2</sub>SO<sub>4</sub>, respectively, for 100 cycles in each electrolyte at scan rates of 5 mV s<sup>-1</sup>.

#### **3.4.1.4 Electrochemical Impedance Spectroscopy**

Electrochemical impedance measurements for PANI-modified electrodes (PANI-modified growth, as described in section 3.4.1.3) were performed in various media (monomer free) using an Autolab/ PGSTAT12 potentiostat, fitted with an FRA impedance module, using GPES software. Frequency spectra were used in the range 65000 – 0.01 Hz at an amplitude of 5 mV at 0.5 V for all samples, which were each carried out in fresh cells. Polymers grown from Oxaline were transferred into Ethaline and 0.5 M H<sub>2</sub>SO<sub>4</sub> respectively, while polymers grown from 1 M H<sub>2</sub>SO<sub>4</sub> were transferred into 0.5 M H<sub>2</sub>SO<sub>4</sub> and Ethaline, respectively at 25 ± 2°C.

#### **3.4.1.5 Charge and Discharge Batteries**

PANI-modified electrodes (PANI, PANI/MoO<sub>2</sub>, PANI/GR and PANI/MoO<sub>2</sub>/GR grown from aqueous and Oxaline) were prepared as described in section 3.4.1.3. After polymerisation, PANI-modified electrodes were washed with deionised water and dried, and then immersed in an electrochemical cell containing battery electrolyte. The PANI-modified electrode was used as the cathode (positive electrode), with a zinc flag (area ~3×1.5 cm) as the counter electrode (negative electrode), and a zinc (diameter ~3 mm) as a reference electrode, at room temperature (25 ± 2°C).

Charge and discharge experiments for the batteries were carried out with an Autolab/PGSTAT12 galvanostat controlled by a computer through GPES software. The batteries grown from aqueous solution were charged and discharged between 0.70 and 1.80 V in various aqueous solutions of 0.50 M ZnCl<sub>2</sub> and 0.20 M NH<sub>4</sub>Cl, 0.50 M NH<sub>4</sub>ClO<sub>4</sub> and 0.20 M Zn(ClO<sub>4</sub>)<sub>2</sub>, 0.50 M NH<sub>4</sub>NO<sub>3</sub> and 0.20 M Zn(NO<sub>3</sub>)<sub>2</sub>, 0.50 M (NH<sub>4</sub>)<sub>2</sub>SO<sub>4</sub> and 0.20 M ZnSO<sub>4</sub> at various current densities.

However, the batteries grown from Oxaline solution were charged and discharged between 1.0 and 2.3 V in various Ethaline solutions of 0.35 M ZnCl<sub>2</sub> and 0.15 M NH<sub>4</sub>Cl, 0.35 M NH<sub>4</sub>ClO<sub>4</sub> and 0.15 M Zn(ClO<sub>4</sub>)<sub>2</sub>, 0.35 M NH<sub>4</sub>NO<sub>3</sub> and 0.15 M Zn(NO<sub>3</sub>)<sub>2</sub>, 0.35 M (NH<sub>4</sub>)<sub>2</sub>SO<sub>4</sub> and 0.15 M ZnSO<sub>4</sub> at various current densities.

### **Coin cell assembly components**

To make a functional coin cell battery, the following components were used, as shown in **Figure 3.4**:

1-Coin case (bottom cap). 2-Top cap. 3-Stainless steel spacers (SUS316L 16 mm diameter, 0.5 mm thickness). 4-Stainless steel wave springs (SUS316L 15 mm × 1.4 mm). 5-Cathode electrode (PANI sample). 6-Anode electrode (Zn 16 mm diameter, 0.12 mm thickness). 7- Separator. 8-Electrolyte. 9-A syringe for dispensing the electrolyte fluid. 10-Gasket. 11- Crimper (Hohsen Corporation CR2025).

### **Coin cell assembly procedure:**

Prior to assembly, the electrodes and the separator were immersed in the battery electrolyte to achieve optimum performance. The gasket, wave spring and spacer were set up in the coin case, respectively. Next, the PANI-modified cathode was placed in the assembly with its platinum surface in contact with the spacer. A small amount of the electrolyte was injected to saturate the coated cathode disc. Then, the separator membrane was placed over the cathode disc and a few drops (2 - 3) of electrolyte were injected onto the separator. The Zn disc anode was then placed on top of the separator membrane. The other spacer was placed on the anode disc, and then the wave spring was inserted. Finally, the cell was closed with the top cap and the cell was ready to be locked by the crimper tool.

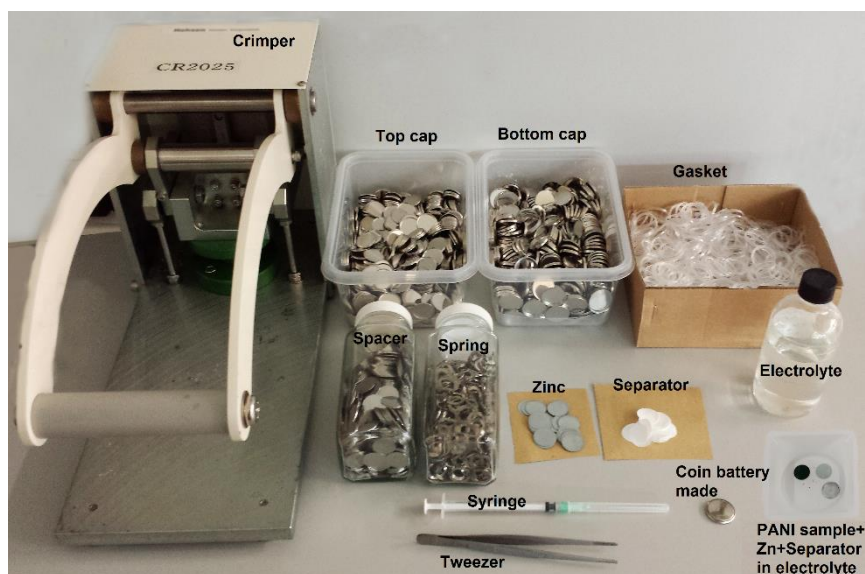


*Figure 3.4: The materials used to make coin battery in our laboratory.*

### **3.4.2 Polyaniline Deposition Using EQCM**

#### **3.4.2.1 PANI Film Deposition from Aqueous Solution**

PANI films were deposited potentiodynamically on a Pt quartz crystal electrode from 0.1 M aniline in 1 M H<sub>2</sub>SO<sub>4</sub> aqueous solution using EQCM, over the potential range -0.16 to 0.96 V vs. Ag/AgCl (sat. KCl) at a scan rate of 10 mV s<sup>-1</sup> for 3 cycles. After film deposition, the film was rinsed with deionised water several times and dried. The mass of film was calculated via the Sauerbrey equation (see sections 4.3.7 and 5.3.9) by measuring the difference in frequencies between the bare crystal in air and the deposited film after drying. In addition, the admittance spectra were studied before measuring the mass change for the film deposited in monomer-free electrolyte (aqueous/DESS) during the redox process in order to characterise whether the films were acoustically thin (rigid) rather than non-rigid (due to viscoelastic effects). It is well known that the Sauerbrey equation is only used for gravimetric analysis if the film behaves in an acoustically thin (rigid) manner.<sup>18</sup> All experiments for PANI growth were performed at room temperature (25 ± 2°C).

The electrochemical behaviour of PANI films during redox switching were studied by transferring the PANI films into different electrolytes (monomer free). Several parameters were investigated in order to study ion-exchange dynamics during oxidation and reduction processes by means of the EQCM. For example, PANI films were

exposed to various electrolytes (0.5 M H<sub>2</sub>SO<sub>4</sub>, Ethaline, and 0.5 M H<sub>2</sub>SO<sub>4</sub>, respectively) to compare their mass and charge responses, the effect of potential windows, various monomer-free DESs, various scan rates, and the effect of temperature (50°C and room temperature) on the mass change for the same PANI film cycled in the same DES electrolyte.

#### **3.4.2.2 PANI Film Deposition from DESs**

PANI films were deposited potentiodynamically on a Pt quartz crystal electrode from 0.25/0.2 M aniline in an Oxaline electrolyte using EQCM, where the best conditions were identified in terms of the amount of charge passed, its rough surface topography (greater porosity), and greatest stability as shown in CV experiments. The potential was scanned from 0.1 to 1.2 V vs. Ag wire at a scan rate of 5 mV s<sup>-1</sup> for three/two cycles. After PANI films were formed by electropolymerisation, the film was rinsed with deionised water several times and dried. Analogous to PANI films deposited from aqueous solution, the mass of PANI films grown from Oxaline were calculated via the Sauerbrey equation. Admittance spectra were also used for characterisation prior to measuring mass change for the deposited film in DESs or aqueous solution during the redox process during gravimetric investigations.<sup>18</sup> All experiments for PANI growth were performed at room temperature (25 ± 2°C).

Ion-transfer dynamics through PANI films during redox switching were also studied, similar to the methods mentioned in section 3.4.2.1, by transferring the PANI films into monomer-free electrolytes. Various parameters were investigated to study the ion-exchange dynamics during the oxidation and reduction process by means of the EQCM. For example, the effect of the polymer thickness, various electrolytes (DESs, monomer free), potential windows, various scan rates, temperatures, and exposing the PANI film to multiple electrolytes such as DES, aqueous solution, and DES sequentially, to see the differences in mass change.

### 3.5 References

1. Q. Zhang, K. De Oliveira Vigier, S. Royer and F. Jerome, *Chemical Society Review*, 2012, **41**, 7108-7146.
2. A. P. Abbott, G. Capper, K. J. McKenzie and K. S. Ryder, *Journal of Electroanalytical Chemistry*, 2007, **599**, 288-294.
3. A. P. Abbott, J. C. Barron, K. S. Ryder and D. Wilson, *Chemistry-A European Journal*, 2007, **13**, 6495-6501.
4. R. G. Compton and C. E. Banks, *Understanding Voltammetry*, Imperial College Press, 2011.
5. R. Bates and J. Macaskill, *Pure and Applied Chemistry*, 1978, **50**, 1701-1706.
6. U. Schröder, J. D. Wadhawan, R. G. Compton, F. Marken, P. A. Suarez, C. S. Consorti, R. F. de Souza and J. Dupont, *New Journal of Chemistry*, 2000, **24**, 1009-1015.
7. D. MacFarlane, S. Forsyth, J. Golding and G. Deacon, *Green Chemistry*, 2002, **4**, 444-448.
8. B. Huber and B. Roling, *Electrochimica Acta*, 2011, **56**, 6569-6572.
9. L. Barrosse-Antle, A. Bond, R. Compton, A. O'Mahony, E. Rogers and D. Silvester, *Chemistry—An Asian Journal*, 2010, **5**, 202-230.
10. A. R. Hillman, K. S. Ryder, V. C. Ferreira, C. J. Zaleski and E. Vieil, *Electrochimica Acta*, 2013, **110**, 418-427.
11. A. R. Hillman, in *Encyclopedia of Electrochemistry*, Vol 3 (A. J. Bard, M. Stratmann, P. R. Unwin), Wiley-VCh, 2003.
12. I. Efimov, A. R. Hillman and J. W. Schultze, *Electrochimica Acta*, 2006, **51**, 2572-2577.
13. A. R. Hillman, *Journal of Solid State Electrochemistry*, 2011, **15**, 1647-1660.
14. R. Schumacher, G. Borges and K. Kanazawa, *Surface Science*, 1985, **163**, L621-L626.
15. D. A. Buttry and M. D. Ward, *Chemical Reviews*, 1992, **92**, 1355-1379.
16. D. S. Viswanath, T. Ghosh, D. H. L. Prasad, N. V. K. Dutt and K. Y. Rani, *Viscosity of Liquids: Theory, Estimation, Experiment, and Data*, Springer Netherlands, 2007.
17. <http://www.originlab.com/>.

18. A. R. Hillman, M. A. Mohamoud and I. Efimov, *Analytical Chemistry*, 2011, **83**, 5696-5707.

## **Chapter 4: Characterisation of the Behaviour of Polyaniline (grown from aqueous electrolytes) in Aqueous Solutions and Deep Eutectic Solvents using EQCM.**

### **Contents**

<b>4.1</b>	<b>Overview .....</b>	<b>75</b>
<b>4.2</b>	<b>Objective .....</b>	<b>76</b>
<b>4.3</b>	<b>Results and Discussion.....</b>	<b>77</b>
4.3.1	Film preparation from H <sub>2</sub> SO <sub>4</sub> /H <sub>2</sub> O (thick film) .....	77
4.3.2	Effect of different acids/anions electrolytes on the growth of polyaniline ..	81
4.3.3	Effect of background/DES electrolytes on PANI stability and reversibility	83
4.3.4	Effect of different anions on PANI film stability at constant thickness.....	86
4.3.5	Morphology and topography of the polymer films .....	89
4.3.6	Selection of polymer for further studies .....	93
4.3.7	Characterisation of the behaviour of PANI using EQCM technique .....	93
4.3.8	Conclusion.....	115
<b>4.4</b>	<b>References.....</b>	<b>118</b>

## 4.1 Overview

Conducting polymers have attracted considerable attention in the last few decades due to their wide range of interesting applications,<sup>1,2</sup> as described in chapter one. One of the main types of conductive polymers, and the most popular, is polyaniline, owing to its chemical, electrochemical and optical properties.<sup>3-7</sup> Generally speaking, previous investigations have shown that the morphology of polyaniline at different stages during electrodeposition can be significantly affected by various factors; for example, the concentration of the acidic solution in the electrolyte bath and the anionic species present during electroformation of the film.<sup>8</sup> Furthermore, it is also dependent on other parameters, such as the amount of deposition charge during cycles, scan rate, potential sweep and concentration of anilinium in the electrolyte bath.<sup>9</sup> Consequently, the influences of the natural anions and background electrolyte concentration with regard to film growth and surface morphology can be said to belong within two categories. The first is that of *compact structure*, and includes anions such as  $\text{BF}_4^-$ ,  $\text{ClO}_4^-$  and  $\text{CF}_3\text{CO}_2^-$  in the electrolyte bath. The second category is that of *open structure*, and includes anions  $\text{SO}_4^{2-}$ ,  $\text{NO}_3^-$  and  $\text{Cl}^-$  in the electrolyte bath during film deposition.<sup>8,10</sup>

In fact, the formation of the polymers and their surface morphology can be empirically analysed via the Scanning Electron Microscopy (SEM) images and Electrochemical Quartz Crystal Microbalance (EQCM) data. Understanding the concepts of these properties and other elementary processes are necessary in the optimisation of desirable specifications of electronic devices. Although many authors have reported the redox cycling dynamics of polyaniline and its structural characteristics,<sup>3,8,10,11</sup> the kinetic and dynamic characterisation of such polymers in DESs have received less attention. Generally, the association between the SEM morphological analysis and the EQCM results may be important in this respect, but this means that comparisons between them are not necessarily justified because the former technique is performed *ex situ*, whilst the latter is *in situ*. For this simple reason, it could be that the voids between networks of film will be filled with solvent *in situ*, the effects of which could clearly never be evaluated through SEM. It is well known that EQCM is suited to the study of mass variation and the doping/dedoping behaviour of polymer films as ion-exchange membranes during redox cycling. Depending on the oxidation reaction, cations are expelled and anions are inserted to satisfy the condition of electroneutrality, and *vice versa*. Following this process, ion transfer is often accompanied by the exchange of

solvent molecules.<sup>12-14</sup> The key point in this work is that the growth of polyaniline film is dependent on the following aspects: (i) the effect of different anions on polymer composition during the nucleation and growth process and (ii) the viscoelastic properties of polyaniline films as a response to diverse background electrolytes (aqueous/non-aqueous). Another important aspect is the influence of the electrolyte composition (monomer free) on the mechanism(s) of ion movement and thus the amount of solvent transfer, with associated ion transfer, into/out of the polymer during redox cycling. In fact, the mechanism of PANI films cycling in non-aqueous electrolytes (deep eutectic solvents) has not, to date, been fully investigated. So, the structural dynamics and kinetics of the resultant polymer should be recognised in these electrolytes. This phenomenon depends on the type of anion present in the electrolytes as well as their viscosity, the latter of which plays a significant role in the diffusion rate of species during the doping and undoping processes. Therefore, in this chapter, the effects of these parameters on the mechanical properties of the film will be studied in more detail via the EQCM technique.

## 4.2 Objective

Many researchers have characterised polyaniline films through cycling (oxidation and reduction) in acidic electrolytes using cyclic voltammetry.<sup>15, 16</sup> EQCM has been used to study ion exchange at the polymer/solution interfaces.<sup>3, 17</sup> The focus of this investigation is not to study the mobility processes of ion/solvent into/out of the polymer, as there are many such studies in the literature; the main goal is, in fact, to (i) characterise the electrochemical behaviour of ion exchange in acidic and DES electrolytes and (ii) compare these results with PANI growth from DESs and analyse the optical and redox behaviour of PANI in the same electrolytes (monomer free) using the same techniques. This directly addresses the main question of this study: what are these mechanisms, and is the behaviour of the conducting polymer [essentially] retained when using aqueous and DES electrolytes? Furthermore, are our observations due to the properties and composition of film or the solution behaviour, *per se*.

Therefore, the key points of this chapter are to describe the reliance of PANI film formation with regards to the following objectives. **The first objective** is to understand the effect of different anions on the growth of the polymer and their effects on its morphology; subsequent to this, we will explore the stability and reversibility of these

films in different environmental systems (aqueous/DES electrolyte) during cyclic voltammetry. **The second objective** is the identification of the response of an acoustic resonator of PANI films (rigid or non-rigid) to background electrolytes by using the Sauerbrey equation.<sup>18</sup> **The third objective** involves the determination of how the individual contributions of cations and anions (ion fractions) effect the dynamics of the film matrix in order to maintain electroneutrality throughout redox switching. This is dependent upon the changing potential sweep, the potential scan rate and the diversity of anions used in different environmental systems (aqueous/DES). In the following sections, we will try to address the above objectives in the context of the preparation and exploitation of polyaniline films in practical applications.

### **4.3 Results and Discussion**

#### **4.3.1 Film preparation from H<sub>2</sub>SO<sub>4</sub>/H<sub>2</sub>O (thick film)**

Initially, polyaniline was electrochemically deposited onto a platinum electrode using cyclic voltammetry between -0.2 V and 1.0 V at a scan rate of 100 mV s<sup>-1</sup> in 1 M H<sub>2</sub>SO<sub>4</sub> and 0.8 M aniline solution over 20 cycles, as shown in **Figure 4.1a**. The rationale behind displaying this graph here is to compare the formation rate of the polyaniline in these conditions with that deposited from DESs (chapter 5) using the same monomer concentration, scan rate and number of cycles. It is well known that the shape (*i* vs. *E*) of polyaniline consists of two oxidation and reduction peaks, and in this our results are similar to those reported in previous studies.<sup>4, 6, 19, 20</sup> The reason given for this form in the literature is that PANI has three forms (leucoemeraldine, emeraldine and pernigraniline),<sup>2, 21</sup> which are formed during electrodeposition of the monomer. The surface coverage and thickness of electroactive PANI film were 1.584×10<sup>-4</sup> mol cm<sup>-2</sup> and 122.7 μm, respectively, which were calculated according to the equations given in section 4.3.1.1. Furthermore, the charge *Q* (C) under the more cathodic peaks can be calculated from the integral of cathodic current with time.<sup>22, 23</sup>

After deposition, the film was rinsed several times with deionised water and cycled in monomer-free solution in order to study the stability and reversibility of the film. **Figure 4.1b** shows film characterised in 0.5 M H<sub>2</sub>SO<sub>4</sub> by cyclic voltammetry from -0.2 to +1.0 V vs. an Ag/AgCl (sat. KCl) reference electrode. The film was then transferred

into Ethaline using a silver wire as the reference electrode. Finally, PANI film was transferred back into 0.5 M H<sub>2</sub>SO<sub>4</sub> at 100 mV s<sup>-1</sup> for 20 cycles. It was observed that CVs of PANI in aqueous solution have two reversible redox couples, which are attributed to the leucoemeraldine form converting to emeraldine, and emeraldine converting to pernigraniline couples. From this figure, it can be seen that the film is clearly losing redox activity and decreasing in stability with each subsequent cycle due to pernigraniline formation. However, cycling PANI film in Ethaline exhibited no redox peaks, indicating a complete lack of electrochemical response of the polymer in Ethaline; this may be related to resistive behaviour, and can be observed in the CV.<sup>24</sup> The main reason for this is that Ethaline has a high viscosity and ions with large ionic radii compared with sulphuric solution; these factors will affect ion mobility during the oxidation and reduction processes, and will be especially evident in the presence of a film with a high thickness (122.7 μm) and lower porosity in the chains of the polymer. Finally, the film was again immersed in 0.5 M H<sub>2</sub>SO<sub>4</sub> to determine whether the film would show electroactivity. It can be seen that film showed about 65 % of its original activity (see **Table 4.1**) and this implies that the polymer had not altered electrochemically.

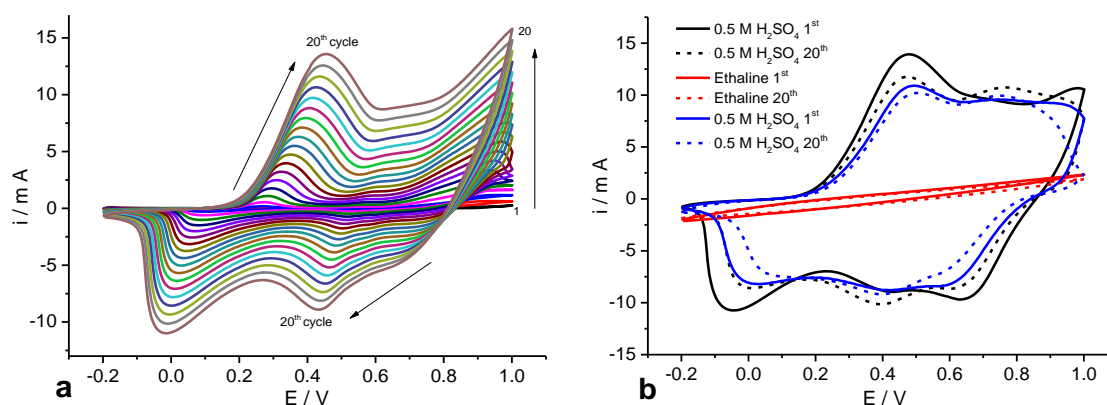


**Figure 4.1:** a) Cyclic voltammogram for the preparation of PANI film ( $\Gamma = 1.58 \times 10^{-4}$  mol cm<sup>-2</sup>) deposited potentiodynamically from 0.8 M aniline / 1 M H<sub>2</sub>SO<sub>4</sub> (-0.2 V to 1.0 V ; 100 mV s<sup>-1</sup>); b) PANI film exposed to the electrolytes (monomer free) 0.5 M H<sub>2</sub>SO<sub>4</sub>, Ethaline, and 0.5 M H<sub>2</sub>SO<sub>4</sub>, respectively, at a scan rate of 100 mV s<sup>-1</sup>; cycles 1 and 20 are shown.

**Table 4.1:** Charge reduction of PANI peaks (see Figure 4.1) exposed to electrolytes (monomer free).

Electrolytes (monomer free)	Q/C <sub>red</sub> 1 <sup>st</sup> cycle	Q/C <sub>red</sub> 20 <sup>th</sup> cycle	% Q <sub>red</sub> retention 20 <sup>th</sup> /1 <sup>st</sup> cycle	% Q <sub>red</sub> total retention
0.5M H <sub>2</sub> SO <sub>4</sub>	0.07611	0.06804	89	<b>65</b>
Ethaline	0.00364	0.0036	98	
0.5M H <sub>2</sub> SO <sub>4</sub>	0.06016	0.05001	83	

#### 4.3.1.1 Film Thickness

There are many methods that can be used to estimate the thickness of the film layer after electrochemical polymerisation. One possible method is by using Faraday's Law. The amount of charge was determined from the final voltammogram of the more cathodic PANI reduction peaks during the deposition process. The time-scale of the process can be calculated from the range of the potential window of the cyclic voltammogram and scan rate. As the time is known, the charge  $Q$  (C) can be calculated as described in equation (4.1).

$$Q = \int_0^t i dt \quad 4.1$$

The charge of the final voltammogram was taken (equation 4.1) in order to determine the number of moles of aniline in the polymer deposit, of coverage  $\Gamma$  (mol cm<sup>-2</sup>).

$$\Gamma = \frac{Q}{nFA} \quad 4.2$$

where  $n$  (0.5) is the number of electrons lost per molecule of aniline to form the emeraldine salt,  $A$  is the area (cm<sup>2</sup>) of the polymer deposit on the substrate and  $F$  is the Faraday Constant (96485 C mol<sup>-1</sup>). The concentration can be calculated from the density  $\rho$  (g cm<sup>-3</sup>) and molar mass  $Mr$  (g mol<sup>-1</sup>) of the monomer and, finally, the thickness of polymer layer was calculated from equation 4.4:

$$c = \frac{\rho}{Mr} \quad 4.3$$

$$h = \frac{\Gamma}{c} \quad 4.4$$

where  $c$  ( $\text{mol cm}^{-3}$ ) is the concentration and  $h$  (cm) is the height (thickness) of the film. These calculations were estimated for a compacted dry polymer film. An increasing thickness of polymer during the CV measurements was probably due to the presence of different species inside the net of the film, causing it to swell.<sup>3, 22, 25, 26</sup>

As an example of the thickness calculations, the data for PANI in **Figure 4.1a** has been employed to determine one particular sample's thickness, as shown below. The data was obtained from the CV of potentiostat, which is connected to a computer, the data from which was transferred to Origin 9.1. Here, the amount of charge (0.06 C, equation 4.1) was calculated by integrating the cathodic current as a function of time digitally. The area,  $A$ , of the Pt working electrode exposed to solution during the deposition process was calculated to be  $0.007854 \text{ cm}^2$ . This was determined using equation 4.5:

$$A = \pi r^2 \quad 4.5$$

where  $r$  is the radius of the Pt working electrode, which was found to be 0.05 cm. Substituting the charge, Faraday Constant, number of electrons and Pt electrode area into equation 4.2 gives the surface coverage of the film.

$$\Gamma = \frac{0.06}{0.5 \times 96485 \times 0.007854} = 1.584 \times 10^{-4} \text{ mol cm}^{-2} \quad 4.6$$

From the density ( $1.02 \text{ g cm}^{-3}$ ) and molar mass ( $93.13 \text{ g mol}^{-1}$ ) of aniline, which will be the same for all samples studied, the concentration can be determined using equation 4.3.

$$c = \frac{1.02}{93.13} = 0.0129 \text{ mol cm}^{-3} \quad 4.7$$

The thickness of film can be determined by substituting the concentration and number of moles of aniline in the polymer into equation 4.4.

$$h = \frac{1.584 \times 10^{-4}}{0.0129} = 0.01227 \text{ cm} = 122.7 \mu\text{m} \quad 4.8$$

### 4.3.2 Effect of different acids/anions electrolytes on the growth of polyaniline

**Figure 4.2** shows polyaniline films prepared using cyclic voltammetry ( $-0.16$  V and  $0.96$  V;  $\nu = 100$  mV s<sup>-1</sup>) from an aqueous solution of  $0.2$  M aniline/ $1$  M aqueous acid ( $\text{H}_2\text{SO}_4$ ,  $\text{HCl}$ ,  $\text{HNO}_3$  and  $\text{HClO}_4$ ). All experiments were performed at room temperature ( $25 \pm 2^\circ\text{C}$ ). In this section, we report the influence of the use of various acids, such as  $\text{H}_2\text{SO}_4$ ,  $\text{HCl}$ ,  $\text{HNO}_3$  and  $\text{HClO}_4$ , as electrolytes on the electropolymerisation of aniline under potentiodynamic conditions. The question that should be addressed here is that of why we are doing these experiments here when they have been done previously and reported in the literature? The reason is that we are attempting to both control the growth of the polyaniline film in aqueous solution, and attempting to understand the electrochemical behaviour of the polymer in different solvent environments. The motivation is one of controlling the growth of the polymer by controlling its conditions.

**Figure 4.2** (a-d) illustrates the  $i$  vs.  $E$  graphs for a number of different anions, those of  $\text{SO}_4^{2-}$ ,  $\text{Cl}^-$ ,  $\text{NO}_3^-$  and  $\text{ClO}_4^-$ , respectively; these results are in agreement with those reported in the literature.<sup>4-6, 23</sup> It is clear from the data that rate of deposition is fastest for  $\text{SO}_4^{2-}$  and slowest for  $\text{ClO}_4^-$ . In other words, the polyaniline grown from the  $\text{H}_2\text{SO}_4$  electrolyte has a higher anodic peak ( $320$   $\mu\text{A}$ ) while the  $\text{HClO}_4$  has a lower anodic peak ( $11$   $\mu\text{A}$ ) under the same conditions (except for the background of the electrolyte). This was attributed to the  $\text{SO}_4^{2-}$  anion tending to interact more strongly with the ion pairs of the anilinium radical cation (polaron) on the polymer chains compared to  $\text{ClO}_4^-$ . Therefore, a greater polymerisation rate is realised in the presence of the  $\text{SO}_4^{2-}$  anion in solution. In this case, the polymerisation rate of the polyaniline films grown is in the order  $\text{SO}_4^{2-} > \text{Cl}^- > \text{NO}_3^- > \text{ClO}_4^-$  is strongly dependent on the type of anion present in the aqueous acid media. As a result, the type of ion has a decisive effect on the thickness and various polymer properties, as shown in **Table 4.2**. The influence of the rate of deposition with different anions has been investigated extensively in the literature.<sup>5, 27-30</sup>

Based on these results, many researchers have indicated that the diversity of ions in solution leads to various changes during the polymerisation process, such as (i) growth and growth mechanisms of polymer, which could involve instantaneous or progressive nucleation in two or three dimensions under diffusional/charge transfer control depending on the electrolyte and, thus, monomer concentration;<sup>30, 31</sup> (ii) the stability of

films are influenced dramatically with the type of anion, which have lyophilic and hydrophilic properties in electrolyte solutions, such that the formation of ion pairs between the anion and the anilinium species during monomer oxidation can have different stabilities<sup>5, 30</sup> (more details in section 4.3.3); (iii) thus, different film thickness with different current values; (iv) the hydration enthalpies and Gibbs free energies associated with ion formation in aqueous solution show a strong relationship with anions that increase the rate of polyaniline formation;<sup>29, 32</sup> (v) in general, different conductivities of the samples, caused by variations in dopants.

From these results, we can conclude that there are two means by which we can characterise the quality of the relationship between polymerisation rate and the properties of the polymer. First, the greatest growth rate of polymer was observed in  $\text{SO}_4^{2-}$  when compared to  $\text{ClO}_4^-$ . Second, SEM and AFM images (see sections 4.3.5.1 and 4.3.5.2, respectively) support film growth rates  $\text{SO}_4^{2-} > \text{Cl}^- > \text{NO}_3^- > \text{ClO}_4^-$  through observation of surface features. Polymers formed in the presence of certain anions  $\text{SO}_4^{2-}$ ,  $\text{NO}_3^-$  and  $\text{Cl}^-$  can have more open morphologies compared to the more compact morphology that can be seen in the present  $\text{ClO}_4^-$ .

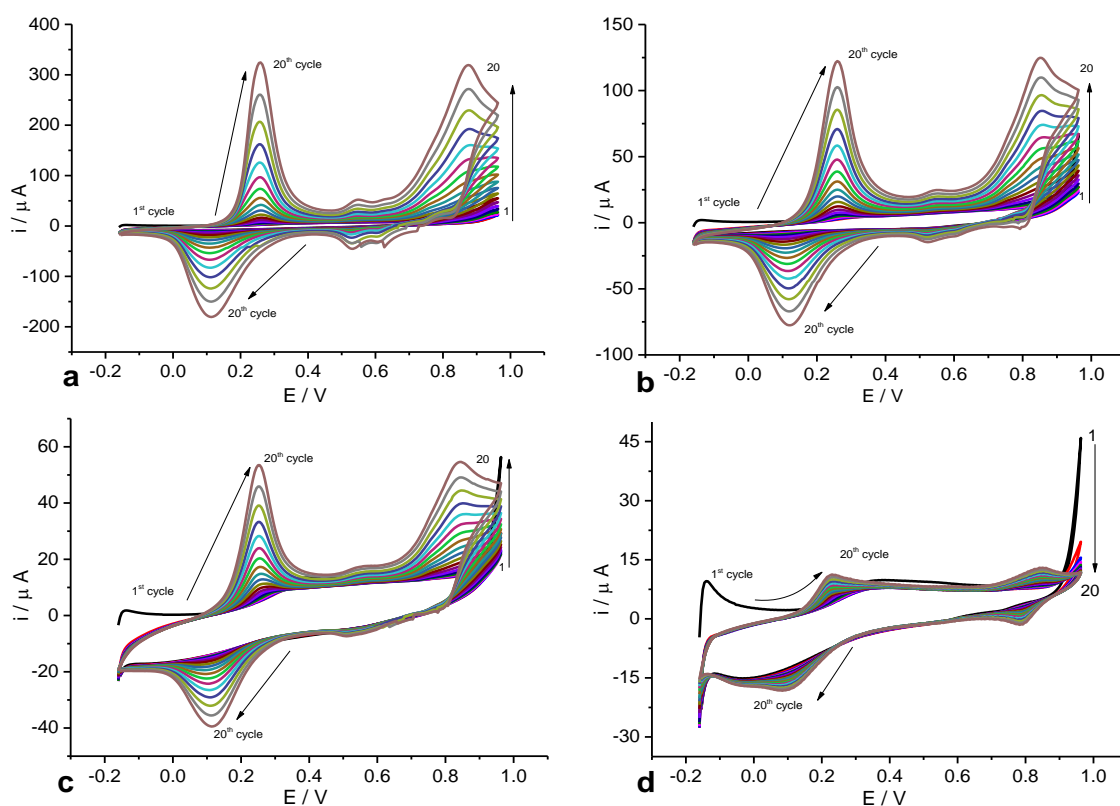


**Figure 4.2:** Cyclic voltammograms for the preparation of PANI film deposited potentiodynamically from 0.2 M aniline in 1 M concentrations of various electrolytes; a)  $\text{H}_2\text{SO}_4$ , b)  $\text{HCl}$ , c)  $\text{HNO}_3$ , and d)  $\text{HClO}_4$  (-0.16 to 0.96 V ;  $100 \text{ mV s}^{-1}$  for 20 cycles).

**Table 4.2:** Redox potentials and current peaks of PANI films deposited from different acidic electrolytes.

Polymer growth from 1 M	Coverage $\Gamma$ mol cm <sup>-2</sup>	Thickness of polymer nm	pH of solution with 0.2 M aniline	Anodic current (i / $\mu$ A)		Anodic potentials (V)		
				I	II	I	II	
a	H <sub>2</sub> SO <sub>4</sub>	1.167 $\times$ 10 <sup>-6</sup>	905	0.27	320	324	0.26	0.87
b	HCl	4.00 $\times$ 10 <sup>-7</sup>	310	0.5	122	125	0.26	0.85
c	HNO <sub>3</sub>	1.383 $\times$ 10 <sup>-7</sup>	107	0.6	54	55	0.25	0.84
d	HClO <sub>4</sub>	5.77 $\times$ 10 <sup>-8</sup>	45	0.7	11	13	0.23	0.84

#### 4.3.3 Effect of background/DES electrolytes on PANI stability and reversibility

In the previous section, we discussed the means by which the electropolymerisation of aniline is dependent on the nature of the anion present in the solution; here we want to characterise the behaviour of those polymers in the same background electrolytes (monomer free) and DESs. The idea here is that each film in **Figure 4.2** is exposed to a similar background electrolyte (i.e. grown in the same monomer-free acid), then transferred to a DES (Ethaline), and finally returned to the first background electrolyte to see if any chemical or physical changes have occurred during the electrochemical process in these systems. All polymers were washed several times with deionised water before subsequent transfer into another electrolyte. Before further discussion of the results below, it should be noted that the polymers have different thickness (see **Table 4.2**), and this will certainly affect their stabilities in the aqueous and DES solutions. The potential windows of the CVs responses for these films were -0.16 V to 0.96 V versus Ag/AgCl (sat. KCl) in the various aqueous solutions, and with an Ag wire in Ethaline.

According to the voltammetric results shown in **Figure 4.3**, we can see several similarities and differences. In the case of the similarities, the current peaks of the polymers cycled in original acid solutions first are similar to those current peaks of the polymer that was grown. It can also be shown that the oxidation peaks are sharp in aqueous solutions (except PANI-HClO<sub>4</sub>) whilst being broad in Ethaline. In addition, the peak potentials of films cycled in all acid electrolytes seems to be very similar. On the other hand, PANI films show the potential peaks shift about 150 mV toward the positive side in the Ethaline electrolyte. This may be a function of Ethaline being able to drive

the proton transfer reaction in this manner, depending on the pH<sup>33, 34</sup> of the medium and the different reference electrodes used in the two media. The activity in terms of current and charge is less in Ethaline than acid media. This is often due to the viscosity of Ethaline being about 40 times greater than that of aqueous acids (see viscosity measurements in section 5.3.1.1 and **Table 9.1** in Appendix) and, consequently, large species have a lower flux through the net of polymer films. As a result, the rate of electrochemical response in the films will decrease during successive potential cycling.<sup>29</sup>

Polymer cycled in H<sub>2</sub>SO<sub>4</sub> shows current peaks and charge values higher than in other samples; we observe that the current peaks and charge values take the following order: PANI-H<sub>2</sub>SO<sub>4</sub> > PANI-HCl > PANI-HNO<sub>3</sub> > PANI-HClO<sub>4</sub>. This is a possible result of the polymers being grown in these different electrolytes (i.e. different anions) showing variations in growth rate and, thus, different thicknesses in the layer deposited on the Pt electrode, which then follow the order given above. The electrochemical stability of each polymer has been determined according to the charge values that were obtained from the polymer cycled in electrolytes. It is clear that polyaniline grown and cycled in H<sub>2</sub>SO<sub>4</sub> has the lowest stability in comparison with polyaniline grown and cycled in HClO<sub>4</sub>, which has the highest stability compared to other films. This is in agreement with previous findings in the literature,<sup>5, 29</sup> according to the order SO<sub>4</sub><sup>2-</sup> < Cl<sup>-</sup> < NO<sub>3</sub><sup>-</sup> < ClO<sub>4</sub><sup>-</sup>. This could be related to the growth conditions of the polymer or the nature of the relevant anion in solution. In order to understand which anions have the greatest effect on the electrochemical stability of polyaniline in an electrolyte, it would be better compare polymers of the same thickness in order to determine whether the electrochemical response can be affected by electrochemical condition or by the mobility of these anions in solution (see section 4.3.4).

However, regardless of the acid used, there is no significant chemical change when the polymer is returned to the relevant aqueous acid because the polymers regenerate to the original electrochemical response. In general, the stability and electroactivity of all films are better after the film has been returned to the original acid (i.e. after being cycled in Ethaline electrolyte), as can be seen in **Table 4.3**. This is possibly due to the morphology of the polymer becoming more porous after being transferred to Ethaline as a result of the large ionic radii of the anions/cations in this solvent, leading to an increase in the number and volume of voids between the polymeric chains. Therefore,

the mobility of ions in aqueous solution subsequent to being transferred out of Ethaline is, relatively speaking, increased, and consequently presents less of an obstruction for ions during the redox process.

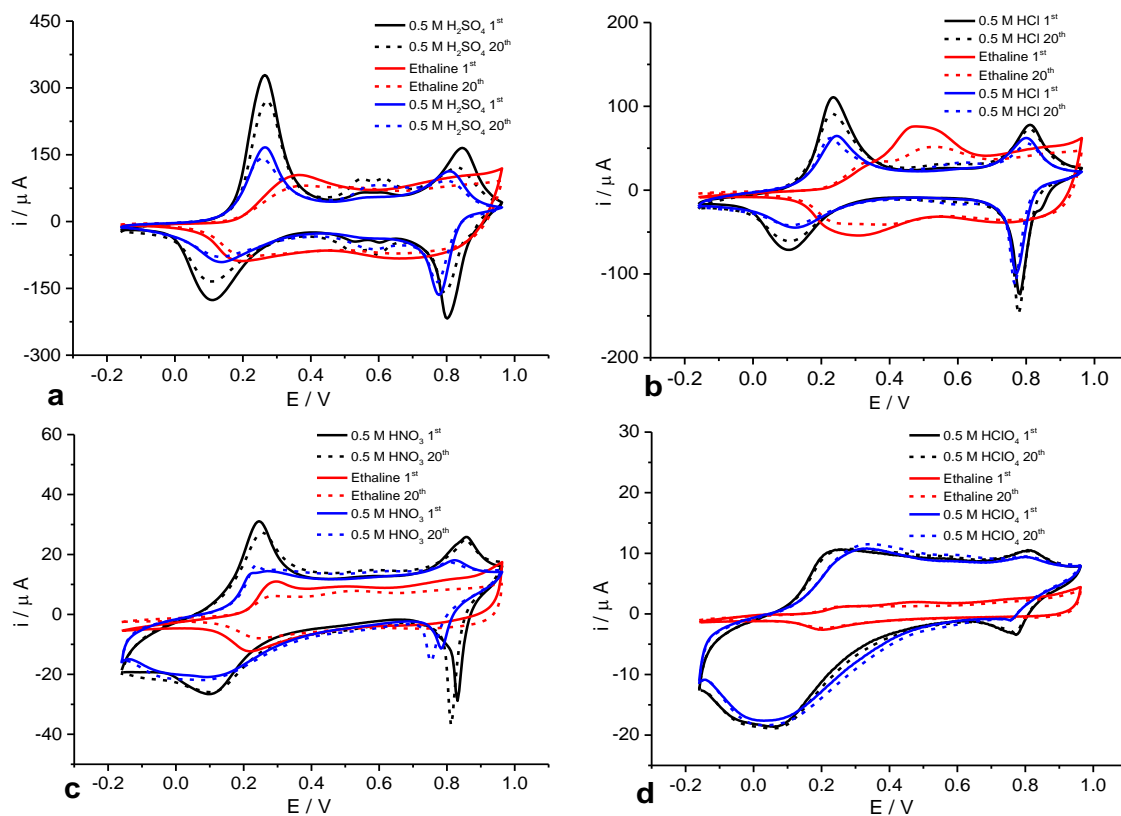


**Figure 4.3:** Voltammetric responses for polyaniline films (Figure 4.2) exposed to background electrolyte (monomer free), Ethaline and then returned to background electrolyte; these are, respectively; a) 0.5 M  $\text{H}_2\text{SO}_4$ , b) 0.5 M  $\text{HCl}$ , c) 0.5 M  $\text{HNO}_3$ , and d) 0.5 M  $\text{HClO}_4$  (-0.16 to 0.96 V;  $100 \text{ mV s}^{-1}$ ), cycles 1 and 20 are shown.

**Table 4.3:** Charge reduction values of PANI (Figure 4.2) exposed to background electrolyte (monomer free), Ethaline and then when returned to the original background electrolyte, respectively.

Electrolytes (free monomer)	Q/C <sub>red</sub> 1 <sup>st</sup> cycle	Q/C <sub>red</sub> 20 <sup>th</sup> cycle	% Q <sub>red</sub> retention 20 <sup>th</sup> /1 <sup>st</sup> cycle	% Q <sub>red</sub> average retention	
<b>a</b>	0.5 M H <sub>2</sub> SO <sub>4</sub>	6.594×10 <sup>-4</sup>	5.752×10 <sup>-4</sup>	87	<b>68</b>
	Ethaline	5.632×10 <sup>-4</sup>	5.130×10 <sup>-4</sup>	91	
	0.5 M H <sub>2</sub> SO <sub>4</sub>	4.664×10 <sup>-4</sup>	4.547×10 <sup>-4</sup>	97	
<b>b</b>	0.5 M HCl	2.108×10 <sup>-4</sup>	1.791×10 <sup>-4</sup>	84	<b>70</b>
	Ethaline	2.758×10 <sup>-4</sup>	2.555×10 <sup>-4</sup>	92	
	0.5 M HCl	1.495×10 <sup>-4</sup>	1.489×10 <sup>-4</sup>	99	
<b>c</b>	0.5 M HNO <sub>3</sub>	4.101×10 <sup>-5</sup>	3.853×10 <sup>-5</sup>	93	<b>94</b>
	Ethaline	3.380×10 <sup>-5</sup>	3.379×10 <sup>-5</sup>	99	
	0.5 M HNO <sub>3</sub>	3.680×10 <sup>-5</sup>	3.861×10 <sup>-5</sup>	104	
<b>d</b>	0.5 M HClO <sub>4</sub>	3.791×10 <sup>-5</sup>	3.615×10 <sup>-5</sup>	95	<b>98</b>
	Ethaline	6.036×10 <sup>-6</sup>	5.960×10 <sup>-6</sup>	98	
	0.5 M HClO <sub>4</sub>	3.508×10 <sup>-5</sup>	3.718×10 <sup>-5</sup>	105	

#### 4.3.4 Effect of different anions on PANI film stability at constant thickness

In this section, we consider the answer the last question above, that of whether the stability of the film is affected by either the polymerisation conditions or by the nature of the ions present in the solution. The requirement here is that PANI films have a similar thickness (in terms of polymer coverage) depending on the charge values.

From our previous studies, polymers grown in H<sub>2</sub>SO<sub>4</sub> and HClO<sub>4</sub> have been chosen based on the differences between their relative growth rates and the best electrochemical stability in different electrolytes (see sections 4.3.2 and 4.3.3). Each polymer was potentiodynamically synthesised in 1 M solutions of the appropriate acid/ 0.2 M aniline with potential windows of -0.16 to 0.96 V and scan rates of 100 mV s<sup>-1</sup>. The thickness of each polymer was controlled by the number of scans (PANI-H<sub>2</sub>SO<sub>4</sub> 20 scans and

PANI-HClO<sub>4</sub> 152 scans) as depending on the values of cathodic charge. As a consequence, the thickness of polyaniline film grown from H<sub>2</sub>SO<sub>4</sub> and HClO<sub>4</sub> were 857 nm and 843 nm, respectively, which is approximately equal. After depositing each film independently, it was cycled in different acid electrolytes (different anions) starting with original acid solutions. In other words, the film was exposed to the same supporting electrolytes as those used for deposition of PANI film electrodes, as well as various other anion electrolytes.

In the case of PANI-H<sub>2</sub>SO<sub>4</sub>, the film was cycled in 0.5 M H<sub>2</sub>SO<sub>4</sub>, HCl, HNO<sub>3</sub>, and HClO<sub>4</sub>, respectively, for 20 scans at scan rate of 100 mV s<sup>-1</sup>. From the charge values (see **Table 4.4**), PANI-H<sub>2</sub>SO<sub>4</sub> is more stable in the perchlorate electrolyte (99 %) and less stable in sulphate (93 %). The electrochemical stability of PANI-H<sub>2</sub>SO<sub>4</sub> in these solutions takes the following order: HClO<sub>4</sub> > HNO<sub>3</sub> > HCl > H<sub>2</sub>SO<sub>4</sub>. Similar observations were made for PANI-HClO<sub>4</sub>, which was also cycled in 0.5 M HClO<sub>4</sub>, HCl, HNO<sub>3</sub>, and H<sub>2</sub>SO<sub>4</sub>, respectively for 20 scans at 100 mV s<sup>-1</sup>. The associated charge values (see **Table 4.4**) indicate that PANI-HClO<sub>4</sub> is also more stable in the perchlorate electrolyte (99 %) and less stable in sulphate (91 %). The electrochemical stability of PANI-HClO<sub>4</sub> in these solutions takes the following order: HClO<sub>4</sub> > HNO<sub>3</sub> > HCl > H<sub>2</sub>SO<sub>4</sub>; these results are in reasonable conformity with previous reports in the literature.<sup>5, 29</sup> Our experimental data show that both electrochemical formation and the stability of the film in the electrolyte depends strongly on the nature of anion present in solution. The reason behind the difference in the stability values can be attributed to the fact that the perchlorate anion is the most lyophilic whilst the sulphate anion is the most hydrophilic. Therefore, perchlorate anions form the most stable ion pairs with the anilinium ions during redox cycling.

Generally, we can conclude from the results above that counter-ions that allow for high stability of the polymer in solution (in the order ClO<sub>4</sub><sup>-</sup> > NO<sub>3</sub><sup>-</sup> > Cl<sup>-</sup> > SO<sub>4</sub><sup>2-</sup>), show the opposing behaviour for growth rate, i.e. lower polymerisation current (in the order ClO<sub>4</sub><sup>-</sup> < NO<sub>3</sub><sup>-</sup> < Cl<sup>-</sup> < SO<sub>4</sub><sup>2-</sup>) and *vice versa*.

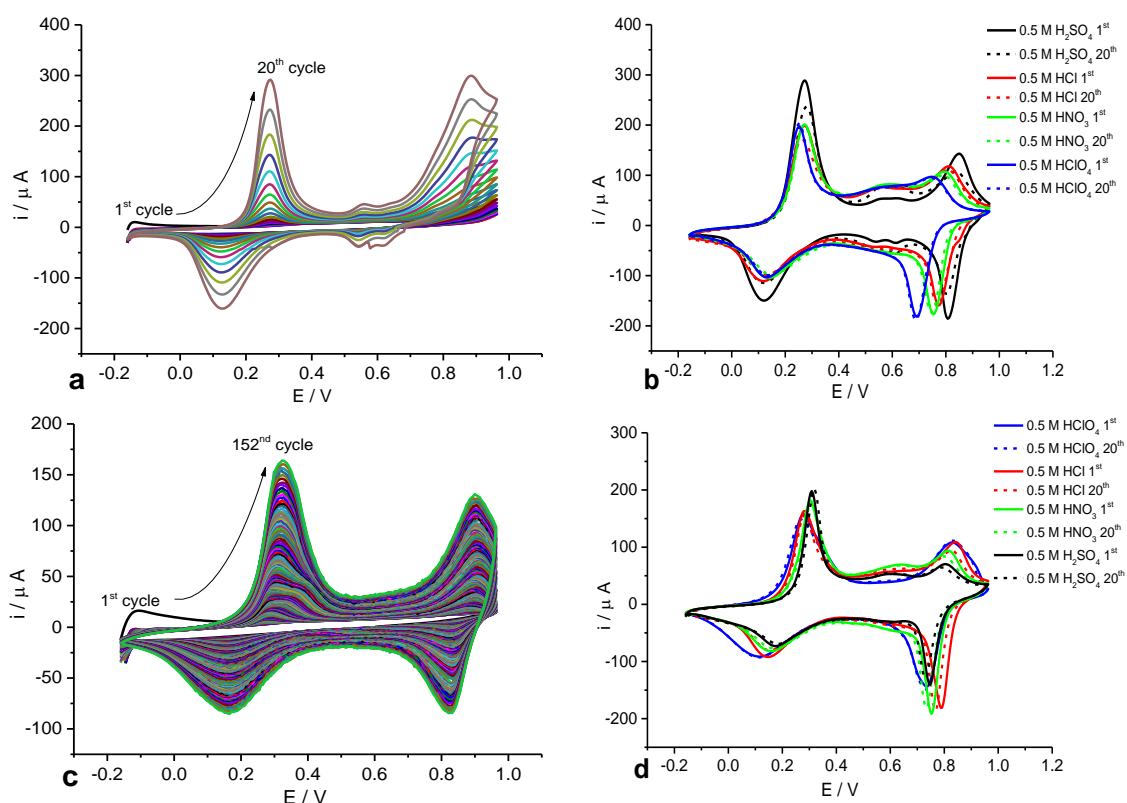


**Figure 4.4:** Cyclic voltammogram for the preparation of PANI film deposited potentiodynamically from 0.2 M aniline in electrolytes; a) 1 M  $H_2SO_4$  and c) 1 M  $HClO_4$  (-0.16 to 0.96V;  $100\text{ mV s}^{-1}$ ). Panels b) and d) show PANI films of a) and c) exposed to different acid electrolytes (monomer free), (-0.16 to 0.96 V;  $100\text{ mVs}^{-1}$ ); cycles 1 and 20 are shown. Colours indicate the electrolytes used.

**Table 4.4:** Charge reduction values of PANI panels (a) and (c) in Figure 4.4 exposed into different acid electrolytes (monomer free).

PANI films made	PANI cycled in electrolytes (monomer free)	$Q/C_{red}$ 1 <sup>st</sup> cycle	$Q/C_{red}$ 20 <sup>th</sup> cycle	% $Q_{red}$ retention 20 <sup>th</sup> /1 <sup>st</sup> cycle
1M $H_2SO_4$	0.5 M $H_2SO_4$	$4.819 \times 10^{-4}$	$4.516 \times 10^{-4}$	93
	0.5 M HCl	$4.473 \times 10^{-4}$	$4.251 \times 10^{-4}$	95
	0.5 M $HNO_3$	$4.815 \times 10^{-4}$	$4.746 \times 10^{-4}$	98
	0.5 M $HClO_4$	$4.728 \times 10^{-4}$	$4.725 \times 10^{-4}$	99
1M $HClO_4$	0.5 M $HClO_4$	$4.455 \times 10^{-4}$	$4.453 \times 10^{-4}$	99
	0.5 M HCl	$4.090 \times 10^{-4}$	$3.871 \times 10^{-4}$	94
	0.5 M $HNO_3$	$4.193 \times 10^{-4}$	$4.013 \times 10^{-4}$	95
	0.5 M $H_2SO_4$	$3.403 \times 10^{-4}$	$3.123 \times 10^{-4}$	91

### **4.3.5 Morphology and topography of the polymer films**

#### **4.3.5.1 Scanning Electron Microbalance (SEM)**

The scanning electron micrographs of the PANI films synthesised in different acidic electrolytes can be seen in **Figure 4.5**. These films are grown potentiodynamically between -0.16 V and 0.96 V at  $100 \text{ mV s}^{-1}$  for 20 cycles. It can be seen that the images shown in panels a, b and c show greater formation of polymer deposit on the electrode surface and, also, their morphologies show an open structure with homogenous fibrous shapes due to the regulation of their growth rates; in comparison, PANI-HClO<sub>4</sub> showed a very smooth layer of polymer with much smaller particles, and the electrode surface seemed uncovered. It was also found that the porosity of these films varies, even though the SEM images of the dry films showed their morphologies were essentially identical in terms of shape (i.e. fibrous). The differences in porosity arise from different anions used in the electrolyte, which leave different sized voids in the associated polymer networks. However, film grown from sulphuric acid media showed more voids between the associated polymeric chains, even though the thickness of the polymer was higher than in other films (because an increase in the thickness of the polymer leads to a decrease in porosity). This might be because during the nucleation and growth process, the thickness is dependent on the nature and size of the ion present in solution, as reported by Cordova *et al.*<sup>30</sup> It seems possible that the morphology and structure of the film can be affected during electrochemical polymerisation by the size of anion present in solution forming larger or smaller holes in the polymer surface.<sup>35</sup> This fact is confirmed by AFM images (**Figure 4.6**) as a result of differences in the thickness, roughness and size of the nodules observed. We also believe that these effects are due to the significant differences in the electron transfer reaction of the polymerisation process, which would be faster in H<sub>2</sub>SO<sub>4</sub> than in HCl, HNO<sub>3</sub> and HClO<sub>4</sub>, respectively, as shown in **Figure 4.2**. This behaviour affects the rate of polymer growth, resulting in different morphologies. Therefore, rapidly grown polymers have an open structure, as observed for H<sub>2</sub>SO<sub>4</sub>, HCl and HNO<sub>3</sub>, whereas the HClO<sub>4</sub>-doped sample has a more compact and smooth structure owing to much slower growth.<sup>5</sup>

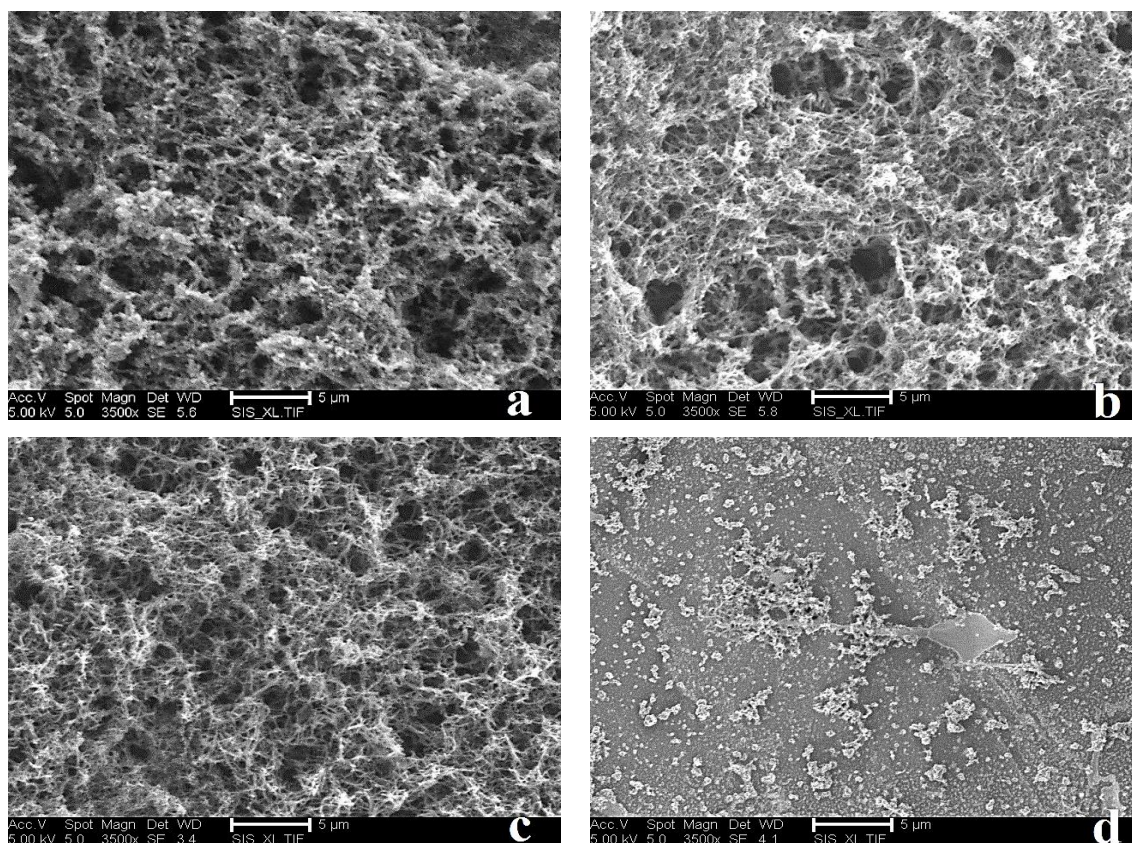


**Figure 4.5:** SEM images of PANI films synthesised with 0.2 M aniline in 1 M of a)  $H_2SO_4$ , b)  $HCl$ , c)  $HNO_3$ , and d)  $HClO_4$  between  $(-0.16$  to  $0.96$  V ;  $100$   $mV$   $s^{-1}$ ) for 20 scans on a Pt electrode (1 mm diameter).

#### 4.3.5.2 Atomic Force Microscopy (AFM)

AFM was employed to characterise the surface and thickness of the polyaniline films obtained from the different [acidic] electrolytes (see **Figure 4.6**). Actually, there are many parameters that affect the surface of polymers, such as concentration of monomer, scan rate, scan number and potential windows, but all these factors were negligible in this instance. The visual comparison was focused on nodule size and an analysis of the roughness of the polymers surfaces, which are the results of using different acids. It was clear that the PANI- $H_2SO_4$  surface displays large nodule sizes in most regions as well as a number of pores, and also a higher roughness compared to the other films formed in  $HCl$ ,  $HNO_3$  and  $HClO_4$ , while the topography of the PANI- $HClO_4$  film shows the smoothest surface (essentially flat). The large nodules of film can be related to a more rapid growth of the polymer under the greater driving force of the current peak. Or, in other words, the differences in nucleation and growth features can be attributed to the amount of charge obtained during the deposition process of these films. From these

observations, it can be concluded that the nucleation and growth mechanism for electropolymerisation of aniline raises interesting subjects for further study, such as the influence of various electrolytes, applying different potential windows and the concentration of the monomer. Here, the results indicate that grain sizes are obviously changed by used different functionalised acid solutions, so it is clear that the resultant morphology depends strongly on the electrolytic medium.

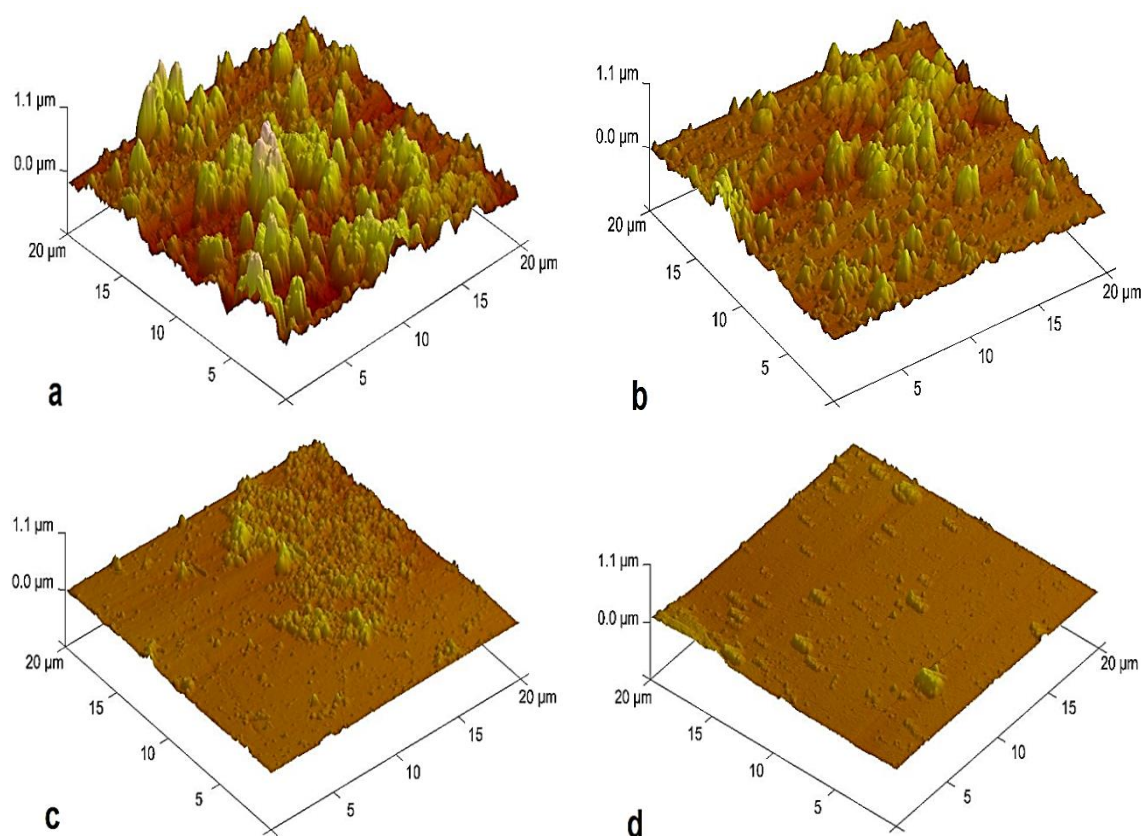


**Figure 4.6:** AFM images of dry PANI electrodeposited from 0.2 M aniline dissolved in 1 M a)  $H_2SO_4$ , b)  $HCl$ , c)  $HNO_3$ , and d)  $HClO_4$  on a Pt electrode (1 mm diameter). Cyclic (-0.16 to 0.96 V;  $100\text{ mVs}^{-1}$ ) for 20 scans.

The average thicknesses of the dry polymer films were estimated using the AFM technique. A scalpel blade was used to carefully remove PANI film from part of a Pt electrode surface, forming a step edge between the film and substrate, as shown in **Figure 4.7** (panels a and b). The outcomes here can be compared with the thickness of polymers determined from charge integration for use the Faraday's Law method. In both methods, the thickness measurements show a slight difference in the two methods (see **Table 4.5**). These observed differences are perhaps due to non-uniform coverage across the available deposition area, instrumental bias, and possibly the presence of

some residual water molecules from the electrolytes, all of which would clearly affect any determination of the true thickness of the polymer film.

Furthermore, the thickness of the polymer depends on various factors such as the composition of the synthesis solutions, which are affected by the amount of charge. In particular, the film grown from the  $\text{H}_2\text{SO}_4$  electrolyte shows a greater thickness and more current density features (i.e. grains) than the films grown from  $\text{HCl}$ ,  $\text{HNO}_3$  and  $\text{HClO}_4$ . This is possibly caused by the charge passed during the growth of the PANI- $\text{H}_2\text{SO}_4$  polymer being larger than in the other films, resulting in a rougher surface. A linear plot of polymer film roughness versus the amount of charge produced by polymerisation of these samples using similar conditions (differing only in the kind of electrolyte solution), is illustrated in **Figure 4.7c**. It is well known that controlling the polymerisation charge makes it possible to control the resultant roughness and thickness of the polymer layer.

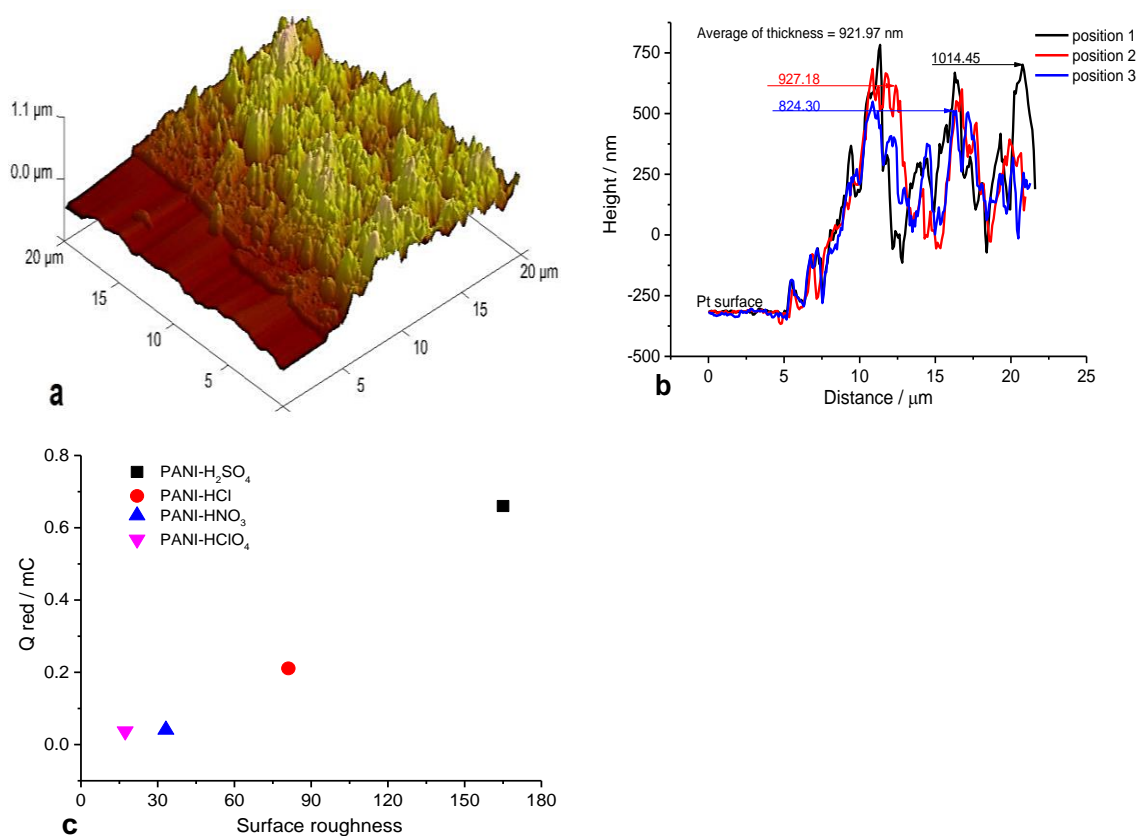


**Figure 4.7:** AFM thickness of PANI film from Figure 4.6 (panel a), b); thickness of film (panel a) measured by AFM and c); charge vs. surface roughness of PANI films.

**Table 4.5:** Thickness of polyaniline films measured by AFM and comparison with those calculated from charge by using Faraday's Law.

PANI films		Thickness (nm) by CVs	Average thickness (nm) by AFM	Roughness (nm) by AFM
a	H <sub>2</sub> SO <sub>4</sub>	905	921	165
b	HCl	310	316	81
c	HNO <sub>3</sub>	107	139	33
d	HClO <sub>4</sub>	45	59	17

#### **4.3.6 Selection of polymer for further studies**

The performance of any electrochemical device is most commonly denoted in terms of I/E output (i.e. a cyclic voltammogram). Here, polyaniline prepared from H<sub>2</sub>SO<sub>4</sub> was used in EQCM studies. The reason for selecting this film was on the basis of the calculation of the charge passed (promising in terms of future charge storage applications); rough surface topography (greater porosity) as well as the initial observations of the polymer film stability. The greater polymerisation rate observed in H<sub>2</sub>SO<sub>4</sub> voltammetric experiments allows for improving this polymer for electronic and optical applications.

The aim in using EQCM is to characterise PANI films in order to understand the correlation between film structure, composition and dynamics. Furthermore, we focus on how conducting polymers behave in aqueous and DES electrolytes during the motion of mobile species between the film and electrolyte via the related change in a mass of rigid film.

#### **4.3.7 Characterisation of the behaviour of PANI using EQCM technique**

##### **4.3.7.1 Growth of PANI Film**

The deposition of the film was carried out using 0.1 M aniline in 1 M H<sub>2</sub>SO<sub>4</sub> by applying a voltage window from -0.16 V to 0.96 V vs. Ag/AgCl (sat. KCl) at a scan rate of 10 mV s<sup>-1</sup> for three cycles, as shown in **Figure 4.8**. After the film deposition onto a 10 MHz AT-cut Pt polished quartz crystal, the experiment was stopped at the reduced

end of the potential cycle ( $E = -0.16$  V) and thoroughly washed with deionised water. The  $i$  vs.  $E$  curve of panel (a) in **Figure 4.8** is same as those reported recently in the literature.<sup>4-6</sup> In this panel, it can be seen that the redox current of the film rises continuously with the increasing number of scans, which implies an autocatalytic reaction is occurring during the electropolymerisation process. The mass change of panel (b) in **Figure 4.8** increased when the voltage reached the polymerisation point  $\sim 0.9$  V because the current peak starts to increase at this point. The mass increase is indicated by the decrease in frequency due to the progressive deposition of polymer with the increasing the number of cycles.

Prior to measuring mass change in electrochemical experiments in monomer-free electrolytes, admittance spectra were recorded as a diagnostic to determine whether the film was showing acoustically 'rigid' (i.e. acoustically thin) behaviour or a non-rigid (i.e. viscoelastic) behaviour in order to use the Sauerbrey equation for gravimetric analysis. It is well known that the quantitative information (mass loading) determined for film can be classified as rigid if its mass lower than 2% of the mass of the quartz plate.<sup>36</sup> In this regard, the mass deposited can be determined by measuring the shift in resonance frequency before and after growth (dry polymer) in air. The resonant frequency of the PANI-loaded crystal is shifted to lower frequency than for the unloaded crystal; the observed difference was 4400 Hz, as seen in panel (d) of **Figure 4.8**. According to the Sauberbery equation, the coefficient between the change of the resonant frequency ( $\Delta f$ ) and the change of mass of the surface layer ( $\Delta m$ ) (within  $\pm 2$  %) for the 10 MHz *AT*-cut quartz crystal used is:  $\Delta m$  (g) =  $-1.1 \times 10^{-9}$   $\Delta f$  (Hz).<sup>37</sup> The change in frequency,  $\Delta f$ , with respect to the reference frequency,  $f_0$ , is related to the additional mass on the crystal due to polymer deposition,  $\Delta m$ , through the Sauerbrey equation. From this equation, the weight of the dry PANI film was found as 4840 ng and the thickness as 175 nm, which are close to the results calculated from the CV method. Normally, a film thickness of about 2  $\mu\text{m}$  or less readily satisfies the necessary criteria to use the Sauerbrey equation, as presented by Hillman *et al.*<sup>38</sup>

The growth behaviour of the polymer deposition has been studied using the admittance spectra illustrated in panel (c) of **Figure 4.8**. The admittance peak reduced by 13 % in the deposition electrolyte due to added mass. There was very little shift and change in peak admittance, but the film was still rigid and the results of acceptable validly for use

in the Sauerbrey equation. Further, the Q factor did not change significantly, meaning that the added mass was both rigidly coupled to, and small, compared to the mass of the crystal.<sup>39</sup> In this work, the admittance-frequency graph has been utilised to characterise the validity of the Sauerbrey equation of an acoustically thin film, for frequency shift can be interpreted gravimetrically.<sup>3</sup>

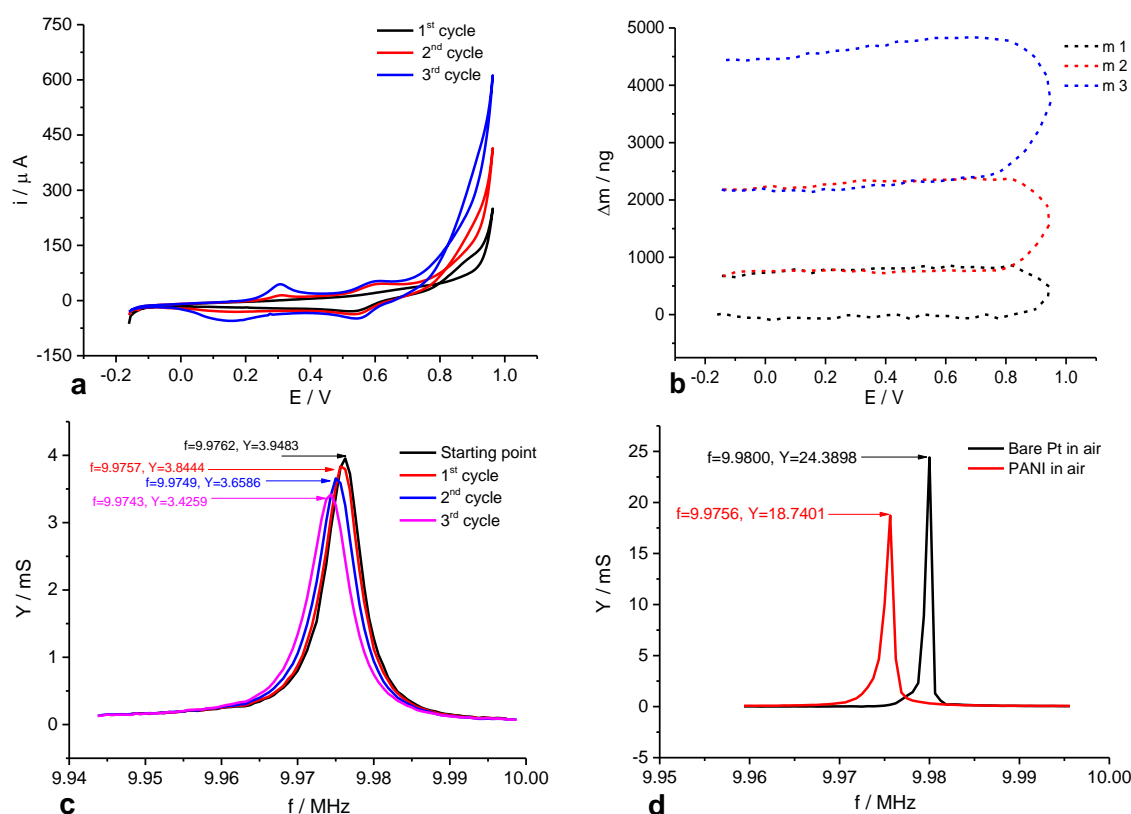


**Figure 4.8:** EQCM data for the deposition of a PANI film ( $\Gamma = 229 \text{ nmol cm}^{-2}$ ) potentiodynamically ( $-0.16 \text{ V}$  to  $0.96 \text{ V}$ ; at  $10 \text{ mV s}^{-1}$ ) from  $0.1 \text{ M}$  aniline/ $1 \text{ M}$   $\text{H}_2\text{SO}_4$ , 3 scans. a)  $i$  vs.  $E$ ; b)  $\Delta m$  vs.  $E$ ; c) crystal admittance spectra,  $Y/\text{mS}$  vs.  $f/\text{MHz}$ , recorded for PANI at the end of each cycle and d);  $Y/\text{mS}$  vs.  $f/\text{MHz}$  for the bare crystal and PANI-loaded crystal in air.

**Table 4.6:** The mass, thickness and surface coverage calculated by EQCM and CV for deposited polyaniline.

PANI sample	Mass ng	Thickness nm	$\Gamma$ $\text{nmol cm}^{-2}$
EQCM	4840	175	225
CV	4903	177	229

Admittance spectra of loaded and unloaded crystals have been studied in different electrolytes. Panel (a) of **Figure 4.9** shows the admittance spectra for the quartz resonator of a film before and after growth in 0.5 M H<sub>2</sub>SO<sub>4</sub> and deposition solution. The admittance peak of the loaded quartz resonator in aqueous electrolyte dropped by 7 % compared with the unloaded. The damping in the admittance peak and shift in resonant frequency is a result of the mass of PANI deposited on the electrode. The characterisation of the viscoelastic properties of PANI was also investigated in Ethaline at both room temperature and at 50°C. It was observed that there was a small decrease in admittance 7 %, which indicates that the film is acoustically thin in Ethaline, as shown in panel (b) of **Figure 4.9**. PANI film in Ethaline shows a lower dissipation of acoustic energy than aqueous solutions due to the higher viscosity of Ethaline, which means the acoustic delay length is proportional to viscosity. On the other hand, the admittance peak in Ethaline at 50°C is higher than in Ethaline at room temperature, with an associated decrease in admittance of about 2 %. This is due to decreasing viscosity with increasing temperature.

All PANI films grown by EQCM in this chapter can be classed as being rigid, having approximately the same surface coverage (due to identical growth conditions), as discussed in **Figure 4.8** c and d, hence it is not essential for this to be presented in this thesis. Generally, the physical-chemical interactions between the film and the medium can be affected by solvent polarity, density, viscosity and the polymer structure and oxidation state, as well as the relative proportions of the ‘open’ and ‘compact’ structures within the polymer film, as confirmed by Randriamahazaka *et al.*<sup>40</sup>

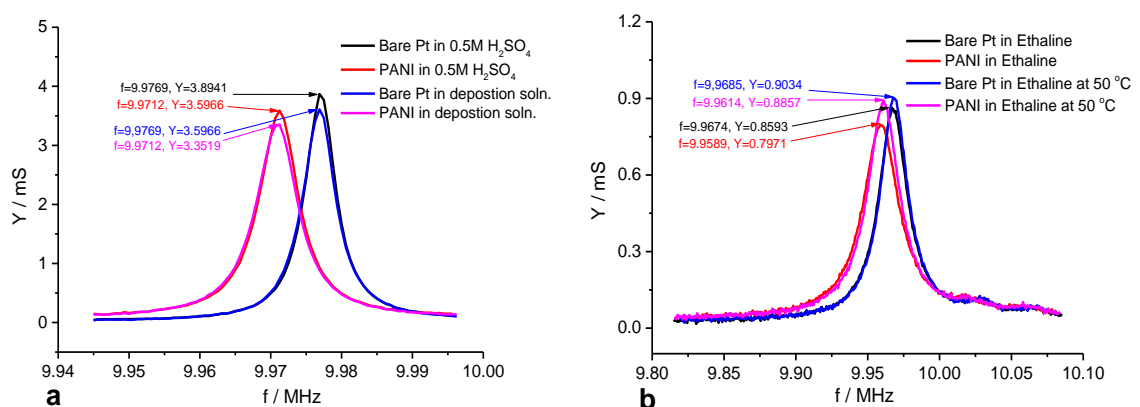


**Figure 4.9:** Acoustic admittance spectra for the bare crystal and PANI-loaded crystal: a) in 0.5 M H<sub>2</sub>SO<sub>4</sub> and deposition electrolyte (0.1 M aniline/1 M H<sub>2</sub>SO<sub>4</sub> aqueous solution) and b); in Ethaline and Ethaline at 50°C. The results are for film ( $\Gamma = 229 \text{ nmol cm}^{-2}$ ).

#### **4.3.7.2 Characterisation of the mass transfer of the film in different solutions using EQCM**

##### **4.3.7.2.1 Effects of wide potential windows on PANI redox cycling**

After washing the polymer (see section 4.3.7.1) with deionised water several times, the prepared film was cycled in various solutions (monomer free) in three steps aqueous, DES and aqueous electrolytes, respectively to explore PANI p-doping dynamics and, thus, to detect the influences of various media on the viscoelastic behaviour of the film during oxidation and reduction cycling. The scan rate was  $10 \text{ mV s}^{-1}$  with an applied voltage of fully reduced film of  $E = -0.16 \text{ V}$  and scanning to fully positive potentials ( $E = 0.96 \text{ V}$ ). The reference electrode was AgCl (saturated KCl) for all PANI film potentials cycled in aqueous solutions with respect to Ag wire in DES. In the beginning, the deposited film was transferred to the same background electrolyte ( $0.5 \text{ M H}_2\text{SO}_4$ ) under the conditions mentioned above, as shown in **Figure 4.10**. It is clear that there is no important change in the mass (linear) in the first stages of the oxidation reaction and this is maybe because a relatively low current is measured. As the polymer is oxidised, the mass starts to increase dramatically at the oxidation point of PANI (ca.  $0.25 - 0.3 \text{ V}$ ). This indicates that the anions ( $\text{SO}_4^{2-}$ ) insert into the film due to the electron/proton that has been removed in the early stages to maintain electroneutrality. The reverse process occurs during the reduction reaction of the film. Prior to replacing PANI from the aqueous acidic solution to Ethaline 200, the film was rinsed with deionised water several times followed by hot Ethaline in order to remove any residual aqueous solution from the voids in the PANI films. In Ethaline 200, the polymer was cycled at  $50^\circ\text{C}$  to reduce the viscosity of electrolyte. The redox potential has been shifted about  $200 \text{ mV}$  towards the positive side and thus the value of the anodic peak is much lower than for the first electrolyte ( $0.5 \text{ M H}_2\text{SO}_4$ ), as shown in panel (a) of **Figure 4.10**. This is possibly due to the diffusion rates for anionic and cationic transfer being affected by the high viscosity of Ethaline compared to aqueous solution. In terms of the mass change of the polymer in Ethaline, it is apparently opposite to that observed in the aqueous solution. Mass change was decreased during the oxidation of the film due to expulsion of cations ( $\text{Ch}^+$ ), while the mass was increased during the reduction, implying the insertion of cations ( $\text{Ch}^+$ ) into the film. This is consistent with the behaviour of pyrrole in Ethaline observed by Hillman *et al.*<sup>41</sup>

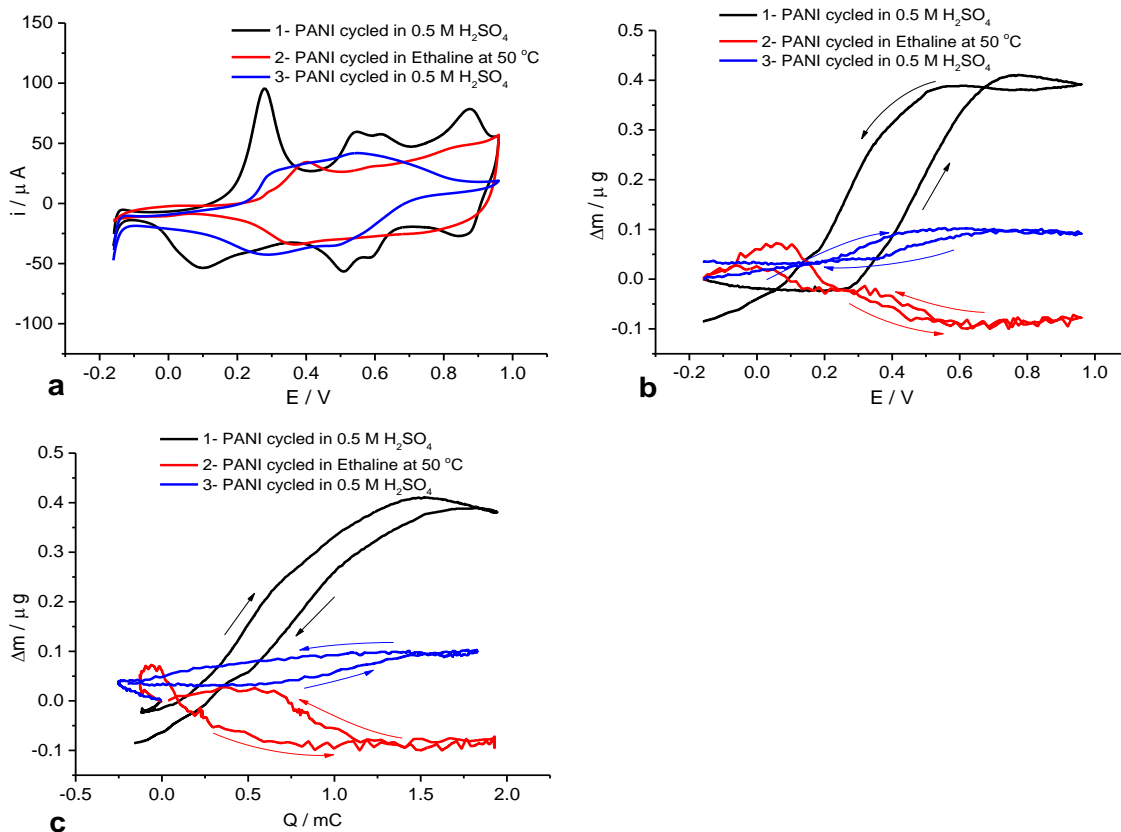


**Figure 4.10:** EQCM data for redox switching of PANI film ( $\Gamma = 229 \text{ nmol cm}^{-2}$ ) exposed to 0.5 M H<sub>2</sub>SO<sub>4</sub>, Ethaline at 50°C and 0.5 M H<sub>2</sub>SO<sub>4</sub>, respectively, at 10 mV s<sup>-1</sup> scan rates. a)  $i$  vs.  $E$ ; b)  $\Delta m$  vs.  $E$ ; c)  $\Delta m$  vs.  $Q$ . The arrows indicate the direction of the changes.

In order to understand the electrochemical response of the polymer in different environments (aqueous and non-aqueous electrolytes), the film was returned to the first electrolyte (0.5 M H<sub>2</sub>SO<sub>4</sub>) it was cycled in. The result clearly showed that the mass change behaviour in the latter case was similar to that observed in the first (H<sub>2</sub>SO<sub>4</sub>) (i.e. the mass response shows a significant increase in the film upon oxidation process, whereas in the reduction process, these trends and changes are reversed). However, we note that the anodic current peaks do not return to their initial values after cycling. In the other words, the electroactivity of the polymer was reduced to almost half its initial value. The failure of the film to return to the same physical state could be for two reasons. The first reason is that the porosity of polymer is likely to be reduced due to the large size of anions and cations of the Ethaline remaining in the net of polymer (a significant memory effect). The second, which might be the more probable, is that a

more oxidised form of PANI at anodic potentials owing to its unstable (pernigraniline) state is present, leads to acid catalysed degradation of the film.<sup>6, 11</sup>

The dynamics behaviour of the species exchanged during redox cycling has been investigated to monitor the evolution of the PANI films. The quantification of the molar mass ( $M_{app}$ ) of counter ions during the PANI redox process can be calculated from the slope of a plot of mass values versus charge.  $M_{app}$  is defined in equation 4.9:

$$M_{app} = zF \left( \frac{\Delta m}{\Delta q} \right) \quad 4.9$$

where  $z$  is the charge of the ions exchanged and  $F$  is the Faraday's constant (96485 C mol<sup>-1</sup>). As  $z$  and  $F$  are constants, the  $M_{app}$  value can be found as the gradient to a plot of mass change vs. the charge ( $\Delta m/\Delta q$ ).

The disagreement in the eventual molar mass values of ions exchanged with the anions and cations that are presented in solution during the redox process is related to the flux of solvent and/or co- and counter ions (in the opposite direction). Generally,  $M_{app}$  values in aqueous solutions are defined as the sum of the molar masses of mobile species conveyed across the polymer/solution interface. Contributions to  $M_{app}$  were possible from *any* mobile species present; these can be anions ( $M_{Anion}$ ), cations ( $\beta M_{Cation}$ ) and/or solvent molecules ( $\alpha M_{Solvent}$ ), as shown in equation 4.10:

$$M_{app} = M_{Anion} + \alpha M_{Solvent} + \beta M_{Cation} \quad 4.10$$

where  $M_{Anion}$ ,  $M_{Solvent}$  and  $M_{Cation}$  are the molar masses of the anion, solvent and cation, respectively, and  $\alpha$  and  $\beta$  are constants representing the number of solvent and cation molecules transferred per anion, respectively.<sup>14, 42</sup>

Equation 4.10 is unresolved as there are more variables than measurements, and this process is called the *underdetermined problem*, therefore the easiest method will be employed, determining the origin of  $M_{app}$ , as this will tend to be the most reasonable, and feasible, scenario. With the one parameter, either anion or cation, equated to zero in equation 4.10 due to the anion/cation being absent, as well as assuming the anion/cation constants to be equal to 1, it becomes possible to determine the parameter  $\alpha$ , the number of transferred solvent molecules for the doping/undoping process of the film (see **Table 4.7**). By considering that the dynamic process of molar mass is dominated by the anion

(as cation exchange is absent), the total mass change is therefore the sum of contributions from anionic and solvent transfers only (equation 4.11) while in the case of a cation-dominated process (with anion exchange absent), the total mass change is the sum of contributions from cation and solvent transfers (equation 4.12).

$$M_{app} = M_{Anion} \pm \alpha M_{Solvent} \quad 4.11$$

$$M_{app} = M_{Cation} \pm \alpha M_{Solvent} \quad 4.12$$

In Ethaline and DESs, the behaviour of PANI film upon redox cycling is generally different from that in aqueous solution because of the absence of a molecular solvent in the DESs. Therefore, a neutral species ( $\alpha M_{neutral}$ ) may have to be used instead of the solvent term ( $\alpha M_{Solvent}$ ), as expressed in equation 4.13, for a reaction dominated by the cation, and as equation 4.14 for a reaction dominated by the anion.

$$M_{app} = M_{cation} \pm \alpha M_{neutral} \quad 4.13$$

$$M_{app} = M_{anion} \pm \alpha M_{neutral} \quad 4.14$$

In this thesis,  $M_{app}$  values during oxidation and reduction processes were reported as overall molar mass exchanges from one end of the potential window to the other in the cyclic voltammograms. In other words, the  $M_{app}$  values were determined as overall molar mass transfers from end-to-end of the potential window used. The detected mass changes provide significant information about the mass exchange due to ion and solvent flux across the polymer/solution interface, which helped to develop PANI as a cathode with a selected battery electrolyte during device usage.

Data ( $\Delta m$  vs.  $\Delta q$ ) presented in panel (c) of **Figure 4.10** shows the molar mass of anion ( $\text{SO}_4^{2-}$ ) ingress into the film during the oxidation scan is around  $+42 \text{ g mol}^{-1}$ , whereas the reduction scan is around  $-46 \text{ g mol}^{-1}$  egress. In contrast, the behaviour of PANI film in Ethaline was changed as cation egress  $\text{Ch}^+$  ( $M_{app} = -8.34 \text{ g mol}^{-1}$ ) was found upon oxidation and a cation ingress  $\text{Ch}^+$  ( $M_{app} = +5.00 \text{ g mol}^{-1}$ ) upon reduction, which is known as the *memory effect*. This is because the film has been transferred to a DES medium, having been prepared in an aqueous acidic medium. Indeed, these results are not the same as the molar masses of  $\text{Ch}^+$  ( $104 \text{ g mol}^{-1}$ ) in Ethaline. This is because of the fact that neutral species ( $\text{EG}_2\text{Cl} \cdot \text{Ch}^+$ ) have participated to satisfy the electroneutrality condition between the polymer and electrolyte during the redox

process. Therefore, the behaviour of the PANI film cycled in DES not only depends on the size of ion or effect of the absent solvent, but it can also be referred to as a mixed cation-anion expulsion/insertion exchange. In the third part of this experiment (i.e. PANI in 0.5 M H<sub>2</sub>SO<sub>4</sub>), the molar mass is lower than that in the first stage in terms of anion (SO<sub>4</sub><sup>2-</sup>) ingress/egress, as reported in **Table 4.7**. The values of  $\alpha$  for the doping and undoping regimes and the identities of mobile species are also given in **Table 4.7**. A negative/positive value of  $\alpha$  (i.e. in the case of the fluxes of the anion and the solvent have the opposite direction) indicates that the replacement of some anions by some solvent molecules in aqueous system during redox processes but in DES, it means the neutral species are replacing cation molecule for a cation-dominated process

**Table 4.7:** Molar masses ( $M_{app}$ ) from  $\Delta m$  vs.  $Q$  graphs for redox switching of PANI ( $\Gamma = 229 \text{ nmol cm}^{-2}$ ) in 0.5 M H<sub>2</sub>SO<sub>4</sub>, Ethaline at 50 °C and 0.5 M H<sub>2</sub>SO<sub>4</sub>, respectively. The potential window was  $-0.16 \leq E / V \leq 0.96$  for the fifth scan at  $10 \text{ mV s}^{-1}$ . + represents a mass increase, - represents a mass decrease.

Electrolytes (monomer free)	Oxidation 5 <sup>th</sup> scan			Reduction 5 <sup>th</sup> scan		
	$M_{app}$ g mol <sup>-1</sup>	$\alpha \sim$	Dominating process	$M_{app}$ g mol <sup>-1</sup>	$\alpha \sim$	Dominating process
0.5M H <sub>2</sub> SO <sub>4</sub>	+42.00	-3.00	SO <sub>4</sub> <sup>2-</sup> in	-46.00	+2.80	SO <sub>4</sub> <sup>2-</sup> out
Ethaline	-8.34	+0.36	Ch <sup>+</sup> out	+5.00	-0.38	Ch <sup>+</sup> in
0.5M H <sub>2</sub> SO <sub>4</sub>	+11.00	-4.72	SO <sub>4</sub> <sup>2-</sup> in	-6.50	+5.00	SO <sub>4</sub> <sup>2-</sup> out

#### 4.3.7.2.2 Effect of limit potential windows on PANI redox cycling

As we indicated in previous section, the overoxidation potential of PANI film could cause deterioration,<sup>43</sup> which leads to poor stability during redox cycling. Mazeikine *et al.* reported the degradation<sup>44</sup> of PANI film caused by the fully oxidised (pernigraniline) form of PANI through application of higher potentials. The strategy here, in order to avoid the above problems, was to limit the applied potential to the first redox peaks of polyaniline. Panel (a) of **Figure 4.11** shows cyclic voltammograms of film cycled in 0.5 M H<sub>2</sub>SO<sub>4</sub> solution between -0.16 V and +0.6 V versus Ag/AgCl (sat. KCl) while the potential window in Ethaline was +0.1 V and +0.7 V versus Ag wire. According to these data, the stability of polyaniline is a better than those seen in section 4.3.7.2.1. It

was observed that the electroactivity of the polymer was recovered to about 87 % after transferral from Ethaline back to aqueous electrolyte. This result indicates that high anodic potentials have a significant effect on the stability of electroactive polymers, identical finding that is entirely in accord with previous studies.<sup>34, 44, 45</sup> However, the current peak in Ethaline is still less than in aqueous solution during the p-doping/n-doping process, the reason for which is the decreased diffusion coefficient values associated with the increased viscosity of the solution.<sup>46</sup>

The mass change shown in panel (b) of **Figure 4.11** is similar to the results found in our previous study, where the mass increase in the aqueous solution during the oxidation was due to anion ( $\text{SO}_4^{2-}$ ) incorporation into the polymer chains; conversely, the mass loss during the reverse scan is due to anion expulsion from the polymer. The overall results consist of two stages: (i) proton egress in the early stages of film oxidation and (ii) anion ingress in the later stages of film oxidation. This means that the mass change in aqueous solution is dominated by anion transfer, because the mass/charge of the anion ( $\text{SO}_4^{2-}$ ) is two orders of magnitude is greater than that of the cation ( $\text{H}^+$ ), as confirmed by a number of studies in the literature.<sup>3, 6, 7, 47, 48</sup> Concerning PANI film in Ethaline, during the oxidation process the mass is reduced, suggesting the cation is ejected from the film, while the increase in mass during the reduction process is attributed to the incorporation of cation ( $\text{Ch}^+$ ) into the film. In case of an Ethaline electrolyte, the overall gravimetric responses towards mass change for PANI in electrolyte are cation dominated during positive cycling and the negative scan. This same behaviour has been reported to some extent in the literature, where cation exchangers egress/ingress during the oxidation and reduction cycles of polypyrrole in the presence of macromolecules (polystyrenesulfonate).<sup>49</sup> Similarly, Hillman *et al.* noted that the mass change of PEDOT film (grown from 0.1 M  $\text{LiClO}_4/\text{CH}_3\text{CN}$  and 0.1 M EDOT monomer) increases upon film oxidation state when it is exposed to a 0.1 M  $\text{LiClO}_4/\text{CH}_3\text{CN}$  electrolyte, whereas the data regarding mass change in the Ethaline indicates a decrease upon film oxidation.<sup>50</sup> To the best of our knowledge, PANI has not been previously investigated in terms of having a cation/anion-domination reaction in DESs.

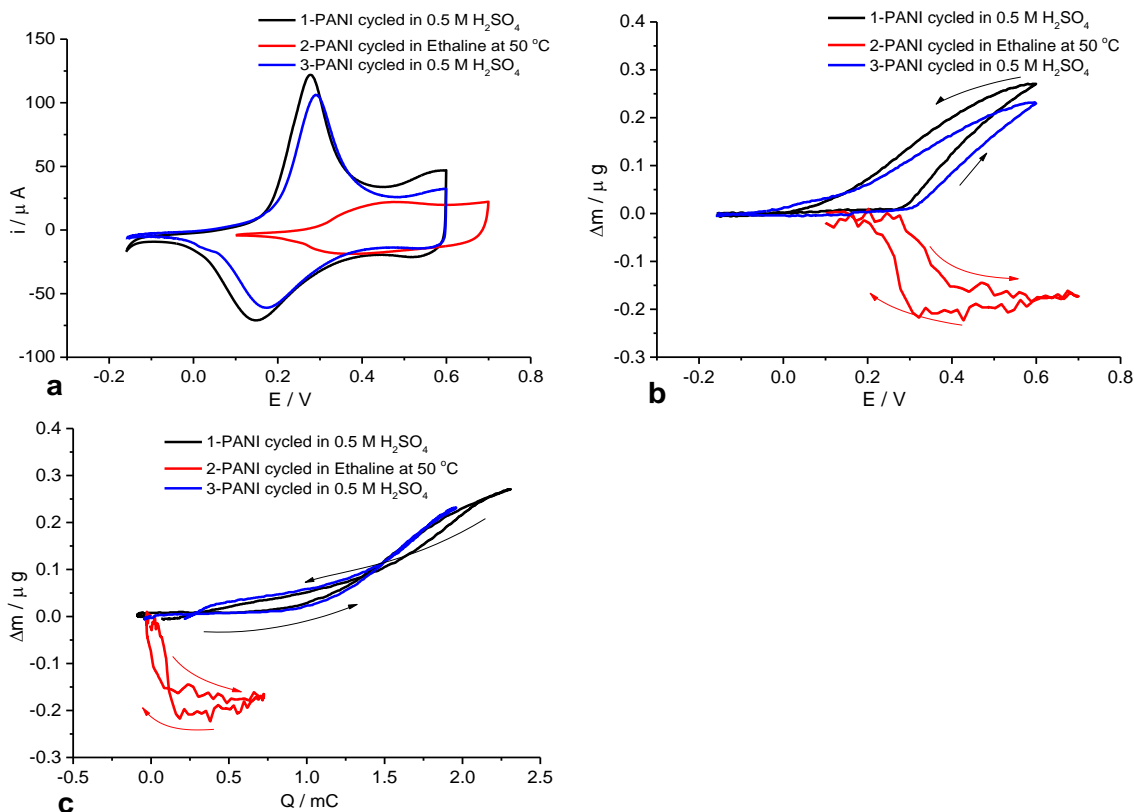


**Figure 4.11:** EQCM data for redox switching of PANI film ( $\Gamma = 231 \text{ nmol cm}^{-2}$ ) exposed to  $0.5 \text{ M H}_2\text{SO}_4$ , Ethaline  $50^\circ\text{C}$  and  $0.5 \text{ M H}_2\text{SO}_4$ , respectively, at  $10 \text{ mV s}^{-1}$  scan rates. a)  $i$  vs.  $E$ ; b)  $\Delta m$  vs.  $E$ ; and c)  $\Delta m$  vs.  $Q$ . The arrows indicate the direction of changes.

Panel c of **Figure 4.11** ( $\Delta m$ - $Q$ ) was determined from charge and mass change responses. In the aqueous solutions used, it was clear that during the oxidation process, mass change was increased as the result of the entry anions into the polymer with the subsequent expulsion of a 4 mole equivalent of solvent molecules ( $\text{H}_2\text{O}$ ) (i.e. 1:4 ratio). Conversely, for the reverse reaction, the mass change was decreased as a result of the expulsion of an anion with the subsequent ingress of a 4 mole equivalent of solvent molecules ( $\text{H}_2\text{O}$ ). Here, the data indicated that the anion and electrolyte fluxes appear to be in opposing directions. The molar masses in Ethaline during oxidation and reduction state are  $-22.60$  and  $+23.40$ , respectively, which are clearly significantly less than the masses of the  $\text{Ch}^+$  cation ( $104 \text{ g mol}^{-1}$ ). This cannot be explained through solvent flux, but can only be attributed to mixed anion-cation incorporation/expulsion transfer. The values of  $\alpha$  and the identities of mobile species for gravimetric results during doping and undoping regimes are reported in **Table 4.8**.

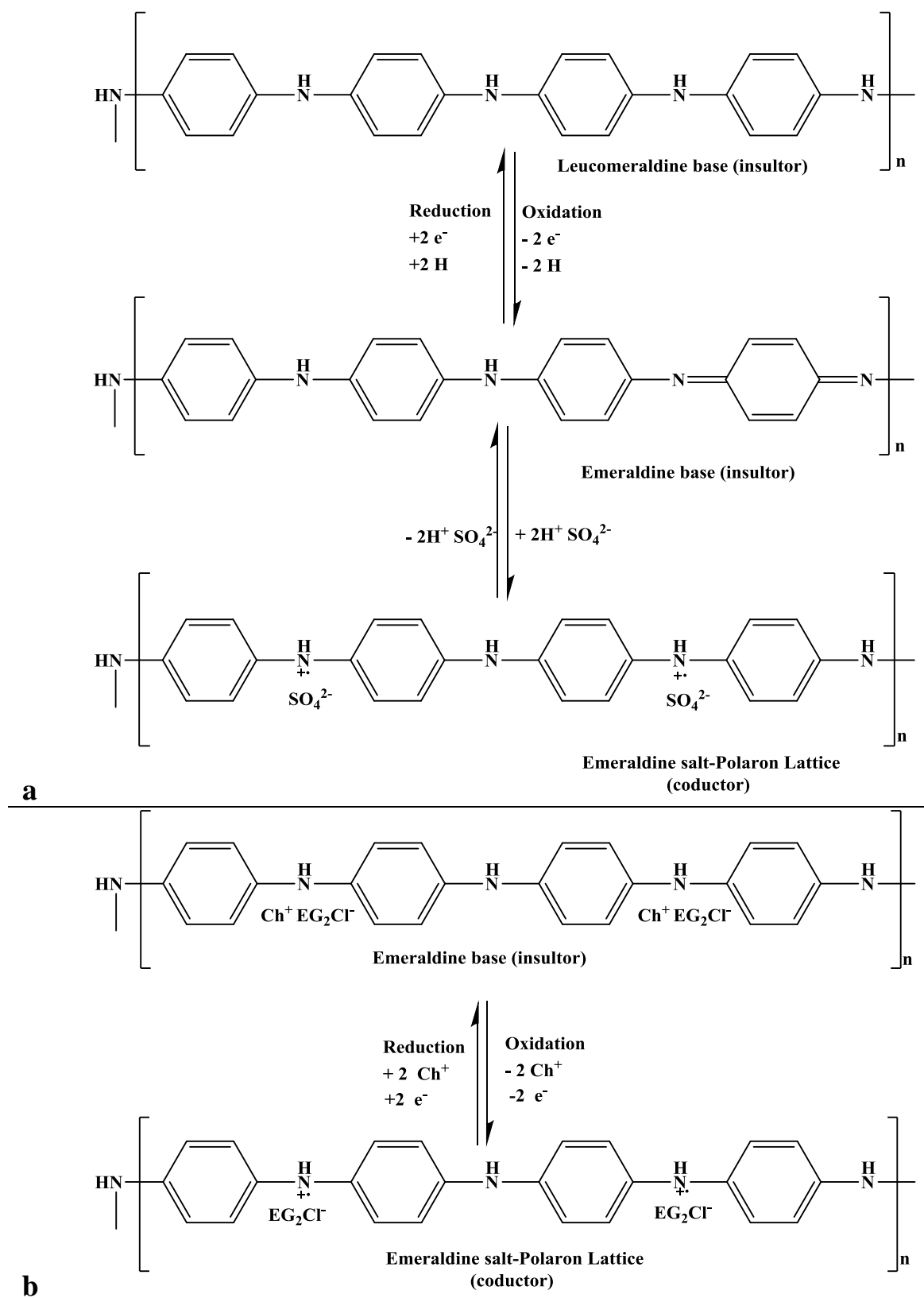


**Figure 4.12:** Schematic representation of PANI oxidation in a) H<sub>2</sub>SO<sub>4</sub> and b) Ethaline electrolytes.

**Table 4.8:** Molar masses ( $M_{app}$ ) from  $\Delta m$  vs.  $Q$  graphs for redox switching of PANI ( $\Gamma = 231 \text{ nmol cm}^{-2}$ ) in 0.5 M  $\text{H}_2\text{SO}_4$ , Ethaline at 50°C and 0.5 M  $\text{H}_2\text{SO}_4$ , respectively. The potential window was  $-0.16 \leq E/V \leq 0.6$  in aqueous while in ethaline was  $0.1 \leq E/V \leq 0.7$  for the fifth scan at  $10 \text{ mV s}^{-1}$ . + represents a mass increase, - represents a mass decrease.

Electrolytes (monomer free)	Oxidation 5 <sup>th</sup> scan			Reduction 5 <sup>th</sup> scan		
	$M_{app}$ g mol <sup>-1</sup>	$\alpha \sim$	Dominating process	$M_{app}$ g mol <sup>-1</sup>	$\alpha \sim$	Dominating process
0.5 M $\text{H}_2\text{SO}_4$	+24.00	-4.00	$\text{SO}_4^{2-}$ in	-24.00	+4.00	$\text{SO}_4^{2-}$ out
Ethaline	-22.60	+0.31	$\text{Ch}^+$ out	+23.40	-0.31	$\text{Ch}^+$ in
0.5 M $\text{H}_2\text{SO}_4$	+24.00	-4.00	$\text{SO}_4^{2-}$ in	-24.00	+4.00	$\text{SO}_4^{2-}$ out

#### 4.3.7.2.3 Effect of Scan Rates

In this section, the influence of scan rate on electrochemical response was investigated in both aqueous and DES electrolytes. The purpose here is to distinguish the kinetic and dynamics of PANI film during redox cycling; whether it is dominated by diffusional control, diffusionless control, or some kind of intermediate. A new polyaniline film was prepared as per the conditions described in section 4.3.7.1, which is then exposed to a fresh 0.5 M  $\text{H}_2\text{SO}_4$  background electrolyte (monomer free) at various scan rates (5, 10, 20, 50 and  $100 \text{ mV s}^{-1}$ ) with a potential window of -0.16 V to 0.6 V, as shown in **Figure 4.13**. The same film was then transferred into an Ethaline medium, as shown in **Figure 4.14**. Cathodic current data from cyclic voltammetry of the film shown in **Figure 4.13a** when normalised and fitted against scan rate ( $\nu$ ) gives a straight line ( $R = 0.99965$ ). A gradual increase of peak current with increasing a scan rate indicates that the flux of materials are adsorbing at the electrode surface. This result is in agreement with that reported in the literature.<sup>51</sup>

In the case of mass change, the EQCM response in **Figure 4.13c** shows that the amount of mass changes in same background electrolytes are vary slightly due to differences in scan rates. These variations are attributed due to the occurrence of fast and slow mass transport into and out of the polymer which are affected by timescale. At high scan rates, the mobility of species is fast (fast kinetics) compared to the rate of electron transfer during the redox processes, so a lower mass change is observed. As a result, the redox system does not maintain an equilibrium state during the potential scan. In

contrast, at slow a scan rate, equilibrium processes are predominant. Therefore, the movement of neutral species is slower than the movement of charged species, resulting in a movement independent of scan rate.<sup>6</sup>

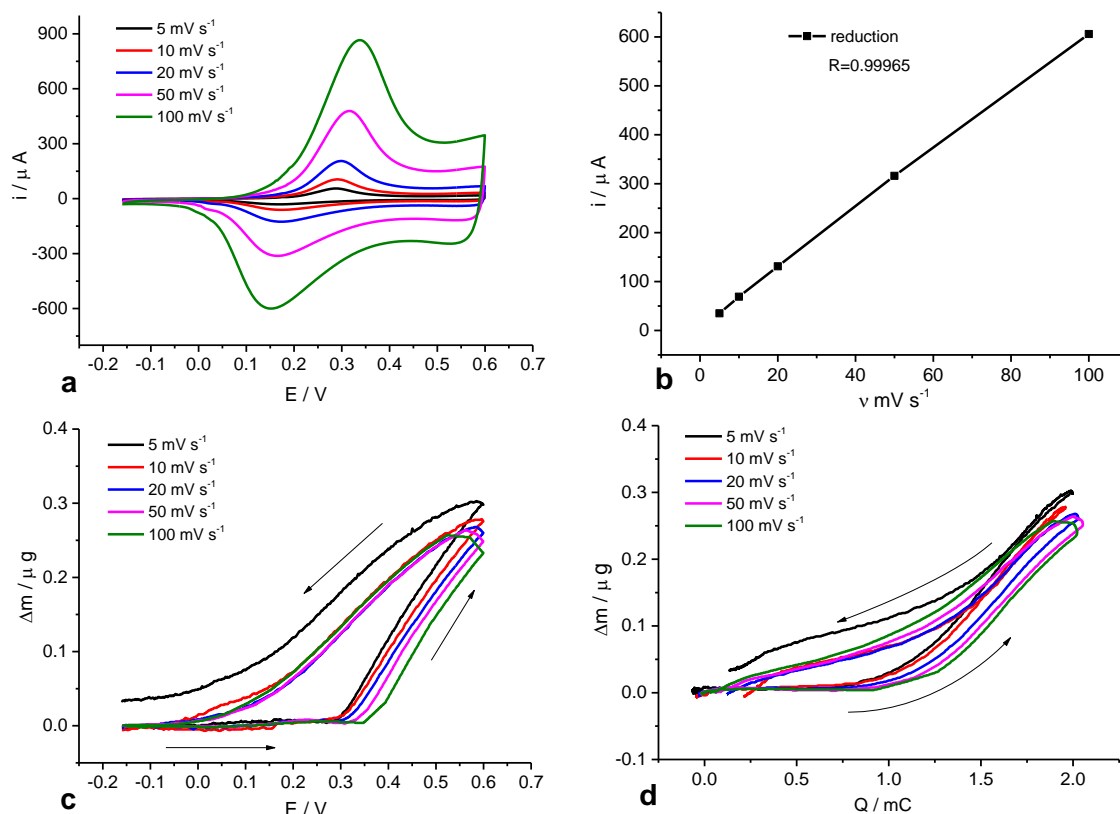


**Figure 4.13:** EQCM data for redox switching of PANI film ( $\Gamma = 221.00 \text{ nmol cm}^{-2}$ ) exposed to  $0.5 \text{ M H}_2\text{SO}_4$  at various scan rates. a)  $i$  vs.  $E$ ; b)  $i$  vs.  $v$ ; c)  $\Delta m$  vs.  $E$ ; and d)  $\Delta m$  vs.  $Q$ . Colours indicate scan rates.

In the Ethaline, the same film was washed several times with deionised water and hot Ethaline to get rid of any residual acid solution. After that, the film was cycled in an Ethaline medium at various scan rates (5, 10, 20, 50 and  $100 \text{ mV s}^{-1}$ ) with a potential window between 0.1 V and 0.7 V, as shown in **Figure 4.14**. Similar to the aqueous system, the cathodic current data recorded during the cyclic voltammetry of the film recorded in **Figure 4.14a**, when normalised and fitted against scan rate ( $v$ ), give a straight-line fit. The main difference in current response between the aqueous solutions and Ethaline is that the value of current peak in the redox process in aqueous solution is higher than that in Ethaline. Regarding mass change, the contrasting quality of film behaviours is illustrated in the ionic liquid (Ethaline) medium in **Figure 4.14c**, which shows the diverse responses in mass change for the same PANI film undergoing p-

doping–undoping in Ethaline solution. Starting from the oxidised PANI state, there is a small mass decrease in the early stages of oxidation, with a significant decrease in film mass at potentials of 0.2 - 0.3 V with respect to scan rate. The reverse state for mass changes tends to occur in the reduction half cycle.

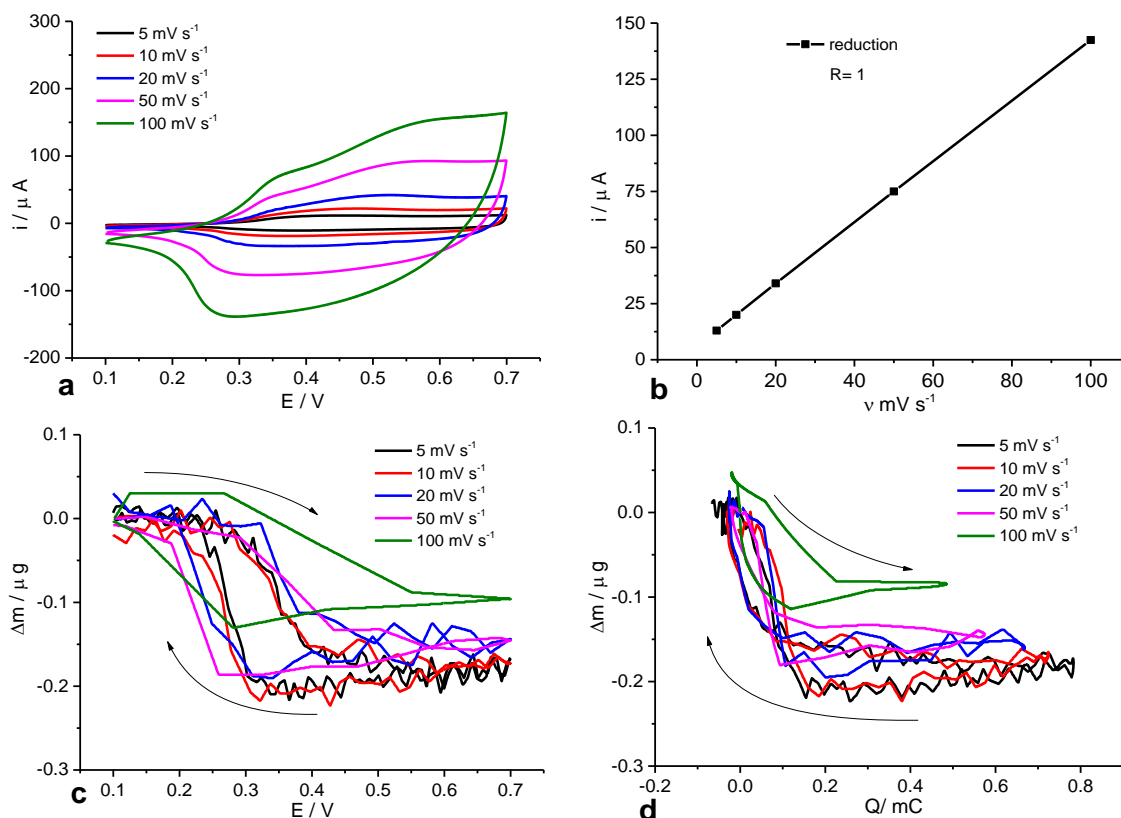


**Figure 4.14:** EQCM data for redox switching of a PANI film ( $\Gamma = 221.00 \text{ nmol cm}^{-2}$ ) exposed to Ethaline at  $50^\circ\text{C}$  at various scan rates. a)  $i$  vs.  $E$ ; b)  $i$  vs.  $v$ ; c)  $\Delta m$  vs.  $E$ ; and d)  $\Delta m$  vs.  $Q$ . Colours indicate scan rates.

A quantitative interpretation may be performed through the mass change vs. charge plots in **Figures 4.13d** and **4.14d**, which are derived from the data in panels (a) and (c) of **Figures 4.13** and **4.14**, respectively. As mentioned previously, the exchanged molar mass values are calculated from end to-end of the redox peaks. The molar mass and  $\alpha$  value of expulsion and incorporation of solvent/neutral species are calculated for all sweep rates in both media, the results of which are presented in **Table 4.9**. The interpretation of the PANI mobile species immersed in the aqueous solution has been given by a number of researchers,<sup>11, 48</sup> but the main goal is to compare the data (ion dynamics) of the polymer in aqueous solution with that in ionic liquids. In Ethaline, these are broadly interpreted along the lines of expulsion of a choline cation because a small amount of neutral species is entered ( $\text{EG}_2\text{Cl}\cdot\text{Ch}^+$  per  $\text{Ch}^+$ ) during the doping

reaction. Conversely, when the mass increase during the reverse scan is due to cation incorporation into the polymer chains, a small amount of neutral species is expelled ( $\text{EG}_2\text{Cl}\cdot\text{Ch}^+$  per  $\text{Ch}^+$ ). Obviously, the data does not correspond with the normal value expected for transfer of either ion present, namely  $+96 \text{ g mol}^{-1}$  for sulphate entry in aqueous electrolytes and  $-104 \text{ g mol}^{-1}$  for choline exit in the Ethaline electrolyte. Remarkably, the failure of the mass and charge responses to reach to their initial values at the end of the complete redox cycle is dependent on scan rate (kinetics of ions in electrolytes). This means that kinetic effects dominate the relative transfer rates of choline and sulphate ions. From the observed results, it is important to consider why there should be such a sharp shift with potential from a point gravimetrically dominated by choline egress to one dominated by chloride ingress at the final points. This is because choline egress is the thermodynamically favoured process; therefore, this process can be proceed as long as choline is available.

**Table 4.9:** Molar masses ( $M_{app}$ ) from  $\Delta m$  vs.  $Q$  graphs for redox switching of PANI ( $\Gamma=221 \text{ nmol cm}^{-2}$ ) in  $0.5\text{M H}_2\text{SO}_4$  and Ethaline at  $50^\circ\text{C}$ . Potential window was  $-0.16 \leq E / V \leq 0.6$  in aqueous while in Ethaline it was  $0.1 \leq E / V \leq 0.7$  for the fifth scan at various scan rate (5, 10, 20, 50 and  $100 \text{ mV s}^{-1}$ ). + represents a mass increase, - represents a mass decrease.

Electrolytes	Scan rates	Oxidation scan			Reduction scan		
		$M_{app}$ $\text{g mol}^{-1}$	$\alpha \sim$	Dominating process	$M_{app}$ $\text{g mol}^{-1}$	$\alpha \sim$	Dominating process
0.5 M $\text{H}_2\text{SO}_4$	5	+ 24.56	-3.97	$\text{SO}_4^{-2}$ in	- 24.00	+4.00	$\text{SO}_4^{-2}$ out
	10	+ 24.12	-3.99	$\text{SO}_4^{-2}$ in	- 26.66	+3.85	$\text{SO}_4^{-2}$ out
	20	+ 24.05	-3.99	$\text{SO}_4^{-2}$ in	- 25.40	+3.92	$\text{SO}_4^{-2}$ out
	50	+ 23.80	-4.01	$\text{SO}_4^{-2}$ in	- 24.34	+3.98	$\text{SO}_4^{-2}$ out
	100	+ 23.67	-4.01	$\text{SO}_4^{-2}$ in	- 24.12	+3.99	$\text{SO}_4^{-2}$ out
Ethaline	5	- 24.77	+0.30	$\text{Ch}^+$ out	+ 25.06	-0.30	$\text{Ch}^+$ in
	10	- 24.1	+0.30	$\text{Ch}^+$ out	+ 24.50	-0.30	$\text{Ch}^+$ in
	20	- 23.32	+0.31	$\text{Ch}^+$ out	+ 23.40	-0.31	$\text{Ch}^+$ in
	50	- 23.32	+0.31	$\text{Ch}^+$ out	+ 23.40	-0.31	$\text{Ch}^+$ in
	100	-23.20	+0.31	$\text{Ch}^+$ out	+19.85	-0.32	$\text{Ch}^+$ in

#### 4.3.7.2.4 Effect of electrolyte composition (different DESs) on PANI redox cycling

In this section, polyaniline film was individually analysed in different DESs having different functional groups (i.e. HBD) using EQCM analysis. The PANI film used in one experiment could not be employed for further use in another DES because DES electrolytes remain in PANI voids that cannot be removed completely from it due to their high viscosity. Therefore, a fresh PANI film was prepared for each experiment in order to characterise each DES. The conditions for growing the polymer were similar to that reported in section 4.3.7.1. Prior to transferring film to each DES, the film was washed several times in the same solution that it was to be recycled in. The scan rate was held at  $10 \text{ mV s}^{-1}$  and the potential sweep ranged from 0.1 to 0.7 V, whilst the temperature was held at  $50^\circ\text{C}$  to allow reasonable comparison with the results previously obtained for Ethaline.

Panels a, c, e, and g of **Figure 4.15** show cyclic voltammograms of polyaniline film exposed to the various electrolyte solutions of Propaline, Oxaline, Glyceline and Reline. These data show several varied and interesting features. First, the redox peak is relatively sharp for PANI in Oxaline due to the greater acidity of this electrolyte in comparison to the others; by contrast, in the Propaline, Glyceline and Reline electrolytes broad peaks were observed. This might imply that as the pH of the solution is varied (i.e. neutral, acidic and alkaline, see **Figure 9.2** in Appendix), so the electroactivity of polyaniline increases with decreasing pH. Second, in terms of current peaks, the highest current peaks, which corresponded to the anodic peaks, were found for PANI in Oxaline at  $53 \mu\text{A}$ , followed by Propaline, Glyceline and Reline at 37, 30 and  $24 \mu\text{A}$ , respectively. This could be due to the fundamental properties of these different hydrogen bond donors; in other words, this observation could be dependent on the nature of the ions present in the solution, as was seen in section 4.3.4. Thus, this effect appears to be related to the conductivity of the electrolyte and its viscosity. It has been found that the conductivity of these electrolytes at  $50^\circ\text{C}$  follows the order: Oxaline > Propaline > Glyceline > Reline, while their viscosities follow the order: Propaline < Oxaline < Glyceline < Reline, as measured in section 5.3.1.

The EQCM data  $\Delta m$  vs.  $t$ , for redox switching of PANI film exposed to DES electrolytes are given in panels b, d, f and h of **Figure 4.15**. Mass declines dramatically for electrochemical cycling of PANI in Propaline and Glyceline, as seen in panels b and f of **Figure 4.15**. The fluctuation of mass until  $\sim 700$  s in Propaline and  $\sim 1400$  s in Glyceline was attributed to the rapid mass change observed for the film after the electrochemical experiment was started. The mass of the film decreased by about  $0.5 \mu\text{g}$  in both electrolytes (Propaline and Glyceline). The reason behind this decrease is most probably due to the expulsion of aqueous electrolyte (from deposition solution) and egress of Propaline/Glyceline (from rinsing solution–film not evolved yet) to reach the stability stage (i.e. equilibrium).

In contrast, the mass change observed in Oxaline and Reline seems to be quite different to those in Propaline and Glyceline, where the mass of the PANI films increased immediately in Oxaline (panel d) and Reline (panel h) on starting the electrochemical experiment. The mass of the film increased by about  $4.6 \mu\text{g}$  after  $\sim 480$  s in Oxaline, while in Reline about it increased by  $8.6 \mu\text{g}$  after  $\sim 2900$  s due to overall DES entrance into the film at equilibrium. The results showed that the mass of the film increased in the Oxaline electrolyte to ca.  $\sim 5 \mu\text{g}$  over 6 cycles, which represented a 4 % increase more than the deposited mass of the film ( $4.8 \mu\text{g}$ ). The mass of the film in Reline increased to ca.  $\sim 8.40 \mu\text{g}$  over 20 cycles, which represented a 58 % increase more than the deposited mass of the film ( $4.9 \mu\text{g}$ ). The reason for these increases could be due to insertion of Oxaline/Reline and aqueous solution into the films. The variation of polymers at equilibrium may be due to the difference in viscosity of these solutions. It is clear that the polymer cycled in Reline needed a long time to reach its equilibrium (stability) state due to Reline having the highest viscosity of the electrolytes used. The stability of these films is identical, with their viscosities following the order: Propaline > Oxaline > Glyceline > Reline.

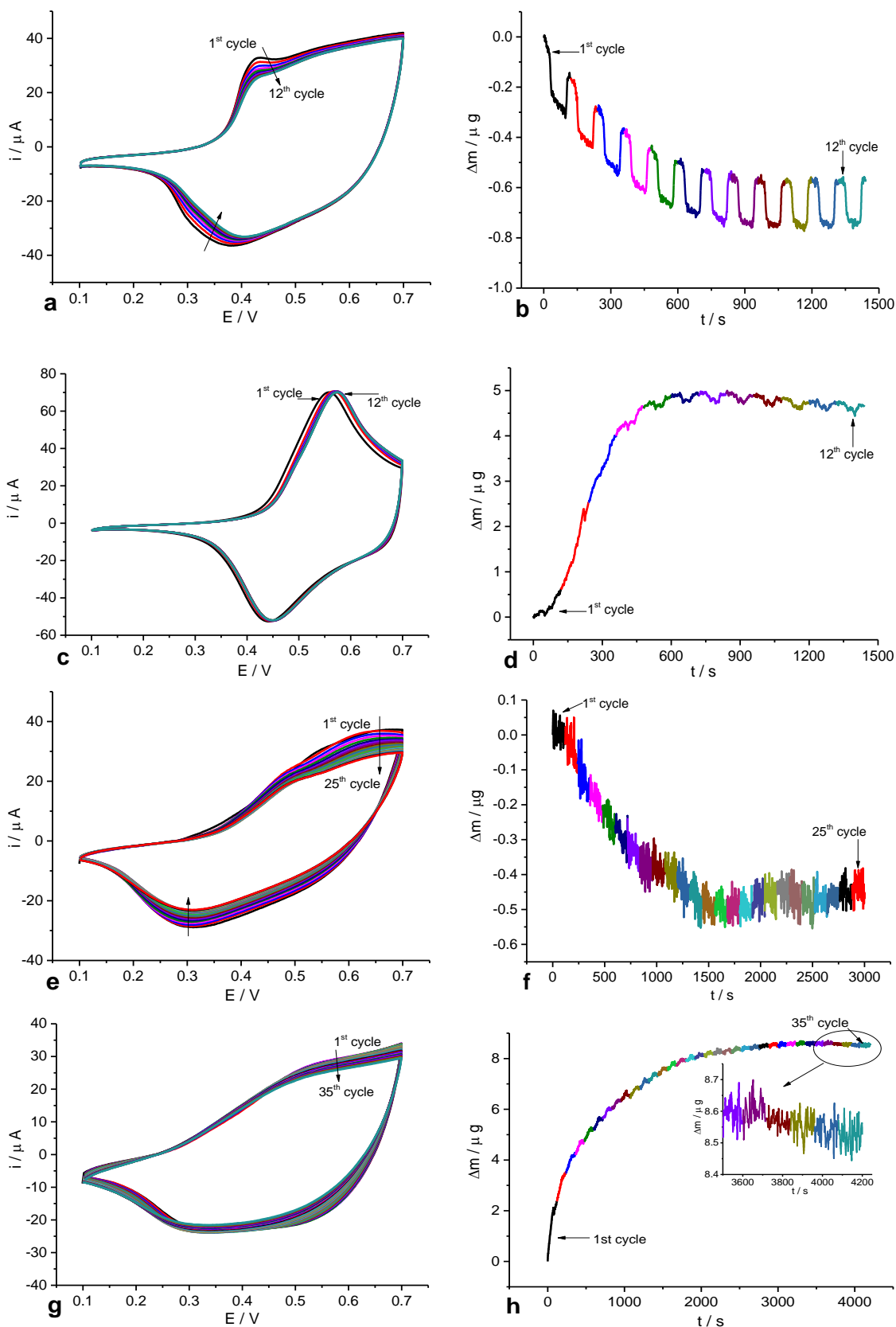


**Figure 4.15:** EQCM data for redox switching of PANI film ( $\Gamma = 229 \text{ nmol cm}^{-2}$ ) exposed to different DES electrolytes at a scan rate of  $10 \text{ mV s}^{-1}$ . Panels: a, c, e, and g show  $i$  vs.  $E$ ; panels b, d, f and h show  $\Delta m$  vs.  $t$ ; for Propaline, Oxaline, Glyceline and Reline, respectively.

The mass change of the last cycle (the stable state) for each of these electrolytes is shown in panel (a) of **Figure 4.16** for comparison. It is obvious that there is no mass change in the film at  $E < 0.35$  V in Propaline and  $E < 0.45$  V in Oxaline. After that, a significant decrease in film mass was observed due to an increasing anodic current peak. In the cathodic half peak, the mass change trends are reversed. These results indicate that PANI film in these electrolytes undergoes a cation-dominated reaction at the redox peak due to cation ( $\text{Ch}^+$ ) egress/ingress, as observed previously for Ethaline. However, the behaviour of the mass change in Glyceline and Reline is the opposite of that observed than in Ethaline, Propaline and Oxaline at  $50^\circ\text{C}$ . It can be seen that mass change shows a slight increase in Glyceline and a slight decrease in Reline during the oxidation peak and, in the reduction state, that the reverse processes take place. This may be related to the low conductivities and high viscosities of these liquids, which affected the mass and charge transport rates during redox switching, as well as the ions naturally present in these electrolytes. As before, the molar mass of ion exchange of PANI films in these electrolytes has been calculated from plots of  $\Delta m$  vs.  $Q$ , as shown in panel (b) of **Figure 4.16**; the data for  $\alpha$  for cations/anions mixed with ion dominated process are presented in **Table 4.10**.

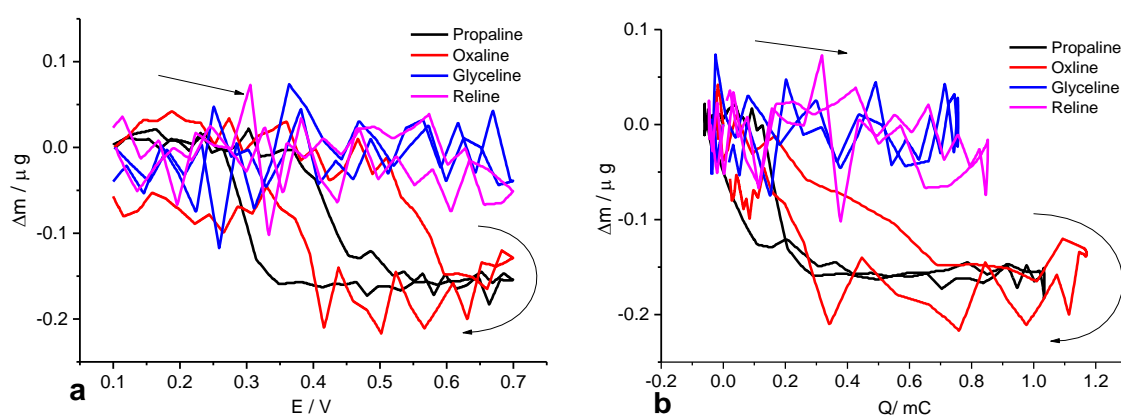


**Figure 4.16:** Panels a)  $\Delta m$  vs.  $E$ ; and b)  $\Delta m$  vs.  $Q$  recorded simultaneously with corresponding cyclic voltammograms in Figure 4.15 for each individual electrolyte. Colours indicate electrolytes.

**Table 4.10:** Molar masses ( $M_{app}$ ) from  $\Delta m$  vs.  $Q$  graphs for redox switching of PANI ( $\Gamma = 229 \text{ nmol cm}^{-2}$ ) in DESs at 50 °C. Potential window was between  $0.1 \leq E / V \leq 0.7$  at  $10 \text{ mV s}^{-1}$ . + represents a mass increase, - represents a mass decrease.

Electrolytes (monomer free)	Oxidation last scan			Reduction last scan		
	$M_{app}$ g mole <sup>-1</sup>	$\alpha_{\sim}$	Dominating process	$M_{app}$ g mole <sup>-1</sup>	$\alpha_{\sim}$	Dominating process
Propaline	-15.80	+0.30	Ch <sup>+</sup> out	+16.60	-0.30	Ch <sup>+</sup> in
Oxaline	-16.22	+0.38	Ch <sup>+</sup> out	+12.72	-0.40	Ch <sup>+</sup> in
Glyceline	+3.73	-0.67	Gly <sub>2</sub> Cl <sup>-</sup> in	-9.03	+0.65	Gly <sub>2</sub> Cl <sup>-</sup> out
Reline	-8.43	+0.37	Ch <sup>+</sup> out	+11.17	-0.36	Ch <sup>+</sup> in

#### 4.3.7.2.5 Effect of temperature on PANI stability in Ethaline

Ethaline has been selected as the best model electrolyte to compare the behaviour of PANI at room temperature,  $25 \pm 2^\circ\text{C}$ , and at  $50^\circ\text{C}$  due to its lower viscosity, good conductivity and ion dynamics behaviour than the other DES's used. The growth conditions of the film were the same as given in section 4.3.7.1. The film was cycled in Ethaline electrolyte at room temperature,  $25 \pm 2^\circ\text{C}$ , and the experiment was stopped after completing the 39<sup>th</sup> cycle. After that, the temperature of the electrolyte was increased to  $50^\circ\text{C}$  and held at this temperature for 1 hour to allow ingress of the hot Ethaline into the chains of the film and to thus increase the porosity of the polymer. Panels a and c of **Figure 4.17** illustrate that the cyclic voltammogram of PANI responses in Ethaline at both room temperature and at  $50^\circ\text{C}$ . The results show that PANI in room temperature Ethaline has a lower current peak, stability and electroactivity than those observed at  $50^\circ\text{C}$ . The anodic current peaks of PANI film cycled in Ethaline at  $25 \pm 2^\circ\text{C}$  and at  $50^\circ\text{C}$  were  $32 \mu\text{A}$  and  $38 \mu\text{A}$ , respectively.

Mass change data ( $\Delta m$  vs.  $t$ ) at various temperatures, given in panels b and d of **Figure 4.17**, during the redox process were quite distinct. At room temperature,  $25 \pm 2^\circ\text{C}$ , the mass was immediately increased during redox cycling of the film in Ethaline until an equilibrium state was reached after  $\sim 2300 \text{ s}$  and showed an approximate  $8.6 \mu\text{g}$  increase in mass. This was due to the entrance of the high-viscosity electrolyte (large ionic radii) into the film, leading to a reduction in the average void radius in the polymeric net and an obstruction to free movement (entry and exit) of ions through the net of film. As a

consequence, the kinetics of the mobile species will decrease, leading to swelling of the polymer during redox switching. However, the mass change behaviour of the film was considerably different in Ethaline at 50°C. **Figure 4.17d** shows that the mass decreases during the oxidation process and increases during the reduction process and that overall, seems to be essentially stable. This indicates that ion transfer dynamics during redox cycling of PANI in Ethaline can be greatly influenced by increasing temperature due to the associated decrease in viscosity of the solution, allowing the ions greater freedom of movement.

It is well known that the viscosity of DESs decreases with increasing temperature, as mentioned in chapter 5 and as is in agreement with data reported in the literature.<sup>52, 53</sup> As the viscosity of the electrolyte decreases with increasing temperature, the frequency and the admittance of the quartz will be increase and, as a consequence, the mechanical resistance (impedance) on the quartz reduces. According to the Sauerbrey equation, mass change is inversely proportional to the change in frequency, so decreases in mass change at high temperature were not related to the electrochemical reaction only but could also be due to a viscosity change. Khalkhali *et al.*<sup>54</sup> investigated how ion-exchange properties can be affected by different temperatures for polypyrrole cycled in electrolytes containing various dopants (p-toluene sulfonate, dodecylsulfate and dodecylbenzenesulfonate counter ions). The results of this study showed that ion-exchange dynamics in the PANI are also affected by the temperature of the Ethaline electrolyte.

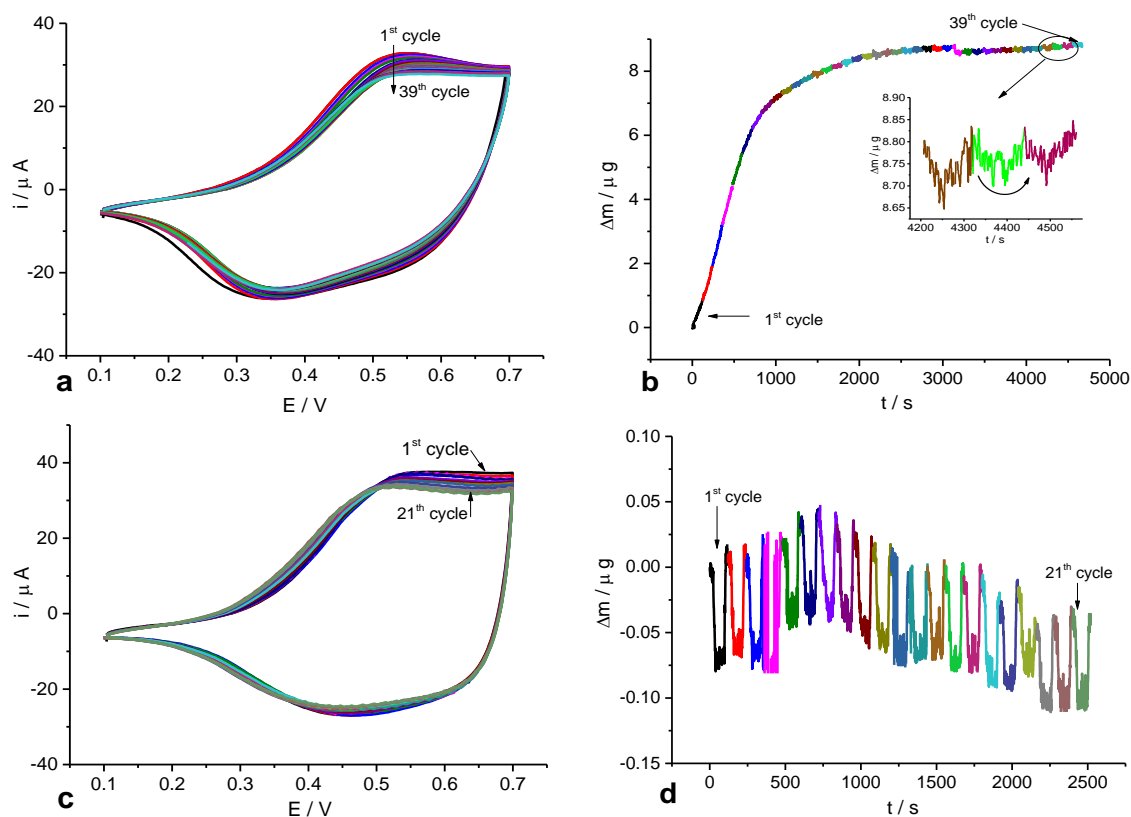


**Figure 4.17:** Panels showing a)  $i$  vs.  $E$ ; and b)  $\Delta m$  vs.  $t$  for PANI film cycled in Ethaline at room temperature ( $25 \pm 2^\circ\text{C}$ ); panels showing c)  $i$  vs.  $E$ ; and d)  $\Delta m$  vs.  $t$  for PANI film cycled in Ethaline at  $50^\circ\text{C}$ .

### 4.3.8 Conclusion

The polyaniline films synthesised in electrolytes having different counter-anions (1 M  $\text{H}_2\text{SO}_4$ , HCl,  $\text{HNO}_3$  and  $\text{HClO}_4$ ), showed various electrochemical responses. These responses were affected on the morphologies, grain size and fibrils of these films, as discovered by using the SEM and AFM techniques. The stability of PANI film in different electrolytes strongly depends on the nature of the anions present in the solution, rather than on the structure of the film (see section 4.3.4). The results showed that polyaniline film has a higher stability in perchlorate solvent compared to other aqueous solutions ( $\text{H}_2\text{SO}_4$ , HCl and  $\text{HNO}_3$ ). Polyaniline growth from  $\text{H}_2\text{SO}_4$  was selected as the best model polymer (due to its high current density, and open structure indicating more pores) to study the mechanisms of this film in aqueous and DES electrolytes using EQCM. In the case of the viscoelastic investigations of electropolymerisation of aniline, the films produced have been characterised using a frequency thickness shear mode acoustic resonator. Although the admittance spectrum

showed that the deposited film had a small viscoelastic nature, the validity of gravimetric measurements via the Sauerbrey equation were successfully fulfilled in the aqueous and DES electrolytes (monomer free). The EQCM studies of electroactive films in aqueous and DES electrolytes having different anions showed a reversible exchange of mobile species transfer accompanying the solvent/neutral species during the doping and dedoping processes. The contributions from exchanged molar mass, as well as the accompanying solvent or anion, were affected by potential due to the various kinetics of anion and solvent transfer. It was found that PANI film in DESs can be successfully transferred from a leucoemeraldine salt to an emeraldine salt, and *vice versa*, during the redox reaction.

In aqueous and DES (Ethaline), when a potentiodynamic control function is utilised, the values of current peaks are linear with scan rate. The magnitude of the mass change of the film cycled in the aqueous and Ethaline electrolytes was found to be dependent on scan rate. The data for the molar mass of solvent/ion flux with the ingress/egress of the anion and/or cation during redox switching of PANI films in aqueous and different DESs, were varied across all available parameters (potential, scan rate, electrolyte and temperature). All PANI films were grown in aqueous solution; the associated mass changes were dominated by anion transfer during redox cycling. On the other hand, cation transfer dominates the control of the oxidation reaction and the reduction reaction for PANI films in Ethaline, Propaline, Oxaline and Reline, while in Glyceline the opposite was observed (i.e. dominated by anion transfer during redox cycling).

PANI films deposited from aqueous solution and transferred to Ethaline electrolyte at 50°C need less time to reach their equilibrium state than other DES electrolytes (Propaline, Oxaline, Glyceline and Reline); this is likely to be related to viscosity, as Ethaline has a lower viscosity than the other DESs used in this chapter. The behaviour of the film cycled in Ethaline at room temperature is completely different from that the same film cycled in Ethaline at 50°C. This is due to the fact that high viscosity of the electrolyte at room temperature left ions salts inside the voids of the polymer branches, which could not then diffuse out of the films so easily due to species colliding with each other, causing obstructions to movement. Therefore, the mass change of the PANI film increases throughout the redox switching process, and the film will undergo swelling until equilibrium is reached. From these outcomes, we can conclude (as per the question

raised in section 4.2) that ion transfer processes in the film during redox cycling in the different media (aqueous and non-aqueous) are quite different. This suggests that various mechanisms can occur during complete redox conversion due to the different sources/sinks of mobile species in each case. However, further research should be undertaken for other conducting polymers in order to understand the effect of electrolyte temperature and other factors such as scan rate, growth conditions and surface population, and fractions of ions, more fully.

#### 4.4 References

1. F. Endres, D. MacFarlane and A. Abbott, *Electrodeposition from Ionic Liquids*, Wiley, 2008.
2. K. M. Molapo, P. M. Ndangili, R. F. Ajayi, G. Mbambisa, S. M. Mailu, N. Njomo, M. Masikini, P. Baker and E. I. Iwuoha, *International Journal of Electrochemical Science*, 2012, **7**, 11859-11875.
3. A. R. Hillman and M. A. Mohamoud, *Electrochimica Acta*, 2006, **51**, 6018-6024.
4. A. Baba, S. Tian, F. Stefani, C. Xia, Z. Wang, R. C. Advincula, D. Johannsmann and W. Knoll, *Journal of Electroanalytical Chemistry*, 2004, **562**, 95-103.
5. S.-J. Choi and S.-M. Park, *Journal of the Electrochemical Society*, 2002, **149**, E26-E34.
6. L. P. Bauermann and P. N. Bartlett, *Electrochimica Acta*, 2005, **50**, 1537-1546.
7. S. L. d. A. Maranhao and R. M. Torresi, *Electrochimica Acta*, 1999, **44**, 1879-1885.
8. S. Pruneanu, E. Csahok, V. Kertesz and G. Inzelt, *Electrochimica Acta*, 1998, **43**, 2305-2323.
9. A. Baba, M.-K. Park, R. C. Advincula and W. Knoll, *Langmuir*, 2002, **18**, 4648-4652.
10. G. Zotti, S. Cattarin and N. Comisso, *Journal of Electroanalytical Chemistry and Interfacial Electrochemistry*, 1988, **239**, 387-396.
11. D. Orata and D. A. Buttry, *Journal of the American Chemical Society*, 1987, **109**, 3574-3581.
12. S. Bruckenstein, J. Chen, I. Jureviciute and A. R. Hillman, *Electrochimica Acta*, 2009, **54**, 3516-3525.
13. A. R. Hillman, S. J. Daisley and S. Bruckenstein, *Electrochemistry Communications*, 2007, **9**, 1316-1322.
14. W. Plieth, A. Bund, U. Rammelt, S. Neudeck and L. Duc, *Electrochimica Acta*, 2006, **51**, 2366-2372.
15. G. G. Wallace, P. R. Teasdale, G. M. Spinks and L. A. P. Kane-Maguire, *Conductive Electroactive Polymers: Intelligent Polymer Systems, Third Edition*, CRC Press, 2008.

16. W.-S. Huang, B. D. Humphrey and A. G. MacDiarmid, *Journal of the Chemical Society, Faraday Transactions 1: Physical Chemistry in Condensed Phases*, 1986, **82**, 2385.
17. G. Inzelt and V. Kertesz, *Electrochimica Acta*, 1997, **42**, 229-235.
18. G. Sauerbrey, *Zeitschrift für Physik*, 1959, **155**, 206-222.
19. A. Y. Obaid, E. H. El-Mossalamy, S. A. Al-Thabaiti, I. S. El-Hallag, A. A. Hermas and A. M. Asiri, *International Journal of Electrochemical Science*, 2014, **9**, 1003-1015.
20. S.-Y. Cui and S.-M. Park, *Synthetic Metals*, 1999, **105**, 91-98.
21. G. Ćirić-Marjanović, *Synthetic Metals*, 2013, **177**, 1-47.
22. A. L. Beresford, *University of Leicester*, 2013, 92-94.
23. L. Duic and Z. Mandic, *Journal of Electroanalytical Chemistry*, 1992, **335**, 207-221.
24. S. Lagoutte, P.-H. Aubert, M. Pinault, F. Tran-Van, M. Mayne-L'Hermite and C. Chevrot, *Electrochimica Acta*, 2014, **130**, 754-765.
25. L. Duic and S. Grigic, *Electrochimica Acta*, 2001, **46**, 2795-2803.
26. W. C. Chen, T. C. Wen and A. Gopalan, *Synthetic Metals*, 2002, **128**, 179-189.
27. Y. Harima, R. Patil, K. Yamashita, N. Yamamoto, S. Ito and A. Kitani, *Chemical Physics Letters*, 2001, **345**, 239-244.
28. H. Okamoto and T. Kotaka, *Polymer*, 1999, **40**, 407-417.
29. H. Tang, A. Kitani and M. Shiotani, *Electrochimica Acta*, 1996, **41**, 1561-1567.
30. R. Cordova, M. A. del Valle, A. Arratia, H. Gomz and R. Schrebler, *Journal of Electroanalytical Chemistry*, 1994, **377**, 75-83.
31. G. M. Morale, M. C. Miras and C. Barbero, *Synthetic Metals*, 1999, **101**, 686.
32. J. Desilvestro and W. Scheifele, *Journal Material Chemistry*, 1993, **3**, 263-272.
33. Y. Kang, M.-H. Lee and S. B. Rhee, *Synthetic Metals*, 1992, **52**, 319-328.
34. H. Ding and S.-M. Park, *Journal of the Electrochemical Society*, 2003, **150**, E33-E38.
35. A. Abd-Elwahed and R. Holze, *Synthetic Metals*, 2002, **131**, 61-70.
36. F. Scholz, *Electroanalytical Methods: Guide to Experiments and Applications*, Springer Berlin Heidelberg, 2010.
37. M. Skompska and A. Tarajko-Wazny, *Electrochimica Acta*, 2011, **56**, 3494-3499.
38. A. R. Hillman, *Journal of Solid State Electrochemistry*, 2011, **15**, 1647-1660.

39. A. P. Abbott, M. Azam, G. Frisch, J. Hartley, K. S. Ryder and S. Saleem, *Physical Chemistry Chemical Physics*, 2013, **15**, 17314-17323.
40. H. Randriamahazaka, C. Plesse, D. Teyssié and C. Chevrot, *Electrochemistry Communications*, 2003, **5**, 613-617.
41. M. A. Skopek, M. A. Mohamoud, K. S. Ryder and A. R. Hillman, *Chemical Communications*, 2009, 935-937.
42. A. Bund and S. Neudeck, *Journal of Physical Chemistry*, 2004, **108**, 17845-17850.
43. T. Kobayashi, H. Yoneyama and H. Tamura, *Journal Electroanalytical chemistry* 1984, **161**, 419-423.
44. R. Mazeikiene and A. Malinauskas, *European Polymer Journal*, 2002, **38**, 1947-1952.
45. A. A. Pud, *Synthetic Metals*, 1994, **66**, 1-18.
46. P. Hapiot and C. Lagrost, *Chemical Reviews*, 2008, **108**, 2238–2264.
47. J. Desilvestro, W. Scheifele and O. Haas, *Journal Electrochemical Society*, 1992, **139**, 2727.
48. G. Inzelt, *Electrochimica Acta*, 2000, **45**, 3865-3876.
49. C. Weidlich, K.-M. Mangold and K. Juttner, *Electrochimica Acta*, 2001, **47**, 741-745.
50. A. R. Hillman, K. S. Ryder, V. C. Ferreira, C. J. Zaleski and E. Vieil, *Electrochimica Acta*, 2013, **110**, 418-427.
51. M. A. Mohamoud, *Journal of Solid State Electrochemistry*, 2013, **17**, 2771-2782.
52. A. P. Abbott, D. Boothby, G. Capper, D. L. Davies and R. K. Rasheed, *Journal of the American Chemical Society*, 2004, **126**, 9142-9147.
53. A. P. Abbott, J. C. Barron, K. S. Ryder and D. Wilson, *Chemistry-A European Journal*, 2007, **13**, 6495-6501.
54. R. A. Khalkhali, W. E. Price and G. G. Wallace, *Reactive and Functional Polymers*, 2003, **56**, 141-146.

## **Chapter 5: Electrochemical Synthesis of Polyaniline from Choline-Based Type (III) Deep Eutectic Solvents and Characterisation of the Properties of Conducting Polymers using EQCM.**

### **Contents**

<b>5.1</b>	<b>Overview .....</b>	<b>122</b>
<b>5.2</b>	<b>Objective .....</b>	<b>123</b>
<b>5.3</b>	<b>Results and discussion .....</b>	<b>124</b>
5.3.1	Viscosity and conductivity measurements of DESs .....	124
5.3.2	Film preparation .....	129
5.3.3	Growth of PANI in Ethaline .....	130
5.3.4	Effect of dopant ions on electrochemical polymerisation of aniline .....	132
5.3.5	Effect of different DES electrolytes on the growth of aniline .....	134
5.3.6	Effect of various electrolytes on PANI stability and reversibility .....	136
5.3.7	Morphology and topography of the polymer films .....	140
5.3.8	Selection of polymer for further study .....	145
5.3.9	EQCM investigations of ions and solvents regarding polyaniline film .....	145
5.3.10	Conclusion .....	164
<b>5.4</b>	<b>References .....</b>	<b>166</b>

## 5.1 Overview

To date, the majority of investigations into electrically conducting polymers have been successfully performed in aqueous and organic electrolytes.<sup>1-3</sup> This may be due to these electrolytes having the appropriate cost, non-flammability and high solubility in terms of dissolution of metal salts, which leads to high conductivity and mass transport.<sup>4</sup> Despite their safety and efficiency, however, these systems suffer from some limitations, such as a small range over their potential windows causing hydrogen evolution, which can be hazardous and generate brittle electrodeposits (“hydrogen embrittlement”).<sup>4-6</sup> This factor can affect the conductivity, lifetime (reproducibility) and performance of a device. For instance, poor electrochemical stability for conducting polymers can occur after only a few cycles in some aqueous electrolytes due to degradation of the polymer in these solutions.<sup>7, 8</sup> In addition, solvent molecular transfer is accompanied by ion transfer between the polymer and electrolyte during the doping and undoping processes. Further, due to the fact that the anion species are particularly large, highly charged or prone to entanglement, they can be rendered immobile. As a result, the cationic species can dominate the transfer.<sup>9</sup>

Recently, in order to overcome some of the above problems, electrodeposition and ion exchange behaviour during the charging and discharging processes of these products has been utilised extensively in ionic liquids,<sup>10-14</sup> because these liquids offer significant enhancement to electrochemical properties, such as a broad potential window, selective products, low environmental impact and high ionic conductivity. These features can improve the sustainable properties of organic semiconductors regarding conductivity, durability, thermal stability and morphology.<sup>11, 15, 16</sup> Deep Eutectic Solvents (DESs) are a special type of ionic liquid discovered by Abbott *et al.*,<sup>17-20</sup> these solvents/electrolytes are a crucial factor in improving electroactivity, and thus the electrochemical stability, of the polymer; further information regarding this subject was reported in chapter one. Moreover, to the best of our knowledge, the use of DESs as background electrolytes in the deposition of electrochemically polymerised aniline has not yet been the subject of extensive scientific study.

In fact, the mechanisms of nucleation, growth and molar mass exchange in conducting polymers are unclear in highly ionic media, and especially in DESs. One reason for this is that the absence of a ‘solvent’ in the standard sense. Anion ingress and cation egress

during charging and discharging are affected by a number of factors such as (i) the type and size of the species in the solvent and (ii) the morphology of the polymer, which itself relies on the electrolyte composition. The purpose of this chapter is to explore the redox chemistry typical to polyaniline (PANI) when electrochemically deposited from type III deep eutectic solvents and then characterising in DESs and aqueous solution. Furthermore, we will concentrate on the redox processes in DESs include unique ion transport (anions or cations), mixed ion transport (anions and cations together), or neutral species. Therefore, the behaviour of PANI film in DESs will be compared to those deposited from aqueous solution in chapter four.

## 5.2 Objective

The purpose of this investigation was to understand the ion dynamics during the charging/discharging process of PANI film growths from DESs and the comparison of these polymer film growths with those from aqueous media (see chapter 4).

The following objectives regarding the study of conducting polymers are focused on in this work. **The initial objective** was to understand the effect of different DES media on the electrochemical growth and morphologies of the polymer, followed by an exploration of the stability and reversibility of these films in different environmental systems (aqueous/DES electrolyte), specifically with regards to their performance during cyclic voltammetry. **The second objective** was the identification of species present and mechanism of the PANI films using EQCM, which involved identification of the response of an acoustic resonator to polyaniline films (rigid or non-rigid) to background electrolytes using the Sauerbrey equation.<sup>21</sup>

**The third objective** of this research was the investigation the behaviour of PANI film in DES solvents (as well as aqueous solution) at room and high temperature by focussing on the redox-driven mass/charge transfer of PANI. Furthermore, EQCM studies, were used to analyse individual contributions of mobile species and solvents (ion fractions) in order to maintain electroneutrality through the redox switching process. This work included the effect of changing timescale (by changing potential scan rate), the potential sweep, physical properties of the film (thickness, growth conditions), the electrolyte composition by changing components of DESs and the

temperature of the electrolyte. Generally, the purpose of the current research was to see whether DESs are more appropriate electrolytes than organic and aqueous solvents in electrochemical devices (charge storage). The questions addressed here was one of identifying the mechanisms involved in these processes, and whether the behaviour of a conducting polymer is predominantly retained between DESs and the aqueous solution, or otherwise. Furthermore, are these behaviours due to the properties and composition of the film or the solution, *per se*. In the following sections, we will attempt to address the above objectives in the context of the preparation and exploitation of polyaniline films in practical applications.

### **5.3 Results and discussion**

#### **5.3.1 Viscosity and conductivity measurements of DESs**

##### **5.3.1.1 Viscosity measurements**

Viscosity of eutectic mixtures is one of the most significant issues affecting mass transport and charge transfer during electropolymerisation of the aniline monomer; therefore, it is crucial that this be addressed here. In this section, rotational viscometry was used to measure the viscosity of DESs. **Figure 5.1** shows the viscosities of type III DESs with/without 1 M H<sub>2</sub>SO<sub>4</sub> (measuring viscosity of DESs with H<sub>2</sub>SO<sub>4</sub> because PANI films were polymerised in DESs of 1 M H<sub>2</sub>SO<sub>4</sub> concentration, and we needed to see effect of the acid solution on the viscosity of the background electrolytes) as a function of temperature using a variety of HBDs with choline chloride as a quaternary ammonium. It can be seen that the viscosity of the ionic liquids are decreased with increasing temperature. This variation in viscosity with temperature is often explained using equation 5.1, which follows the Arrhenius Law.<sup>18, 22</sup>

$$\ln \eta = \ln \eta_0 + \frac{E_\eta}{RT} \quad 5.1$$

Here,  $\eta$  is absolute viscosity,  $\eta_0$  is a constant,  $R$  is the gas constant,  $T$  is the absolute temperature and  $E_\eta$  is the activation energy of viscous movement.

In this study, our results show that the viscosity of Ethaline seems to be lower than any other DES, while Maline displays the highest viscosity. Oxaline and Glyceline are of

intermediate viscosities; however, the viscosity of Glyceline exhibits a higher viscosity than Oxaline at temperatures above 40°C. As the temperature is raised, the viscosity decreases; this same sensitivity has been reported in previously in the literature.<sup>4, 18, 20, 23</sup> In general, the properties of these liquids are often attributed to van der Waals forces and hydrogen bonding, therefore the high viscosity of DESs and ionic liquids (ILs) are caused by the strong affinity between each individual components (ions/molecules) by means of hydrogen bonding and Coulombic forces.<sup>24</sup>

On the other hand, the viscosity of a solution of 1M H<sub>2</sub>SO<sub>4</sub> in the various DESs used herein (Ethaline, Propaline, Glyceline and Reline) tends to be more viscous than the pure DES electrolytes (i.e. without 1 M H<sub>2</sub>SO<sub>4</sub>). For example, the viscosity of Ethaline was 40 cP at 25 °C, compared to 1 M H<sub>2</sub>SO<sub>4</sub> in Ethaline, where it becomes 48 cP. This is due to the increasing number and the size of the ions in the solution (i.e. increased H-bonding), as a result, the range of available cavity sizes in solution is reduced, hence affecting mass transport properties. It was found that the difference in viscosity between a pure DES and its associated admixture with 1 M H<sub>2</sub>SO<sub>4</sub> shows a *relative* decrease with increasing temperature. This is because of the increase in free volume in the solution. Abbott and co-workers interpreted this in terms of the viscosity of the fluid being decreased by the increasing free volume, a process which can be described in detail by *hole theory*.<sup>25</sup> Therefore, at high temperature, the mobility of ions is increased due to ionic components containing empty spaces as a result of the thermal fluctuations causing localised density changes.<sup>6, 25</sup> This has been confirmed in previous studied,<sup>6</sup> the researchers in this case highlighting the fact that the interaction between the choline cation and the corresponding HBD becomes weaker by increasing the temperature. Conversely, the formation of a large number of hydrogen bonds leads to an increase in the viscosity of the ionic liquids.

Panels c and d of **Figure 5.1** describe  $\ln \eta$ , acquired from a rotating cylinder, versus reciprocal temperature for DESs, wherein it is possible to calculate flow activation energy from equation 5.1. The activation energies of DESs with/without added acid are listed in the **Table 5.1**. It has previously been shown that a large ratio of the size of the ion to hole radius in ionic liquids leads to high activation energies liquids compared with conventional liquids and high temperature molten salts.<sup>19, 20</sup> These magnitude of these activation energies not only relates to the available hydrogen bonding interactions,

but is also correlated to the ratio of the size of the ions compared to the size of the holes. In Ethaline, the activation energy is lower than for other DESs, which is thought to be due to weaker hydrogen bonding and the larger void volume. By contrast, Maline and Reline have large  $E_\eta$  values, which arise from the energy required to form and increase the average radius of the holes in the electrolyte that control mass transport. It was observed that the viscosity and activation energies of ionic liquids were significantly affected by many factors, such as water content, temperature and the chemical nature of the electrolyte compounds. The mobile species present and the void magnitude (free volume) were also key variables in the fluidity of deep eutectic solvents, and thus their associated mobilities and mass transport properties.

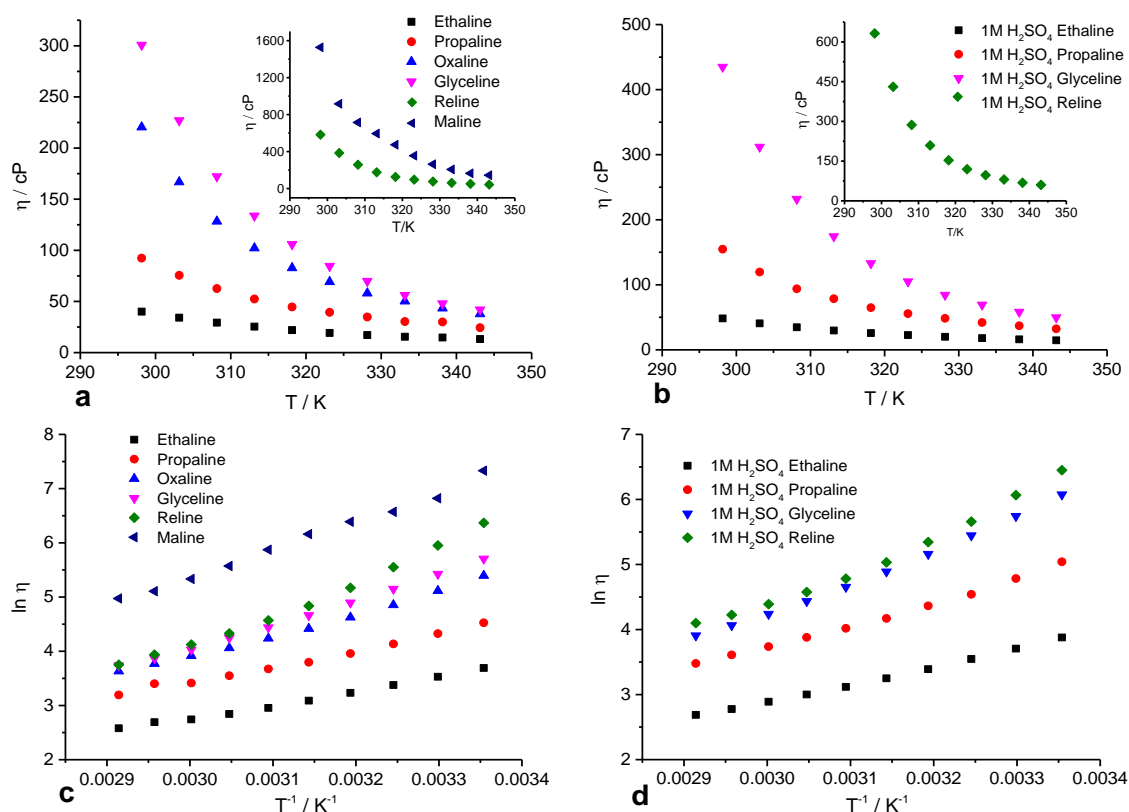


**Figure 5.1:** Plot of viscosity vs. temperature for a) a variety of DESs and b) 1 M H<sub>2</sub>SO<sub>4</sub> admixtures with each DES. Panels c) and d) are plots of the natural log of the viscosity vs. reciprocal temperature for the same variety of DESs and their admixtures with 1M H<sub>2</sub>SO<sub>4</sub>, respectively.

**Table 5.1:** Values of activation energies of viscosity flow for different DESs over a temperature range of 25 - 70 °C as found from **Figure 5.1**.

No.	DESs	Activation energy kJ mol <sup>-1</sup>	1 M H <sub>2</sub> SO <sub>4</sub> / DESs	Activation energy kJ mol <sup>-1</sup>
1	Ethaline	21	Ethaline	23
2	Propaline	24	Propaline	29
3	Oxaline	33	-	-
4	Glyceline	37	Glyceline	41
5	Reline	42	Reline	47
6	Maline	46	-	-

### 5.3.1.2 Conductivity measurements

Because of the high relative viscosities of ionic liquids, most such liquids tend to have relatively low conductivities at room temperature. The ionic conductivity of ILs and DESs generally depends on the mobility of species in ionic fluids rather than ionic activity.<sup>19, 26</sup> **Figure 5.2** shows the conductivity of type III DESs (with/without 1 M H<sub>2</sub>SO<sub>4</sub>) as a function of temperature. It is clear that the electrical conductivity of DESs is strongly increased as the temperature increases; the data shown here are analogous to those observed in previous studies.<sup>4, 20</sup> The highest conductivity is found for Ethaline, while both Maline and Reline have much lower conductivities owing to their higher viscosities. Abbott and co-workers debated the idea that since the size of the ions and the availability of vacant sites limits the viscosity of an ionic liquid, that “the movement of species within these systems is controlled by the ease of migration through voids, which in turn is controlled by the dimensions of the vacant sites”.<sup>20</sup> The conductivity of these systems, will be also limited by the availability of suitably sized vacancies in the liquid. Similar to the viscosity results, the conductivities of DESs without/with 1 M H<sub>2</sub>SO<sub>4</sub> have been fitted to equation 5.2:<sup>27</sup>

$$\ln \sigma = \ln \sigma_0 - \frac{E \wedge}{RT} \quad 5.2$$

In contrast, the conductivity of a 1 M H<sub>2</sub>SO<sub>4</sub> admixture with DESs is considerably lower than that observed in the pure equivalent DES. This difference in characteristics, as shown by viscosity properties, is likely to be due to diversity in liquid density, which results from the differing degrees of hydrogen bonding in the two systems. The

conductivity decreases observed for this system could be due to the large anion ( $\text{SO}_4^{2-}$ ) clusters reducing ion mobility.

The activation energies for conduction ( $E_A$ ) are listed in **Table 5.2**, which are gained according to **Figure 5.2c, d** and equation 5.2. The value of  $E_A$  for pure Ethaline was 14  $\text{kJ mol}^{-1}$  which become 16  $\text{kJ mol}^{-1}$  on addition of  $\text{H}_2\text{SO}_4$  as more charge carriers were added to the system. This means that the ion mobility controls the conductivity due to the space of the free volume, not the actual number of charge carriers present. In other words, the ideas proposed above reinforce the idea that the conductivity due to ion mobility is controlled by the density of voids, not the density of charged species. This is because restriction of mass transport can be affected by decreasing the availability of voids of suitable dimensions in the liquid, leading to the fluid becoming more viscous.<sup>19, 20</sup> The results of the conductivity measurements recorded for the various DES systems were analysed to indicate whether these are also dominated by the availability of suitably sized vacancies in the liquid.

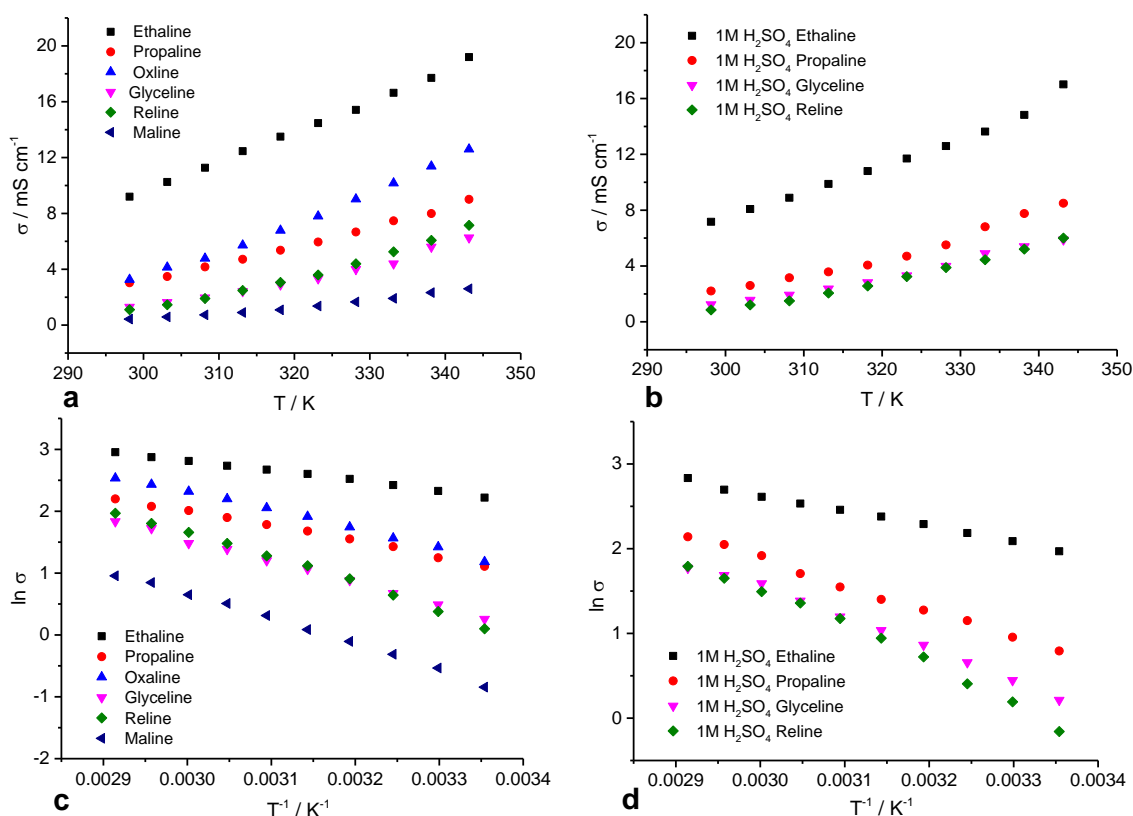


**Figure 5.2:** Plot of conductivity vs. temperature for a) a variety of DESs and b) 1M  $\text{H}_2\text{SO}_4$  admixtures of DESs. Panels c) and d) are plots of the natural log of conductivity vs. reciprocal of temperature for the same variety of DES and their 1M  $\text{H}_2\text{SO}_4$  admixtures, respectively.

**Table 5.2:** Activation energies of conductivity for the various DESs givens in Figure 5.2.

No.	DESs	Activation energy kJ mol <sup>-1</sup>	1 M H <sub>2</sub> SO <sub>4</sub> / DESs	Activation energy kJ mol <sup>-1</sup>
1	Ethaline	14	Ethaline	16
2	Propaline	20	Propaline	26
3	Oxaline	25	-	-
4	Glyceline	29	Glyceline	30
5	Reline	34	Reline	37
6	Maline	35	-	-

### 5.3.2 Film preparation

In this chapter, polyaniline films were synthesised electrochemically from its monomer solution in DESs onto a conducting substrate in order to compare with the polymer films prepared in Chapter four. The growth conditions for the PANI films used in this chapter are given in the **Table 5.3**.

**Table 5.3:** Experimental conditions for the deposition of PANI films used in this chapter in different electrolytes and supporting electrolytes. The potential windows were 0.0 to 1.2 V, with a scan rate of 100 mV s<sup>-1</sup> for 20 cycles at room temperature.

No.	Monomer concentration	Electrolytes	Supporting electrolytes	Results
1.	0.5 M aniline	Ethaline	-----	No PANI film
2.	0.5 M aniline	Ethaline	0.2 M LiCl	No PANI film
3.	0.5 M aniline	Ethaline	1M H <sub>2</sub> SO <sub>4</sub>	Weak PANI film
4.	0.8 M aniline	Ethaline	1M H <sub>2</sub> SO <sub>4</sub>	PANI film
5.	0.8 M aniline	90 % Vol Ethaline: 10 % Vol Water	1M H <sub>2</sub> SO <sub>4</sub>	PANI film
6.	0.8 M aniline	Ethaline	1M *HCl	PANI film
7.	0.8 M aniline	Ethaline	1M *HNO <sub>3</sub>	PANI film
8.	0.8 M aniline	Ethaline	1M *HClO <sub>4</sub>	PANI film
9.	0.8 M aniline	90 % Vol Propaline: 10 % Vol Water	1M H <sub>2</sub> SO <sub>4</sub>	PANI film
10	0.8 M aniline	90 % Vol Glyceline: 10 % Vol Water	1M H <sub>2</sub> SO <sub>4</sub>	PANI film

11	0.8 M aniline	90 % Vol Reline: 10 % Vol Water	1M H <sub>2</sub> SO <sub>4</sub>	PANI film
12	0.8 M aniline	90 % Vol Maline 10 % Vol Water	-----	PANI film
13	0.8 M aniline	Oxaline	-----	PANI film
14	0.8 M aniline	Ethaline	3 M **Oxalic acid	PANI film

Notes:

\* These acids contain certain amounts of water (see 2.1)

\*\* Anhydrous oxalic acid

### 5.3.3 Growth of PANI in Ethaline

Ethaline (200) (a deep eutectic solvent) was initially chosen as the electrolyte to study the electropolymerisation of aniline by cyclic voltammetry. Looking at the pure liquid in **Figure 5.3a** as well as with added 0.2 M LiCl (**Figure.5.3b**), in the first oxidation scan, one peak is well -defined. The first peak, observed at 1.0 V and 1.1 V in these solvents, might be caused by the oxidation of –NH<sub>2</sub>, as has been reported previously.<sup>28</sup> On further potential cycling, the oxidation currents of these peaks decreased rapidly. However, no appreciable film growth was observed on the electrode surface, even after 40 cycles. This may be because these solvents have no proton source, leading to a lack of any reaction during the oxidative and reductive processes. This implies that the oligomer is formed but the radical cation of the oligomer couples could not react to form the polymer film due to the non-acidic medium. Likewise, Brett *et al.* showed that electrodeposition of EDOT in pure deep eutectic solvents wasn't successful due to the fact that radicals are not formed in these conditions.<sup>29</sup>

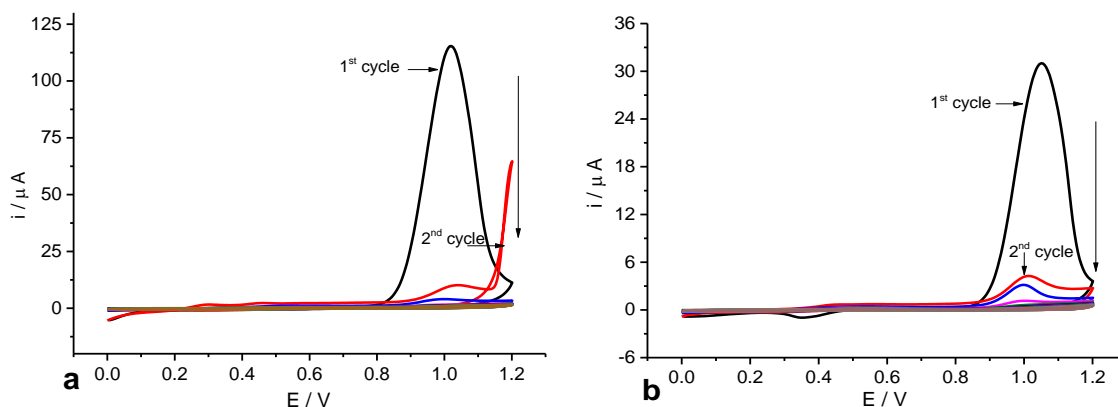


**Figure 5.3:** CVs of PANI film on a Pt electrode (1 mm diameter) from 0.5 M aniline in (a) Ethaline and (b) Ethaline (0.2 M LiCl) over 20 scans. The scan rate was 100 mV s<sup>-1</sup>.

In order to achieve the polymerisation of aniline in the Ethaline electrolyte, sulphuric acid (1 M H<sub>2</sub>SO<sub>4</sub>) was added as a supporting electrolyte to provide a proton source, with the resulting CVs shown in **Figure 5.4a**. It is clear that the deposition of polyaniline on the electrode surface probably occurs, and indeed, there is a small increase in the redox peaks between scans, but the interaction was very weak and, as a consequence, the redox peaks are not particularly apparent.

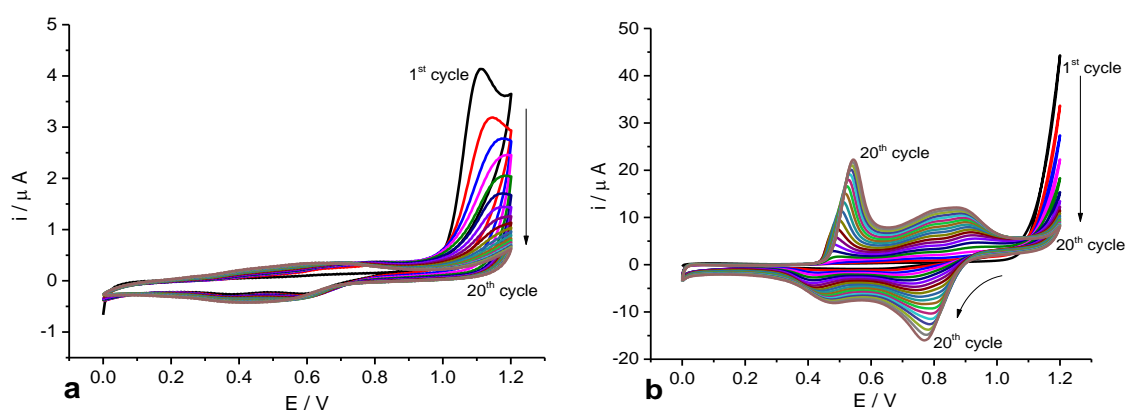


**Figure 5.4:** CVs of PANI film on a Pt electrode (1 mm diameter) from (a) 0.5 M aniline in Ethaline + 1 M H<sub>2</sub>SO<sub>4</sub> and (b) 0.8 M aniline in Ethaline + 1 M H<sub>2</sub>SO<sub>4</sub> solutions over 20 scans. The scan rate was 100 mV s<sup>-1</sup>.

However, a significant development, in the form of the successful synthesis of polymer via electropolymerisation from a 0.8 M aniline and 1 M H<sub>2</sub>SO<sub>4</sub> in Ethaline electrolyte precursor is illustrated in **Figure 5.4b**. It was noticed that a film of PANI was subsequently grown from this solution scan upon scan. Here, apparently, there were two factors that influenced the deposition of PANI in Ethaline. Firstly, acidic conditions<sup>30</sup> and secondly, increasing the concentration of the monomer, as has been emphasised in the literature.<sup>31</sup> The CVs shape for PANI in Ethaline is similar to that found in aqueous solution, in that it has two redox peaks. However, its formation does not follow an autocatalytic mechanism as in aqueous media, the peak current is decreased at maximum potential (i.e. nucleation loop), and increasing the number of scans leads to the development of a couple of redox pairs. It should be noted that PANI films formed in aqueous acidic liquids (PANI-H<sub>2</sub>O) are prepared by the coupling of refined benzenoid rings (leucoemeraldine base, LB), exchanged benzenoid and quinoid rings (emeraldine salt, ES), and refined quinoid rings (pernigraniline base, PB).<sup>32-34</sup>

The electrochemical result can be explained by two electrons and two protons conveyed between various states of PANI in acidic aqueous solutions (see **Figure 1.4b**). In

comparison with the well-known CV-PANI-H<sub>2</sub>O system, we can associate the first redox process (located at 0.41 V in the CVs of **Figure 5.4b**) with the oxidative transition from LB to ES, and its reverse reduction in the negative-moving potential deviation. Similar to the first redox process, the second redox pair at 0.82 V is probably further oxidation of ES to PB and its reverse reaction. A third wave has been assigned to the redox activity of the *p*-benzoquinone/ hydroquinone (BQ/HQ) side species formed upon the above oxidation of PB. In addition, the potential changes in the redox process from the minimum limit to the maximum limit of CV-PANI- Ethaline indicated a  $\Delta E$  value of more than 150 mV, and its reversibility is higher compared to CV-PANI-H<sub>2</sub>O due to loss of protons in aqueous media.<sup>32,33</sup>

### 5.3.4 Effect of dopant ions on electrochemical polymerisation of aniline

The influence of anions doping during the growth of PANI film has also been examined in Ethaline via cyclic voltammetry. These anions act as a supporting electrolyte solution during the electropolymerisation, and they substantially impact on redox potentials and current densities.<sup>35</sup>

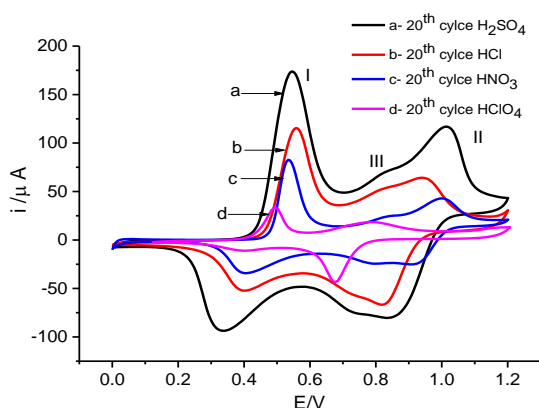


**Figure 5.5:** CVs of PANI films on a Pt electrode (1 mm diameter) from 0.8 M aniline in Ethaline, having 1 M of (\*a); H<sub>2</sub>SO<sub>4</sub>, (b); HCl, (c); HNO<sub>3</sub> and (d); HClO<sub>4</sub>. The scan rate was 100 mV s<sup>-1</sup>, 20 scans shown. \*a has 10 % Vol of deionised water used.

Here, we grow polyaniline from different inorganic acids (H<sub>2</sub>SO<sub>4</sub>, HCl, HNO<sub>3</sub> and HClO<sub>4</sub>) in Ethaline on a platinum electrode. The aim of this section of work is to emphasise the effect of dopant ions upon current density and successive cycles of electropolymerisation of aniline and compared with the PANI films, which were grown from the same acid but in the aqueous background electrolyte described in the last chapter (section 3.3.2). Generally, dopant ions may lead to a diversity of film conductivity values compared with undoped patterns, and the latter may have lower

conductivities. As can be seen in **Figure 5.5** and **Table 5.4** the highest anodic current peak (175  $\mu\text{A}$ ) and polymerisation rates were exhibited for the  $\text{SO}_4^{2-}$  doped solutions, whereas the  $\text{ClO}_4^-$  doped solutions represented the lowest anodic current peak (34  $\mu\text{A}$ ), and a lower polymerisation rate was obtained. This may be due to charge density of anions used affecting the oxidation potential of the monomer. In addition, some anions, such as  $\text{HSO}_4^-$  and  $\text{Cl}^-$ , tend to be strongly adsorbed on the external face of the working electrode. Conversely,  $\text{ClO}_4^-$  anions probably do not have this property on the external area of the electrode. Furthermore, three instances of redox pairs formed in PANI films that were prepared from Ethaline solutions containing the acids  $\text{H}_2\text{SO}_4$ ,  $\text{HCl}$  and  $\text{HNO}_4$ . According to a recent study, the first oxidation state (I) can be attributed to transfer from the LB to ES form, while the second oxidation peak (II) responds to ES converse to PB. Peak III was assigned to the presence of crosslinking in the polyaniline caused by the reaction of nitronium species being present as intermediates. Alternatively, peak III has been assigned to overoxidation products.<sup>35</sup>

In contrast, the PANI film, which was synthesised in Ethaline in the presence of  $\text{HClO}_4$ , shows two peaks, I and II. The lack of the central peak III is probably due to the missing crosslinking or overoxidation reaction as compared to the polymers formed in  $\text{H}_2\text{SO}_4$ ,  $\text{HCl}$  and  $\text{HNO}_4$  solutions.<sup>35, 36</sup> It can be said that the data for polyaniline grown from Ethaline in the presence of these inorganic acids is in good agreement with our last result in terms of growth rate of the polymer (see section 4.3.2) and follows the order  $\text{SO}_4^{2-} > \text{Cl}^- > \text{NO}_3^- > \text{ClO}_4^-$ . By using Faraday's Law, the thickness of polymer has been estimated from the amount of charge, which was determined from the final voltammogram of the more cathodic reduction peaks of PANI during the deposition process. All details and equations on this subject can be seen in section 3.3.1.1.

**Table 5.4:** Redox potentials and current peaks of PANI films deposited from Ethaline using different supporting electrolytes.

Polymer growth from 1 M		Thickness of polymer (nm)	Anodic current (i/ $\mu\text{A}$ )			Anodic potentials (V)		
			I	II	III	I	II	III
a	$\text{H}_2\text{SO}_4$	948	175	118	71	0.55	1.0	0.83
b	$\text{HCl}$	543	116	60	53	0.55	0.94	0.81
c	$\text{HNO}_3$	281	86	40	17	0.52	1.0	0.81
d	$\text{HClO}_4$	131	34	15	-	0.49	0.79	-

### 5.3.5 Effect of different DES electrolytes on the growth of aniline

The influence of the DES composition on the nucleation and growth mechanism of polyaniline has not yet been investigated. **Figure 5.6** (a-f) demonstrates the CVs observed during the electrodeposition of PANI films in electrolytes of Ethaline, Propaline, Glyceline, Reline, Maline and Oxaline at  $25 \pm 2^\circ\text{C}$ .

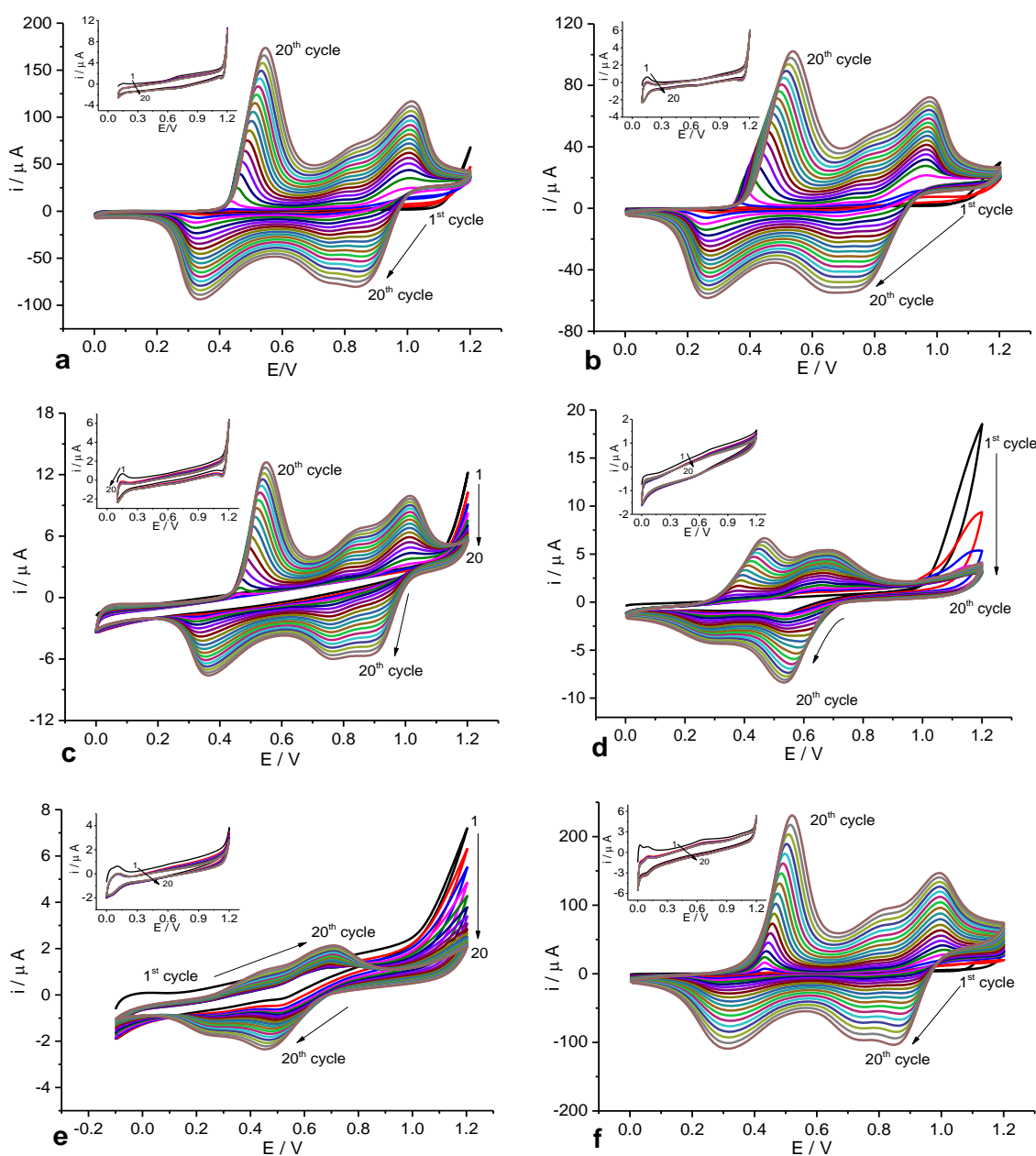


**Figure 5.6:** CVs of PANI on a Pt electrode from 0.8 M aniline + 1 M  $\text{H}_2\text{SO}_4$  in (\*a) Ethaline (\*b) Propaline, (\*c) Glyceline, (\*d) Reline, (\*e) Maline and (f) Oxaline over 20 scans. The scan rate was  $100 \text{ mV s}^{-1}$ . The insert shows CVs of the background electrolyte without aniline. \*background electrolyte consisted of 10 % Vol  $\text{H}_2\text{O}$ :90 % DES

In order to reduce the viscosity of the solvent and increase the growth rate of the film, all DESs except Oxaline, were diluted with 10 % Vol deionised water. The results show that the lowest polymerisation rates were obtained from Maline, Reline, and Glyceline ( $I = 1, 7$  and  $13 \mu\text{A}$ , respectively, see **Table 5.5**) due to their high viscosities, which affected their current densities.<sup>32</sup> Electropolymerisation in Ethaline in the presence of 10 % Vol deionised water showed a higher capacitive current than in **Figure 5.4b**. This was due to the effect of the water<sup>37</sup> as the  $\text{H}_2\text{SO}_4$  reacts with  $\text{H}_2\text{O}$  to produce  $\text{HSO}_4^-$  and  $\text{H}_3\text{O}^+$ . This may lead to an increased number of protons, which play a key role in increasing PANI adherence by improving the mobility of the ionic species. The second reason is that the viscosities of all DES reduce when the water is added and, water-DES mixtures are not homogeneously mixed but there is a “microscopic” phase separation between them.<sup>38</sup>

The highest polymerisation rates and current density were achieved in the Oxaline electrolyte. This considers a new method for growth of PANI electrochemically from DESs. There are many factors that may have an effect on these results. Firstly, high viscosity and low conductivity of some electrolytes, such as Maline, Reline and Glyceline, cause a decrease in electropolymerisation rates. It is well known that the mobility of the ionic species is in turn affected by the viscosity of the medium; this effect was previously studied in section 5.3.1. Another factor that may be related to the type of HBD structure in each electrolyte, and how these structures react with the ion pair of anilinium and consequently, effect on the rate of polymerisation of the aniline monomer. It could be argued that Oxaline, having a large number of carboxylic groups as well as two  $\text{H}_2\text{O}$  molecules present to each oxalic acid moiety (added to reduce the viscosity of the medium) might have a significant influence on the growth of polymeric chains. In other words, the protons from the carboxylic acid play an important role in the charge transport in an Oxaline medium, unlike in Ethaline, Propaline and other DESs.<sup>19, 32</sup> However, Maline also has carboxylic groups, but it tends to have a lower current density due to its higher viscosity than Oxaline and, as a consequence, mass and charge transfer rates are reduced in such a viscous medium. The second reason may be regarded to acidity, anilinium pKa is 4.6, malonic acid is (pKa is 3.4, 5.2) which less acidity than oxalic acid (pKa is 1.2, 4.2) as a result the nucleation and growth process for PANI-Oxaline is to be fast than PANI-Maline.

The shifting oxidation and reduction waves of conducting polymers are related to an increased thickness of the polymer, and may be due to different aspects, for example: heterogeneous electron-transfer kinetics due to mass transfer limits the electrochemical process or a loss in electrical conductivity of the electrolyte, in counter-ion mobility or limited conjugated network.<sup>39</sup> It should also be mentioned that the electrodeposition of aniline has been performed successfully in an Ethaline 200 electrolyte containing 3 M anhydrous oxalic acid. The anodic current peak was 36  $\mu\text{A}$ , which will be compared to the other PANI films observed in this study. Compared with aqueous electropolymerisation, the redox peaks of the polymerisation of aniline carried out in DESs are relatively broad, similar to  $\text{HClO}_4$ , while in  $\text{H}_2\text{SO}_4$ ,  $\text{HCl}$  and  $\text{HNO}_3$ , sharp peaks are observed. Thicker films with lower degrees of reversibility are formed with aqueous solvents compared to DESs over 20 scans at  $100 \text{ mV s}^{-1}$ .

**Table 5.5:** Redox potentials and current peaks at the redox peaks of PANI films deposited from DES electrolytes having different hydrogen bond donors.

Polymer growth from 1 M		Thickness of polymer (nm)	Anodic current ( $i/\mu\text{A}$ )			Anodic potentials (V)		
			I	II	III	I	II	III
a	Ethaline	949	173	120	72	0.55	1.00	0.80
b	Propaline	652	102	73	49	0.54	0.97	0.79
c	Glyceline	64	13	7	10	0.55	1.00	0.8
d	Reline	45	7	5	-	0.48	0.68	-
e	Maline	14	1	2	-	0.44	0.72	-
f	Oxaline	1277	231	147	95	0.53	1.00	0.80

### 5.3.6 Effect of various electrolytes on PANI stability and reversibility

Analogous to those polymers observed in aqueous studies, **Figure 5.7** and **Table 5.6** illustrate the exceptional stability of polyaniline films prepared from DESs. In order to investigate the redox stability of polymers, all films prepared in DESs (section 5.3.5) were initially cycled in the same background solution that they were grown in, after which they were rinsed with deionised water several times, treated with 0.5 M  $\text{H}_2\text{SO}_4$ , and then rinsed again with deionised water. They were then placed in the same electrolyte in which they were synthesised in the absence of aniline. In aqueous

solution, we used a more negative potential sweep, between -0.2 and 1.0 V, to prevent the overoxidation of PB. However, the potential window employed for DESs was between 0.0 and 1.2 V, with the scan rate in both systems held at  $100 \text{ mV s}^{-1}$ . There is a potential shift, but this is mainly a manifestation of the different reference electrodes necessarily used in the two media. In general, the stability of all of PANI-DESs in aqueous solution were clearly higher than DES electrolytes, and films clearly maintained their redox activities. This is possibly due to DESs being denser than aqueous solution.

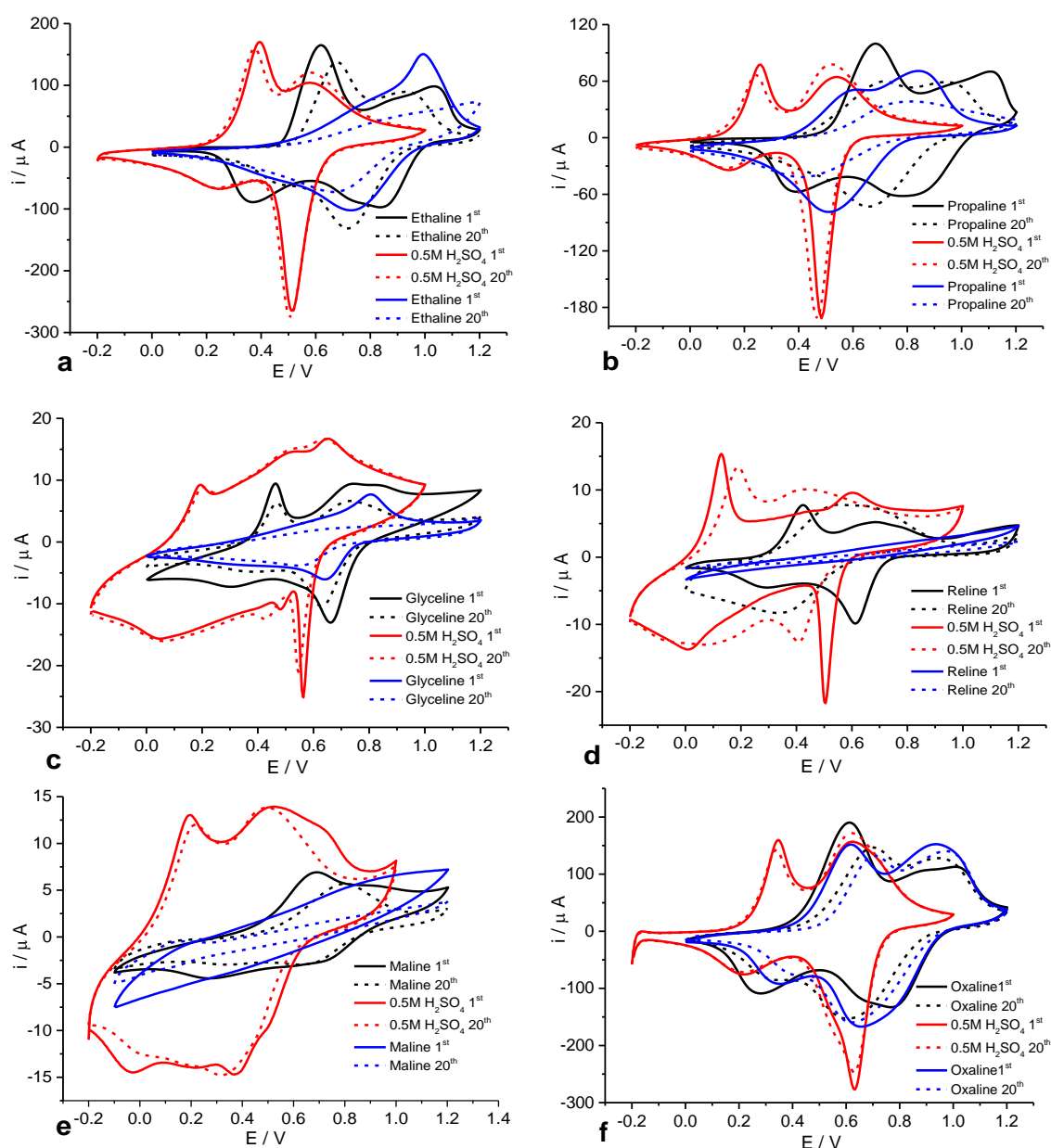


**Figure 5.7:** CVs explain the stability of PANI films exposed to background electrolyte (monomer free),  $0.5 \text{ M H}_2\text{SO}_4$  and then returned to background electrolyte again. The electrolytes are (a) Ethaline, (b) Propaline, (c) Glyceline, (d) Reline, (e) Maline and (f) Oxaline. The scan rate was  $100 \text{ mV s}^{-1}$ , cycles 1 and 20 are shown.

From the data above, the minimum electroactive stabilities were found in PANI-Maline and PANI-Reline, **Figures 5.7e** and **5.7d**, respectively, when these polymers were transferred back into their background electrolytes. This could be related to many factors, such as the high viscosity and low conductivity of these solvents causing the movement of ions transported between the polymer and electrolyte to be very slow, and with the resultant obstruction in the movement of ions that would occur. Furthermore, the weak degree of polymerisation which was achieved in this polymer, owing to the highly viscous electrolyte, can affect their structural stability. The electroactivity of PANI in Ethaline (**Figure 5.7a**) prolongs the cycle life compared to the polymers prepared from Propaline, Glyceline, Reline and Maline. However, it was dramatically decreased in the current peaks after the film was returned to Ethaline. This could be due to a combination of deprotonation as well the polymer probably suffering from dissolution and/or irreversible damage, i.e., change in structure at the extended potential employed.

Remarkably, PANI-Oxaline film showed a better redox stability in comparison to other polymers after being cycled in Oxaline, aqueous solution, and Oxaline, respectively. This might be due to the proton source of the carboxylic group (COOH) in Oxaline supporting the intensity of oxidation and reduction for the film by a combination of the anion dopant into the polymer rather than OH<sup>-</sup> in Ethaline, Propaline, and Glyceline, and CO-NH<sub>2</sub> in Reline.<sup>11, 12, 32</sup> In addition to the reasons mentioned above, Marmisolle stated that as a result of the reduction of the electrically active area of the PANI/electrolyte interface, changes in the impedance and voltammetric response can occur during electrochemical cycling.<sup>40</sup> Innis *et al.* said that the stability of polyaniline and polypyrrole electrochemically synthesised from ILs can be affected by nitrogen/non-nitrogen purges dried upon hydrophobic RTILs” such as tetrabutylammonium hexafluorophosphate (TBA PF<sub>6</sub>) and, the results showed that polymer films cycled in TBA PF<sub>6</sub> are more stable with N<sub>2</sub> than without N<sub>2</sub>.<sup>11, 12</sup> According to our experimental data, the electrochemical stability of films synthesised from different hydrogen bond donors take the following order: PANI-Oxaline > PANI-Ethaline > PANI-Propaline > PANI-Gyceline > PANI-Reline > PANI-Maline.

**Table 5.6:** Explains charge values of PANI stability in each electrolyte: a) Ethaline, b) Propaline, c) Glyceline, d) Reline, e) Maline and f) Oxaline. The charge is calculated from integration the current of the reduction peak with time in the cyclic voltammogram. Charges of cycles 1 and 20 are shown.

PANI cycled in electrolytes		Q/C red. 1 <sup>st</sup> cycle	Q/C red. 20 <sup>th</sup> cycle	% Q red. retention 20 <sup>th</sup> /1 <sup>st</sup> cycle	% Q red. average retention
<b>a</b>	Ethaline	$4.942 \times 10^{-4}$	$4.165 \times 10^{-4}$	84	<b>58</b>
	0.5 M H <sub>2</sub> SO <sub>4</sub>	$4.883 \times 10^{-4}$	$5.022 \times 10^{-4}$	102	
	Ethaline	$4.149 \times 10^{-4}$	$2.852 \times 10^{-4}$	69	
<b>b</b>	Propaline	$3.511 \times 10^{-4}$	$2.653 \times 10^{-4}$	76	<b>37</b>
	0.5 M H <sub>2</sub> SO <sub>4</sub>	$2.605 \times 10^{-4}$	$2.771 \times 10^{-4}$	106	
	Propaline	$2.474 \times 10^{-4}$	$1.313 \times 10^{-4}$	53	
<b>c</b>	Glyceline	$2.897 \times 10^{-5}$	$2.129 \times 10^{-5}$	73	<b>35</b>
	0.5 M H <sub>2</sub> SO <sub>4</sub>	$5.680 \times 10^{-5}$	$5.584 \times 10^{-5}$	98	
	Glyceline	$1.763 \times 10^{-5}$	$1.019 \times 10^{-5}$	58	
<b>d</b>	Reline	$2.406 \times 10^{-5}$	$1.725 \times 10^{-5}$	72	<b>39</b>
	0.5 M H <sub>2</sub> SO <sub>4</sub>	$3.355 \times 10^{-5}$	$3.352 \times 10^{-5}$	99	
	Reline	$9.299 \times 10^{-6}$	$5.252 \times 10^{-6}$	56	
<b>e</b>	Maline	$1.377 \times 10^{-5}$	$8.640 \times 10^{-6}$	63	<b>22</b>
	0.5 M H <sub>2</sub> SO <sub>4</sub>	$5.538 \times 10^{-5}$	$4.851 \times 10^{-5}$	88	
	Maline	$2.988 \times 10^{-6}$	$1.445 \times 10^{-6}$	48	
<b>f</b>	Oxaline	$6.784 \times 10^{-4}$	$6.309 \times 10^{-4}$	93	<b>89</b>
	0.5 M H <sub>2</sub> SO <sub>4</sub>	$6.154 \times 10^{-4}$	$6.271 \times 10^{-4}$	102	
	Oxaline	$6.741 \times 10^{-4}$	$6.032 \times 10^{-4}$	89	

### **5.3.7 Morphology and topography of the polymer films**

#### **5.3.7.1 Scanning Electron Microbalance (SEM)**

The morphology of PANI-DES was investigated by SEM, and different morphologies were formed in layers grown in different background electrolytes. These films were grown potentiodynamically between 0.0 V and 1.2 V at  $100 \text{ mV s}^{-1}$  for 20 cycles, for which high resolution images of polyaniline films are presented in **Figure 5.8**. In particular, the figures demonstrate different sizes of the grains and chains. The latter is strongly based on the composition of the solution, notably on the type of counterions present.<sup>41, 42</sup> In the case of PANI formed from Reline and Maline (panels d and e, respectively), the pictures display many tiny globules linked together with a regular microstructure and low coverage of the electrode surface, whereas the image of the PANI-Glyceline electrolyte (**Figure 5.8c**) shows that film chains seem to be fibrous, connecting to each other with void spaces and with low coverage of the electrode area.

However, the images shown in panels a, b and f show higher coverage of the electrode surface and, also, that their morphologies could be homogenous in shape due to the high degree of regulation of the growth rate in comparison with the polymer films mentioned above (panels c, d and e). In the case of films made from Ethaline and Propaline, the chains of film connected together to make an agglomerated shape with a porous, fibrous morphology, while PANI formed from the Oxaline electrolyte has small sized circular grains connected to each other, and could be more porous and homogenous than other types. This is mainly due to the nucleation and growth process, which is dependent on the nature and size of the ion present in solution, as reported by Cordova *et al.*<sup>43</sup> This fact was shown in section (5.3.5) as the electron transfer reaction of the polymerisation process would be faster in Oxaline than for other DESs.

As mentioned in previous sections, the differences in porosity are a result of the different sizes of anions that were used. The latter (counterions) caused different sizes of voids to form in the polymer networks, which may have had an effect on the thickness of these polymers. This seems to be possible: the film morphology (compactness, swelling) could be decided during electrochemical polymerisation by choosing the size and kind of anion present in solution in order to make larger or smaller holes in the polymer surface. Large holes in the film morphology are considered to be one of the most significant factors in improving electrochemical stability because

the movement of cations and/or anions will be easier through the polymer network. It can be concluded that grains of the polymer films prepared in DES solutions are more compact, and considerably different from polymers grown from aqueous solutions. The sizes of the grains were also different from each other. This fact is also confirmed by the AFM images seen in **Figure 5.9** as a result of the differences in the thickness, roughness and size of the nodules in these films.

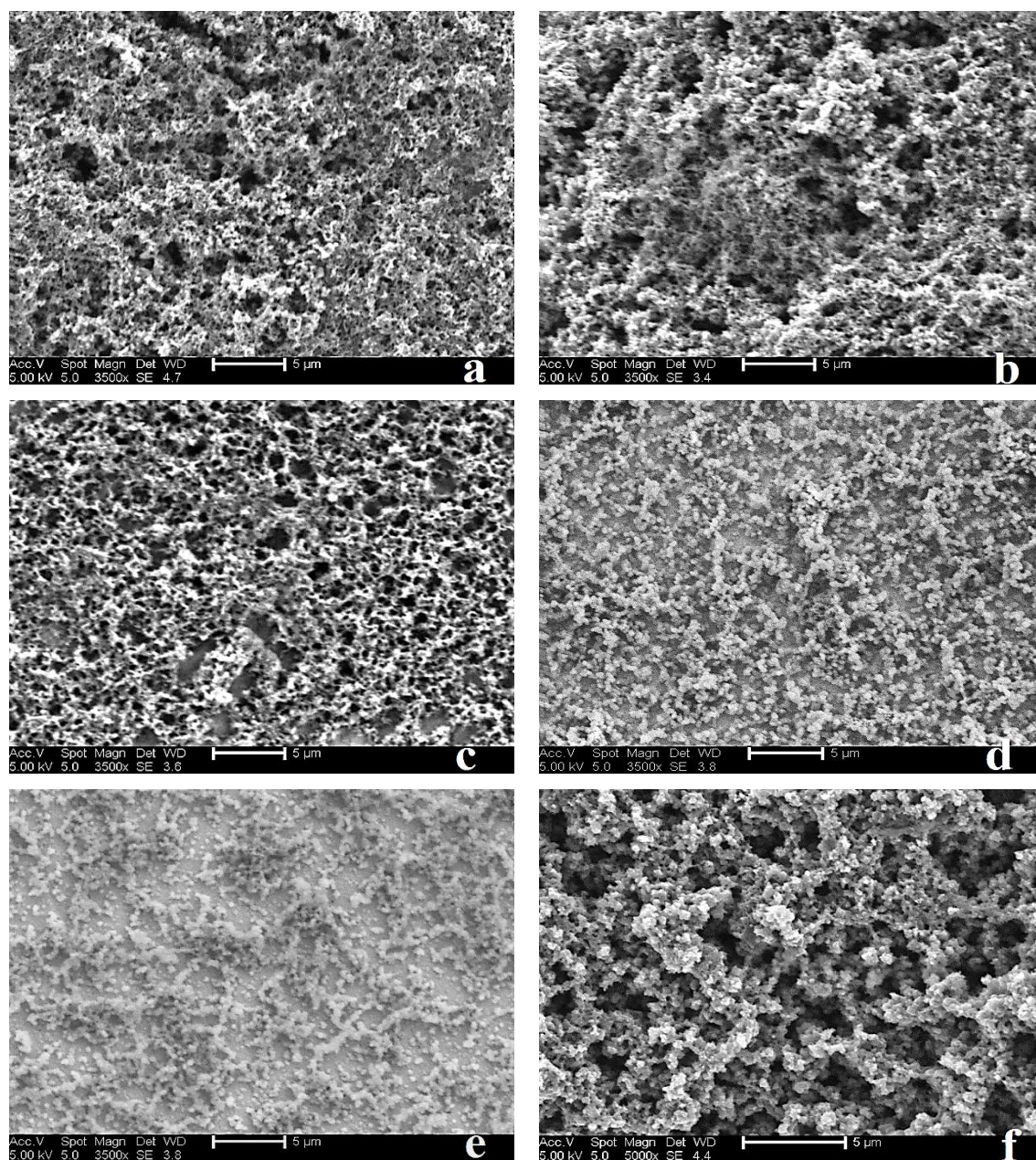


**Figure 5.8:** SEM pictures taken *ex-situ* in SE mode for Pt electrodes modified with CV-PANI-1 M H<sub>2</sub>SO<sub>4</sub> from 0.8M aniline in a) Ethaline b) Propaline, c) Glyceline d) Reline e) Maline and f) Oxaline as prepared with 20 scans between 0.0 and 1.2 V at 100 mV s<sup>-1</sup>.

### 5.3.7.2 Atomic Force Microscopy (AFM)

**Figure 5.9** compares surface topographies of polyaniline films made from different DES electrolytes using the same electropolymerisation conditions, such as potential window, scan rate, cycle numbers, type and size of electrode. In the same manner as SEM, AFM images demonstrated that the growth of polymer films is strongly dependent on the compositions of the electrolyte, it is also obvious that the thickness and roughness in the films increases the faster the polymerisation process occurs.<sup>44</sup> As can be observed from these images, PANI-Oxaline and then PANI-Ethaline have larger-sized nodules and are more porous than other polymers. In contrast, surface images of polymers made from Glyceline and Reline seem to have a small globular morphology with different sized particles, depending on the chemical nature of the anion. The surface morphology of PANI-Maline is very smooth and has the lowest roughness compared with other films. This might be due to the poor polymerisation process which had occurred. It may be noticed that polyaniline grown from DESs have various surface characterisations that are not observed for those formed from aqueous solutions.

The formation of polymeric nodules is dependent on deposition mechanism, and in this case there are a range of sizes of small nucleation centres on electrode substrate from nonhomogeneous/ homogeneous contributions, leading to different globular formation.<sup>45, 46</sup> Further work will be required to understand this phenomenon.

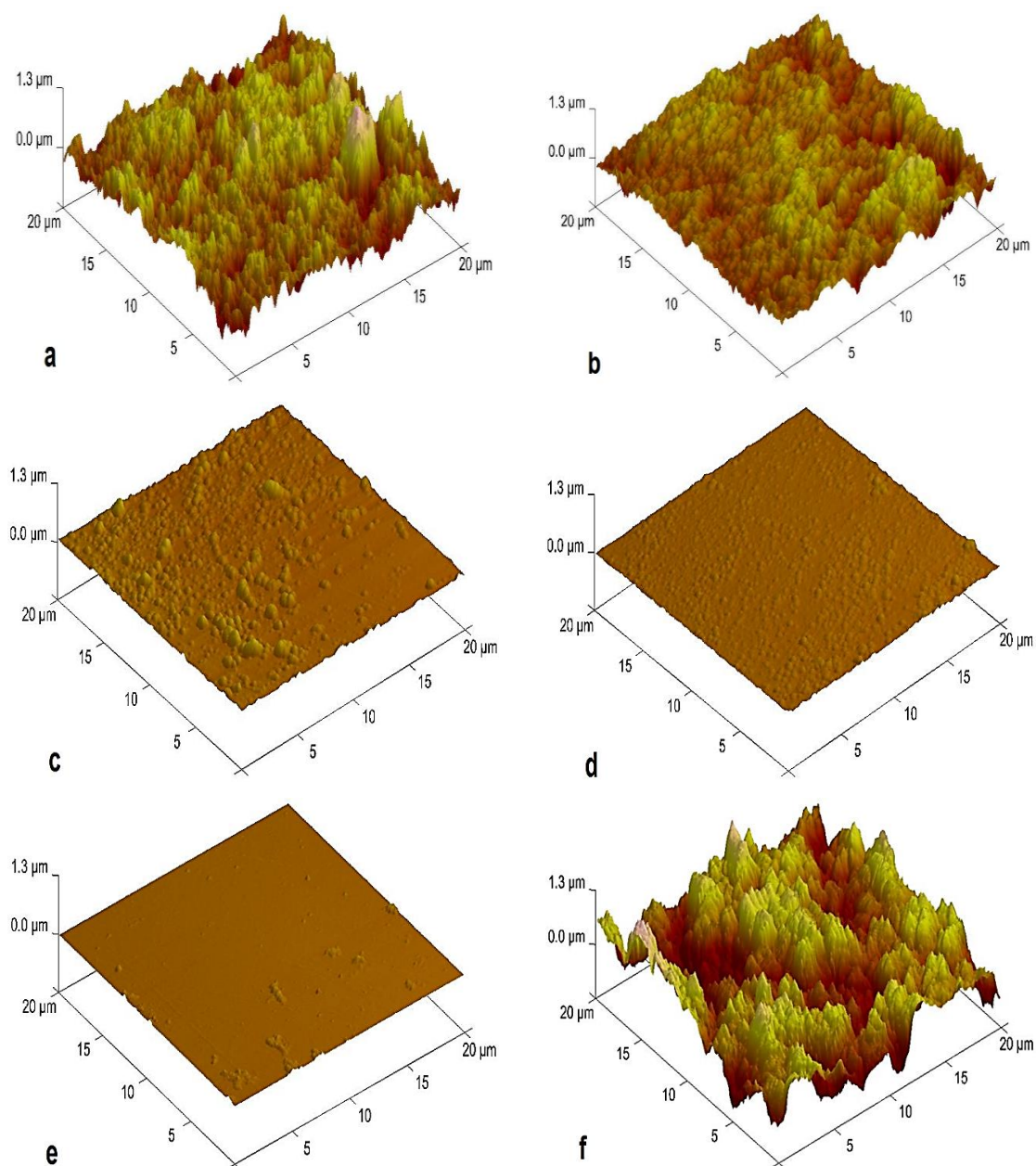


**Figure 5.9:** AFM images of dry PANI electrodeposited from 0.8M aniline dissolved in 1 M  $H_2SO_4$  in a) Ethaline, b) Propaline, c) Glyceline, d) Reline, except e) Maline and f) Oxaline on a Pt electrode (1 mm diameter). Cycling the voltage between 0.0 V to 1.2 V;  $100\text{ mV s}^{-1}$  for 20 scans.

Similar to section 4.3.5.2, film thickness was measured using AFM, with the images shown in **Figure 5.10a** given as examples of this. It is well known that the thickness of polyaniline increases with the amount of charge passed during the electropolymerisation process, and this leads to an increase in the roughness values of these polymers.<sup>45-47</sup> **Table 5.7** compares the thickness obtained by AFM with the thickness acquired on the basis of the charge passed during the reduction process.

**Figure 5.10c** showed a good linear relationship in a plot of polymer film roughness versus the amount of charge yielded from polymerisation. It can be concluded that controlling the polymerisation charge allows for a significant degree of control over the roughness and thickness of the resulting polymer layer.

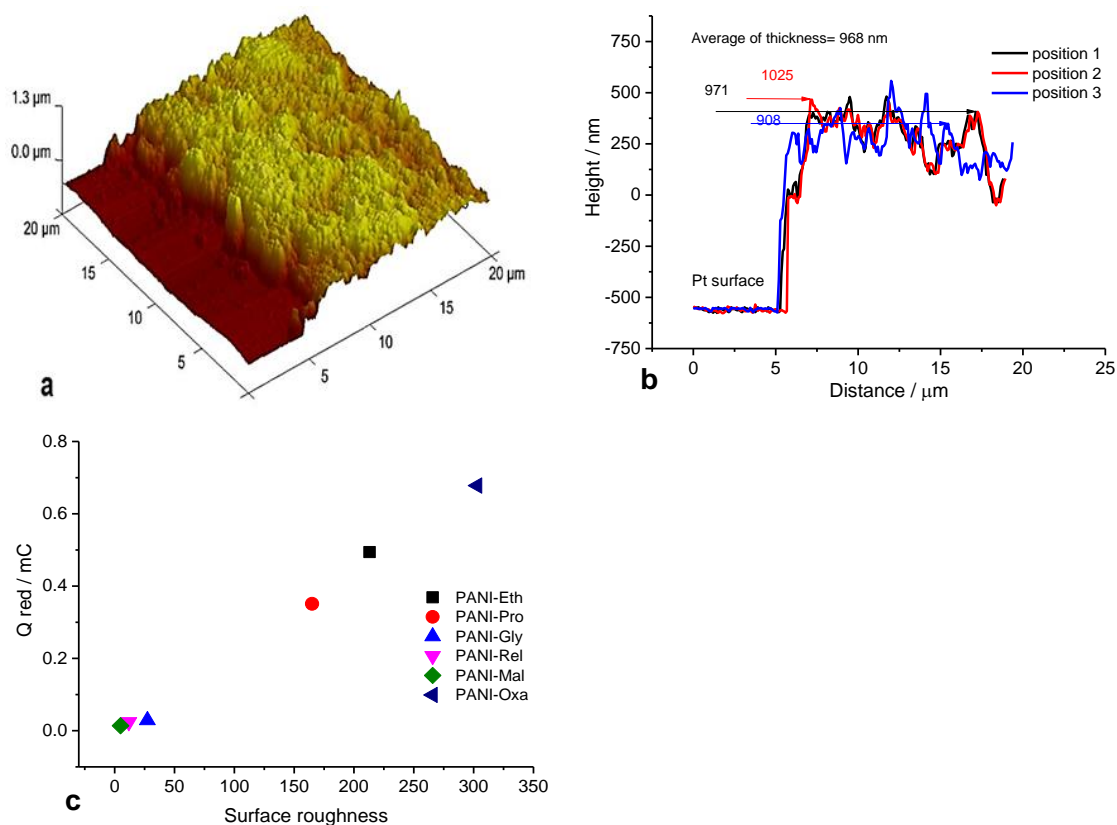


**Figure 5.10:** Film from **figure 5.9** (panel a), b) thickness of film (panel a) measured by AFM, and c) charge vs. surface roughness of PANI films.

**Table 5.7:** Thickness of polyaniline films measured using AFM compared to those calculated by charge passed from Faraday's law.

PANI films		Thickness (nm) by CVs	Average thickness (nm) by AFM	Roughness (nm) by AFM
a	Ethaline	949	968	213
b	Propaline	652	672	165
c	Glyceline	64	37	27
d	Reline	45	45	12
e	Maline	14	n/a	5
f	Oxaline	1277	1286	303

### **5.3.8 Selection of polymer for further study**

Here, polyaniline prepared from Oxaline was selected for EQCM studies. The reason for selecting this particular film were on the basis of the amount of charge passed (promising in terms of future charge storage applications), its rough surface topography (greater porosity) as well as the initial observations of this particular polymer film's stability. The greater polymerisation rate observed in Oxaline voltammetric experiments allows for the improvement of this polymer for electronic and optical applications. The aim of the EQCM experiments was to characterise the behaviour of PANI films through an understanding of the correlation between film structure, composition and dynamics. Furthermore, we focus on how conducting polymers behave in DES and aqueous electrolytes during the motion of mobile species between the film and electrolyte via the related change in mass of the rigid film.

### **5.3.9 EQCM investigations of ions and solvents regarding polyaniline film**

#### **5.3.9.1 Growth of PANI in Oxaline using the EQCM technique**

The deposition of the film was performed using 0.25 M aniline in an Oxaline electrolyte by applying a voltage from 0.0 to 1.2 V vs. Ag wire at a scan rate of 5 mV s<sup>-1</sup> for three cycles, as shown in **Figure 5.11**. After film deposition onto a 10 MHz AT-cut Pt-polished quartz crystal, the experiment was stopped at the reduced end of the potential cycle ( $E = 0.0$  V) and washed with deionised water several times. The ( $i$  vs.  $E$ ) curve of panel (a) in **Figure 5.11** is different to those reported in the last chapter (polyaniline grown from aqueous media). Here, it is important to note that the redox current of the film rises continuously with an increasing number of scans, probably due to the number of sites available for monomer oxidation on the surface of the Pt electrode. However, it can be deduced from this graph that the peak at the polymerisation point decreases after each scan, a behaviour that was the complete opposite of that observed for aqueous electrolytes. The mass of the film in panel (b) of **Figure 5.11** increased when the voltage reached the polymerisation potential (nucleation loop) at ~1.15 V when the peak current starts to increase. It is obvious that the mass of the film increases more significantly with an increasing number of cycles due to the decrease in frequency. The result of this study is different to those found for aqueous media, where the increase in

weight for a given scan is not greater than that observed in any previous scan. This increase may be related to the evolution of redox reactions with the increasing number of scans.

The same strategy as used in chapter four was undertaken, using admittance spectra to evaluate and validate if the film was acoustically ‘rigid’ (i.e. acoustically thin) or non-rigid (i.e. viscoelastic).<sup>48, 49</sup> The deposited mass can be determined by measuring the shift in resonance frequency before and after growth (dry polymer) in air. The resonant frequency of a PANI-loaded crystal shows a shift to lower frequency than the unloaded crystal, for which a difference of 4569 Hz was found, as seen in panel (d) of **Figure 5.11**. According to the Sauerbrey equation, the coefficient between the change of the resonant frequency ( $\Delta f$ ) and the change of mass of the surface layer ( $\Delta m$ )  $\pm 2$  % for the 10 MHz AT-cut quartz crystal used is:  $\Delta m$  (g) =  $-1.1 \times 10^{-9} \Delta f$  (Hz).<sup>50</sup> The change in frequency,  $\Delta f$ , with respect to the reference frequency  $f_0$ , is linearly related to the mass added by polymer deposition,  $\Delta m$ . From the Sauerbrey equation, the weight of the dry PANI film was calculated as 5025 ng with a thickness of 182 nm. These values are close to those measured from the cyclic voltammetry peak (see **Table 5.8**).

The growth behaviour of the polymer deposition has been studied using admittance spectra, as illustrated in panel (c) of **Figure 5.11**. The graph of admittance shows a progressive decrease of about 11 % from the starting resonant frequency due to added mass and the viscoelastic behaviour of the film. There is very little shift and change in peak admittance, but the film was still rigid and the validity regarding the Sauerbrey equation was deemed to be acceptable. Further, the Q-factor did not change considerably, meaning that the added mass was rigidly coupled and small compared to the mass of the crystal.<sup>51</sup>

**Table 5.8:** Mass, thickness, and surface coverage calculated by EQCM and CV for deposited PANI.

PANI sample	Mass (ng)	Thickness (nm)	$\Gamma$ (nmol cm <sup>-2</sup> )
EQCM	5025	182	235
CV	5150	183	240

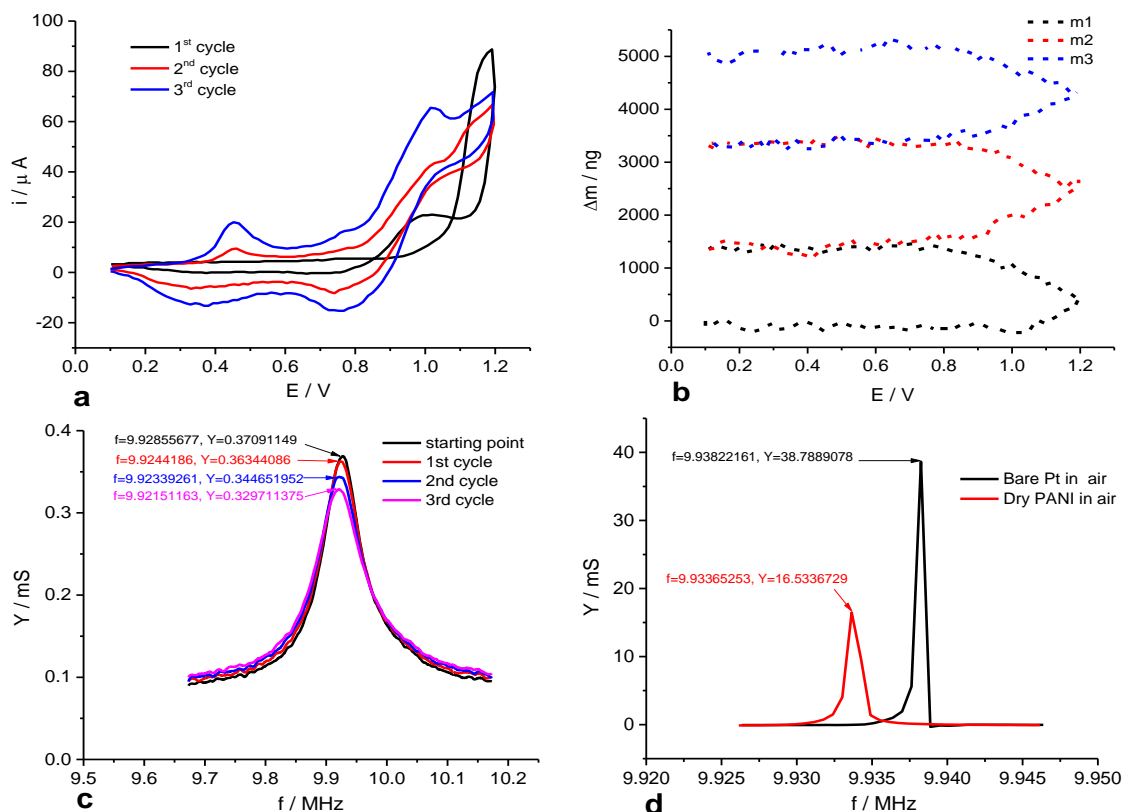


**Figure 5.11:** EQCM data for the potentiodynamic deposition of a PANI film (0.0 to 1.2 V; at  $5 \text{ mV s}^{-1}$ ) from 0.25 M aniline/Oxaline, 3 scans. a)  $i$  vs.  $E$ ; b)  $\Delta m$  vs.  $E$ ; c) crystal admittance spectra,  $Y/\text{mS}$  vs.  $f/\text{MHz}$ , recorded for PANI at the end of each cycle and d);  $Y/\text{mS}$  vs.  $f/\text{MHz}$  for bare crystal and PANI-loaded crystal in air.

### 5.3.9.2 Characterisation of the mass transfer of the film in different solutions using EQCM

#### 5.3.9.2.1 PANI redox cycling in DESs at room temperature

In this section, the PANI film was cycled in various DESs using the EQCM mechanism (in each electrolyte, a fresh film was grown using the same conditions described in section 5.3.9.1). The main purpose of this step was to monitor and study the interaction behaviour of anions and cations entering into the polymer. **Figure 5.12** shows the long-term cycling performance of PANI in Oxaline, Ethaline and Glyceline electrolytes, applying voltage from 0.05/0.1 V to 1.15/1.2 V at a scan rate of  $5 \text{ mV s}^{-1}$  for 38 cycles. The panels on the left show that the steady state cyclic voltammograms of these polymers are not stable and the plateau of anodic/cathodic peaks suffers from different changes in the CV shape, leading to combination, in most cases, with continuously decreasing current peaks. This might be caused by simultaneous degradation of the

polymeric materials as a result of emeraldine  $\rightarrow$  pernigraniline transitions which can occur at high anodic potentials in the voltammograms, i.e.  $\sim 1.15$  V.<sup>8</sup>

Interesting observations have been found for the PANI films produced in these DESs. It was observed that the mass-change kinetics during the redox cycles of PANI film in DESs are very different to the results for those produced by cycling in aqueous solutions. These curves show the emergent mass increase during the oxidation state caused by the insertion of anions; indeed, the mass change was still continuously increasing irreversibly during the reduction reactions. This is as a consequence of the incorporation of ions and/or solvents into the film, the latter becoming highly swollen due to the ingress of a large amount of species into its matrix until it reaches saturation state; it subsequently shrinks by expelling cations and anions during redox states. It is noticeable that the shrinking process (mass decrease) is smooth and slower than the initial mass increase due to the movement of ions being affected by the reduction in the free volume to a fraction of its original value, thereby hindering the molecular diffusion rate. The initial rise response to portion mass increase in the film (deposited mass is 5025 nm) about 100 % for PANI in Oxaline (mass of film increase to  $5 \mu\text{g} = 5000$  ng in Oxaline), while mass of film increase 75 % in Ethaline ( $3.75 \mu\text{g} = 3750$  ng) and 60 % in Glyceline ( $3 \mu\text{g} = 3000$  ng). If we assume that this may be feasible due to the increase solvent into the film, this indicates that the polymers may be not rigid (viscoelastic) in DES at room temperature or strongly affected by high viscosity of DESs but these polymers show rigid behaviour and stable mass change when transfer into 0.5 M  $\text{H}_2\text{SO}_4$  (**Figures 5.12g** and f, the mass of film increase 9 % in 0.5 M  $\text{H}_2\text{SO}_4/\text{H}_2\text{O}_4$ ).

Analogous results were found by Pruneanu *et al* after a PANI electrode was cycled in 5-sulfosalicylic acid (HSSA) instead of  $\text{HClO}_4$ . The results showed that the swelling and compact structure of the PANI film depends heavily on the nature of the electrolyte.<sup>52</sup> Here, the interpretation of these results is more complicated and the contribution of electron diffusion and charge transport across the polymer/solution interface is strongly influenced by the type and size of the species in the electrolyte, as well as its viscosity.

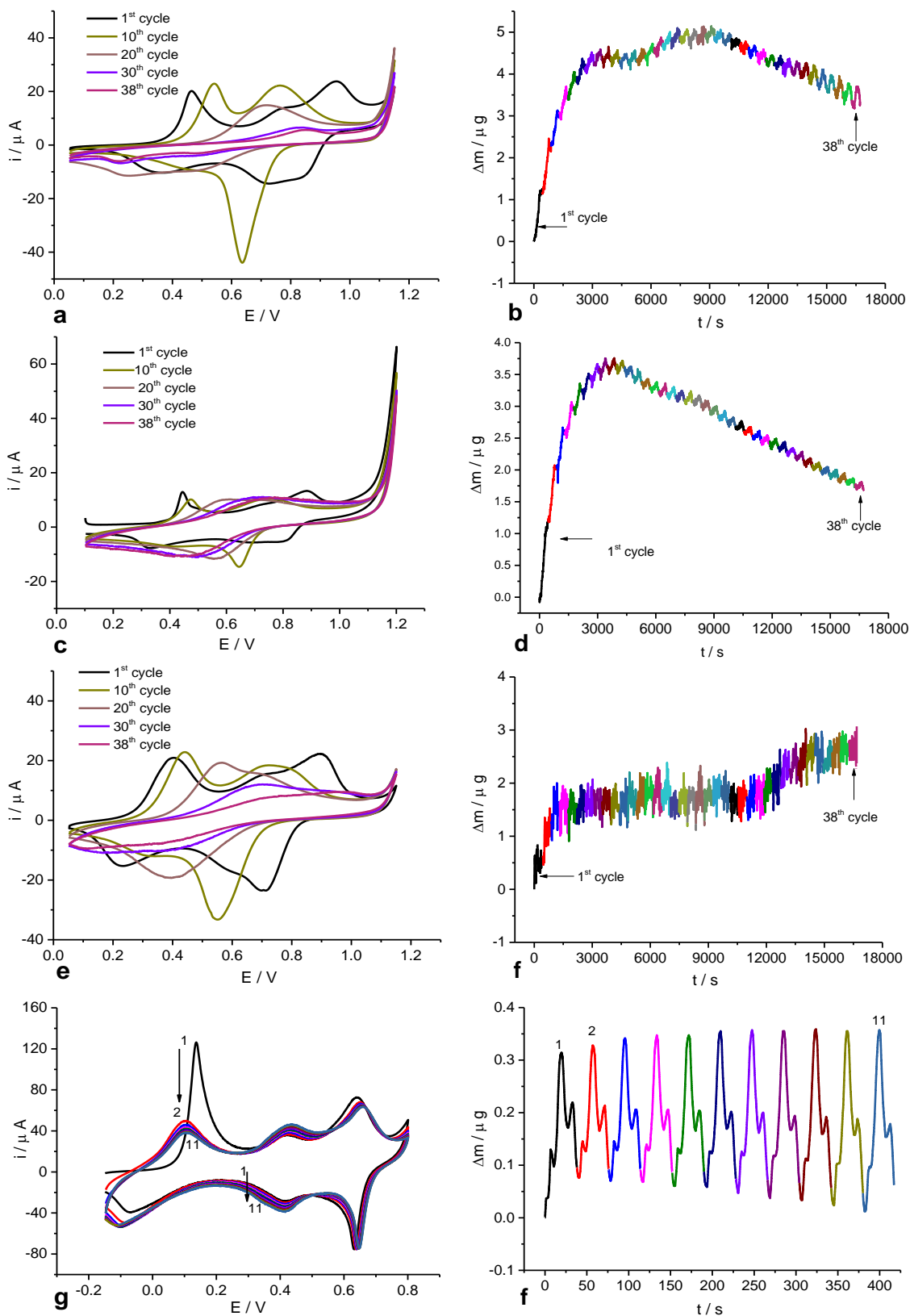


**Figure 5.12:** EQCM data for redox switching of a PANI film from Oxaline exposed to different DES electrolytes at a scan rate  $5 \text{ mV s}^{-1}$ . Panels: a, c, and e, are  $i$  vs.  $E$  in Oxaline, Ethaline and Glyceline, respectively, while panels: b, d and f are  $\Delta m$  vs.  $t$  for these same electrolytes, respectively. Panels g)  $i$  vs.  $E$  and f)  $\Delta m$  vs.  $t$  for PANI film grown from Oxaline exposed to  $0.5 \text{ M H}_2\text{SO}_4/\text{H}_2\text{O}$  at a scan rate  $5 \text{ mV s}^{-1}$

**Figure 5.13a** shows the mass change vs potential window for the first scan of PANI film in an Oxaline electrolyte. The result clearly shows that the mass change is increased for both reactions (oxidation *and* reduction). However, it is clear that the dynamics behaviour of the species exchanged during redox cycling has been changed after the polymer reaches steady state. For example, for scan number 38, mass is increased during oxidation, and during reverse cycling it is decreased, as seen in **Figure 5.13c**. The quantification of the molar mass ( $M_{app}$ ) for counter ions during the redox process of PANI can be calculated from Faraday's constant from the slope of a plot of mass values versus charge, as explained in equation 4.10.

The data ( $\Delta m$  vs.  $Q$ ) presented in panels b and d of **Figure 5.13** was calculated from end to end redox cycling. In the case of the first cycle, the result showed the molar mass of anions (Ox.Cl<sup>-</sup>) that ingress into the film doing oxidation is around +28.64 g mol<sup>-1</sup>, whereas during reduction it was found as being around +34.04 g mol<sup>-1</sup>. Indeed, these results are not the same as the molar mass of Ox.Cl<sup>-</sup> (126 g mol<sup>-1</sup>) in Oxaline; this is because the flux of the ions is accompanied by a neutral species (a combination of anion and cation) during the redox process. As mentioned previously, the disagreement in the eventual molar mass values of ion exchange with the actual anions and/or cations that are presented in solution during redox process is related to the flux of solvent and/or co and counter ions (in opposite directions). Therefore, the physical properties of the PANI film transferred in DES are not readily attributable to only the single ion, ion size or the effective lack of solvent, but should rather be considered as a mixed anion – cation entry/withdrawal in the same or opposite directions.

In order to calculate the number of cations and anions that egress and ingress, respectively, in DESs, equations 4.13 and 4.14 have been used. This analysis was based on whether the process in question was a cation- or anion-dominated mass exchange. A negative sign of  $\alpha$  indicates to the replacement of the cations by salt solvent for a cation-dominated process, and *vice versa* for an anion-dominated process. The values of  $\alpha$  and the identities of the mobile species proposed as fits for the observed gravimetric results for the redox reactions are shown in **Table 5.9**.

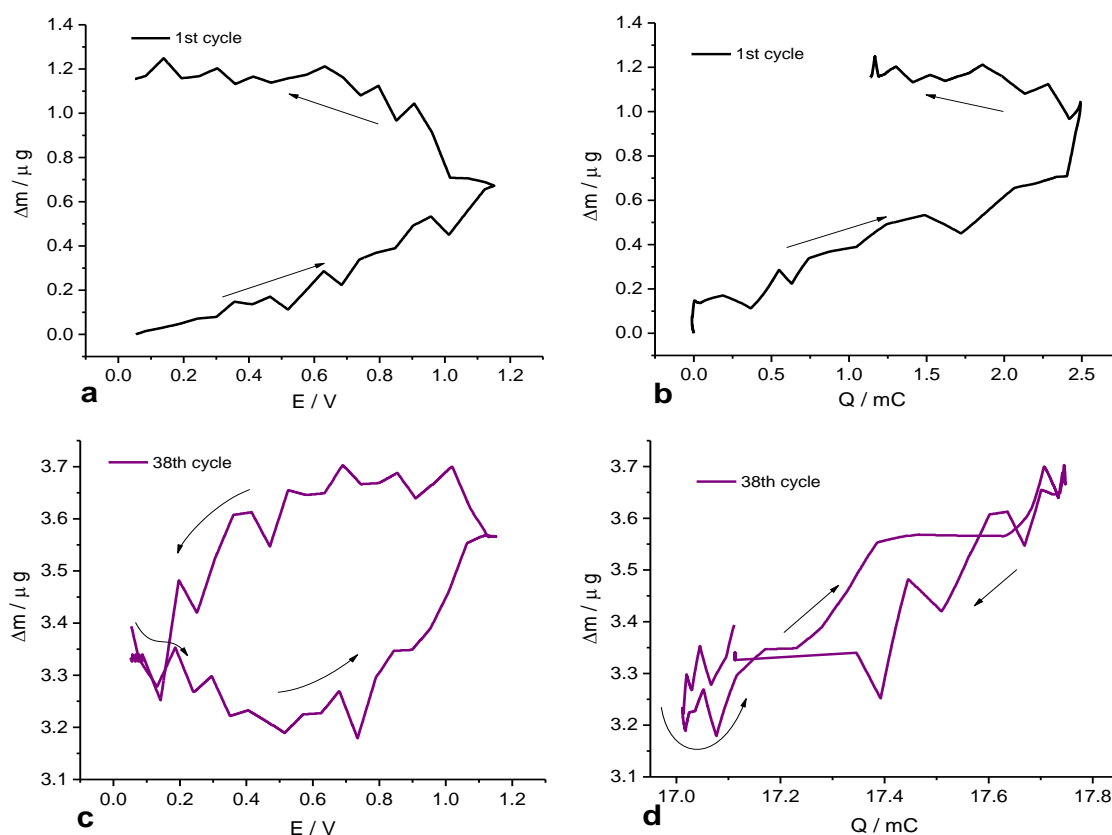


**Figure 5.13:** Panels a) and c) show  $\Delta m$  vs.  $E$  for PANI film cycled in an Oxaline electrolyte at  $5 \text{ mV s}^{-1}$ , while panels b) and d) show  $\Delta m$  vs.  $Q$  for scans 1 and 38. Numbers indicate cycle number.

**Table 5.9:** Molar masses ( $M_{app}$ ) determined from  $\Delta m$  vs.  $Q$  graphs for redox switching of PANI in DESs at  $25^\circ\text{C}$ . + represents a mass increase, - represents a mass decrease.

Electrolytes	Cycle number	Oxidation reaction			Reduction reaction		
		$M_{app}$ $\text{g mol}^{-1}$	$\alpha$	Dominating process	$M_{app}$ $\text{g mol}^{-1}$	$\alpha$	Dominating process
Oxaline	1 <sup>st</sup> cycle	+28.64	-0.42	OxCl <sup>-</sup> in	+34.04	-0.40	OxCl <sup>-</sup> in
	38 <sup>th</sup> cycle	+66.72	-0.26	OxCl <sup>-</sup> in	-56.89	+0.30	OxCl <sup>-</sup> out
Ethaline	1 <sup>st</sup> cycle	+28.59	-0.50	EG <sub>2</sub> Cl <sup>-</sup> in	+69.36	-0.34	EG <sub>2</sub> Cl <sup>-</sup> in
	38 <sup>th</sup> cycle	+06.56	-0.58	EG <sub>2</sub> Cl <sup>-</sup> in	-13.03	+0.56	EG <sub>2</sub> Cl <sup>-</sup> out
Glyceline	1 <sup>st</sup> cycle	+22.65	-0.61	Gly <sub>2</sub> Cl <sup>-</sup> in	+14.69	-0.63	Gly <sub>2</sub> Cl <sup>-</sup> in
	38 <sup>th</sup> cycle	+28.80	-0.59	Gly <sub>2</sub> Cl <sup>-</sup> in	-19.89	+0.61	Gly <sub>2</sub> Cl <sup>-</sup> out

#### 5.3.9.2.2 Effect of electrolyte composition on PANI redox cycling at 50°C

It is well known that high positive potentials result in susceptibility degradation<sup>53, 54</sup> or deterioration<sup>7, 55</sup> of the polymeric materials during continuous cycling of potentials. This was revealed in a section 5.3.9.1 by cyclic voltammetry, where the degradation of potentiodynamically synthesised PANI films was obtained at 1.15 V. This problem was avoided here by limiting the applied potential to the first redox peaks of PANI i.e. 0.8 V. Secondly, we cycled the polymer film in DESs at high temperature (50 °C) in order to decrease the viscosity of these solvents. This step leads to an increase in the speed of electron transfer between the  $\pi$ -conjugated system in the polymeric matrix, as well as increasing the transport of ionic species between the polymer and solution. Finally, polyaniline was deposited from 0.2 M aniline in Oxaline solution for two cycles with a potential window of 0.1 to 1.2 V at scan rate of 5 mV s<sup>-1</sup>, the significance of which was that the new polymer was grown was a reduced thickness. The weight, thickness and surface coverage of the PANI film thus produced were 2749 ng, 100 nm and 128 nmol cm<sup>-2</sup>, respectively.

In this work, polyaniline films were individually analysed in different DESs having different ion sizes and functional groups using EQCM analysis. Because DES electrolytes in PANI voids could not be removed fully due to their high viscosities, films could only be employed for a single DES. A fresh PANI film (similar to that presented in section 5.3.9.2.2) was prepared for each DES. Prior to transferring the film to each DES, it was washed several times in the same solution it was to be recycled in. For all solvents, the scan rate was kept at 5 mV s<sup>-1</sup>, the potential was swept from 0.1 to 0.8 V and the temperature was 50°C.

Panels a, c, e and g of **Figure 5.14** show cyclic voltammograms of polyaniline film exposed to various DESs, in this instance Ethaline, Propaline, Oxaline, and Glyceline, separately. These graphs show several varied and interesting features. First, the redox peak (especially for oxidation) is relatively sharp for PANI in Oxaline, due to the greater acidity of this solution. However, in Ethaline, Propaline and Glyceline, broad peaks are observed. This might imply that these solutions are varied (i.e. neutral, acidic and alkaline). Second, in terms of current peaks, the highest current peak found for the anodic peaks was that of PANI in Oxaline, at 7.2  $\mu$ A, followed by Ethaline, Propaline

and Glyceline at 4.1, 3.5 and 2.5  $\mu\text{A}$ , respectively. This could be due to the fundamental properties of these different hydrogen bond donors. In other words, it is dependent on the nature of the ions present in the solution, as shown in the previous chapter. Thus, it would seem related to the conductivity of the electrolyte and its viscosity. It has been found that the conductivity of these electrolytes at 50 °C follows the order: Ethaline > Oxaline > Propaline > Glyceline, while the viscosity follows the order: Ethaline < Propaline < Oxaline < Glyceline, as seen in section 5.3.1. The pressing question here is why is the current peak of polyaniline in Ethaline is less than in Oxaline when the latter has a lower conductivity and higher viscosity from the first? This may be related to the acidity of the Oxaline medium.

The EQCM data  $\Delta m$  vs.  $t$  for redox switching of PANI film exposed in DES electrolytes is given in panels b, d, f and h of **Figure 5.14**. High stability to mass change of a PANI film has been observed in Ethaline and Propaline at 50°C. However, mass changes in PANI in Oxaline declined by 0.99  $\mu\text{g}$  during electrochemical cycling. The reason behind the decrease in mass is probably due to expulsion of electrolyte (from the deposition solution) to reach the stability stage. In Glyceline, the behaviour of mass change seems to be the opposite to that of Oxaline in the initial redox process (i.e. before the film reaches its equilibrium state). The mass of PANI increased by about 1.2  $\mu\text{g}$  after 600 seconds in this liquid (panel h) during the electrochemical experiment. The reason for this increase could be due to the ingress of Glyceline and Oxaline (from the growth of the polymer) solution into the film. The variation of polymers in reaching equilibrium may be due to the difference in the ratio between ion size in the electrolyte and the hole size in the polymer. This study has found that polymer cycled in DESs at 50°C needed less time to reach its stable state than at room temperature due to the decrease in viscosity and consequent increased rate of ionic mobility of these electrolytes.

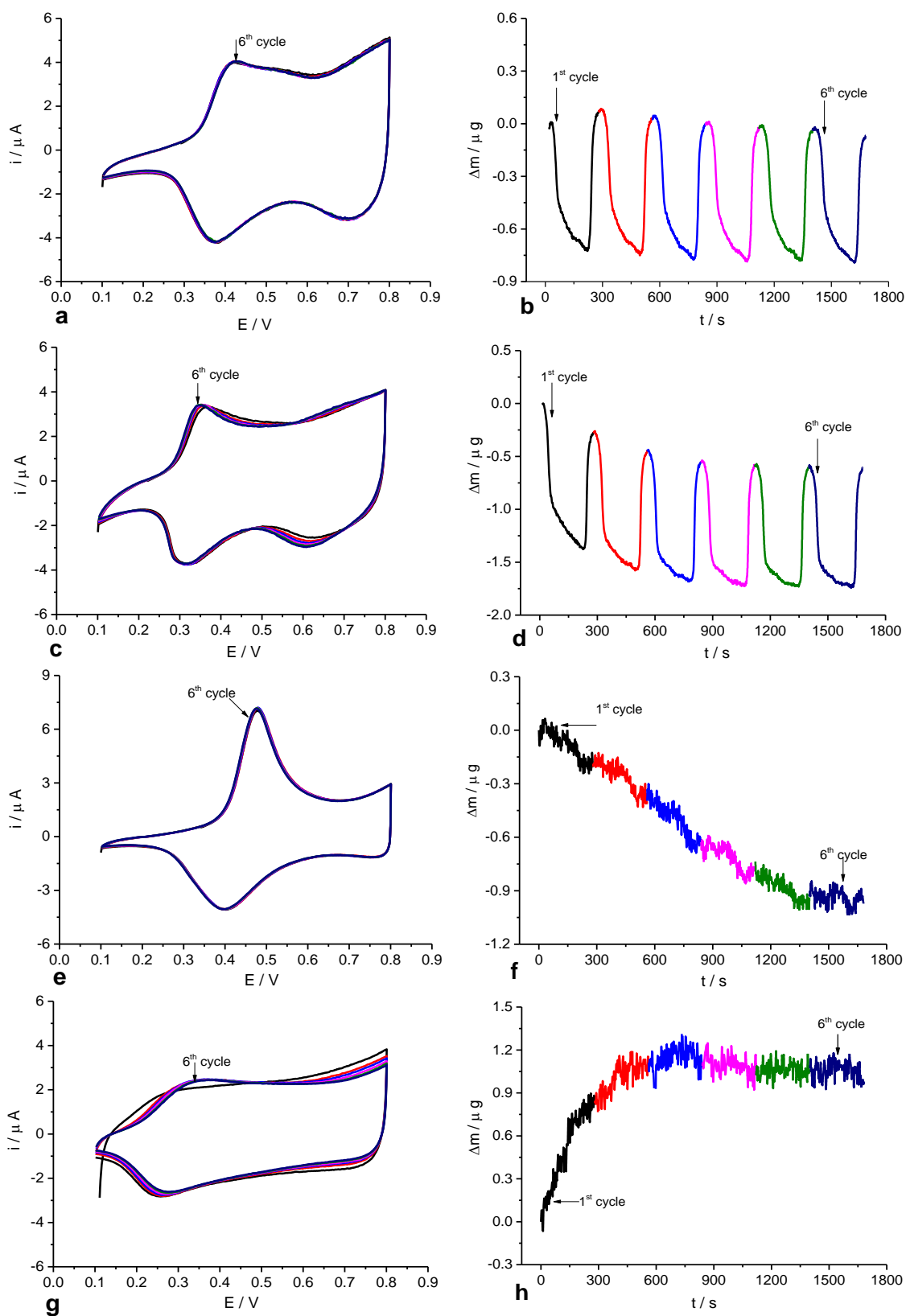


**Figure 5.14:** EQCM data for redox switching of a PANI ( $\Gamma = 128 \text{ nmol cm}^{-2}$ ) exposed to DESs at a  $5 \text{ mV s}^{-1}$  scan rate. Panels: a, c, e and g are  $i$  vs.  $E$ ; while panels b, d, f and h are  $\Delta m$  vs.  $t$ ; for Ethaline, Propaline, Oxaline and Glyceline, respectively.

The mass change of the last cycle (stable state) for these electrolytes is presented in panel (a) of **Figure 5.15** for reasons of comparison. It is obvious that there was no mass change in the film at  $E < 0.30$  V in Propaline and 0.35 V in Ethaline. After that, a significant decrease in film mass occurred due to an increasing anodic current peak. In the cathodic half peak, the mass change trends are reversed. These results indicate that PANI film in these electrolytes is cation-dominated reaction for the oxidation peak due to egress of the choline cation ( $\text{Ch}^+$ ) and ingress of the  $\text{Ch}^+$  for the reduction peak, as previously explained for PANI growth from aqueous solutions that were then cycled in Ethaline and Propaline. However, the mass change behaviour in Oxaline and Glyceline differed to that observed in Ethaline and Propaline electrolytes at  $50^\circ\text{C}$ . It can be seen that there is no measurable mass change for either Oxaline or Glyceline during the CV redox cycle. This may be related to the high viscosities of these solutions, which has consequent effects on the mass and charge transport rates during redox switching. It is clear that charge transport in these mixtures is predominantly controlled by ion mobility. Hillman *et al* found a similar shape ( $\Delta m$  vs.  $E$ ) when transferring PEDOT film into  $0.1 \text{ mol/dm}^3 \text{ TEABF}_4/\text{CH}_3\text{CN}$  at various scan rates.<sup>56</sup>

Similar to before, the molar mass of the ion exchanged across the PANI films in these electrolytes has been calculated from an end to end of plot of  $\Delta m$  vs.  $Q$ , as shown in panel (b) of **Figure 5.15**; the  $\alpha$  value and associated data for the cation and anion transferred are presented in **Table 5.10**.

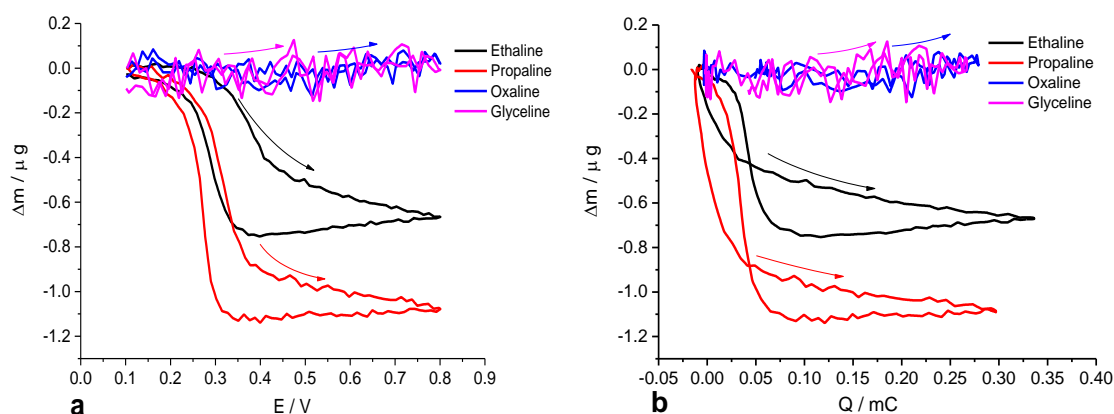


**Figure 5.15:** Panels a)  $\Delta m$  vs.  $E$ ; and b)  $\Delta m$  vs.  $Q$  recorded simultaneously with corresponding cyclic voltammograms in Figure 5.14 for each individual electrolyte. Each colour indicates a specific electrolyte (see graph keys).

**Table 5.10:** Molar masses ( $M_{app}$ ) from  $\Delta m$  vs.  $Q$  graphs for redox switching of PANI ( $\Gamma = 128 \text{ nmol cm}^{-2}$ ) in DESs at  $50^\circ\text{C}$ . The potential window was between  $0.1 \leq E / V \leq 0.8$  at scan rate  $5 \text{ mV s}^{-1}$ . + represents a mass increase, - represents a mass decrease.

Electrolytes	Oxidation last scan			Reduction last scan		
	$M_{app}$ $\text{g mol}^{-1}$	$\alpha$	Dominating process	$M_{app}$ $\text{g mol}^{-1}$	$\alpha$	Dominating process
Ethaline	-192.06	-0.33	$\text{Ch}^+$ out	+186.16	+0.31	$\text{Ch}^+$ in
Propaline	-342.40	-0.82	$\text{Ch}^+$ out	+331.85	+0.78	$\text{Ch}^+$ in
Oxaline	n/a	n/a	-	n/a	n/a	-
Glyceline	n/a	n/a	-	n/a	n/a	-

### 5.3.9.2.3 Effect of temperature on PANI redox cycling in Ethaline

The swelling and shrinking of polyaniline film is substantially affected by the cycling in DES electrolytes at high temperature and room temperature, as was found above. Therefore, it would be interesting to compare mass change behaviour of a given film at room- and high temperature within one experiment. **Figure 5.16** shows the mass change behaviour for PANI film as a function of the time when cycled in an Ethaline electrolyte in the following three steps. In the first step, the film was cycled in Ethaline at  $50^\circ\text{C}$  between 1 and 51 scans. The result showed that, at high temperature and over 28 cycles that, the mass decreased (by  $\sim 0.55 \mu\text{g}$ ), which represented 20 % of the total mass of the film ( $2.8 \mu\text{g}$ ). Thereafter, from scans 28 – 51, the mass remained essentially constant, as shown in **Figure 5.16**. In this process, the mass change was dominated by the cation during the oxidation and reduction cycles.

In contrast, the onset of any substantial swelling starts when the polymer is cycled in Ethaline at room temperature (see scan 52). It was observed that the mass of the film increased by  $\sim 6.5 \mu\text{g}$  over the first 19 scans, which represented about twice the total mass of the film. This could be due to the increasing viscosity of the solution at this temperature, which has an impact on the mobility of ions causing their accumulation at oxidised sites and their trapping by cations in the voids of the polymer film, so consequently they show low mobilities. The decrease in mass did not occur during the doping and undoping reaction between 52 - 70 scans and the film continued to increase in mass, causing it to swell. However, although the mass change showed a gradual

increase in this system, the mass decreased during the oxidation peak and increased during the reduction peak between scans 70 to 80.

A similar trend in mass change was observed during the third step of this experiment, when the polymer was cycled in Ethaline at 50°C. Between scans 81 and 86, the mass was decreased during the oxidation process and increased during the reduction, recording a decrease of 2.1  $\mu\text{g}$  owing to the egress of Ethaline from the film network. After six scans during this step, the mass remained essentially constant, showing a decrease in the mass during the doping process and an increase in the mass during the undoping process. This phenomenon can be explained by the fact that the swelling, shrinking and stability of polyaniline can be strongly dependent on the temperature of the DES with time. This study has found that PANI film cycled in Ethaline at room temperature took longer to reach its equilibrium state compared to the same electrolyte at higher temperature (50°C). This could be related to slow mass and charge transport processes in DES electrolytes due to their high viscosity.

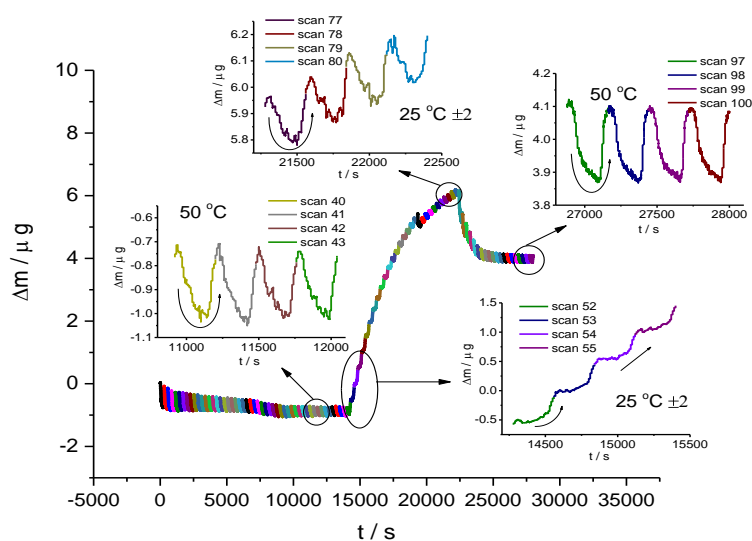


**Figure 5.16:** An explanation ( $\Delta m$  vs.  $t$ ) for PANI film ( $\Gamma = 130 \text{ nmol cm}^{-2}$ ) cycled in Ethaline, varying the temperature between 50°C and room temperature ( $25 \pm 2^\circ\text{C}$ ) at a scan rate of  $5 \text{ mV s}^{-1}$ .

The observed changes in mass as a function of the potential window for PANI film in Ethaline during the redox process are reported in panels a, c, e and g of **Figure 5.17**. Here we concentrate on molar mass exchange, which are calculated from end to end for the redox reactions reported in panels b, d, f and h of **Figure 5.17** (here, an initial charge of each panel of zero was taken). The results were found by the product of the slope of a  $\Delta m$  vs.  $Q$  plot and Faraday's constant (using equations 4.13 and 4.14).

When the electrolyte at high temperature, the  $M_{app}$  for the first and fortieth scans indicated the egress of the choline cation ( $\text{Ch}^+$ ) and ingress of  $\text{Ch}^+$ , about 0.26 ( $\text{Ch}^+$ ,  $\text{EG}_2\text{Cl}^-$ ) removed per  $\text{Ch}^+$  expelled from the film for first cycle, which represented an  $\alpha$  value of -0.26. The doping and undoping  $M_{app}$  values and related  $\alpha$  values are reported in **Table 5.11**. However, the profile of the mass behaviour changed during the cycling of the film in Ethaline at room temperature. The average  $M_{app}$  for PANI in Ethaline at room temperature over 52 cycles showed the ingress of  $19.24 \text{ g mol}^{-1}$  of the  $\text{EG}_2\text{Cl}^-$  anion during the first part of the redox cycle and  $98.85 \text{ g mol}^{-1}$  ingress in the second part. The expulsion of a neutral species from film in order to achieve electroneutral equilibrium during the charge and discharge processes were -0.53 and -0.23, respectively. The gravimetric response in this system was altered after a couple of cycles. It is clear that scan 77 exhibited a cation-based mechanism during the redox phase. The average doping  $M_{app}$  indicated the egress/ingress of a choline cation during the redox processes. During oxidation process,  $\sim 0.23$  of ( $\text{Ch}^+$ ,  $\text{EG}_2\text{Cl}^-$ ) entered per  $\text{Ch}^+$  expelled from the film and -0.23 ( $\text{Ch}^+$ ,  $\text{EG}_2\text{Cl}^-$ ) expelled per  $\text{Ch}^+$  entering the film. Finally, when the PANI film was retuned back into Ethaline at  $50^\circ\text{C}$ , the mechanisms of mass change are similar to first step of this investigation, which is also at high temperature. The data for doping and undoping  $M_{app}$  values and the related  $\alpha$  values are reported in **Table 5.11**.

It can be concluded that the reason the mass did not return to its initial value after each cycle could be due to the retention of certain species in the film after discharge, which are likely to be neutral species. The mass change of PANI in Ethaline at room temperature is dominated by anions transfer (before the film reaches steady state), whereas high temperature ( $50^\circ\text{C}$ ) processes are dominated by cation transfer. This means that the polymer in Ethaline was greatly influenced by temperature due to the associated variation in the viscosity of the solution. As mentioned in the early sections of this chapter, the viscosity of DESs decreases with increasing temperature, in agreement with the results obtained in chapter four. As the viscosity of the electrolyte decreases with increasing temperature, the frequency and the admittance of the quartz will be increased and, as a consequence, the mechanical resistance (impedance) on the quartz is reduced. According to the Sauerbrey equation, mass is inversely proportional to frequency, so decrease in the mass change at high temperature were not related to electrochemical reactions only, but could also be due to viscosity change.

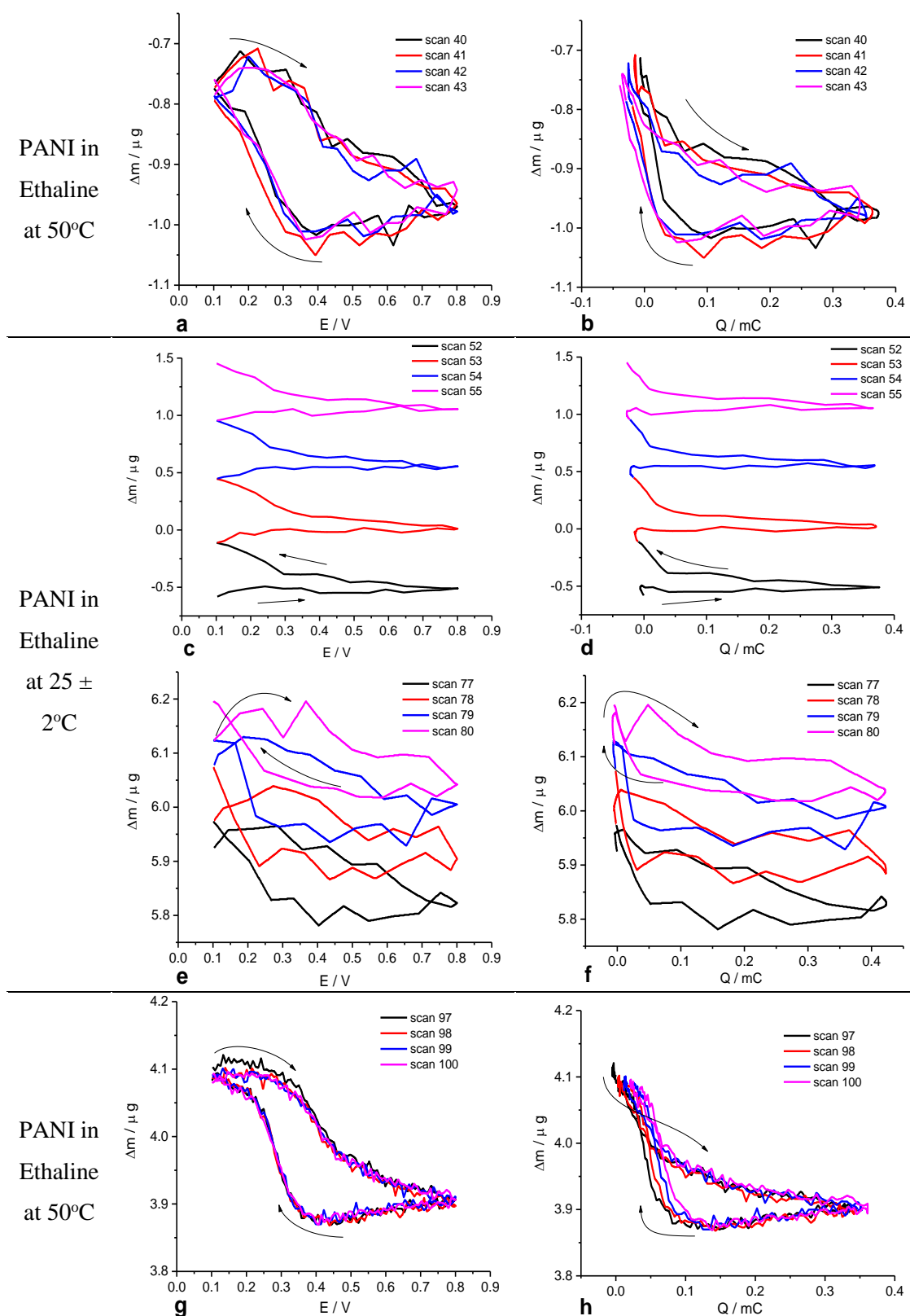


**Figure 5.17:** EQCM data for redox switching of a PANI film ( $\Gamma = 130 \text{ nmol cm}^{-2}$ ) exposed to Ethaline at  $50^\circ\text{C}$ ,  $25 \pm 2^\circ\text{C}$ , and  $50^\circ\text{C}$ , respectively, at a scan rate of  $5 \text{ mV s}^{-1}$ . Panels a), c), e) and g) show  $\Delta m$  vs.  $E$ , while panels b), d), f) and h) show  $\Delta m$  vs.  $Q$ . The arrows indicate the direction of change.

**Table 5.11:** Molar masses ( $M_{app}$ ) from  $\Delta m$  vs.  $Q$  graphs for redox switching of PANI in DESs at 50 and 25°C. + represents a mass increase, - represents a mass decrease.

Electrolytes	Cycle number	Oxidation reaction			Reduction reaction		
		$M_{app}$ g mol <sup>-1</sup>	$\alpha$	Dominating process	$M_{app}$ g mol <sup>-1</sup>	$\alpha$	Dominating process
Ethaline 50°C	1 <sup>st</sup> cycle	-172.14	-0.26	Ch <sup>+</sup> out	+135.35	-0.12	Ch <sup>+</sup> in
	40 <sup>th</sup> cycle	-82.53	+0.08	Ch <sup>+</sup> out	+70.64	-0.13	Ch <sup>+</sup> in
Ethaline 25 ± 2°C	52 <sup>st</sup> cycle	+19.24	-0.53	EG <sub>2</sub> Cl <sup>-</sup> in	+ 98.85	-0.23	EG <sub>2</sub> Cl <sup>-</sup> in
	77 <sup>th</sup> cycle	-42.04	+0.23	Ch <sup>+</sup> out	+43.07	-0.23	Ch <sup>+</sup> in
Ethaline 50°C	81 <sup>st</sup> cycle	-243.03	-0.53	Ch <sup>+</sup> out	+39.82	-0.24	Ch <sup>+</sup> in
	97 <sup>th</sup> cycle	-59.66	+0.17	Ch <sup>+</sup> out	+55.82	-0.18	Ch <sup>+</sup> in

#### 5.3.9.2.4 Effect of different environmental electrolyte on PANI redox cycling

The aim of the work reported here was to compare the mass change of polyaniline grown from Oxaline with polymer grown in aqueous solution (chapter 4) to understand if the mass transfer behaviour of the film in DES/aqueous is identical or otherwise. Panel (a) of **Figure 5.18** shows cyclic voltammograms of film cycled in Ethaline, 0.5 M H<sub>2</sub>SO<sub>4</sub> solution and Ethaline, respectively. The potential window in Ethaline was between +0.1 V and +0.8 V versus Ag wire, while in aqueous solution it was between -0.15 V and +0.8 V versus Ag/AgCl (sat. KCl). It is clear that the electroactivity of the polymer has recovered to about 64 % of its original value after being transferred back to Ethaline (step 3). This indicates that the electroactive stability of the polymer was affected due to the significant decrease in the high anodic potential in this experiment. The mass change in panel (b) of **Figure 5.18** is similar to the results found in our previous study, where the mass is decreased during the oxidation reaction as a result of removing the cation (Ch<sup>+</sup>) from the polymer net; the increase in mass change during the reduction process was attributed to the incorporation of cation (Ch<sup>+</sup>) into the film. However, in aqueous solution, the mass is increased during the oxidation reaction due to the injection of anions (SO<sub>4</sub><sup>2-</sup>) into the polymer chains. Conversely, the mass is decreased when scanning in reverse, showing that anions are moving out of the polymer (the reasons for which are reported in section 4.3.7.2.2). A similar mass change

behaviour with different polymers (mass increases upon film during the oxidation stage and decreases during the reduction stage) has been noted in the literature.<sup>2, 13</sup>

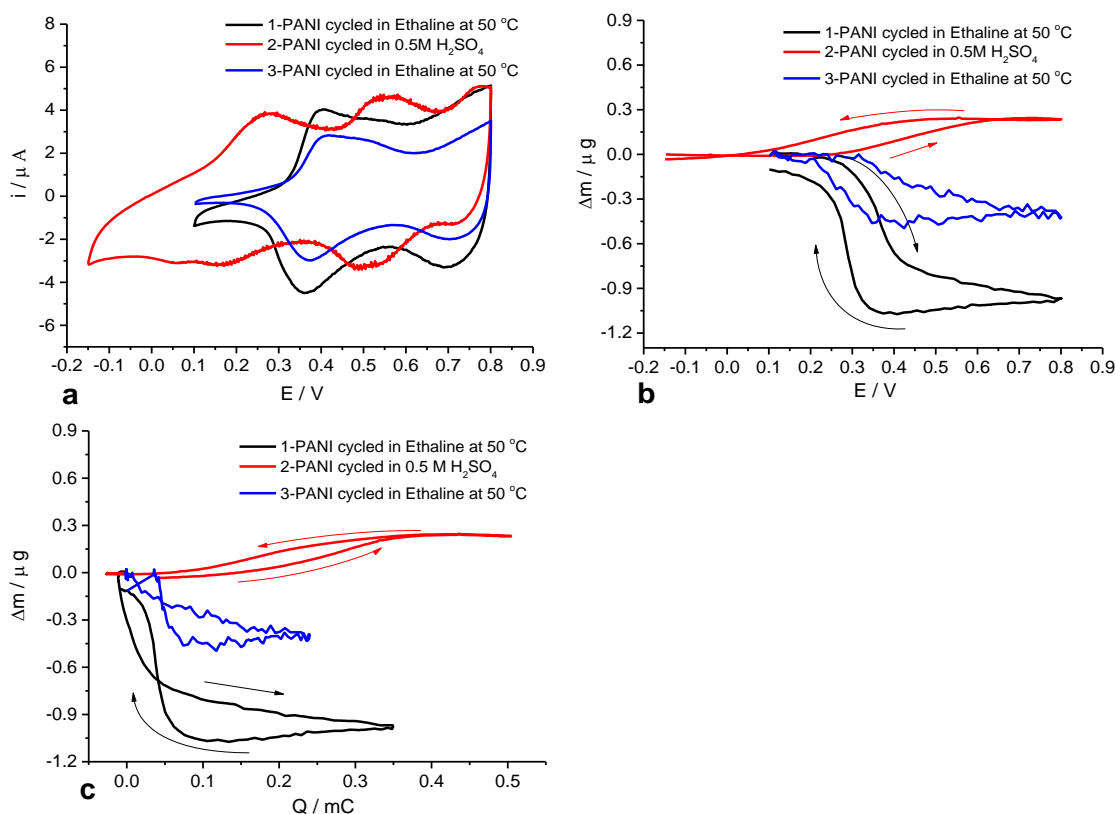


**Figure 5.18:** EQCM data for redox switching of PANI film exposed to Ethaline at 50°C, 0.5 M H<sub>2</sub>SO<sub>4</sub> and Ethaline at 50°C, respectively, at 5 mV s<sup>-1</sup> scan rates. a) *i* vs. *E*; b)  $\Delta m$  vs. *E*; and c)  $\Delta m$  vs. *Q*. The arrows indicate the direction of change.

The molar mass changes vs. charge, calculated from end to end oxidation and reduction regimes, are shown in **Figure 5.18c**. The molar masses in Ethaline during the oxidation and reduction states equal -251 and +241 g mol<sup>-1</sup>, respectively, which are significantly greater than the Ch<sup>+</sup> cation molar mass (104 g mol<sup>-1</sup>). This can be interpreted as the fluxes of the cation and the neutral species transfer into/out the film during redox process at the same direction. In the aqueous solution, the molar mass for doping indicated an entry mass of 96 g mol<sup>-1</sup>, which is attributed to the sulphate anion (SO<sub>4</sub><sup>2-</sup>). Conversely, a decrease of 94 g mol<sup>-1</sup> in the molar mass upon reduction indicated anions (SO<sub>4</sub><sup>2-</sup>) being expelled, with ~0.11 (H<sub>2</sub>O) entered per sulphate anion (SO<sub>4</sub><sup>2-</sup>) leaving the film. The mass-exchanged in the third stage (i.e. PANI in Ethaline) is significantly lower than in the first stage in terms of choline cation egress as reported in **Table 5.12**.

**Table 5.12:** Molar masses ( $M_{app}$ ) from  $\Delta m$  vs.  $Q$  graphs for redox switching of PANI in Ethaline at 50°C, 0.5 M H<sub>2</sub>SO<sub>4</sub>, and Ethaline at 50°C, respectively. Potential window was  $-0.15 \leq E / V \leq 0.8$  in aqueous solution, while in Ethaline was  $0.1 \leq E / V \leq 0.8$  for the fifth scan, with a scan rate of 5 mV s<sup>-1</sup>. + represents a mass increase, - represents a mass decrease.

Electrolytes (monomer-free)	Oxidation 5 <sup>th</sup> scan			Reduction 5 <sup>th</sup> scan		
	$M_{app}$ g mol <sup>-1</sup>	$\alpha$	Dominating process	$M_{app}$ g mol <sup>-1</sup>	$\alpha$	Dominating process
Ethaline	-251	-0.56	Ch <sup>+</sup> out	+241	+0.52	Ch <sup>+</sup> in
0.5 M H <sub>2</sub> SO <sub>4</sub>	+96	a/n	SO <sub>4</sub> <sup>-2</sup> in	-94	+0.11	SO <sub>4</sub> <sup>-2</sup> out
Ethaline	-179	-0.29	Ch <sup>+</sup> out	+156	+0.2	Ch <sup>+</sup> in

### 5.3.9.2.5 Effect of Scan Rates

In this work, the influence of scan rate on electrochemical response has been successfully investigated in an Ethaline electrolyte. As we indicated in chapter four, the purpose here is to distinguish film dynamics during redox cycling; diffusional control, diffusionless control or some intermediate between these two extremes. A new polyaniline film was prepared as per section 5.3.9.2.2, and was then exposed to fresh Ethaline electrolyte (monomer-free) at various scan rates (5, 10, 20, 50 and 100 mV s<sup>-1</sup>) with a potential window of 0.1 V to 0.8 V, as shown in **Figure 5.19**. Cathodic current data taken from cyclic voltammetry of the film is shown in panel (a) of **Figure 5.19**, when normalised and fitted against scan rate ( $v$ ) gives a straight line ( $R = 0.99997$ ). A gradual increase of redox currents with scan rate indicates that a diffusion controlled process occurs (i.e. a reversible reaction). In the case of mass change, the EQCM response in panel (c) of **Figure 5.19** shows that the magnitude of the mass change in the Ethaline electrolyte varies with scan rate. Generally, the mass changes in the film decline upon p-doping, whilst the reverse occurs in the reduction half-cycle. It can be also seen that the largest mass change occurred at the lowest scan rate (5 mV s<sup>-1</sup>), while the lowest mass change was produced at the highest scan speed (100 mV s<sup>-1</sup>). These variations are attributed to the occurrence of fast and slow anion/cation transport into and out of the polymer. At high scan rates, the mobility of species is fast (high kinetics) during the redox processes, where a lower mass change is obtained. By contrast, at a slow a scan rate, an equilibrium process predominates as the movement of the neutral species is slower than the movement of the charged species, therefore a higher mass

change occurs because there is enough time for mass transport to maintain its rate with the electrode dynamics.<sup>57, 58</sup>

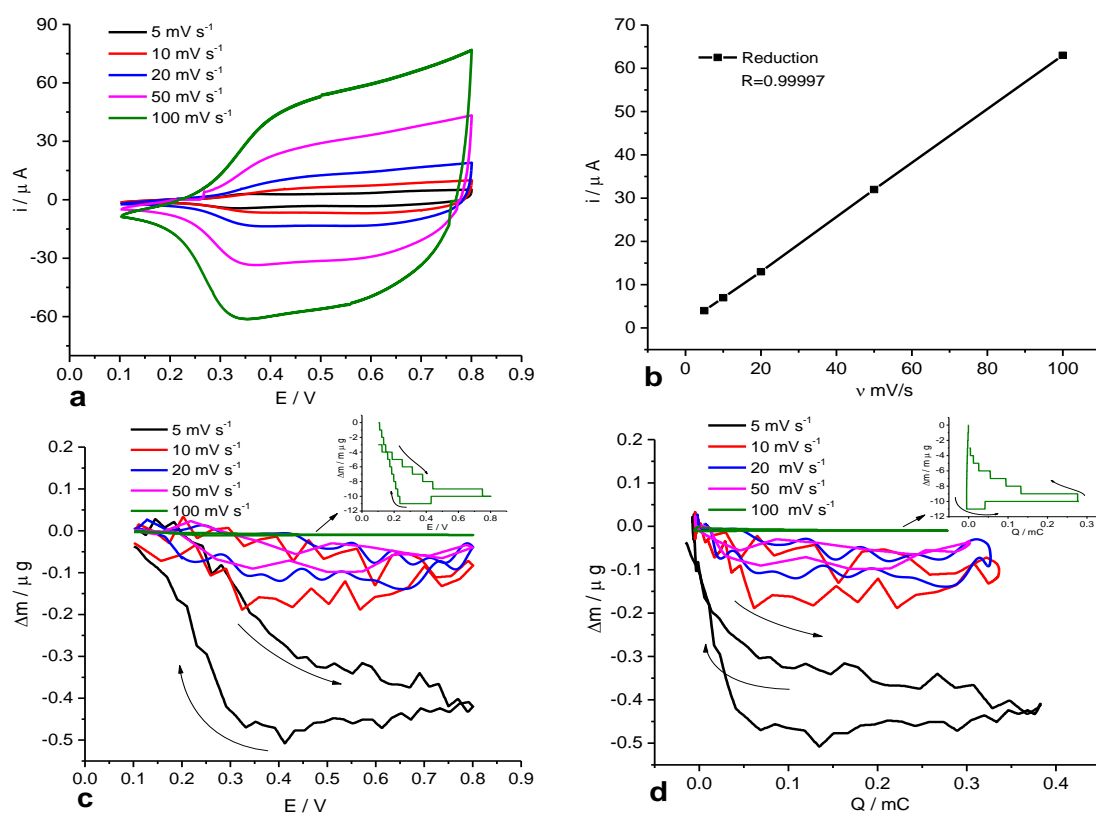


**Figure 5.19:** EQCM data for redox switching of PANI film exposed to Ethaline at various scan rates. a)  $i$  vs.  $E$ ; b)  $i$  vs.  $v$ ; c)  $\Delta m$  vs.  $E$ ; and d)  $\Delta m$  vs.  $Q$ . Colour indicate scan rates.

A quantitative interpretation of molar mass obtained from end to end for the doping and undoping regimes of PANI in Ethaline can be gained by plotting mass change vs. charge, as seen in **Figure 5.19d**. The molar mass and  $\alpha$  values for the expulsion and incorporation of ions calculated for all sweep rates are reported in **Table 5.13**. Obviously, the data do not correspond with the values expected for the transfer of either ion present, namely  $104 \text{ g mol}^{-1}$  for  $\text{Ch}^+$  injection or entry into the polymer. In general, the failure of mass and charge responses to reach to their initial values at the end of the complete redox cycle is dependent on scan rate (kinetics of ions in electrolytes). This means kinetic effects are associated with the relative transfer rates of cations and anions.

**Table 5.13:** Molar masses ( $M_{app}$ ) from  $\Delta m$  vs.  $Q$  graphs for redox switching of PANI in Ethaline at 50°C. Potential window in Ethaline was  $0.1 \leq E / V \leq 0.8$  for the fifth scan at various scan rate (5, 10, 20, 50 and 100  $mV s^{-1}$ ). + represents a mass increase, - represents a mass decrease.

Electrolytes	Scan rates	Oxidation 5 <sup>th</sup> scan			Reduction 5 <sup>th</sup> scan		
		$M_{app}$ g mol <sup>-1</sup>	$\alpha$	Dominating process	$M_{app}$ g mol <sup>-1</sup>	$\alpha$	Dominating process
Ethaline	5	-115.50	-0.04	Ch <sup>+</sup> out	+96.72	-0.03	Ch <sup>+</sup> in
	10	-44.56	+0.23	Ch <sup>+</sup> out	+51.85	-0.20	Ch <sup>+</sup> in
	20	-34.76	+0.26	Ch <sup>+</sup> out	+51.28	-0.20	Ch <sup>+</sup> in
	50	-27.00	+0.29	Ch <sup>+</sup> out	+43.69	-0.23	Ch <sup>+</sup> in
	100	-03.50	+0.38	Ch <sup>+</sup> out	+02.50	-0.38	Ch <sup>+</sup> in

### 5.3.10 Conclusion

This chapter has described the electrochemical polymerisation of aniline in DESs (type III) on a Pt electrode surface for the first time and surface characterisation studies of the polymers were conducted. The results showed excellent polymerisation rate and high stability was exhibited by PANI (Oxaline) compared to other eutectics. This is related to many factors which effect the electrochemical growth of PANI in this report. Firstly, the composition of the background solution, in terms of being different hydrogen bond donors (HBD), such as alcohols, amines, and carboxylic acids as well as water content, is important. These formulations can be used to enhance the conductivity, stability and reproducibility effects observed for conducting polymers. Secondly, the inorganic acids used in some PANI-DES as supporting electrolytes affect electrochemical, optical and conducting characteristics of films. The morphology of the films created in DESs were examined by comparing with those grown in aqueous solutions using SEM and AFM. It noticeable that the polymers' structures are changed in these systems depending on the nature of the anions present in solution.

In this instance, polyaniline growth from Oxaline was selected as a model polymer (due to high current density, more pores in the structure and high redox stability) to study the mechanism of the formation of this film in DESs and in aqueous solutions by using an *in situ* EQCM technique. It was found that PANI film cycled in DES at room

temperature demonstrated greater swelling and needs greater time to reach its equilibrium state than when cycled in high temperature DES electrolytes. This may be related to the large size of the anions present and, thus, the high viscosity of these solvents, which obstruct the motion of molecules.

The admittance spectra was shown that PANI film deposited from DESs possible partially viscoelastic nature and, it can be used for gravimetric measurements in the monomer-free aqueous and DES electrolytes. The magnitude of the mass change of the films in DESs is dependent on the scan rate. All PANI films are grown in DES solution showed the mass changes are dominated by cation transfer processes during oxidation and reduction cycling at high temperature. However, at room temperature, the anion transfer processes are dominated during redox cycling before the film reaches steady state. When PANI films, prepared from DES (Oxaline), are transferred to aqueous solution change from cation transfer domination during oxidation process to anion transfer domination during redox processes. Oxaline and Glyceline gravimetric analysis was not measurable mass change by these solvents due to their high viscosity.

Conclusions show that various mechanisms may occur during the complete redox conversion due to different sources/sinks of mobile species in each case, rather than just the polymer structure itself, potential window, scan rate and temperature. Despite these results, it is difficult to confirm whether deep eutectic solvents are more appropriate electrolytes for electropolymerisation of aniline than aqueous solutions. It is crucial that more work is done to interpret the correlation between DES properties and polymer performance. These results provide a platform that will allow researchers to develop further research in this field. As a result of their many chemical and electrochemical applications DESs will probably become considered as green and eco-friendly alternatives to ionic liquids, and as solvents in their own right.

## 5.4 References

1. A. R. Hillman and M. A. Mohamoud, *Electrochimica Acta*, 2006, **51**, 6018-6024.
2. C. Weidlich, K.-M. Mangold and K. Juttner, *Electrochimica Acta*, 2001, **47**, 741-745.
3. R. Bhadani, *Asian Journal of Research Chemistry*, 2013, **7**, 637-640.
4. A. P. Abbott and K. J. McKenzie, *Physical Chemistry Chemical Physics*, 2006, **8**, 4265-4279.
5. F. Endres, D. MacFarlane and A. Abbott, *Electrodeposition from Ionic Liquids*, Wiley, 2008.
6. E. L. Smith, A. P. Abbott and K. S. Ryder, *Chemical Reviews*, 2014, **114**, 11060-11082.
7. T. Kobayashi, H. Yoneyama and H. Tamura, *Journal Electroanalytical Chemistry*, 1984, **161**, 419-423.
8. A. A. Pud, *Synthetic Metals*, 1994, **66**, 1-18.
9. M. A. Skopek, M. A. Mohamoud, K. S. Ryder and A. R. Hillman, *Chemical Communications*, 2009, 935-937.
10. K. Sekiguchi, M. Atobe and T. Fuchigami, *Journal of Electroanalytical Chemistry*, 2003, **557**, 1-7.
11. P. C. Innis, J. Mazurkiewicz, T. Nguyen, G. G. Wallace and D. MacFarlane, *Current Applied Physics*, 2004, **4**, 389-393.
12. J. H. Mazurkiewicz, P. C. Innis, G. G. Wallace, D. R. MacFarlane and M. Forsyth, *Synthetic Metals*, 2003, **135-136**, 31-32.
13. A. R. Hillman, K. S. Ryder, V. C. Ferreira, C. J. Zaleski and E. Vieil, *Electrochimica Acta*, 2013, **110**, 418-427.
14. F. Zhao, M. Wang, Y. Ma and B. Zeng, *Journal of Chromatography A*, 2011, **1218**, 387-391.
15. W. Lu, A. G. Fadeev, B. Qi, E. Smela, B. R. Mattes, J. Ding, G. M. Spinks, J. Mazurkiewicz, D. Zhou, G. G. Wallace, D. R. MacFarlane, S. A. Forsyth and M. Forsyth, *Science*, 2002, **297**, 983-987.
16. A. R. Hillman, K. S. Ryder, C. J. Zaleski, V. Ferreira, C. A. Beasley and E. Vieil, *Electrochimica Acta*, 2014, **135**, 42-51.

17. A. P. Abbott, G. Capper, D. L. Davies, R. K. Rasheed and V. Tambyrajah, *Chemical Communications*, 2003, 70-71.
18. A. P. Abbott, *Chemical Physics and Physical Chemistry*, 2004, **5**, 1242-1246.
19. A. P. Abbott, D. Boothby, G. Capper, D. L. Davies and R. K. Rasheed, *Journal of the American Chemical Society*, 2004, **126**, 9142-9147.
20. A. P. Abbott, J. C. Barron, K. S. Ryder and D. Wilson, *Chemistry-A European Journal*, 2007, **13**, 6495-6501.
21. G. Sauerbrey, *Zeitschrift für Physik*, 1959, **155**, 206-222.
22. A. P. Abbott, *Chemical Physics and Physical Chemistry*, 2005, **6**, 2502-2505.
23. G. Yu, D. Zhao, L. Wen, S. Yang and X. Chen, *AIChE Journal*, 2012, **58**, 2885-2899.
24. A. P. Abbott, P. M. Cullis, M. J. Gibson, R. C. Harris and E. Raven, *Green Chemistry*, 2007, **9**, 868-872.
25. A. P. Abbott, G. Capper and S. Gray, *Chemical Physics and Physical Chemistry*, 2006, **7**, 803-806.
26. Q. Zhang, K. De Oliveira Vigier, S. Royer and F. Jerome, *Chemical Society Review*, 2012, **41**, 7108-7146.
27. J. O. M. Bockris, A. K. N. Reddy and M. E. Gamboa-Aldeco, *Modern Electrochemistry 2A: Fundamentals of Electrode Processes*, Springer US, 2001.
28. S. Mu, *Synthetic Metals*, 2004, **143**, 259-268.
29. K. P. Prathish, R. C. Carvalho and C. M. A. Brett, *Electrochemistry Communications*, 2014, **44**, 8-11.
30. G. G. Wallace, P. R. Teasdale, G. M. Spinks and L. A. P. Kane-Maguire, *Conductive Electroactive Polymers: Intelligent Polymer Systems, Third Edition*, CRC Press, 2008.
31. J. Zang, Y. Wang, X. Zhao, G. Xin, S. Sun, X. Qu and S. Ren, *International Journal of Electrochemical Science*, 2012, **7**, 1677 - 1687.
32. P. M. Fernandes, J. M. Campiña, C. M. Pereira and F. Silva, *Journal of the Electrochemical Society*, 2012, **159**, G97-G105.
33. P. M. V. Fernandes, J. M. Campiña, N. M. Pereira, C. M. Pereira and F. Silva, *Journal of Applied Electrochemistry*, 2012, **42**, 997-1003.
34. F. F. Bazito, L. T. Silveira, R. M. Torresi and S. I. Cordoba de Torresi, *Physical Chemistry Chemical Physics* 2008, **10**, 1457-1462.
35. A. Abd-Elwahed and R. Holze, *Synthetic Metals*, 2002, **131**, 61-70.

36. D. D. Borole , U. R. Kapadi, P. P. Kumbhar and D. G. Hundiwale, *Materials Letters*, 2002, **56**, 685–691.
37. J. Heinze, B. A. Frontana-Urbe and S. Ludwigs, *Chemical Reviews*, 2010, **110**, 4724-4771.
38. C. D’Agostino, L. F. Gladden, M. D. Mantle, A. P. Abbott, I. A. Essa, A. Y. Al-Murshedi and R. C. Harris, *Physical Chemistry Chemical Physics*, 2015, **17**, 15297-15304.
39. X. Li, *Electrochimica Acta*, 2009, **54**, 5634-5639.
40. G. Ćirić-Marjanović, *Synthetic Metals*, 2013, **177**, 1-47.
41. G. Inzelt, *Electrochimica Acta*, 2000, **45**, 3865-3876.
42. G. Inzelt, *Conducting Polymers: A New Era in Electrochemistry*, Springer-Verlag Berlin Heidelberg, 2008.
43. R. Cordova, M. A. del Valle, A. Arratia, H. Gomz and R. Schrebler, *Journal of Electroanalytical Chemistry*, 1994, **377**, 75-83.
44. K. Bieńkowski, M. Strawski and M. Szklarczyk, *Journal of Electroanalytical Chemistry*, 2011, **662**, 196-203.
45. M. J. Giz, S. L. de Albuquerque Maranhao and R. M. Torresi, *Electrochemistry Communications*, 2000, **2**, 377–381.
46. J. K. Avlyanov, J. Y. Josefowicz and A. G. MacDiarmid, *Synthetic Metals*, 1995, **73**, 205-208.
47. E. C. Venancio, C. A. R. Costa, S. A. S. Machado and A. J. Motheo, *Electrochemistry Communications*, 2001, **3**, 229-233.
48. F. Scholz, *Electroanalytical Methods: Guide to Experiments and Applications*, Springer Berlin Heidelberg, 2010.
49. A. R. Hillman, *Journal of Solid State Electrochemistry*, 2011, **15**, 1647-1660.
50. M. Skompska and A. Tarajko-Wazny, *Electrochimica Acta*, 2011, **56**, 3494-3499.
51. A. P. Abbott, M. Azam, G. Frisch, J. Hartley, K. S. Ryder and S. Saleem, *Physical Chemistry Chemical Physics*, 2013, **15**, 17314-17323.
52. S. Pruneanu, E. Csahok, V. Kertesz and G. Inzelt, *Electrochimica Acta*, 1998, **43**, 2305-2323.
53. R. Mazeikiene and A. Malinauskas, *European Polymer Journal*, 2002, **38**, 1947-1952.

54. E. Salamifar, M. A. Mehrgardi and M. F. Mousavi, *Electrochimica Acta*, 2009, **54**, 4638-4646.
55. T. Kobayashi, H. Yoneyama and H. Tamura, *Journal of Electroanalytical Chemistry and Interfacial Electrochemistry*, 1984, **177**, 281-291.
56. A. R. Hillman, S. J. Daisley and S. Bruckenstein, *Electrochimica Acta*, 2008, **53**, 3763-3771.
57. J. Wang, *Analytical Electrochemistry*, Wiley-VCH, 2001.
58. L. P. Bauermann and P. N. Bartlett, *Electrochimica Acta*, 2005, **50**, 1537-1546.

## **Chapter 6: Synthesis, Characterisation and Electrochemical Supercapacitor Properties of MoO<sub>2</sub>-Graphite-Polyaniline Composite Electrodes.**

### **Contents**

<b>6.1</b>	<b>Overview .....</b>	<b>171</b>
<b>6.2</b>	<b>Background .....</b>	<b>173</b>
6.2.1	Carbon composite .....	173
6.2.2	Metal oxides composite .....	175
<b>6.3</b>	<b>Objective .....</b>	<b>175</b>
<b>6.4</b>	<b>Results and discussion .....</b>	<b>176</b>
6.4.1	Stability and capacitance of PANI film during redox cycling .....	176
6.4.2	Effect of MoO <sub>2</sub> particles on stability and capacitance .....	178
6.4.3	Effect of GR particles on stability and capacitance.....	183
6.4.4	Effect of GR particles and MoO <sub>2</sub> on stability and capacitance .....	187
6.4.5	Capacitance retention .....	192
6.4.6	Effect of scan rates on the CVs and capacitance of PANI .....	194
6.4.7	Conductivity Measurements .....	196
6.4.8	Electrochemical impedance spectroscopy study .....	198
6.4.9	Spectroscopy studies .....	203
6.4.10	Thermogravimetric analysis of polyaniline composite .....	207
6.4.11	Morphology and topography of the polymer films .....	210
6.4.12	Conclusion.....	215
<b>6.5</b>	<b>References.....</b>	<b>217</b>

## 6.1 Overview

The increasing demand for the energy storage in electric vehicles and portable systems which need high power has led to considerable attention being given to electrochemical capacitors (also called supercapacitors) over the last decade.<sup>1-3</sup> Conducting polymers and metal oxides are expected to play a key role in optimising longer cyclability<sup>4</sup>, higher power density<sup>5</sup> and higher energy density<sup>6</sup> compared with traditional Electric Double Layer Capacitors (EDLCs).<sup>7</sup> Depending on their charge storage mechanisms, supercapacitors can be categorised into two types: (i) electrical double-layer capacitors (EDLCs) are carbon-based materials which generate their energy storage from the charge accumulated between the electrode and electrolyte interface, and (ii) redox supercapacitors. Compared with EDLCs, the latter are dependent on transition-metal oxides, such as RuO<sub>2</sub>, or conducting polymers, such as polyaniline. These materials have been widely studied as pseudo-capacitors due to faradaic reactions occurring within the active material of the electrodes.<sup>8-11</sup> Some metal oxides, such as RuO<sub>2</sub>, can give high specific capacitances, but are expensive, while other metal oxides, made from low cost materials, have low specific capacitances. Conducting polymers for pseudocapacitor applications have been extensively studied because of their low cost, ease of synthesis and high charge density in comparison with metal/metal oxides. As a result, conducting polymers can alternatively be employed instead of metal/metal oxides in supercapacitor applications.<sup>12</sup>

Generally, Electrically Conducting Polymers (ECPs) exhibit good capacitances with poor stabilities during the redox process. This is because these polymers suffer from a degree of volumetric change as a result of swelling, shrinkage, and then degradation of the polymer. Moreover, electrochemical cycling of each ECP is based on its working potential range, and this will be limited due to isolating states and/or structural degradation, which can be caused by overoxidation.<sup>13-15</sup> On the other hand, carbonaceous substances such as Carbon Nanotubes (CNTs), Activated Carbon (AC), and Mesoporous Carbon (MC) give good stability, but have limited capacitances due to the microstructures found in such materials. Recently, composite materials based on various carbon materials and conducting polymers such as PANI have been investigated as supercapacitor electrodes. As a result, extremely high capacitances and improved cycling have been accomplished due to synergetic incorporation of the mechanical

characteristics of carbonaceous materials and the excellent conductivity of ECPs.<sup>16-19</sup> Most research into supercapacitors concentrates on composite materials by incorporation of conducting polymers with carbonaceous compounds and/or metal oxides; some examples of such are PANI/MnWO<sub>4</sub> nanocomposites<sup>20</sup>, polypyrrole/carbon aerogel composite<sup>21</sup>, H<sup>+</sup> and Fe<sup>3+</sup> doped/co-doped PANI/multiwalled carbon nanotubes (MWCNTs) nanocomposites<sup>22</sup> and polypyrrole/graphene (PPy/GR) nanocomposite films prepared by electrochemical polymerisation on indium tin oxide (ITO) from aqueous solution.<sup>8</sup>

Significant improvements from those reported in the literature have been generally achieved in the capacitance of composite electrodes. This has been determined by the following parameters: (i) structural morphology, which provides good oxidation and reduction capacity, (ii) high conductivity, which depends on doping–dedoping rates (low charge transfer resistance), and (iii) increased porosity, which results in a high surface area. In the case of electrochemical performance, several advantages are achieved because (i) polymerisation and doping processes are presented at the same time, (ii) the rate of polymerisation can be easily regulated via the applied potential, and (iii) the constant potential applied in CA allows for uniform, adherent film deposition.<sup>23</sup> The preparation of conducting polymers with carbonaceous material/metal oxides composites has been successfully achieved by chemical and electrochemical methods; however, challenges remain, such as the high cost of CNTs, unsatisfactory redox and electroactive properties shown by electrostability and their own mechanical and thermostability insufficiencies. This may be due to the efficiency of the preparation method, the quality of the solutions used and the types of composite materials.<sup>12</sup> Therefore, the improved fabrication of PANI-GR-Metal oxide composites with large specific surface areas, high redox stabilities and desired functional groups through simple and efficient means remains difficult.

In the present work, we attempt a method to optimise the power and the energy densities of PANI-based supercapacitors by using a graphite (GR) material and molybdenum dioxide (MoO<sub>2</sub>) as an electrode template. The fabrication of composites for PANI-GR- MoO<sub>2</sub> are achieved by using electrochemical polymerisation in both aqueous and DES electrolytes. Various composite electrodes were also examined using cyclic voltammetry in order to improve charge-discharge stability in the voltage ranges of the supercapacitors.

## 6.2 Background

### 6.2.1 Carbon composite

Carbon has seen a growing interest as a practical electrode material in recent years due to its highly attractive characteristics in electrochemical applications. It is available in different forms such as glassy carbon, black carbon, carbon nanotubes (CNTs), carbon fibres, powdered graphite, graphene, pyrolytic graphite and highly ordered pyrolytic graphite (HOPG). Typically, these forms can exist in two- and/or three-dimensional electrodes. Typical two-dimensional carbon-based electrodes are carbon cloth, black carbon, activated carbon and carbon-polymer composite. In general, these are characterised by their high electrical conductivity, good thermal and mechanical stability, large surface area, a wide potential window with slow oxidation kinetics and, in many cases, enhanced electrocatalytic activity.<sup>24, 25</sup> The difference in whole carbon structures may be related to carbon's unique hybridisation properties. The ground state electronic configuration of the carbon atom is  $1s^2 2s^2 2p^2$ . The small energy gap between the  $2s$  and  $2p$  orbitals, facilitates the effective promotion of an electron from a  $2s$  orbital (lower energy state) to the vacant  $2p$  orbital (higher energy state). This electron promotion permits carbon to hybridise into  $sp$ ,  $sp^2$  and  $sp^3$  configurations, resulting in diverse molecular structures such as linear structures, planar structures and tetrahedral structures, respectively.<sup>26</sup> Research and development in this chapter will focus on graphite particles.

Graphite crystal is composed of many flat layers of hexagons in three-dimensional sheets formed in the earth's crust. It may be recognised by its grey/black colour, high melting point and brittleness. It has good thermal and electrical conductivity. A single layer of graphite is called graphene, where each carbon atom tightly is connected to three other carbons atoms by covalent bonds to form planar hexagonal rings in a layer that is itself planar.

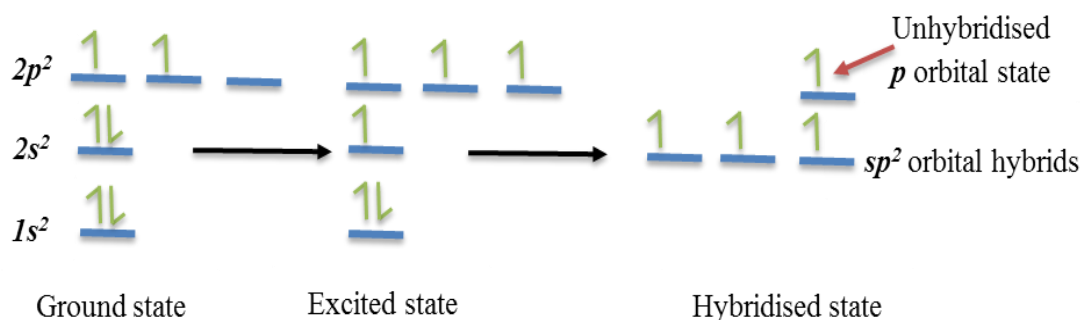


**Figure 6.1:** Atomic carbon  $sp^2$  hybridisation, as observed in graphite

The hybridisation of graphite forms  $sp^2$  type orbitals, directed  $120^\circ$  apart on a plane due to one electron from an  $s$ -orbital combining with two  $p$ -orbitals, which allows for the formation of a trigonal planar shape. The interaction of these electrons can lead to the formation of  $\sigma$ -bonding between carbon atoms on a planar layer. The free  $p_z$ -orbital electron can overlap with other  $p_z$ -orbitals orientated in the same direction to form a delocalised  $\pi$ -type orbital, with overlap being most effective if they are parallel (which defines an out-of-plane  $\pi$ -bond). This allows graphite to conduct heat and electricity. The layers of graphene in graphite are held together by weak van der Waals forces, and are detached by a distance of 0.335 nm. As a result, graphite is anisotropic, as seen in **Figure 6.2**. In addition, the graphene sheets can be easily separated from each other, resulting in such physical properties in graphite such as its soft and lubricating nature.<sup>26-</sup>

28

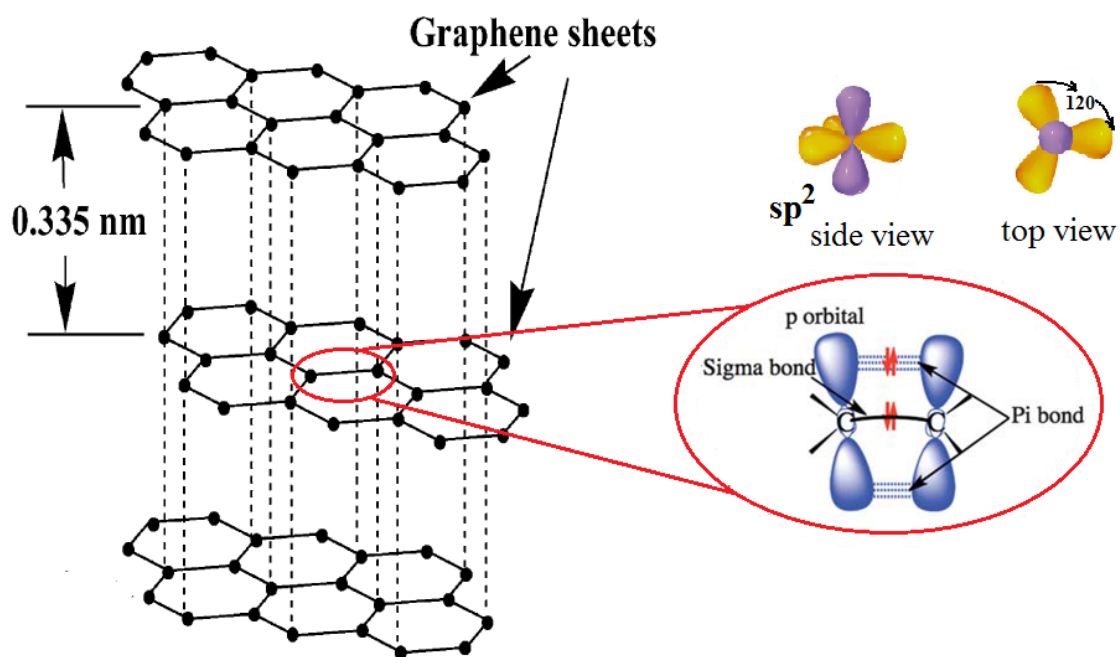


**Figure 6.2:** Atomic layering structure of graphite.<sup>26</sup>

### **6.2.2 Metal oxides composite**

Nanostructured materials involving transition metal oxides have attracted a great deal of attention and are used in various applications such as catalysts, electrochemical supercapacitors, lithium-ion batteries,<sup>6</sup> and sensors.<sup>29</sup> The properties of these structures are based on particle size, shape and surface area. The efficiency of batteries and electrochemical supercapacitors are improved when nanofibre and nanowire structures made of metal oxides having high surface area are used in their fabrication.<sup>30</sup> The most extensively used transition-metal oxide electrodes are RuO<sub>2</sub><sup>31</sup>, MnO<sub>2</sub><sup>32</sup>, NiO<sup>33</sup>, Co<sub>3</sub>O<sub>4</sub> and V<sub>2</sub>O<sub>5</sub> for various potential applications and thus, perform, enhanced energy and power density.<sup>9</sup>

Amongst the many metal oxides studied with conducting polymers as electrode materials, molybdenum oxides are widely studied as materials in the energy storage, catalysis, sensing objectives and optoelectronics due to their low cost and the promise of high electroactivity over a wide range of potentials. However, its capacitive implementations are limited as a result of poor ionic and electronic conductivity, which can affect electrochemical performance. In order to overcome these drawbacks, molybdenum oxide was incorporated into polymer composites, especially polyaniline (good capacitances with poor stability during the redox process) or graphite and its derivatives.<sup>34</sup> PANI-MoO<sub>x</sub> composites have been synthesised using the chemical polymerisation of aniline with ammonium persulphate (as an oxidising agent) using monoclinic anilinium trimolybdate dihydrate nanowires, formed upon the mixing of ammonium heptamolybdate with aniline in an acidic aqueous solution as a precursor.<sup>35</sup> Bian *et al.* also synthesized a self-doped polyaniline (SPAN) with molybdenum oxide (MoO<sub>x</sub>) composite by electrodeposition of MoO<sub>x</sub> and SPAN. The result was improved electroactivity over a wide potential range of up to 1.4 V between -0.6 to 0.8 V vs. Saturated Calomel Electrode (SCE). This pseudocapacitive behaviour proceeds from synergism of actions between organic and inorganic components.<sup>36</sup>

### **6.3 Objective**

In this chapter, we employ a simple approach to improve the electrochemical stability and capacitance performance of polyaniline growth from DES and aqueous solutions by the incorporation of graphite and MoO<sub>2</sub> particles. The purpose of incorporating the

species is to modify the internal architecture of the polymer so as to increase ion/solvent transfer and improve charge storage and possibly stability and performance. Incorporation of carbon nanoparticles is an obvious target, but these are difficult to see in the film and hence to measure and quantify. Therefore, a metal oxide and graphite micro-particles are selected, such that the particles are easily detected in SEM. A series of questions (objectives) can be set in this work. **The first question** is whether we can incorporate graphite and metal oxides with polyaniline film during the electropolymerisation process in DES/ aqueous solutions. **The second question** is how incorporation of these particles might influence the electrochemical stability, consistent morphology, conductivity, impedance spectroscopy and thermal stability of the polyaniline composite. In the following sections, we will try to address the above questions in the context of the preparation and exploitation of polyaniline composites in supercapacitance applications.

## **6.4 Results and discussion**

### **6.4.1 Stability and capacitance of PANI film during redox cycling**

Polyaniline films were electrochemically deposited on a Pt electrode (active area = 0.55 cm<sup>2</sup>) from 0.2 M aniline in Oxaline (**Figure 6.3a**) and in 1 M H<sub>2</sub>SO<sub>4</sub> (**Figure 6.3d**) at fixed scan rate of 5 mV s<sup>-1</sup> using cyclic voltammetry. The potential window in an Oxaline background electrolyte was 0.0 to 1.2 V over 15 scans while in aqueous solution -0.25 to 0.8 V over 6 scans was used. It is clear that two redox peaks were observed in the CV curves indicating the two exchange forms between the leucoemeraldine ↔ emeraldine and emeraldine ↔ pernigraniline states of the polymer.<sup>37</sup> From growth results, the mass and capacitance of the polymers were determined from the discharge time. Consequently, discharge values were calculated by the integration of the (*i* × *t*) curve along with the application of Faraday's Law. The relatively low current value for PANI-Oxaline resulted from slow ion transport rates due to the high viscosity of the solvent, as described in previous chapters. The specific capacitance (F/g) of the PANI electrode can be estimated from the CV curves according to the following two equations:

$$C_{sp} = \frac{i}{r \times m} \quad 6.1$$

$$C_{sp} = \frac{Q}{\Delta V \times m} \quad 6.2$$

where  $i$  is the average cathodic current,  $r$  is the scan rate,  $Q$  is discharge value,  $\Delta V$  is the electrochemical potential window and  $m$  is the mass of the active material (i.e. where polymer mass is determined based on a coulometric assay of the amount initially deposited).<sup>9, 11, 38, 39</sup> The specific capacitance values found for the PANI-Oxaline and PANI-H<sub>2</sub>O by two methods above were 545 F/g (Growth charge 0.03564 C) and 628 F/g (Growth charge 0.09849 C), respectively. The electrochemical stability of these polymers was studied in three steps. In the first step, the film was cycled for 100 cycles in the same environmental system in which it was deposited, then transferred into a different system, for example 0.5 M H<sub>2</sub>SO<sub>4</sub>, and finally back to the original system at a constant scan rate of 5 mV s<sup>-1</sup>, as shown in panels b and e of **Figure 6.3**; these experiments are termed ‘bracketed experiments’. This process shows whether the changes in the electroactivities of the films when transferred between multiple electrolytes are related to the properties and composition of the film (chemical changes) or the behaviour of the monomer-free electrolyte (e.g. ion mobility).

For DESs, Ethaline was selected as the most suitable electrolyte for studying doping/dedoping reactions according to the EQCM data recorded in previous chapters. **Figures 6.3c** and **f** exhibit the specific capacitance for PANI-Oxaline and PANI-H<sub>2</sub>O over 100 cycles cycled in each electrolyte. Initially, the capacitance increases slightly for 20-30 cycles due to swelling of the film, after which it decrease scan upon scan. 15 % PANI-Oxaline and 21 % PANI-H<sub>2</sub>O of the capacitance was lost in the first electrolyte the film was cycled in (i.e. the first step). It is notable that the shape of the CV curves for typical peaks recorded for the third step for each polymer appeared as a single redox peak following the rapid decrease in capacitance. This drop is attributed to two causes. The initial reason is poor electron transfer, arising from a lack of porosity in the polymer leading to solvent and charge carriers being unable to transfer in any significant volume into the film network (see panels a and b of **Figures 9.4** in the appendix). The second cause may have been due to degradation of the polymer electrode during the redox process.<sup>9, 40</sup>

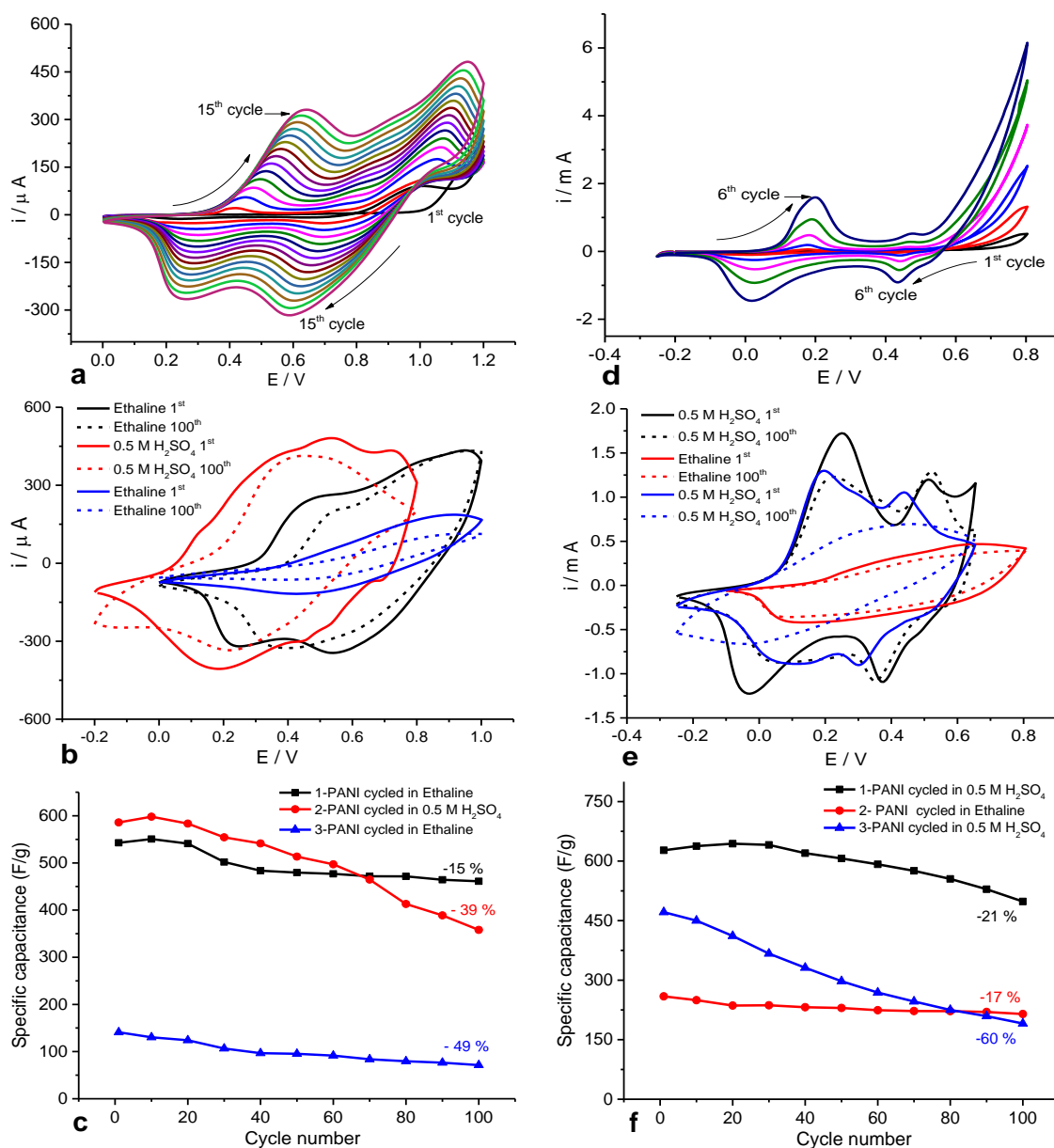


**Figure 6.3:** Panels: a), b) and c) show the CV of PANI film prepared from 0.2 M aniline in Oxaline, electrochemical redox stability and specific capacitance versus cycle numbers, respectively. Panels: d), e) and f) show CV of PANI film prepared from 0.2 M aniline in 1 M H<sub>2</sub>SO<sub>4</sub> aqueous solution, electrochemical redox stability and specific capacitance versus cycle numbers, respectively. The scan rate in both systems was 5 mV s<sup>-1</sup>.

#### 6.4.2 Effect of MoO<sub>2</sub> particles on stability and capacitance

In order to improve the permeability of the polymer network to the electrolyte and obtain high electrochemical performance, the porosity of the PANI films must be increased. This allows faster ion transport into and out of the film. The novel

composites based on electrochemically conducting polymers (PANI) and metal oxide ( $\text{MoO}_2$ ) were carefully fabricated using cyclic voltammetry. This process was followed by a three-step method, as shown in **Figure 6.4a**. Firstly, a thin layer of PANI was deposited on a Pt electrode ( $0.55 \text{ cm}^2$ ) [5 cycles for PANI in an Oxaline deposition electrolyte (0.0 to 1.2 V vs Ag wire,  $\nu = 5 \text{ mV s}^{-1}$ ) and 1 cycle for aqueous solution (-0.25 to 0.8 V vs Ag/AgCl,  $\nu = 5 \text{ mV s}^{-1}$ ]. Secondly,  $\text{MoO}_2$  particles ( $\sim 3 \text{ mg}$ ) were dispersed on the PANI surface. The modified electrode was then put in an oven at  $50^\circ\text{C}$  for 24 h. In the third step, PANI was again electrodeposited onto the  $\text{MoO}_2$ -PANI-modified electrode using CV (for 10 cycles in an Oxaline deposition electrolyte and 5 cycles for aqueous solution) at  $5 \text{ mV s}^{-1}$ . The potential range after particle addition for the deposition film formed in Oxaline was -0.2 to 1.3 V versus Ag wire, and between -0.25 and 0.8 V versus Ag/AgCl in aqueous solution. It can be seen from **Figures 6.5a** and **d** that  $\text{MoO}_2$  particles dramatically increased the current of the two well-defined redox couples in both electrolytes compared to the pure polyaniline deposition. In addition, the shape of CVs and redox potentials are obviously different to the pure PANI samples in previous sections. The changes in current peaks, as well as in redox potentials, are due to the incorporation of  $\text{MoO}_2$  particles with the conducting polymer, resulting in a high surface area. The mechanism of incorporating the PANI with molybdenum dioxide is thought to result from a fairly complex interaction, as shown in **Figure 6.4b**. Here, PANI obtains protonated and becomes anilinium cation due to oxidation reaction. When  $\text{MoO}_2$  particles are added to the PANI surface,  $\text{MoO}_2$  particles could be placed at the core of that complex. Further PANI occurs strictly on the surfaces of  $\text{MoO}_2$  in the complex with the addition of the aniline monomer solution by H-bonding and/or strong electrostatic force attraction with nitrogen atoms present in PANI chains.

The results show higher capacitance values compared to those reported previously for pure PANI films (**Figure 6.3**). As an example, the specific capacitance for PANI/ $\text{MoO}_2$  grown from Oxaline was 557 F/g (Growth charge 0.03935 C), whilst that found for pure PANI was 545 F/g (Growth charge 0.03564 C). In the instance of polymers grown from aqueous solution, the specific capacitance for PANI/ $\text{MoO}_2$  was 632 F/g (Growth charge 0.3831 C), whilst that found for pure PANI was 628 F/g (Growth charge 0.09849 C), as evaluated from cathodic peaks according to equation 6.2.

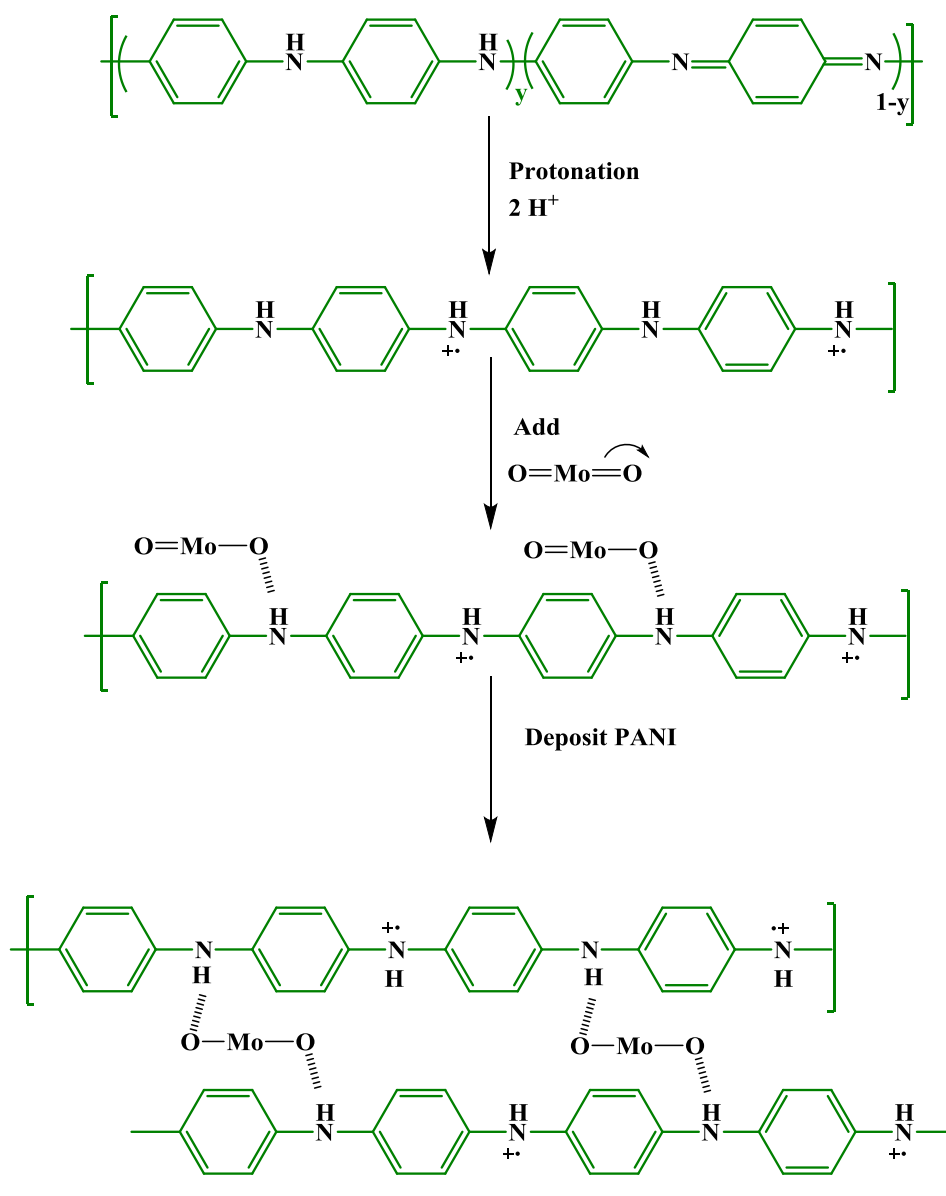
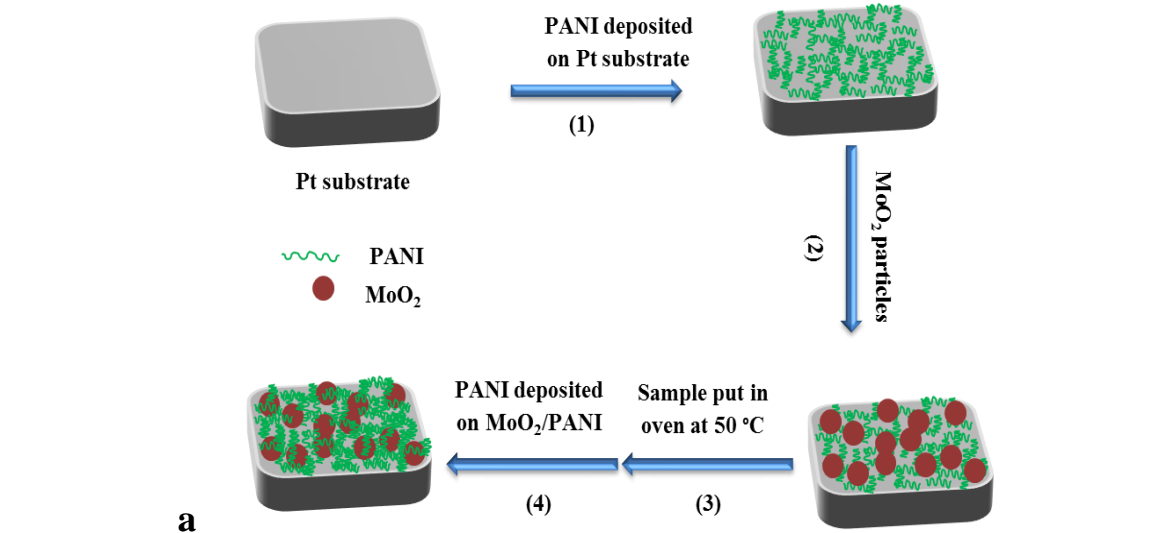


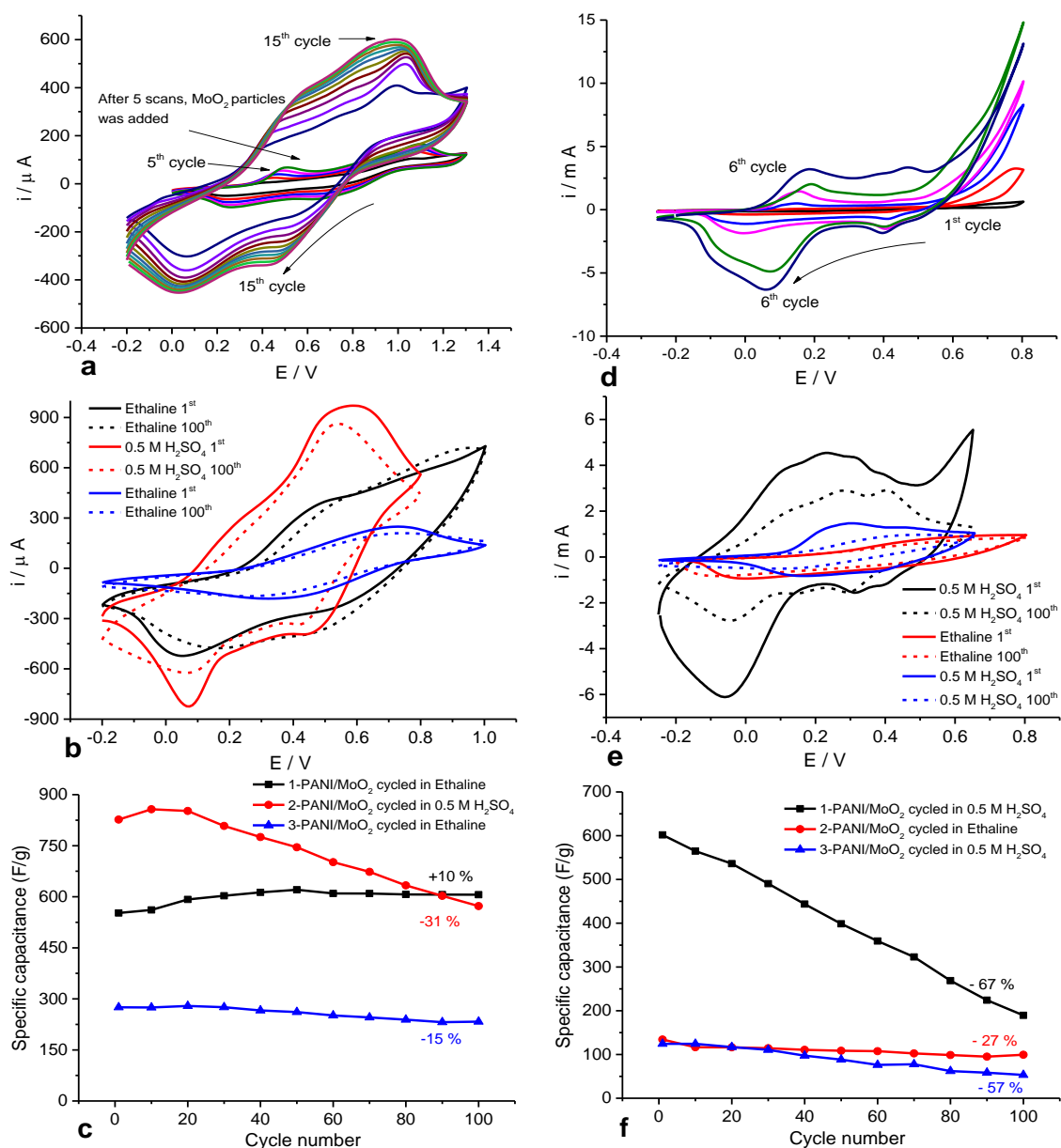
**Figure 6.4:** a) Synthetic route to the fabrication of polyaniline/MoO<sub>2</sub> composite b) The conjugated network formed between PANI and MoO<sub>2</sub>.

The electrochemical stability of these composites was tested using the same strategy as described in previous sections and can be seen in panels b and e of **Figure 6.5**. For example, PANI-MoO<sub>2</sub> grown from Oxaline was cycled for 100 cycles in Ethaline, aqueous solution and Ethaline, sequentially at a fixed scan rate of 5 mV s<sup>-1</sup>. Similarly, the PANI-MoO<sub>2</sub> grown from aqueous solution was cycled for 100 cycles in aqueous electrolyte, Ethaline and aqueous electrolyte, sequentially at fixed scan rate of 5 mV s<sup>-1</sup>.

The specific capacitance values of these materials were calculated based on them being conducting polymers using equation 6.2. Initially, there is an increase in capacitance for PANI-MoO<sub>2</sub>-Oxaline in Ethaline, which then remains stable over 100 cycles up to 10 % over the initial value. The capacitance of the polymer electrode is dramatically increased when the film is transferred to 0.5 M H<sub>2</sub>SO<sub>4</sub> due to further proton doping into the polymer composite and, as a result of the decrease in the viscosity of the electrolyte (compare to Ethaline), allowing faster ion transport into and out of the film. However, the capacitance data started to decrease rapidly after 30 cycles, and over 100 cycles it decreased by 31 % from the initial capacitance. In the third electrolyte, the polymer failed to reach its previous capacitance after being returned to Ethaline. This is may be due to degradation of the polymer composite or obstruction of the diffusion of species, such that mass transfer reduces the electrochemical process. It is noteworthy that the capacitance of the film in Ethaline (third step) dropped by 15 % from its initial over 100 cycles. This implies that the stability of the PANI-Mo electrode is greatly improved in Ethaline compared to aqueous solution. This agreement was also found in the PANI-Mo electrode grown in sulphuric acid and cycled in Ethaline.

Poor stability was shown to exist when the film was electrochemically cycled in 0.5 M H<sub>2</sub>SO<sub>4</sub> solution, with a recorded drop in capacitance of 67 %, whereas the cycling stability of the same film in Ethaline over 100 scans showed only a 27 % decrease in capacitance. The low capacitance value of the film in Ethaline compared to that in 0.5 M H<sub>2</sub>SO<sub>4</sub> is due to the high viscosity of the former solution. The data showed that the long-term redox cycling stability of PANI film with regards to its supercapacitance properties can be considerably improved by adding MoO<sub>2</sub> particulates, but can be affected by its environment, i.e., the electrolyte. In addition, the two redox peaks exhibit

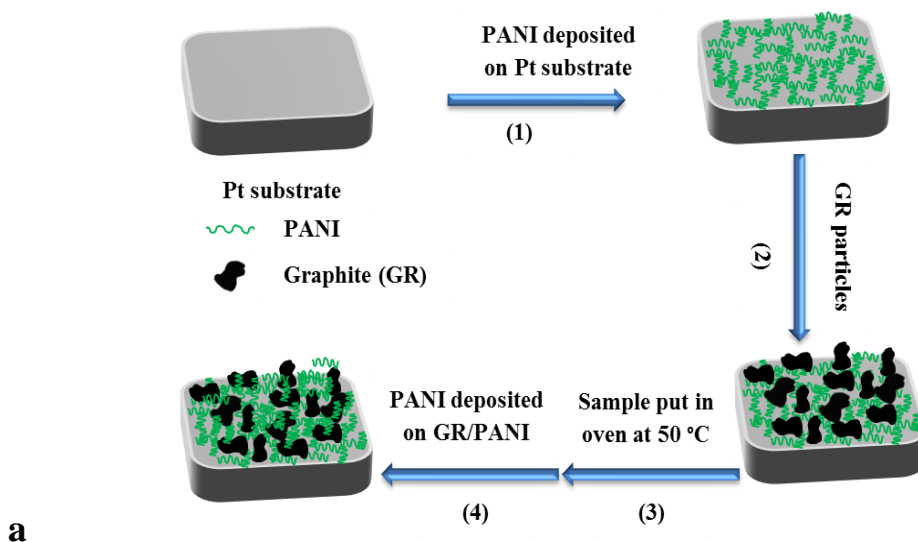
deviations in each electrolyte, and appear as one redox peak after long-term charge and discharge measurements.



**Figure 6.5:** Panels: a), b) and c) show the CV of PANI/MoO<sub>2</sub> electrode prepared from 0.2 M aniline in Oxaline, electrochemical redox stability and specific capacitance versus cycle numbers, respectively. Panels: d), e) and f) show CV of PANI/MoO<sub>2</sub> electrode prepared from 0.2 M aniline in 1 M H<sub>2</sub>SO<sub>4</sub> aqueous solution, electrochemical redox stability and specific capacitance versus cycle numbers, respectively. The scan rate in both systems was 5 mV s<sup>-1</sup>.

### 6.4.3 Effect of GR particles on stability and capacitance

In this section, polyaniline film was fabricated with graphite particles (GR) on a Pt substrate ( $0.55 \text{ cm}^2$ ) using the same method described in **Figure 6.6a**. **Figure 6.7a** and **d** show the electrodeposition of aniline with graphite particles in Oxaline and 1 M  $\text{H}_2\text{SO}_4/\text{H}_2\text{O}$ , respectively. After growing PANI on GR particles ( $\sim 3 \text{ mg}$ ) (i.e. third step, for 10 cycles in Oxaline and 5 cycles in aqueous solution at scan rate of  $5 \text{ mV s}^{-1}$  in both systems), the data exhibited significantly higher current peaks in both electrolytes than those seen for pure PANI and PANI/ $\text{MoO}_2$ . This enhancement in current peaks originated from the high surface area of the modified electrode, resulting in high electrical conductivity (due to fast ion transfer) as a consequence of the presence of graphite particles and their incorporation into the polyaniline film during the electrochemical process. The specific capacitance calculated for PANI/GR-Oxaline was  $573 \text{ F/g}$  (Growth charge  $0.07049 \text{ C}$ ), whilst that found for PANI/GR- $\text{H}_2\text{O}$  was  $741 \text{ F/g}$  (Growth charge  $0.47261 \text{ C}$ ), as evaluated from cathodic peaks according to equation 6.2. The interaction between GR and PANI is presumably that shown in **Figure 6.6b**, where the PANI chains can be stacked on the surface of graphite or graphene sheets through multiple interactions, such as  $\pi$ - $\pi$  coordination, hydrogen bonding and electrostatic attraction.<sup>41</sup>



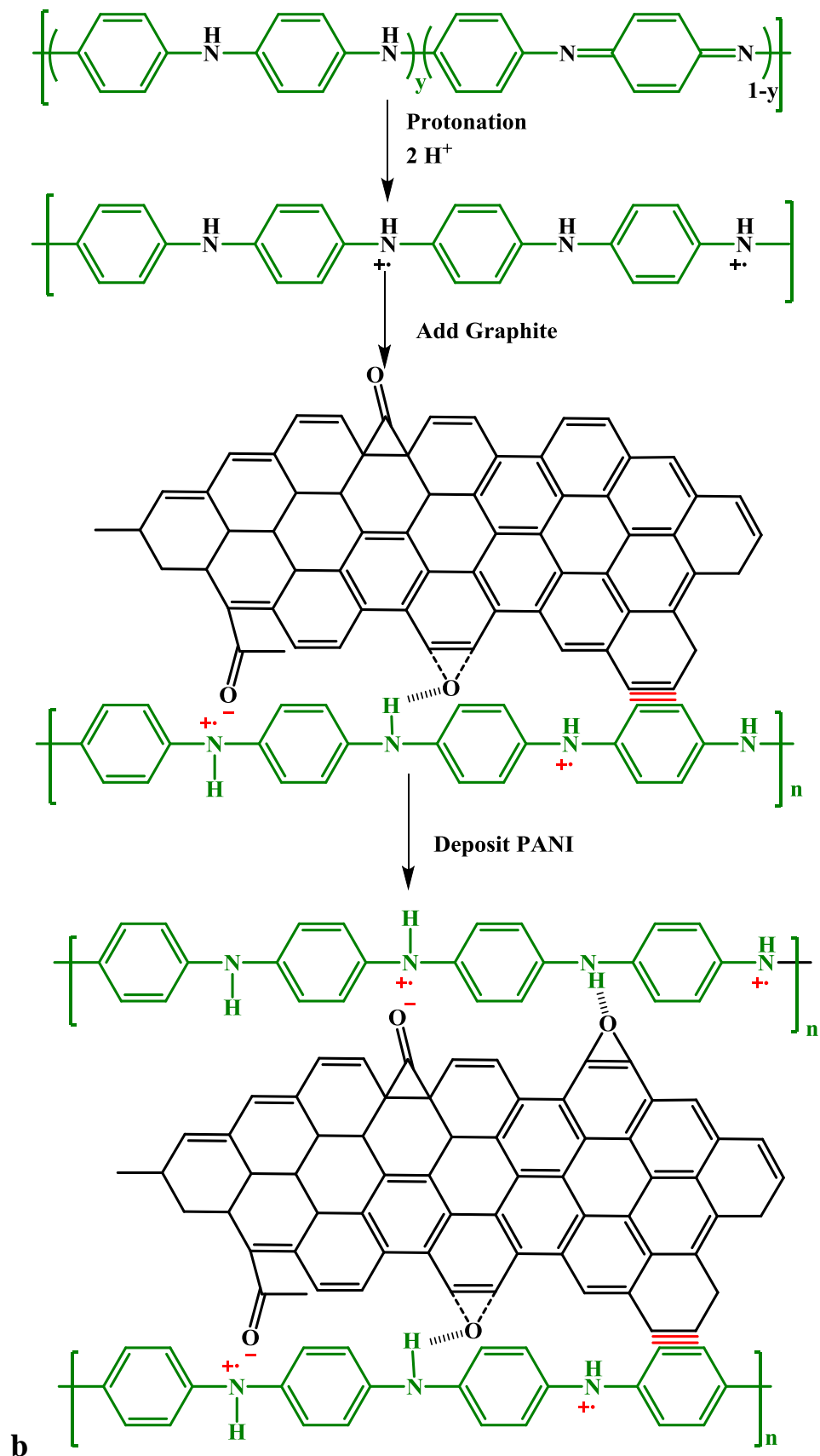


**Figure 6.6:** a) Synthetic route to the fabrication of polyaniline/graphite system. b) The conjugated network process between PANI and graphene single sheet of graphite composite.

**Figures 6.7b** and e show long-term measurements of the charge and discharge process for these polymers, where PANI/GR-Oxaline was cycled in Ethaline (0 – 1 V), 0.5 M H<sub>2</sub>SO<sub>4</sub> (-0.2 – 0.8 V) and Ethaline, respectively, for 100 cycles in each electrolyte, and PANI/GR- H<sub>2</sub>O was cycled in 0.5 M H<sub>2</sub>SO<sub>4</sub> (-0.25 – 0.65 V) and Ethaline (-0.2 – 0.8 V) and 0.5 M H<sub>2</sub>SO<sub>4</sub>, respectively, at 5 mV s<sup>-1</sup> for 100 cycles in each electrolyte. From discharge measurements, specific capacitance values were determined. All data determined for polymers containing GR particles show higher capacitances and better stability during long-term cycling in monomer-free electrolytes.

The specific capacitance of PANI/GR-Oxaline in Ethaline dropped 3 % from the initial value over 100 cycles and 8 % in the third step (when it was transferred back into Ethaline). Final capacitance retention after 300 cycles in different electrolytes was 83 %. In the case of PANI/GR-H<sub>2</sub>O, high electrochemical performance was seen during cycling of the polymer in 0.5 M H<sub>2</sub>SO<sub>4</sub>. The first time this was performed, the specific capacitance was slowly declined by about 11 % over 100 cycles, whereas the capacitance values gradually increased in the same electrolyte after transferal from Ethaline by about 3 %. The eventual capacitance retention after 300 cycles in various electrolytes was 69 % of the original value. High redox stability has been obtained for PANI/GR-H<sub>2</sub>O in Ethaline but with poor capacitance. This was attributed to high solvent viscosity and the thickness of the modified electrode, both of which influence ion ingress and egress through the film.

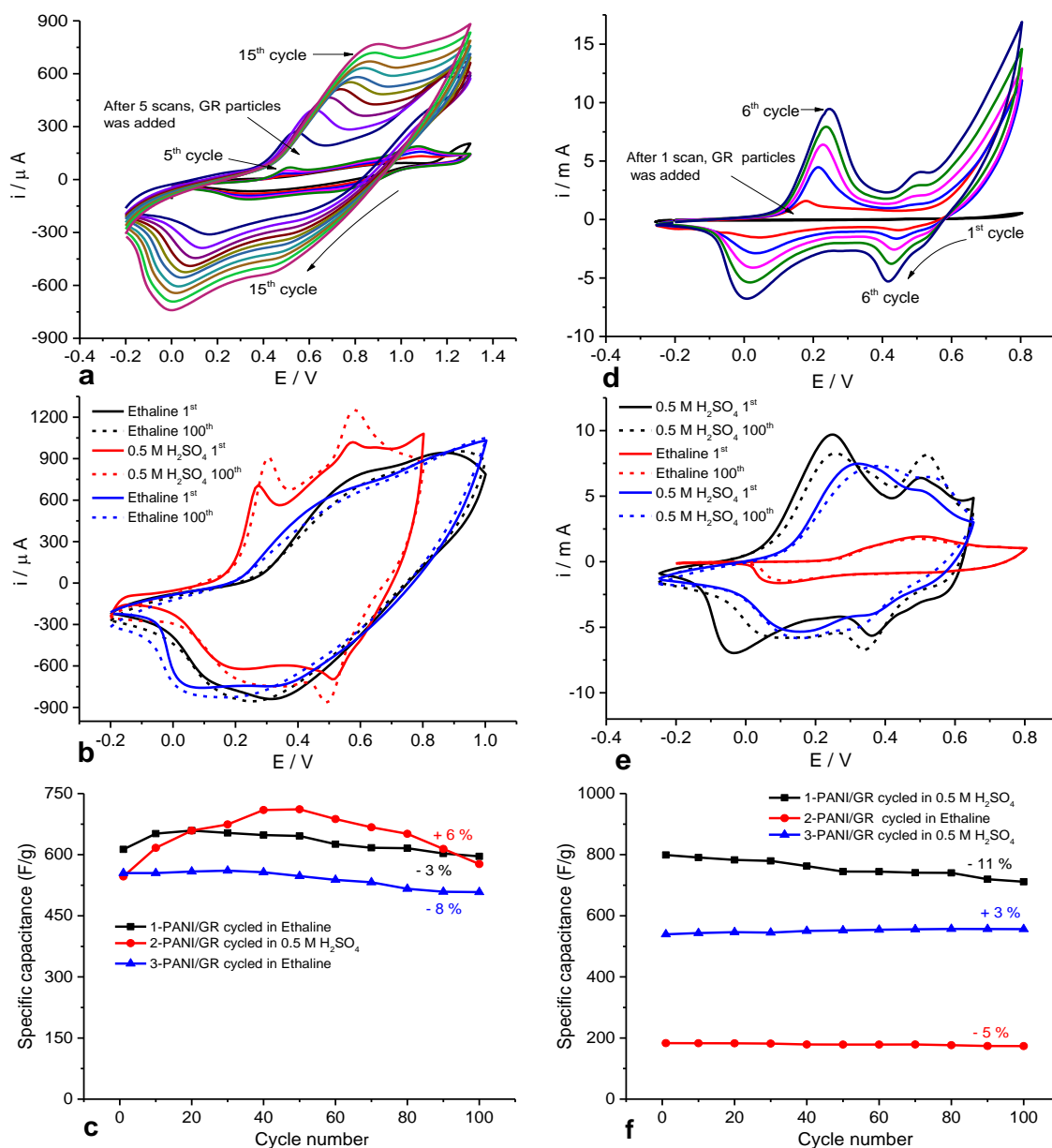


**Figure 6.7:** Panels: a), b) and c) show CV of PANI/GR electrode prepared from 0.2 M aniline in Oxaline, electrochemical redox stability and specific capacitance versus cycle numbers, respectively. Panels: d), e) and f) show CV of PANI/GR electrode prepared from 0.2 M aniline in 1 M H<sub>2</sub>SO<sub>4</sub> aqueous solution, electrochemical redox stability and specific capacitance versus cycle numbers, respectively. The scan rate in both systems was 5 mV s<sup>-1</sup>.

The specific capacitances and stabilities of the PANI/GR in this investigation are significantly better compared to those reported previously for polymer-carbon composite systems such as graphene oxide/PANI,<sup>12</sup> PANI/SWCNT composite<sup>38</sup> and polypyrrole/carbon aerogel composite materials.<sup>21</sup> It can be concluded from these results that GR particles significantly enhance the electrochemical performance of the

polyaniline after incorporation. Thus, optimisation of the cycling stability of PANI/GR composites was based on the high porosity of the composite, which occurred as a cooperative effect between the polymer matrix and graphite particles making the mass transfer for PANI/GR easier owing to the more extended conjugated network. Therefore, the stability of the capacitance of PANI/GR-Oxaline to cycling is better than that of PANI/GR-H<sub>2</sub>O.

#### **6.4.4 Effect of GR particles and MoO<sub>2</sub> on stability and capacitance**

A ternary PANI/GR/MoO<sub>2</sub> composite was synthesised on a Pt substrate (0.55 cm<sup>2</sup>) using cyclic voltammetry and the same strategy described in above was used to investigate the capacitance stability of this new modified polymer in sulphuric acid solution and DES electrolyte.

The PANI/MoO<sub>2</sub>/GR-modified electrodes were prepared from aqueous and Oxaline electrolytes through a stepwise method, as shown in **Figure 6.8a**. For PANI deposition from Oxaline, the first step was deposition of a thin layer of PANI on Pt (0.55 cm<sup>2</sup>) from 0.2 M aniline / Oxaline, using 5 potentiodynamic scans (0.0 to 1.2 V vs Ag wire,  $\nu = 5 \text{ mV s}^{-1}$ ). Secondly, the deposition solution was removed from the cell, then ca. 3 mg of GR+MoO<sub>2</sub> (3:1) particles were dispersed on the PANI surface and the electrode held at 50°C for 24 h. In the third step, further PANI was electrodeposited using the same deposition solution (10 cycles, -0.2 to 1.3 V vs Ag wire,  $\nu = 5 \text{ mV s}^{-1}$ ). The same strategy described above was used for PANI-modified electrodes prepared from aqueous 0.2 M aniline / 1 M H<sub>2</sub>SO<sub>4</sub> solution, but with a potential range -0.25 to 0.8 V versus Ag/AgCl. In the first stage, one potential cycle was used and in the last step five cycles were used (all at  $\nu = 5 \text{ mV s}^{-1}$ ). After polymerisation, each PANI composite modified electrode was cycled (100 cycles;  $\nu = 5 \text{ mV s}^{-1}$ ) in different monomer-free solutions: Ethaline, 0.5 M H<sub>2</sub>SO<sub>4</sub>, and Ethaline, sequentially, for films grown from Oxaline; and 0.5 M H<sub>2</sub>SO<sub>4</sub>, Ethaline and 0.5 M H<sub>2</sub>SO<sub>4</sub>, sequentially for films grown from 1 M H<sub>2</sub>SO<sub>4</sub> aqueous solution.

**Figure 6.9a** and d show the growth behaviour of PANI/GR/MoO<sub>2</sub> in Oxaline and 1 M H<sub>2</sub>SO<sub>4</sub>, respectively. In both electrolytes, the cyclic voltammograms of these composite polymers showed various changes in shape compared to previous results but they still responded to redox reaction progress. The shapes of the CVs for PANI/MoO<sub>2</sub>/GR in Oxaline, displayed the highest enhanced electrochemical performance in comparison to

previous modified electrodes. There were also changes in the redox peaks, with the anodic peak potential shifting towards the more positive side while the cathodic peak shifting towards more negative potentials. This originated from the incorporation of the three components as follows: (i) the rise in the electrical conductivity can be attributed to MoO<sub>2</sub>, as described by the CV measurements of the PANI/MoO<sub>2</sub> sample; (ii) the high overall specific capacitance which showed a dependence on the pseudo-capacitance, can be associated with the PANI;<sup>42</sup> and (iii) a high surface area is supplied by graphite, which significantly reduces structural damage to the PANI during the redox processes (as found by the CV measurements of the PANI/GR sample) and which additionally contributed to an increased capacitance in the composite.<sup>39</sup>

The capacitance values from the cyclic voltammetry experiments, as found using equation 6.2, were also calculated for PANI/GR/MoO<sub>2</sub>-Oxaline as 576 F/g (Growth charge 0.06685 C) and for PANI/GR/MoO<sub>2</sub>-H<sub>2</sub>O as 792 F/g (Growth charge 0.5011 C) from their respective cathodic peaks. The interactions between GR, MoO<sub>2</sub> and PANI are expected to be as shown in **Figure 6.9b**, where the PANI chains can be stacked on the surface of graphene sheets through the same multiple interactions as shown in **Figure 6.8b**, whereas MoO<sub>2</sub> can interact by H-bonding and/or strong electrostatic force attraction with the nitrogen atom.

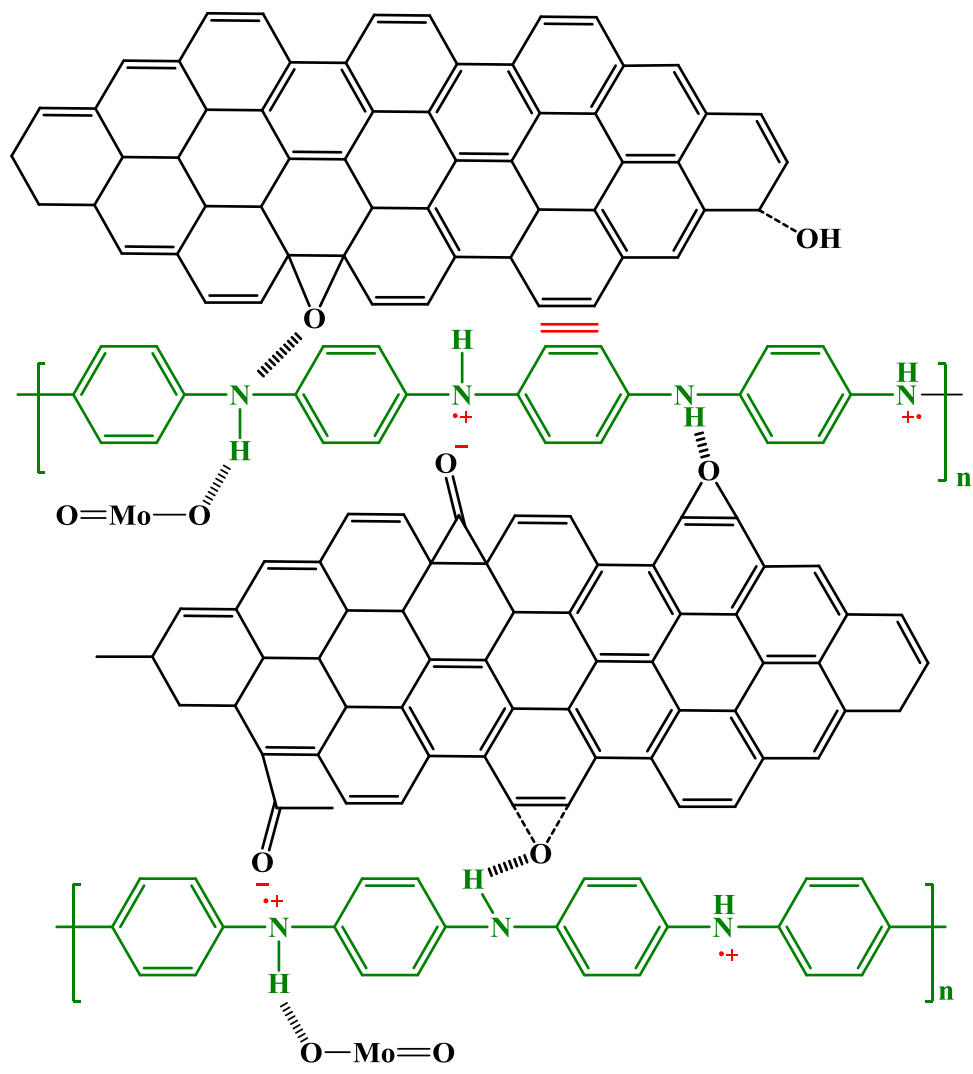
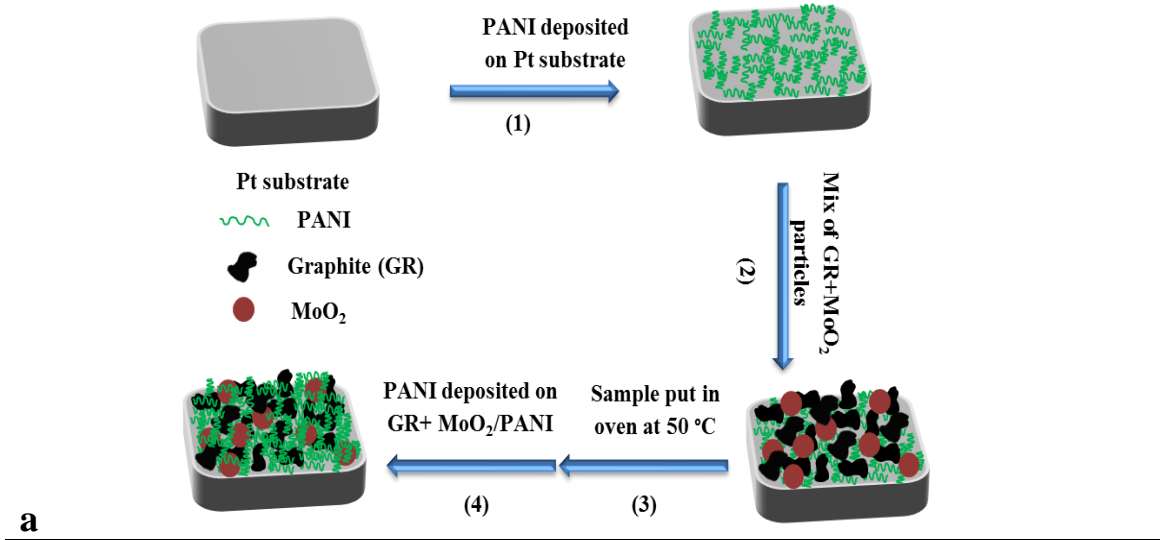


**Figure 6.8:** a) Synthetic route to the fabrication of PANI/MoO<sub>2</sub>/GR composite. b) The conjugated network interactions between PANI/ MoO<sub>2</sub>/GR.

After growth, ternary composite electrodes were examined in one electrolyte, for example Ethaline, transferred to another, for example 0.5 M H<sub>2</sub>SO<sub>4</sub>, and then returned to the initial electrolyte, all at a scan rate of 5 mV s<sup>-1</sup> for 100 cycles in each electrolyte. The reason for this, as mentioned in previous chapters, was to show if there were any changes in the electroactivities of the films when transferred to multiple electrolytes. These differences can be related to the polymer behaviour due to the electrolyte medium (e.g. ion mobility), or chemical changes that could be attributed to transferral of the polymer from one solvent to another (e.g. from H<sub>2</sub>SO<sub>4</sub> to DES). **Figure 6.9b** demonstrates the behaviour of PANI/MoO<sub>2</sub>/GR-Oxaline in Ethaline, 0.5 M H<sub>2</sub>SO<sub>4</sub> and Ethaline, respectively, while **Figure 6.9e** shows the behaviour of PANI/MoO<sub>2</sub>/GR-H<sub>2</sub>O in 0.5 M H<sub>2</sub>SO<sub>4</sub>, Ethaline and 0.5 M H<sub>2</sub>SO<sub>4</sub>, respectively. The CVs of both polymers remained the same even after extended cycling in various electrolytes.

In the case of PANI/MoO<sub>2</sub>/GR-Oxaline, after exposure to Ethaline over 100 cycles the capacitance increased by 3 % from its original value (first cycle). After transferring the film into 0.5 M H<sub>2</sub>SO<sub>4</sub>, there was a gradual rise in capacitance over 40 cycles, and then a subsequent decrease in capacitance resulting in a net decrease of about 4 % relative to the initial value. After exposure to 0.5 M H<sub>2</sub>SO<sub>4</sub> for the second time and subsequent transferral back to Ethaline, the trend of capacitance behaviour showed a lower value than in Ethaline (i.e. in the first step, as shown in **Figure 6.9c**), that increased with scan number until scan 50, thereafter dropping slowly resulting in a net increase in the value of capacitance of 3 % over 100 cycles.

For PANI/MoO<sub>2</sub>/GR-H<sub>2</sub>O cycled in 0.5 M H<sub>2</sub>SO<sub>4</sub> as its first monomer-free electrolyte, the capacitance initially increased during the first 10 scans, then remained stable until 100 cycles had been completed, giving a net increase of 7 % of its original value (first cycle). The specific capacitances of the same polymer in Ethaline were lower than in 0.5 M H<sub>2</sub>SO<sub>4</sub>, with values between 195 F/g – 185 F/g. This is related to the movement of ions, whose mobilities are low in this fluid due to its high viscosity. Despite low values of capacitance for the polymer in this electrolyte, it shows high electrical stability over 100 scans. Upon third exposure to 0.5 M H<sub>2</sub>SO<sub>4</sub>, the capacitance started with much lower values in comparison to the first exposure to 0.5 M H<sub>2</sub>SO<sub>4</sub>, probably due to the remnants of some of the Ethaline solution within the gaps in the polymer, causing a reduction of the gap size between polymeric chains. However, it can be seen that the capacitance values increase with an increasing number of scans, reaching 3 %

over its initial value. Compared with previous studies, lower capacitance values have been obtained than for ternary composite electrodes, though with different methods of fabrication consisting of graphene/MnO<sub>2</sub>/polyaniline<sup>43</sup>, multiwalled carbon nanotube/polyaniline/MnO<sub>2</sub><sup>44</sup>, reduced graphene oxide/molybdenum oxide/polyaniline<sup>34</sup> and manganese ferrite/graphene/polyaniline.<sup>45</sup> This means the improved capacitance values are strongly dependant on the quality and quantity of the ingredients used, as well as cell formation for electrochemical study.

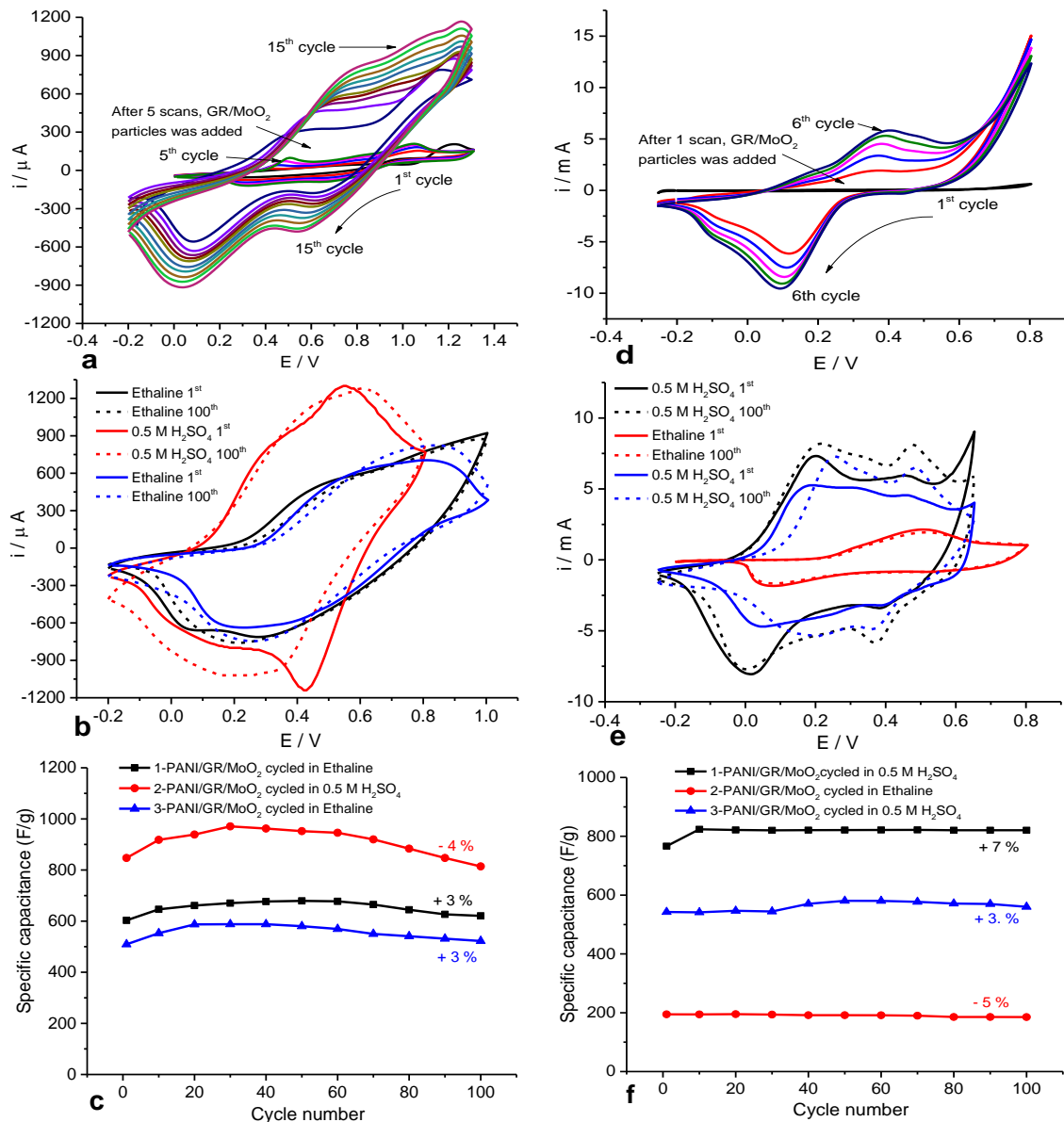


**Figure 6.9:** Panels: a), b) and c) show CV of PANI/MoO<sub>2</sub>/GR electrode prepared from 0.2 M aniline in Oxaline, electrochemical redox stability and specific capacitance versus cycle numbers, respectively. Panels: d), e) and f) show CV of PANI/MoO<sub>2</sub>/GR electrode prepared from 0.2 M aniline in 1 M H<sub>2</sub>SO<sub>4</sub> aqueous solution, electrochemical redox stability and specific capacitance versus cycle numbers, respectively. The scan rate in both systems was 5 mV s<sup>-1</sup>.

From the data in **Figure 6.9**, it is clear that a lower loss in electroactivity was found in the PANI/MoO<sub>2</sub>/GR composite. This means that these experiments showed high improvements in capacitance values and electrochemical stability. One of many findings to emerge from this investigation is that no irreversible chemical changes occurred in the polymer when changing from sulphuric acid solution to DES and back to the acid medium, or *vice versa*. The differences observed in capacitance values when the polymer was transferred between sulphuric acid and DES are likely to relate to kinetics and ion transport, which are strongly affected by the viscosity of the solution.

#### **6.4.5 Capacitance retention**

**Figure 6.10** shows a summary of the normalised specific capacitance values of all PANI composite electrodes performed in previous sections for 300 cycles in different electrolytes to compare their lifetime stabilities. As shown in panel a of **Figure 6.10**, pure PANI grown in an Oxaline background electrolyte and then sequentially cycled in Ethaline, 0.5 M H<sub>2</sub>SO<sub>4</sub> and Ethaline, exhibited the poorest capacitance retention (13 %), whereas the best capacitance retention (87 %) was obtained for the PANI/MoO<sub>2</sub>/GR film. The capacitance retention over 300 cycles of all polymers composites has the sequence PANI/MoO<sub>2</sub>/GR > PANI/GR > PANI/MoO<sub>2</sub> > PANI with values of 87 %, 83 %, 42 % and 13 %, respectively, correspond to their initial specific capacitances.

Panel b of **Figure 6.10** shows the cycling stability of polymer composites fabricated in 1 M 0.5 M H<sub>2</sub>SO<sub>4</sub> as the background electrolyte and then sequentially cycled in 0.5 M H<sub>2</sub>SO<sub>4</sub>, Ethaline and 0.5 M H<sub>2</sub>SO<sub>4</sub> at a scan rate 5 mV s<sup>-1</sup> for 300 cycles overall. The composite that exhibited the best capacitance retention was found as 73 % for PANI/MoO<sub>2</sub>/GR, whilst the worst capacitance retention was found for PANI/MoO<sub>2</sub> (9 %). The capacitance retention follows the order PANI/MoO<sub>2</sub>/GR > PANI/GR > PANI > PANI/MoO<sub>2</sub>, with values of 73 %, 70 %, 30 % and 9 %, respectively. This data demonstrates that the long-term cycling stability of the PANI film-based supercapacitors can be significantly improved by adding a mix of GR and MoO<sub>2</sub> particles (an optimal amount), or only graphite. Because these particles offer active PANI chains with a large surface area,<sup>46</sup> they may hence maintain the electrochemical stability of the PANI structure during the charge and discharge processes. In addition, the presence of GR and/or MoO<sub>2</sub> in the PANI material's structure increases the free volume (porosity) of the electrode, as shown in the associated SEM (**Figure 6.18**). As a

result, this process prevents variation in the volume of the PANI which arises from the swelling and shrinkage of the PANI during the redox reactions. This reduces the resistance to charge transfer of the electrode/solution interfacial region, which resulting in excellent rate capability and increased ionic conductivity. Remarkably, PANI/MoO<sub>2</sub> electrode growth from aqueous solution and Oxaline had the poorest stability to cycling in 0.5 M H<sub>2</sub>SO<sub>4</sub>, as seen in the rapidly declining capacitance values when cycled in the 0.5 M H<sub>2</sub>SO<sub>4</sub> solution, but at the same time showing excellent electrochemical stability in Ethaline, so these compounds are more stable in Ethaline than in acidic conditions. This means that an acid electrolyte may be considered the main reason for this problem. Some researchers have claimed that MoO<sub>x</sub>, as a solid-state electrode, can be dissolved in acidic media.<sup>47</sup> Hydrogen molybdenum oxide bronze can be formed at slightly higher pH due to cathodic reduction of MoO<sub>x</sub>.<sup>48</sup> It can be said that the electrochemistry of PANI/molybdenum species in aqueous media is very complex and the specific capacitance and capacitance retention are dependent on electrode composites and the electrolyte (monomer free) that will be cycled.

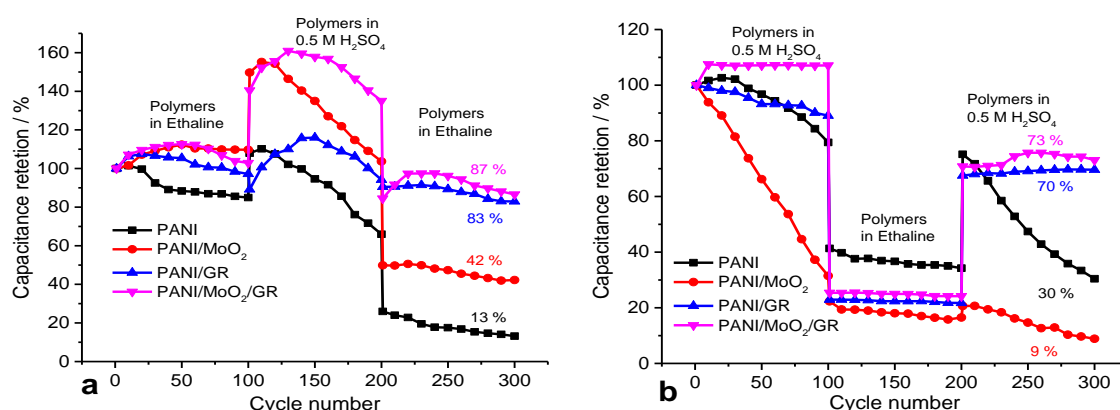


**Figure 6.10:** Capacitance retention characteristics for 300 cycles in different electrolytes acquired from long-term electrochemical stability measurements of samples of PANI, PANI/MoO<sub>2</sub>, PANI/GR and PANI/MoO<sub>2</sub>/GR as made in a) Oxaline, and b) 1 M H<sub>2</sub>SO<sub>4</sub>/H<sub>2</sub>O.

#### **6.4.6 Effect of scan rates on the CVs and capacitance of PANI**

PANI and PANI/MoO<sub>2</sub>/GR were synthesised from Oxaline in the same way as described in previous sections. After growth, the polymers were immersed in Ethaline (monomer free) separately at five different scan rates (5, 10, 20, 50, and 100 mV s<sup>-1</sup>) using cyclic voltammetry. The films were then examined by the chronoamperometry double step method in the same experimental solution over times equal to the time of each scan rate in an order to compare capacitance values in both methods. In the CVs, polymers were cycled in an Ethaline electrolyte between 0.0 and 1.3 V for PANI electrodes whereas the PANI doped with MoO<sub>2</sub>/GR (1:3) composite electrode was cycled between -0.2 and 1.3 V versus Ag wire. CVs can provide useful information about the behaviour of redox reactions on the surface of the electrode. It is well known that two reduction and two oxidation peaks appear in the CV scans, indicating exchange reactions between the leucoemeraldine/emeraldine and emeraldine/permigraniline states of the PANI film.<sup>37</sup> Therefore, here, the capacitance was largely dependent on the redox reactions, so the shapes of the CVs are distinct from the shape characteristic of electric double-layer capacitance, which tends to be like an ideal rectangle.<sup>9, 49</sup>

From CV curves (**Figures 6.11a** and **b**), the rise of current peak with increasing scan rate indicates a good rate capability for PANI and PANI/MoO<sub>2</sub>/GR composite electrodes, and thus in all scan rates the CVs seem to show symmetric shapes during charge and discharge processes. However, redox peaks are decreased, and, ultimately, completely disappeared from the CV at higher scan rates. The deviation from the ideal CV form and the disappearance of redox peaks are the result of increased scan rates. The oxidation peak is shifted toward more the positive side and the reduction peak to the negative side. This is due to the increased resistance of the working electrode (at increased scan rates). Variation in the CVs can also be caused by a rapid decrease in the concentration of ions on the electrode surface such that the ions in solution cannot maintain the electroneutrality of the electrode due limited diffusion rates into the active material of the electrode. As a result, the pseudocapacitance arising from the doping and undoping reactions is weak, and in this case specific capacitance is supplied by only double layer capacitance because the shape of the CV is more likely to be a rectangular. Conversely, at low scan rates, lots of electrochemical species are provided on the electrode surface due to predominating equilibrium conditions during the redox

process, leading to large charge storage formation arising from both pseudocapacitance and double-layer capacitance.<sup>50, 51</sup>

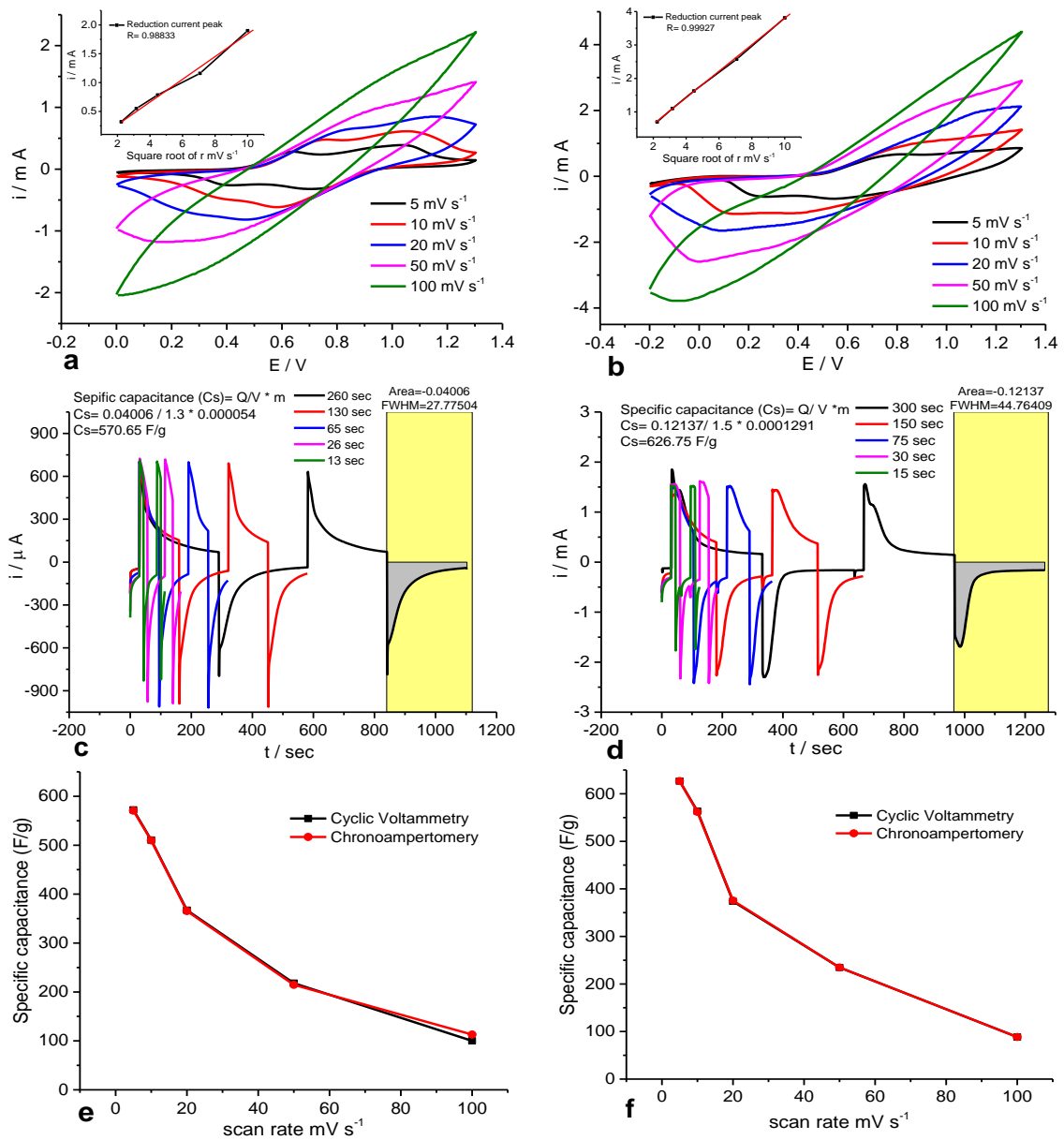


**Figure 6.11:** CV curves for a) PANI and b) PANI/MoO<sub>2</sub>/GR cycled in Ethaline at different scan rate of 5, 10, 15, 20, 50 and 100 mV s<sup>-1</sup>. Panels c) and d) show chronoamperometry curves for PANI and PANI/MoO<sub>2</sub>/GR, respectively, cycled in Ethaline at different time scales equal to scan rate times. Panels e) and f) show specific capacitance versus scan rate for the PANI and the PANI/MoO<sub>2</sub>/GR electrodes, respectively, in both methods.

The specific capacitance values (**Figures 6.11e** and **f**) of the pure PANI and PANI doped with MoO<sub>2</sub>/GR are determined from CV curves recorded at various scan rates in an Ethaline electrolyte according to equation 6.2. As an example, the specific capacitance of PANI/MoO<sub>2</sub>/GR was found to be 623 F/g at scan rate of 5 mV s<sup>-1</sup>, whereas it decreases to 89 F/g at a scan rate of 100 mV s<sup>-1</sup> for the reasons mentioned above. The analogous strategy in the capacitance values recorded for PANI film in Ethaline (i.e. the capacitance determined from the CVs as a function of scan rate). The insets in **Figures 6.11a** and **d** show reduction current peak versus the square root of the scan rate for the PANI and PANI/MoO<sub>2</sub>/GR films measured in an Ethaline electrolyte. The results gave a better proportional relationship (straight line) between reduction current peak and square root of the scan rate for the PANI/MoO<sub>2</sub>/GR electrode than for PANI. This is due to the MoO<sub>2</sub> and GR particles increasing the porosity in the electrode and thus decreasing its resistance to charge transfer. As a consequence, the diffusion-controlled reaction for the PANI/MoO<sub>2</sub>/GR film occurred, hence signifying ideal capacitive behaviour. Similar results were observed using the chronoamperometry double steps method to calculate specific capacitance values of both polymers. In general, our results for specific capacitance values as function of scan rate are decreased, in agreement with those reported in the literature.<sup>23, 52, 53</sup>

#### **6.4.7 Conductivity Measurements**

The conductivity of the polymer composite electrodes was determined using the van der Pauw four-probe method. Dry polymer powder (polymer powder made by cyclic voltammetry using big Pt plate (1.5 cm<sup>2</sup>) as working electrode) was compressed into discs by employing a standard 13 mm disc compressor (30 ton press C-300 Research and Industrial Instruments Company, London, England). It is well known that conductivity can be measured from the facility for electron transfer in the material, and this is represented by the current density per unit of electric field. The unit of measurement of conductivity is Siemens per meter, but commonly Siemens per centimetre (S cm<sup>-1</sup>) is used.<sup>54</sup>

The electrical conductivities of the polymer composites that were measured by the van der Pauw four-probe way can be calculated employing the following equation:

$$\sigma = \frac{\ln 2}{\pi R d} \quad 6.3$$

Here,  $\sigma$  is the electrical conductivity (in  $\text{S cm}^{-1}$ ) of the sample,  $R$  the slope of the voltage vs. current graph,  $d$  is thickness of the polymer disc (cm).

**Table 6.1:** Conductivity values of polyaniline composites

Polymers	Conductivity $\text{S cm}^{-1}$	
	Polymer made from Oxaline electrolyte	Polymer made from 1 M $\text{H}_2\text{SO}_4/\text{H}_2\text{O}$ electrolyte
PANI	1.83	1.25
PANI/MoO <sub>2</sub>	6.83	5.71
PANI/GR	9.87	18.0
PANI/MoO <sub>2</sub> /GR	14.0	19.1
Graphite	2.95	
MoO <sub>2</sub>	-	

**Table 6.1** gives the electrical conductivities ( $\sigma$ ) for all PANI composite materials fabricated in each electrolyte (i.e. Oxaline and 1 M  $\text{H}_2\text{SO}_4/\text{H}_2\text{O}$ ). Pure samples of PANI-Oxaline and PANI- $\text{H}_2\text{O}$  exhibited the lowest conductivity in this study, with values of 1.83 and 1.25  $\text{S cm}^{-1}$ , respectively, whereas GR particles had a much higher conductivity (2.92  $\text{S cm}^{-1}$ ), close to that graphene or pristine graphite.<sup>11, 55</sup> The high electrical conductivity of the graphite material plays a key role in improving the electrical conductivity, energy density and capacitance of PANI, as discussed above. The conductivity of PANI/MoO<sub>2</sub> is enhanced dramatically to 6.83  $\text{S cm}^{-1}$  and 5.71  $\text{S cm}^{-1}$  compared to the pure PANI sample, where the conductivity of PANI/MoO<sub>2</sub>- $\text{H}_2\text{O}$  decreases a little in comparison to PANI/MoO<sub>2</sub>-Oxaline. This is probably due to the effect of the sulphuric acid on the MoO<sub>2</sub> particles, as explained previously. The maximum conductivity was gained for samples of PANI/MoO<sub>2</sub>/GR and PANI/GR grown from aqueous solution, found as 19.1 and 18.0  $\text{S cm}^{-1}$ , respectively.

By contrast, the conductivities of PANI/MoO<sub>2</sub>/GR-Oxaline and PANI/GR-Oxaline are 14.0 and 9.87  $\text{S cm}^{-1}$ , respectively. Nevertheless, the electrical conductivities of both composites are much lower than those acquired from aqueous solution in terms of

composites; they are much higher than that of the pure PANI and PANI/MoO<sub>2</sub> samples due to the differences in the morphologies of the composites. Polymers (PANI/MoO<sub>2</sub>/GR and PANI/GR) grown from Oxaline have shorter chains than polymers grown from aqueous solution, and consequently their conductivities will be lower due to their decreased degree of oxidation and doping during the oxidation and reduction processes. The second reason is that an increasing amount of graphite in the polymer composite or heterogeneous distribution leads to a decrease in the conductivity of the sample, as observed by Zhang *et al.*<sup>11</sup>

In general, it can be said that electrical conductivity is increased for PANI doped with GR and/or MoO<sub>2</sub> particles, which can be attributed to the  $\pi$ - $\pi$  interactions between the PANI polymer backbone and the aromatic structure of the graphite sheets. In addition, the type of dopant ion can have an effect on the conductivity of the polymer.<sup>56</sup> Improvements have generally been found in the literature for the electrical conductivities obtained for polyaniline composite materials consisting of PANI/graphite nanocomposite containing 1.5 wt% graphite nanosheet (33.3 S cm<sup>-1</sup>) compared to other samples with 4 wt% graphite nanosheet (~29 S cm<sup>-1</sup>) and 0 wt% graphite nanosheet (~5 S cm<sup>-1</sup>, i.e. pure PANI),<sup>57</sup> and polyaniline-graphene oxide composites. In the latter case, the conductivities were generally dependent on the ratio of the mass of aniline monomer to the graphene oxide as 90:10, 50:50, and 20:80, whose resultant composites are called PAGO10 (16.87 S cm<sup>-1</sup>), PAGO50 (17.5 S cm<sup>-1</sup>), and PAGO80 (0.004 S cm<sup>-1</sup>), respectively.<sup>11</sup>

#### **6.4.8 Electrochemical impedance spectroscopy study**

Electrochemical Impedance Spectroscopy (EIS) measurements have also been studied in this chapter. The purpose of the current study was to understand the electrochemical properties of each electrode material in depth, as well as confirming the conductivities of the compounds. The range of frequencies used was between 65000 Hz and 0.01 Hz at an amplitude of 5 mV and recorded at +0.5 V (0.5 V was selected after samples were measured at different applied potentials in both systems). Nyquist plots (plots of the imaginary component of the impedance ( $-Z''$  / ohm) versus the real component ( $Z'$  / ohm)) were used in the interpretation of the obtained EIS data.

The impedance spectra were analysed based on an equivalent circuit model to that shown in the **Figure 6.12**. It is based on the resistance of solution ( $R_s$ ), the constant-phase element (CPE), the charge transfer resistance ( $R_{ct}$ ) and Warburg impedance ( $Z_w$ ). The results calculated for the electrochemical properties of these polymers were determined by best fits using the in-built GPES software. The impedances calculated for all polymers are reported in **Table 6.2**. A semi-circular arc represents a high to medium frequency area, while a straight line indicates a low frequency area. Both are formed in all plots, and an ideal capacitor exhibits a steeper low frequency region due to vertical axis to imaginary  $Z$  (see section 2.3.2 for a detailed explanation of the terms ‘semi-circular’ and ‘straight lines’).

Generally, the semicircle running from maximum to medium frequencies is attributed to the charge transfer reaction at the electrolyte/electrode interface (solution resistance,  $R_s$ ), whilst the diameter of the curve gives an estimate of the charge transfer resistance ( $R_{ct}$ ). The linear section (beside the semicircle) in the low frequency region belongs to the Warburg impedance, which results from the ionic diffusion process in the electrode.<sup>58, 59</sup> The charge transfer resistance can be deduced from the diameter of the semicircles. Here, a smaller diameter of semicircle indicates a lower charge transfer resistance and, consequently, a higher electronic conductivity.<sup>60, 61</sup>

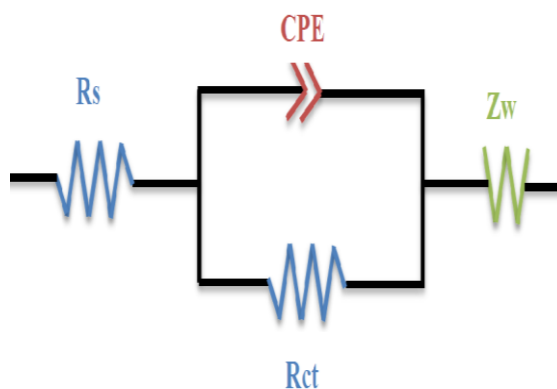


**Figure 6.12:** The equivalent circuit diagram for the Nyquist plot used to represent an electrochemical reaction with both kinetic (charge transfer) and mass transport.

As can be seen from **Figure 6.13a**, the diameter of the semicircle for the pure PANI electrode in Ethaline is much bigger than for other composite materials in the maximum to minimum frequency region. By contrast, the PANI/GR electrode has the smallest semi-circular diameter, which indicates the lowest charge transfer resistance, and hence

the highest electronic conductivity, compared to other polymer composites. The  $R_{ct}$  values of PANI, PANI/MoO<sub>2</sub>, PANI/GR and PANI/MoO<sub>2</sub>/GR at +0.5 V are 395, 173, 24 and 57  $\Omega$ , respectively. According to these values, the electrical conductivity of the polymers in Ethaline take the following order: PANI/GR > PANI/MoO<sub>2</sub>/GR > PANI/MoO<sub>2</sub> > PANI as reported in **Table 6.2**. The same polymers (i.e. **Figure 6.13a**) were transferred to 0.5 M H<sub>2</sub>SO<sub>4</sub> after rinsing with deionised water several times, and the same conditions (i.e. the range of the frequencies and potential) were carried out for all polymers individually, as shown in **Figure 6.13b**. It is clear from **Figure 6.13b** and **Table 6.2** that the same order of  $R_{ct}$  and  $Z_w$  values were obtained when the polymer materials were transferred to aqueous solution. This may be due to the influence of the faradaic charge transfer processes in this highly conducting composite during the investigation.

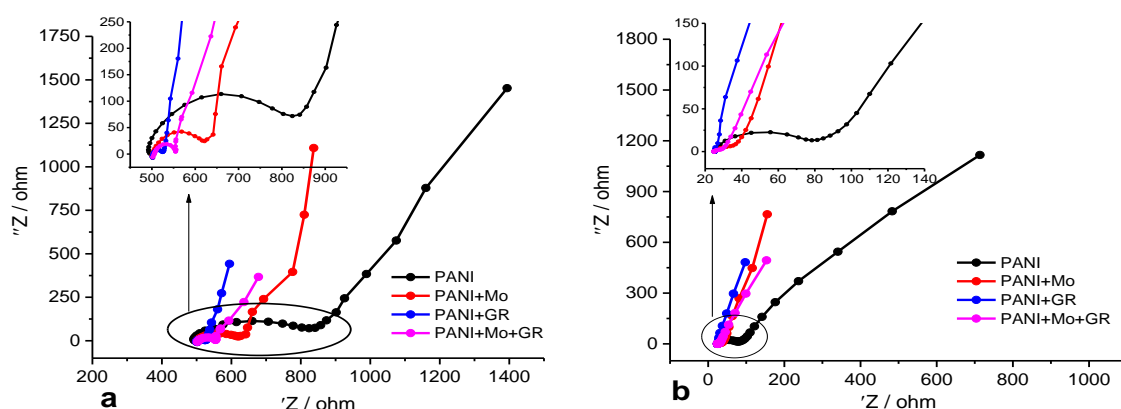


**Figure 6.13:** Nyquist plots from impedance spectra for PANI composite electrodes grown in Oxaline (as explained previously), collected in the range 65000 Hz to 0.01 Hz at an amplitude of 5 mV in a) Ethaline and b) 0.5 M H<sub>2</sub>SO<sub>4</sub>.

**Figure 6.14** represents the Nyquist plots of the PANI composite materials fabricated in aqueous solution (described previously) and immersed in (a) 0.5 M H<sub>2</sub>SO<sub>4</sub> and (b) Ethaline, respectively. The frequency range, amplitude and voltage are similar to those mentioned above. It can be seen from the data below that PANI/MoO<sub>2</sub> in aqueous solution has the highest  $R_{ct}$  value and lowest  $Z_w$ , which are the result of a high interfacial resistance between the electrode materials and solution. Hence, poor charge propagation behaviour occurred in the high frequency region, with low ion diffusion in the low frequency region. This result is expected because the lowest capacitance value

was when the fabricated polymer was cycled in 0.5 M H<sub>2</sub>SO<sub>4</sub> (see previous sections), and may be related to solvation problems between the solid MoO<sub>2</sub> material and sulphuric acid solution, as discussed earlier. Apparently, the PANI/GR and PANI/MoO<sub>2</sub>/GR electrodes maintain a much lower resistance and higher conductivity (Warburg impedance) than the PANI and PANI/MoO<sub>2</sub> electrodes in both electrolytes. Consequently, the electrical conductivity of the polymers in aqueous/Ethaline takes the order PANI/GR > PANI/MoO<sub>2</sub>/GR > PANI > PANI/MoO<sub>2</sub>, and *vice versa* with R<sub>ct</sub> values.

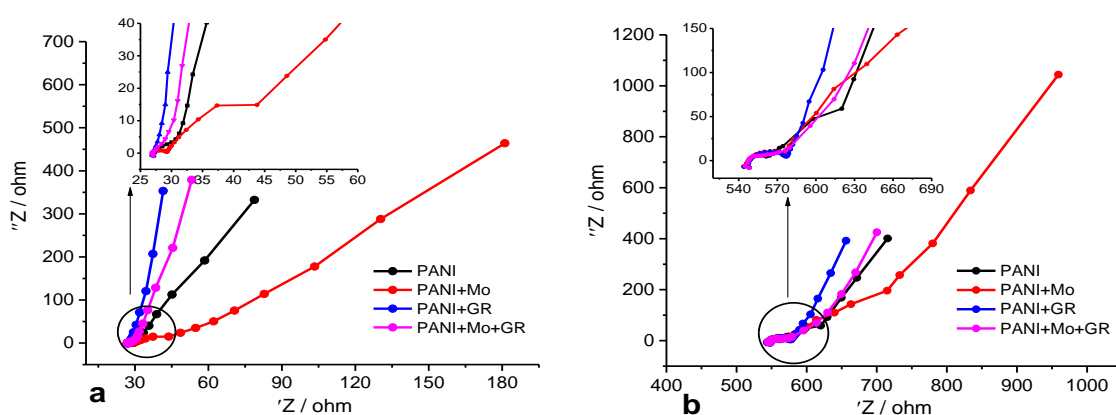


**Figure 6.14:** Nyquist plots from impedance spectra for PANI composite electrodes grown in 1 M H<sub>2</sub>SO<sub>4</sub>/H<sub>2</sub>O (as explained previously), collected in the range 65000 Hz to 0.01 Hz at an amplitude of 5 mV in a) 0.5 M H<sub>2</sub>SO<sub>4</sub> and b) Ethaline.

This study has shown that PANI/GR and PANI/MoO<sub>2</sub>/GR have a much lower charge resistance (semicircular diameter) than other polymers. This is favourable primarily to three-dimensional graphite, which can make electron transfer from PANI chains easier within the whole electrode. As a result, this reduces the internal resistance, leading to a high capability electrode for supercapacitors.<sup>10, 46, 62</sup> The above data exhibit that PANI on a three-dimensional graphite constituent can supply a remarkable synergistic growth for improving electrical conductivity, in terms of super-capacitive performance, over PANI and PANI/MoO<sub>2</sub>.

**Table 6.2:** The estimated impedance parameters of the three electrodes

Samples	Background electrolyte	In 0.5 M H <sub>2</sub> SO <sub>4</sub>				In Ethaline			
		R <sub>s</sub> (Ω)	R <sub>ct</sub> (Ω)	CPE (F)	Z <sub>w</sub> (Ω)	R <sub>s</sub> (Ω)	R <sub>ct</sub> (Ω)	CPE (F)	Z <sub>w</sub> (Ω)
PANI	Oxaline	28	53	1.88×10 <sup>-5</sup>	0.006	730	395	7.31×10 <sup>-5</sup>	0.004
PANI/MoO <sub>2</sub>	Oxaline	24	22	3.12×10 <sup>-3</sup>	0.031	505	173	2.55×10 <sup>-4</sup>	0.013
PANI/GR	Oxaline	20	3.5	8.536×10 <sup>-3</sup>	0.081	430	24	1.93×10 <sup>-4</sup>	0.036
PANI/MoO <sub>2</sub> /GR	Oxaline	24	9.7	8.30×10 <sup>-3</sup>	0.050	560	57	1.36×10 <sup>-4</sup>	0.034
PANI	1 M H <sub>2</sub> SO <sub>4</sub> /H <sub>2</sub> O	28	7.80	1.32×10 <sup>-2</sup>	0.105	619.5	52	9.22×10 <sup>-4</sup>	0.016
PANI/MoO <sub>2</sub>	1 M H <sub>2</sub> SO <sub>4</sub> /H <sub>2</sub> O	28	22.98	4.63×10 <sup>-3</sup>	0.023	573	37	3.97×10 <sup>-4</sup>	0.007
PANI/GR	1 M H <sub>2</sub> SO <sub>4</sub> /H <sub>2</sub> O	27	0.323	4.22×10 <sup>-2</sup>	0.278	548	31	2.77×10 <sup>-4</sup>	0.026
PANI/MoO <sub>2</sub> /GR	1 M H <sub>2</sub> SO <sub>4</sub> /H <sub>2</sub> O	31	0.176	4.57×10 <sup>-1</sup>	0.152	527	33	3.77×10 <sup>-4</sup>	0.022

## 6.4.9 Spectroscopy studies

### 6.4.9.1 Fourier Transformation Infrared Spectrum (FTIR)

Further investigations by spectroscopic methods were performed for PANI, PANI/MoO<sub>2</sub>, PANI/GR and PANI/MoO<sub>2</sub>/GR polymer composites to identify the functional groups and conjunction reactions. The FTIR results obtained are shown in **Figure 6.15** and reported in detail in **Table 6.3**. Here, we are characterising the adsorption peaks of pure PANI–Oxaline and comparing with other composites, as follows: the peak at 3225 cm<sup>-1</sup> corresponds to the NH stretching of aromatic amines, while an aromatic C-H stretch can be assigned in the range between 2816 and 2960 cm<sup>-1</sup>. The peaks at 1582 and 1500 cm<sup>-1</sup> are associated with C=N and C=C stretching modes for the quinoid and benzenoid units of the polymer, respectively. The absorption peak at 1302 cm<sup>-1</sup> is attributed to a C–N stretching mode of the benzenoid ring. The peak at around 1250 cm<sup>-1</sup> is due to the conducting protonated form of polyaniline. The C–H peak, which represents an in-plane bending mode, can be seen at 1150 cm<sup>-1</sup>. The band at 824 cm<sup>-1</sup> corresponds to an out-of-plane C–H bending mode.

Compared to MoO<sub>2</sub> in PANI composite electrodes, all these peaks appeared in the FTIR spectra of the PANI/MoO<sub>2</sub> and PANI/MoO<sub>2</sub>/GR composites, which are analogues to pure PANI film. However, there are some peaks observed in these composites which are *not* observed for pure PANI film. For example, an additional peak in the PANI/MoO<sub>2</sub> and/or PANI/MoO<sub>2</sub>/GR composite spectrum, which is due to Mo–O, appears in the region at 927 - 874 cm<sup>-1</sup> while the wide peak at 3558 cm<sup>-1</sup>, which may be attributed to an O–H stretching mode, indicates that the composites are successfully incorporated. Results similar to the above were also observed in previous work on the composite of PANI and MoO<sub>x</sub>, and were due to inorganic and organic interactions.<sup>36, 47, 63</sup>

The identity of the functional groups present, in the case of GR particles in GR–PANI and PANI/MoO<sub>2</sub>/GR composites, are supported by the recorded FTIR spectra. In the case of GR only, the peaks at observed at ~1750 cm<sup>-1</sup> may be related to C=O stretching vibrations in the carboxylic acid and carbonyl groups due to impurities in the graphite. It also exhibits two peaks that appear at 1630 and 1458cm<sup>-1</sup>, which correspond to aromatic C=C vibrations, while the peak at 1592 cm<sup>-1</sup> is due to a C–C stretch in an

aromatic ring, and other peaks at 1592, 1362, 848 and 2200  $\text{cm}^{-1}$ , were confirmed by comparison to the literature.<sup>64</sup>

All functional groups for PANI/GR and PANI/MoO<sub>2</sub>/GR are observed, but with slight frequency shifts in some peaks and the appearance of other new peaks. For example, the absorption peak around 3597  $\text{cm}^{-1}$  could belong to an O–H stretching mode, which could overlap with the N–H stretching of aromatic amines. There is also a slightly broader peak at 2960  $\text{cm}^{-1}$  than observed for pure PANI, which may be caused by the strong association between carboxyl C=O and hydroxyl O–H via dynamic hydrogen bonding. Additionally, a new feature, which appears around 1671 - 1688  $\text{cm}^{-1}$  for the PANI/GR and PANI/MoO<sub>2</sub>/GR composites, may be related to the C=O of an amide group, and is at nearly the same frequency as the band at 1750  $\text{cm}^{-1}$ , which is assigned to pure graphite. This suggests an acylation reaction between the amino groups on PANI and the carboxylic groups on GR has occurred, a suggestion that is corroborated by the literature.<sup>41, 65, 66</sup> The wide peak for PANI/GR at 835  $\text{cm}^{-1}$  could be related to the strong interaction between the CH out-of-plane bending mode of PANI and the graphite. The peak observed at 2200  $\text{cm}^{-1}$  may be attributed to carbon dioxide, which is evolved when the experiment is done in the absence of a nitrogen environment.<sup>67</sup>

These modified composites indicate the carboxyl/hydroxyl groups from graphene oxide (which are produced by the reaction of graphite with Oxaline/aqueous electrolyte during the electrodeposition process), are associated with the nitrogen of the PANI backbone, introduced via the same doping process into the PANI backbone. Moreover, the shift phenomena observed in the spectra of these composites results from the  $\pi$ – $\pi$  interaction and hydrogen bonding between the doping graphite or graphene oxide sheets and the polymer backbone. This shifting in positions of peaks is a result of structural changes in the polymer backbone. Furthermore, the interaction between the groups in PANI/GR, and thus PANI/MoO<sub>2</sub>/GR composites indicates a strong reaction between the graphite/graphene and the quinoid ring of the pure polymer.<sup>68</sup> The FTIR spectrum of the composites synthesised from aqueous solution exhibits similar features to polymers prepared from the Oxaline electrolyte, the data for which are reported in **Table 6.3** and the FTIR spectrum for which can be seen in **Figure 6.15b**. Overall, the FTIR features analysed in our results are in good agreement with previous studies reported in the literature.<sup>34, 41, 57, 69, 70</sup>

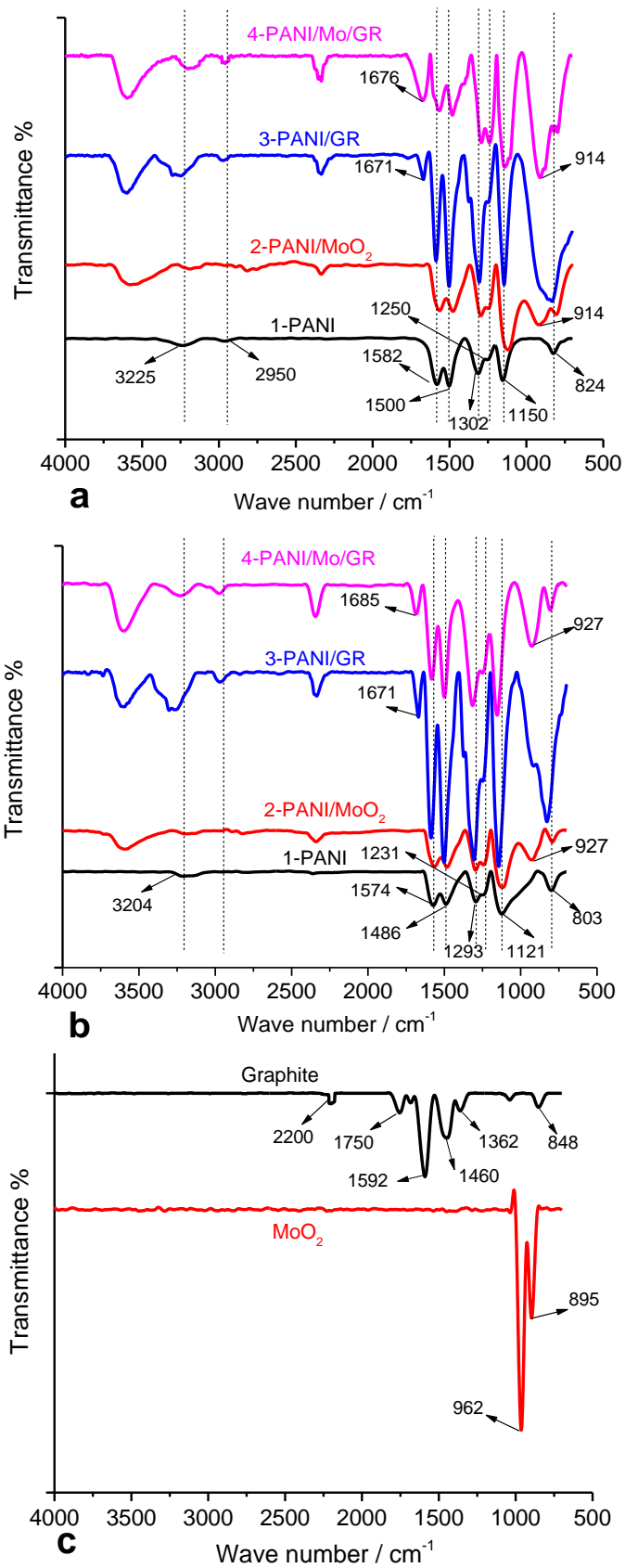


**Figure 6.15:** FTIR spectra of a) PANI composite grown in an Oxaline background electrolyte, b) PANI composite grown in a 1 M  $\text{H}_2\text{SO}_4/\text{H}_2\text{O}$  background electrolyte and c) graphite and  $\text{MoO}_2$  particles.

**Table 6.3:** The positions and assignments of the main absorption bands in the FTIR spectra of various PANI composite materials

Type of the vibrations / Frequency cm <sup>-1</sup>	Polymers growth from Oxaline				Polymers growth from 1 M H <sub>2</sub> SO <sub>4</sub> /H <sub>2</sub> O			
	PANI	PANI/Mo	PANI/GR	PANI/MoO <sub>2</sub> /GR	PANI	PANI/Mo	PANI/GR	PANI/MoO <sub>2</sub> /GR
O-H.....N-H	-	3570	3597	3597	-	3592	3602	3600
N-H stretching aromatic amines	3225	3186	3275	3191	3204	3186	3275	3222
C-H stretching aromatic	2950	2816	2960	2960	-	2830	2960	2960
N-C=O	-	-	1671	1676	-	-	1671	1688
C=N stretching of quinoid ring	1582	1565	1587	1570	1574	1561	1587	1574
C=C stretching of benzenoid ring	1500	1447	1503	1482	1486	1480	1499	1499
C-N bond stretch	1302	1300	1305	1297	1293	1293	1305	1314
Polaron bond of -N=Q=N/ C-H bend	1250	1240	1240	1240	1231	1234	1239	1248
C-H in plane	1150	1120	1142	1138	1121	1116	1138	1150
Mo-O	-	874 - 914	-	874 - 914	-	927	-	927
C-H out of plane	824	803	835	812	803	800	820	803

#### **6.4.10 Thermogravimetric analysis of polyaniline composite**

Thermal Gravimetric Analysis (TGA) is considered a significant technique in the investigation of the change in mass of a material (especially polymers) as a function of temperature. By this technique, the amount of solvent or other volatile materials lost, and the degradation of polymers, can be determined. It also characterises the polymers in terms of suitable applications, depending on the temperature at which decomposition is seen to take place. Generally speaking, there are three stages of weight loss in conducting polymers that depend on the framework composition, and which have been ascribed to:

##### ***1. Loss of solvent or water***

In the initial step, at around 70 - 150°C, the water or solvent and small molecules will be removed from the polymer backbone. Normally, these solvents arise as a consequence of polymer materials that are synthesised in the presence of water or other electrolytes, hydrating the dopant anions, and washing the final compound. Therefore, it is difficult to lose these solvents at low temperatures in the oven, but polymers will lose water and solvent molecules upon the application of sufficient heat.<sup>71,72</sup>

##### ***2. Loss of dopant anions***

In the second stage, the dopant anions, which were employed in the polymerisation process, will be lost from the polymeric backbone, ca. 150 - 350°C, based on the strength of heating, and the kind of dopant ions. Additionally, at the high end of this temperature range, the final step, degradation of the polymer itself, will probably occur.<sup>71-73</sup>

##### ***3. Backbone degradation***

In this step, ca. 350 - 650°C, a sharp mass loss occurs that will continue until complete destruction of the polymeric material. This takes place mainly due to breaking of the polymer backbone upon reaching high temperatures, and the nature of the polymer itself.<sup>71-73</sup>

**Figure 6.16** shows the stability of the PANI composite materials (electrodeposition in DES and aqueous electrolytes) against thermal degradation using the TGA technique. It is observed from the TGA curve of PANI-Oxaline that there are three stages to the thermal degradation process of weight loss as discussed above. More specifically, the initial stage is attributed to solvent loss between 60 and 126°C, the second step

corresponds to the evolution of the dopant (choline cation/Ox.Cl<sup>-</sup>) from the main structure of the polymer at 129 – 238°C, with the final stage of weight loss observed at 452°C due to degradation of the polymer backbone. Remarkably, this indicates that with increasing temperature, the mass of the sample decreases until complete decomposition of the polyaniline.

**Table 6.4:** Stages of weight loss of the polymer

Conducting polymer composite	Temp. loss of water/solvent (°C)	Temp. loss of dopant ions (°C)	Temp. backbone degradation (°C)
PANI-Oxaline	60 - 126	129 – 238	452
PANI/MoO <sub>2</sub> -Oxaline	70	219	472
PANI/GR-Oxaline	64	235	476
PANI/MoO <sub>2</sub> /GR-Oxaline	66	250	478
PANI-H <sub>2</sub> SO <sub>4</sub> /H <sub>2</sub> O	58	215	458
PANI/MoO <sub>2</sub> -H <sub>2</sub> SO <sub>4</sub> /H <sub>2</sub> O	61	220	469
PANI/GR-H <sub>2</sub> SO <sub>4</sub> /H <sub>2</sub> O	64	221	470
PANI/MoO <sub>2</sub> /GR-H <sub>2</sub> SO <sub>4</sub> /H <sub>2</sub> O	64	211	461

The TGA thermograms of PANI/MoO<sub>2</sub>, PANI/GR and PANI/MoO<sub>2</sub>/GR composite, as shown in **Figure 6.16a**, nearly follow the same stages of weight loss as pure PANI, the data for which are reported in **Table 6.4**. On the other hand, the total weight loss in the degradation temperature regime for each material is different, which may be due to the interaction of bonds between chains and composite, the existence of which was confirmed by FTIR studies, having an impact on the thermal stability of polymer.<sup>20, 74</sup> The total mass loss up to 452°C in PANI, PANI/MoO<sub>2</sub>, PANI/GR and PANI/MoO<sub>2</sub>/GR composite grown in Oxaline were found as 37 %, 30 %, 21 % and 16 %, respectively. This clearly shows that the weight loss of PANI/MoO<sub>2</sub>/GR and PANI/GR is less than for PANI and the PANI/MoO<sub>2</sub> composite, indicating the improved thermal stability for the PANI composite due to the synergistic effect between (i) graphite (having a high thermal stability), and (ii) MoO<sub>2</sub> and PANI.<sup>10, 57</sup>

Similar TGA features were noted for the other composites electrodeposited from aqueous solution (1 M H<sub>2</sub>SO<sub>4</sub>/H<sub>2</sub>O). It is observed that the degradation of the polymer PANI, PANI/MoO<sub>2</sub>, PANI/GR and PANI/MoO<sub>2</sub>/GR are a little lower than their counterparts grown in the Oxaline electrolyte. It should be mentioned that the difference in both systems in the second stage of mass loss in these composites indicates the release of ionic H<sub>2</sub>SO<sub>4</sub> from the polymer chain as the protonating dopant (counter-ion connected with positively charged nitrogen). According to the TGA curves reported in **Figure 6.16b**, the total mass removed up to 458°C in PANI, PANI/MoO<sub>2</sub>, PANI/GR and PANI/MoO<sub>2</sub>/GR was found as 40 %, 29 %, 25 % and 17 %, respectively. Similar to the polymers above, the composites with graphite/MoO<sub>2</sub> components show better thermal stability with lower mass loss when compared with other polymers (i.e. the PANI and the PANI/MoO<sub>2</sub> grown in aqueous solution). From the results above, we can conclude that the composites with graphite, or graphite with MoO<sub>2</sub>, have enhanced the thermal stability compared to those composites without graphite present. The thermal stability of compounds prepared from Oxaline electrolyte show greater stability compared to those prepared from acidic media. Due to the high thermal stabilities required in some industrial applications, PANI/GR and PANI/MoO<sub>2</sub>/GR composites could well be a suitable alternate to pure PANI.

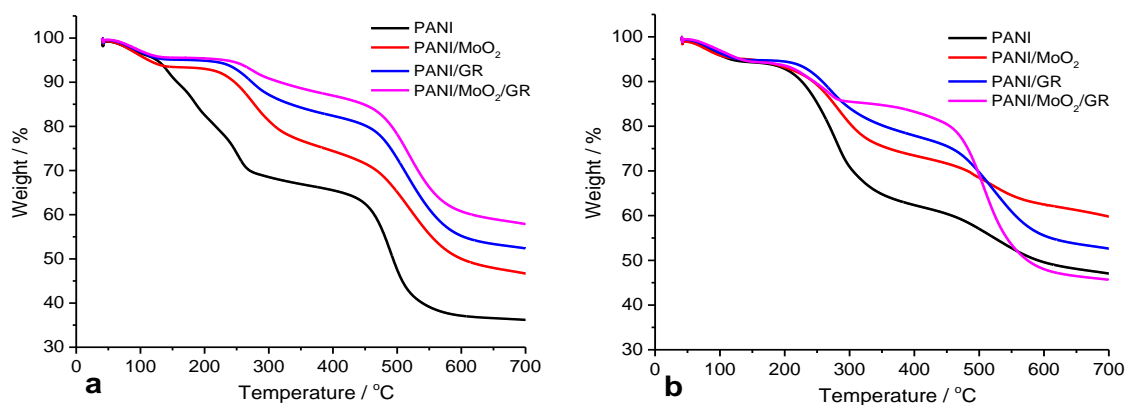


**Figure 6.16:** The TGA curves of a) PANI composite synthesised from an Oxaline electrolyte and b) PANI composite synthesised from a 1 M H<sub>2</sub>SO<sub>4</sub>/H<sub>2</sub>O electrolyte. The colours represent the type of polymer composite.

## 6.4.11 Morphology and topography of the polymer films

### 6.4.11.1 Scanning Electron Microbalance

Primarily, the surface morphology of graphite and MoO<sub>2</sub> particles was characterised by Scanning Electron Microscopy (SEM). It is well known that GR consists of multiple graphene layers, and these layers are connected with each other without any modification, forming a graphite sheet.<sup>41</sup> The size of particles were measured by this technique, and for graphite were found to be 2 - 12  $\mu\text{m}$ , whereas for MoO<sub>2</sub> particles sizes of less  $\mu\text{m}$  - 20  $\mu\text{m}$  were found, as shown in **Figure 6.17**.

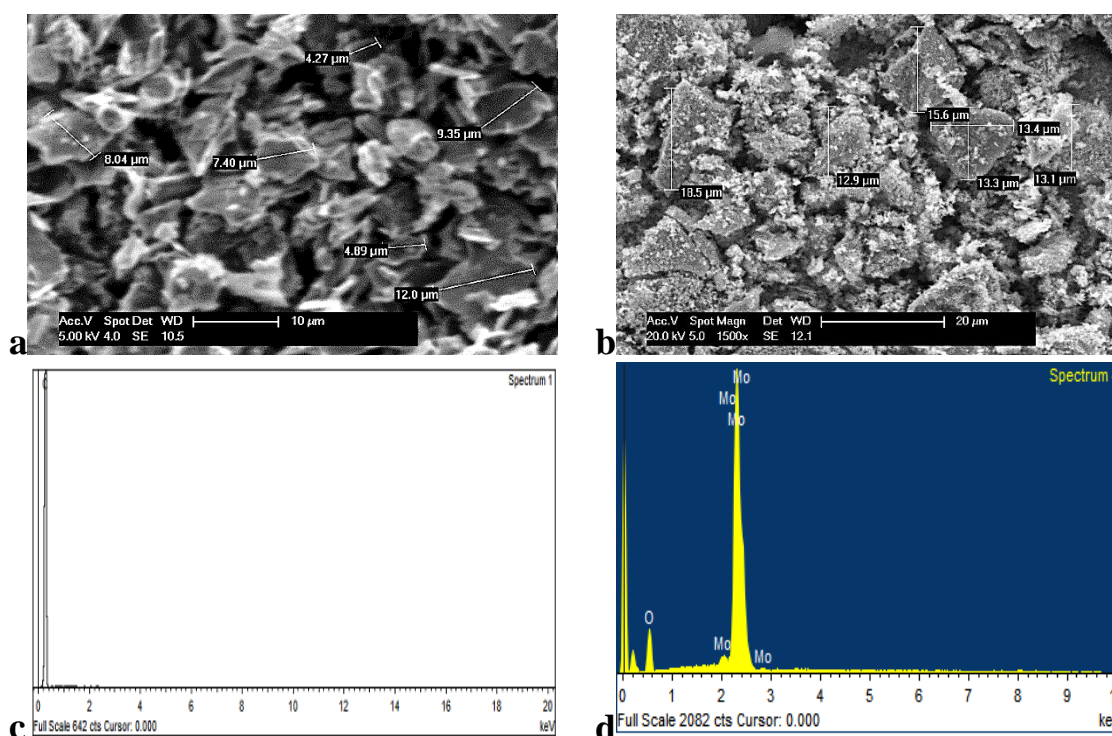


**Figure 6.17:** SEM images of a) graphite, b) MoO<sub>2</sub>, EDX spectrums of graphite of c) and d) MoO<sub>2</sub> are also show.

Based on the SEM images above, Energy Dispersive Analysis by X-ray (EDAX) of the PANI composite electrodes has been performed, whose data showed the presence of molybdenum (Mo) and oxygen (O) in the sample, as well as the PANI itself. These elements have been shown to be present in PANI/MoO<sub>2</sub> and PANI/MoO<sub>2</sub>/GR composites and mainly arise from the MoO<sub>2</sub> particles. The morphology of the resulting PANI, PANI/MoO<sub>2</sub>, PANI/GR, and PANI/MoO<sub>2</sub>/GR-coated electrodes were also analysed by SEM, as shown in **Figure 6.18**. For comparison, the SEM image, of a pure PANI-Oxaline sample panel (a) is homogeneously distributed like small grains and an agglomerated structure, whereas PANI-H<sub>2</sub>O, shown in panel (b), exhibits a uniform

fibrous morphology from hundreds of nanometres to a few micrometres in length, and hundreds of nanometres in width. The results are shown in panels c and d of **Figure 6.18**, representing PANI/MoO<sub>2</sub> electrodes prepared from Oxaline and aqueous solution, respectively. It seems that electropolymerisation of PANI with MoO<sub>2</sub> results in a more porous morphology in this composite than is observed for pure PANI. In addition, the PANI chains are perfectly anchored on the surface of MoO<sub>2</sub> particles, which are shown in **Figures 16.18c** and d.

For the PANI/GR-Oxaline and PANI/GR-H<sub>2</sub>O composites shown in panels e and f, respectively, of **Figure 6.18**, the SEM images show that graphite/graphene oxide layers interact uniformly with the PANI chains. As can be seen, small sized, circular grains of PANI/GR-Oxaline were formed, and chains uncoated (i.e. uncovered) the whole surface of graphite, while the nanofibers of PANI/GR-H<sub>2</sub>O are thinner compared to those of the pure PANI-H<sub>2</sub>O, as can be shown in panel (f) of **Figure 6.18**, and these nanofibres are surrounded and cover the entire surface of the GR sheets. This is due to the rapid growth of PANI in aqueous solution compared to that in DES because the background electrolyte is less viscous than Oxaline. Most significantly, it can be seen that PANI/GR-Oxaline has a more porous structure than PANI/GR-H<sub>2</sub>O, which makes the polymer more electrochemically stable during redox cycling, even when the electrolyte used has a high viscosity. This point is emphasised by results shown in sections 6.4.2 - 6.4.4. The SEM morphologies of the ternary composite samples of PANI/MoO<sub>2</sub>/GR have been found to vary not only with the factors mentioned above, but also due to the strong interactions between the GR sheets, MoO<sub>2</sub> and PANI chains, as shown in **Figures 6.18 g** and h. For example, for PANI/MoO<sub>2</sub>/GR samples grown from aqueous solution, the PANI nanofibres were of various lengths and widths, and were not homogenous structures as seen for PANI and PAN/GR samples. This may be attributed to the effect of MoO<sub>2</sub> on the growth of PANI chains in the present of GR. In other words, a large number of nucleation sites are proved to connect PANI networks with GR and MoO<sub>2</sub> as substrates as evidenced by some research groups, relative to ternary composite samples.<sup>39, 43, 75</sup> A summary of the main findings and of the principal issues and ideas that have arisen in the study of morphologies of PANI composite electrodes is that GR and MoO<sub>2</sub> particles can be easily incorporated into PANI chains and increase the porosity of the films. This enhances the stability of the polymer backbone, making its cycle life longer.

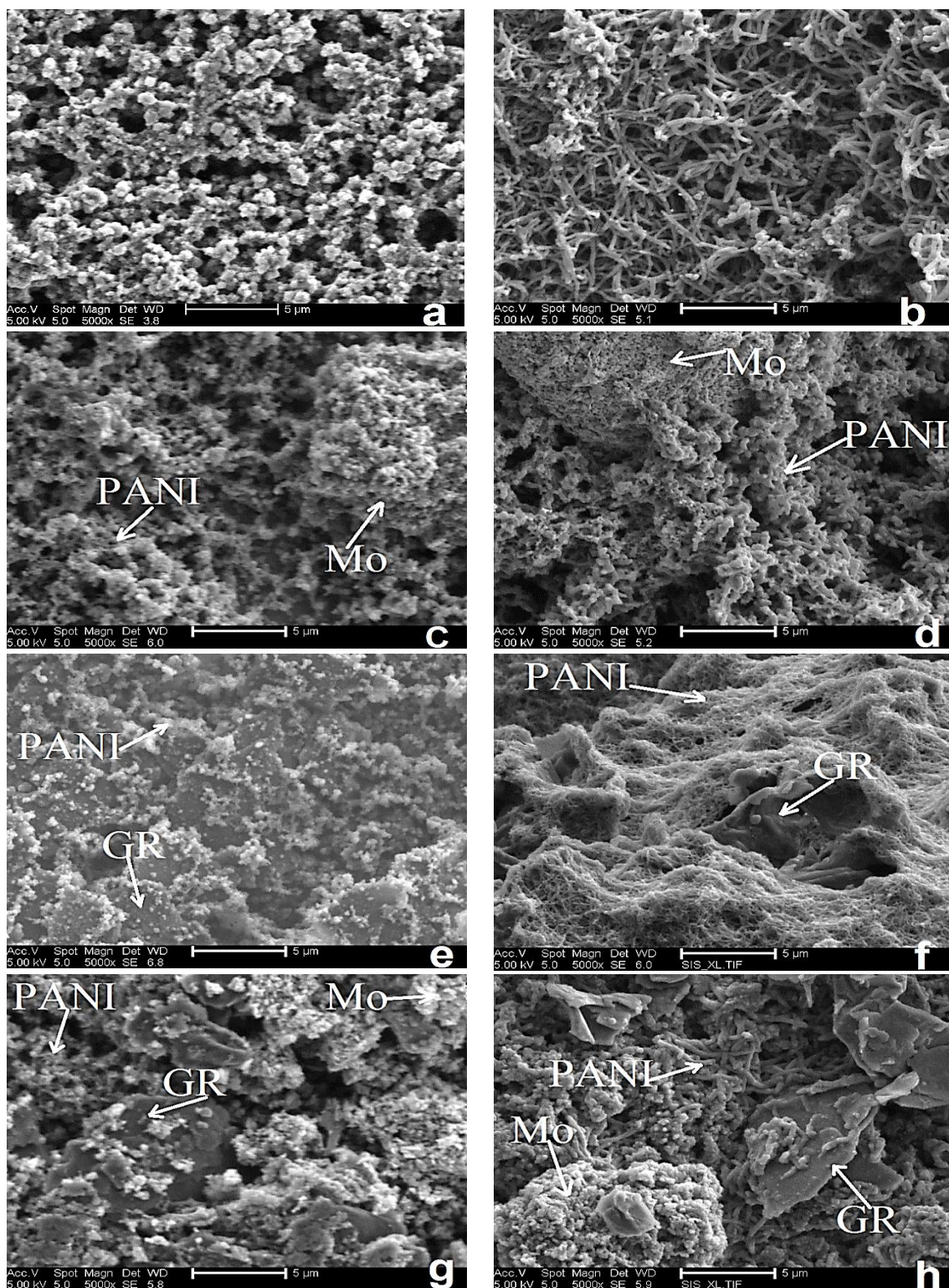


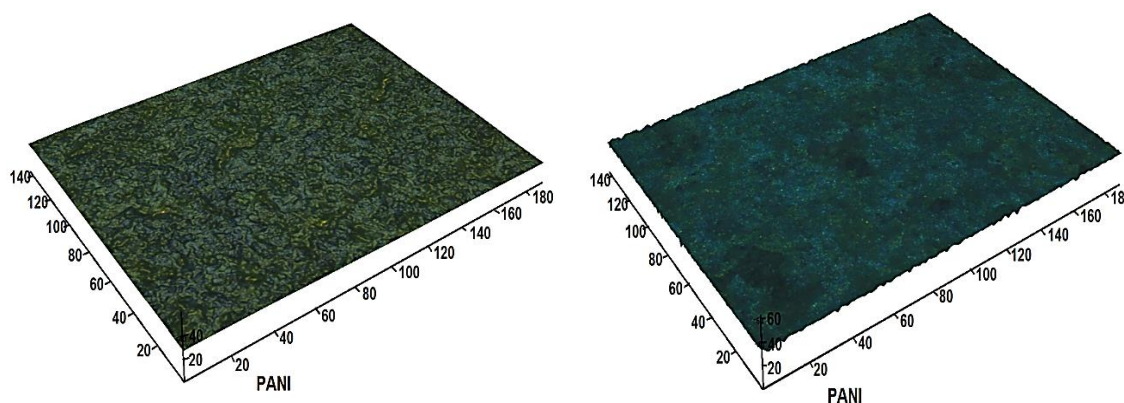
**Figure 6.18:** SEM images of PANI, PANI/MoO<sub>2</sub>, PANI/GR and PANI/MnO<sub>2</sub>/GR composite films before their cycled in electrolytes (monomer free). The left-hand images show samples prepared from an Oxaline electrolyte, while the right-hand images show samples prepared in an aqueous electrolyte.

### 6.4.11.2 3D-Zeta Optical spectroscopy

The surface morphology of the PANI composite electrodes was also characterised using a Zeta-20 Optical 3D microscope, as seen in **Figure 6.19**. It is difficult to measure an accurate thickness for the PANI composite by AFM due to the resolution of the machine being limited for film thicknesses greater than 4  $\mu\text{m}$  and, additionally, due to the distribution of GR and  $\text{MoO}_2$  particles on PANI not being on a uniform level. The thickness of the PANI formed on the Pt electrode has been estimated by using a 3D microscope and taking an average thickness determined over four points. The average surface roughness value, Ra, and thickness of the electrodes are reported in **Table 6.5**.

*Table 6.5: The average of thickness and roughness of PANI composite electrodes prepared from Oxaline and aqueous solutions.*

Samples	Polymers grown from DES		Polymers grown from 1 M $\text{H}_2\text{SO}_4/\text{H}_2\text{O}$	
	Average of Thickness / $\mu\text{m}$	Average of Roughness / $\mu\text{m}$	Average of Thickness / $\mu\text{m}$	Average of Roughness / $\mu\text{m}$
PANI	2	0.1059	3	0.30
PANI/ $\text{MoO}_2$	13	0.6000	15	0.9061
PANI/GR	9	0.6888	17	0.8082
PANI/ $\text{MoO}_2$ /GR	10	0.7449	18	1.032



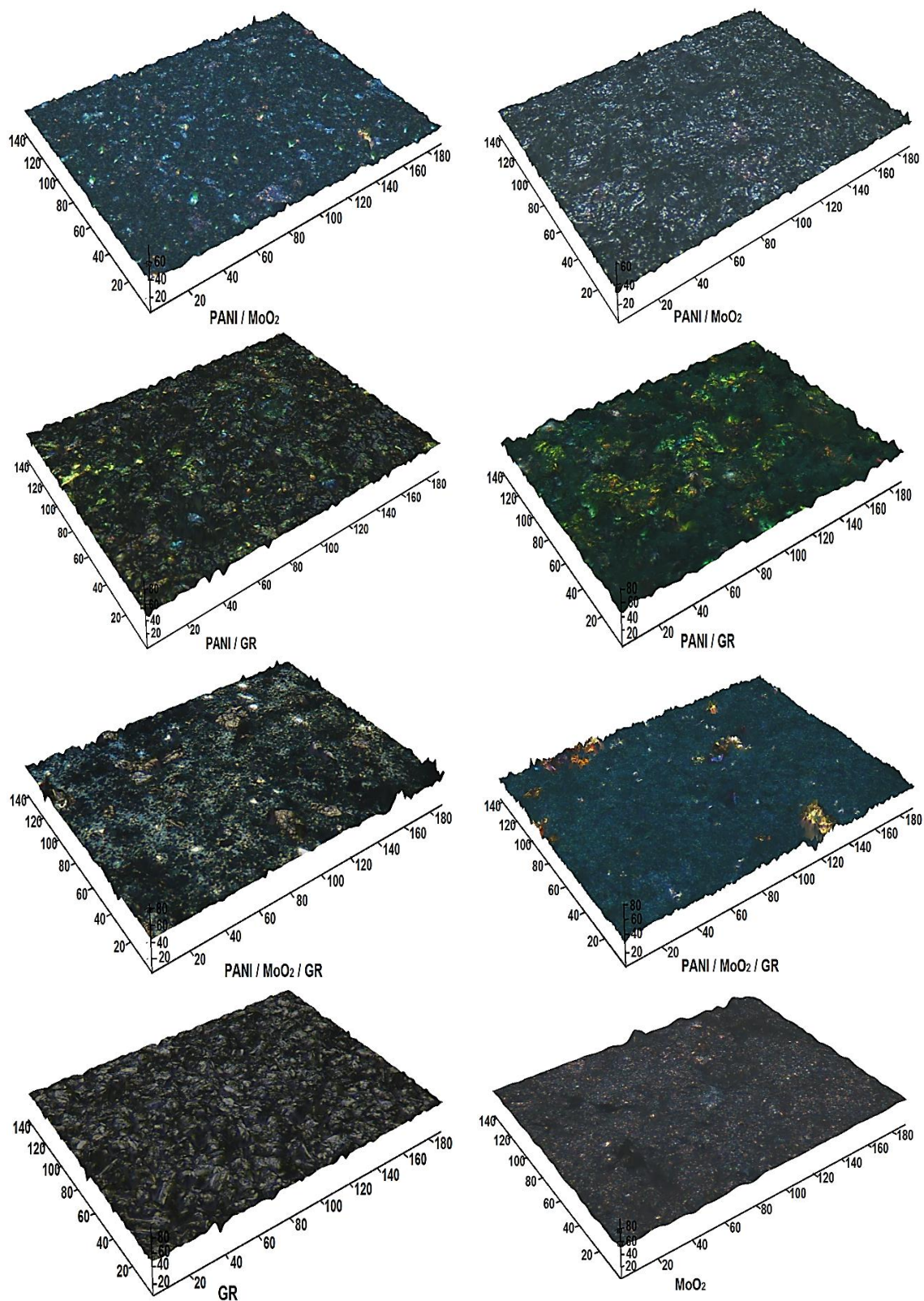


**Figure 6.19:** 3D optical microscopy images for PANI, PANI/MoO<sub>2</sub>, PANI/GR and PANI/MoO<sub>2</sub>/GR composite electrodes. The left-hand images show those grown from Oxaline and the right-hand images show those grown from aqueous solution, graphite and MoO<sub>2</sub>

#### **6.4.12 Conclusion**

Several electrically conducting composites based on the aniline monomer have been successfully fabricated through incorporation of PANI chains with graphite and molybdenum dioxide particles in both DES and aqueous electrolytes via an electrodeposition technique. This was proven by structural analysis and morphology studies conducted using FTIR spectroscopy and SEM techniques, respectively. The electrochemical stability of the electrode has been evaluated from changes that occurred in the CV shapes during long-term redox cycling. It was clear, after growth, that polymers cycled in different environmental systems showed variations and deviations in the associated CV peak shape during the doping/dedoping processes in the PANI films. This is presumably due to swelling and shrinking of polymers, which led to a degradation of the electrode surface.<sup>41</sup> However, the CV shapes of PANI/GR and PANI/MoO<sub>2</sub>/GR remained relatively unchanged and more stable compared to those of PANI and PANI/MoO<sub>2</sub> in both electrolytes (Ethaline and aqueous solutions).

For polymers grown in Oxaline, the highest retention values were found to be for PANI/MoO<sub>2</sub>/GR 87 % and PANI/GR 83 %, whereas the lowest retention was found for PANI/MoO<sub>2</sub> 42 % and PANI 13 % over 300 cycles. Conversely, in the case those polymers grown in aqueous solution, capacitance retention follows the order PANI/MoO<sub>2</sub>/GR > PANI/GR > PANI > PANI/MoO<sub>2</sub>, with associated values of 73 %, 70 %, 30 % and 9 %, respectively, relative to their initial specific capacitances over 300 cycles. It was found that PANI/GR and PANI/MoO<sub>2</sub>/GR electrodes in bracketed experiments were not influenced by chemical changes, and remained as electroactive when transferred between multiple electrolytes (e.g. DES, H<sub>2</sub>SO<sub>4</sub>/H<sub>2</sub>O and DES, respectively, or *vice versa*), but the pure PANI and the PANI/MoO<sub>2</sub> showed there was a loss in electroactivity of the polymers when they were transferred between multiple electrolytes due to changes in polymer structure, causing polymer degradation.

The noticeable deviation in the potential redox peaks and change in the CV shape were also obtained when the PANI and the PANI/MoO<sub>2</sub>/GR composite were cycled in Ethaline (monomer free) at different scan rates. This result showed that the capacitance of the polymer decreases with an increasing scan rate of the reaction. In addition, PANI/MoO<sub>2</sub>/GR has a better electrochemical reversibility and diffusion-controlled reaction compared to pure PANI film. With regard to the conductivity of the polymer

composite, this was found to be dramatically improved by addition of graphite particles and/or molybdenum oxide, which are attractive for electrochemically preferred power devices with a wide range of applications. SEM measurements showed that the PANI composite films grown in Oxaline were more compact and porous than the modified polymers produced from an acidic medium. Differences in heat resistance properties for PANI composite electrodes were observed by thermogravimetric measurements. PANI/GR and PANI/MoO<sub>2</sub>/GR degraded with a lower mass loss than observed for pure PANI and PANI/MoO<sub>2</sub>, indicating that thermal stability increased on incorporation of graphite particles.

In summary, it can be said that pure graphite or graphite mixed with MoO<sub>2</sub> particles played an important role in improving the properties of polyaniline when they are incorporated with it. Consequently, they have improved long-term charge/discharge stability, capacitance values, conductivity, porous morphology, mechanical properties, and good behaviour in impedance spectroscopy. These features were enhanced due to interactions between GR sheets and PANI chains, involving hydrogen bonds,  $\pi$ - $\pi$  coordination, and electrostatic interactions, as well as obtaining a fast electron transfer rate in the microstructure of the PANI/MoO<sub>2</sub>-modified electrode. Furthermore, this investigation not only supplies a new method for the synthesis of multifunctional PANI composite materials with graphite and/or metal oxides, but develops an attractive material with a wide range of potential applications in the areas of energy storage and power density.

## 6.5 References

1. V. Gupta and N. Miura, *Journal of Power Sources*, 2006, **157**, 616-620.
2. W. F. Mak, G. Wee, V. Aravindan, N. Gupta, S. G. Mhaisalkar and S. Madhavi, *Journal of the Electrochemical Society*, 2012, **159**, A1481-A1488.
3. X. Li, H. Song, Y. Zhang, H. Wang, K. Du, H. Li, Y. Yuan and J. Huang, *International Journal of Electrochemical Science*, 2012, **7**, 5163-5171.
4. V. Ruiz, C. Blanco, M. Granda and R. Santamaría, *Electrochimica Acta*, 2008, **54**, 305-310.
5. C. Portet, P. L. Taberna, P. Simon, E. Flahaut and C. Laberty-Robert, *Electrochimica Acta*, 2005, **50**, 4174-4181.
6. X. Hu, Z. Deng, J. Suo and Z. Pan, *Journal of Power Sources*, 2009, **187**, 635-639.
7. S. Yang, I.-J. Kim, M.-J. Jeon, K. Kim, S.-I. Moon, H.-S. Kim and K.-H. An, *Journal of Industrial and Engineering Chemistry*, 2008, **14**, 365-370.
8. Y. S. Lim, Y. P. Tan, H. N. Lim, N. M. Huang and W. T. Tan, *Journal of Polymer Research*, 2013, **20**, 1-10.
9. A. Inamdar, Y. S. Kim, J. S. Sohn, H. Im, H. Kim, D.-Y. Kim, R. S. Kalubarme and C. J. Park, *Journal of the Korean Physical Society*, 2011, **59**, 145-149.
10. A. K. Das, S. K. Karan and B. B. Khatua, *Electrochimica Acta*, 2015, **180**, 1-15.
11. K. Zhang, L. L. Zhang, X. S. Zhao and J. Wu, *Chemistry of Materials*, 2010, **22**, 1392-1401.
12. H. Wang, Q. Hao, X. Yang, L. Lu and X. Wang, *Electrochemistry Communications*, 2009, **11**, 1158-1161.
13. M. Oh, S.-J. Park, Y. Jung and S. Kim, *Synthetic Metals*, 2012, **162**, 695-701.
14. J. M. Ahn, A. I. Inamdar, Y. Jo, J. Kim, W. Jung, H. Im and H. Kim, *Journal of the Korean Physical Society*, 2014, **64**, 182-185.
15. E. Frackowiak, V. Khomenko, K. Jurewicz, K. Lota and F. Béguin, *Journal of Power Sources*, 2006, **153**, 413-418.
16. R. R. Salunkhe, J. Tang, N. Kobayashi, J. Kim, Y. Ide, S. Tominaka, J. H. Kim and Y. Yamauchi, *Chemical Science*, 2016, **7**, 5704-5713.
17. X. Zhang, H. Zhang, C. Li, K. Wang, X. Sun and Y. Ma, *Royal Society of Chemistry Advances*, 2014, **4**, 45862-45884.

18. J. Kim, J. Lee, J. You, M.-S. Park, M. S. Al Hossain, Y. Yamauchi and J. H. Kim, *Materials Horizons*, 2016, **3**, 517-535.
19. J. Foroughi, G. M. Spinks, S. R. Ghorbani, M. E. Kozlov, F. Safaei, G. Peleckis, G. G. Wallace and R. H. Baughman, *Nanoscale*, 2012, **4**, 940-945.
20. S. Saranya, R. K. Selvan and N. Priyadharsini, *Applied Surface Science*, 2012, **258**, 4881-4887.
21. H. An, Y. Wang, X. Wang, L. Zheng, X. Wang, L. Yi, L. Bai and X. Zhang, *Journal of Power Sources*, 2010, **195**, 6964-6969.
22. D. Ghosh, S. Giri, A. Mandal and C. K. Das, *Applied Surface Science*, 2013, **276**, 120-128.
23. Y. Jo, W.-J. Cho, A. I. Inamdar, B. C. Kim, J. Kim, H. Kim, H. Im, K.-H. Yu and D.-Y. Kim, *Journal of Applied Polymer Science*, 2014, **131**, 40306.
24. R. C. Alkire, D. M. Kolb, J. Lipkowski and P. N. Ross, *Chemically Modified Electrodes*, John Wiley & Sons, 2009.
25. R. L. McCreery, *Chemical Reviews*, 2008, **108**, 2646-2687.
26. R. Sengupta, M. Bhattacharya, S. Bandyopadhyay and A. K. Bhowmick, *Progress in Polymer Science*, 2011, **36**, 638-670.
27. M. Wissler, *Journal of Power Sources*, 2006, **156**, 142-150.
28. D. D. L. Chung, *Journal of Materials Science*, 2002, **37**, 1475-1489.
29. X.-L. Luo, J.-J. Xu, W. Zhao and H.-Y. Chen, *Analytica Chimica Acta*, 2004, **512**, 57-61.
30. S. A. Iranagh, L. Eskandarian and R. Mohammadi, *Synthetic Metals*, 2013, **172**, 49-53.
31. J. P. Zheng and T. R. Jow, *Journal of the Electrochemical Society*, 1995, **142**, L6-L8.
32. Y. U. Jeong and A. Manthiram, *Journal of the Electrochemical Society*, 2002, **149**, A1419-A1422.
33. J.-H. Kim, S. H. Kang, K. Zhu, J. Y. Kim, N. R. Neale and A. J. Frank, *Chemical Communications*, 2011, **47**, 5214-5216.
34. X. Xia, Q. Hao, W. Lei, W. Wang, H. Wang and X. Wang, *Journal of Materials Chemistry*, 2012, **22**, 8314.
35. P. Saini, *Fundamentals of Conjugated Polymer Blends, Copolymers and Composites: Synthesis, Properties, and Applications*, Wiley, 2015.
36. L.-J. Bian, H.-L. He and X.-X. Liu, *RSC Advances*, 2015, **5**, 75374-75379.

37. J. Liu, M. Zhou, L.-Z. Fan, P. Li and X. Qu, *Electrochimica Acta*, 2010, **55**, 5819-5822.
38. V. Gupta and N. Miura, *Electrochimica Acta*, 2006, **52**, 1721-1726.
39. J. Kim, H. Ju, A. I. Inamdar, Y. Jo, J. Han, H. Kim and H. Im, *Energy*, 2014, **70**, 473-477.
40. X. Li, *Electrochimica Acta*, 2009, **54**, 5634-5639.
41. Y. Yang, M. h. Diao, M. m. Gao, X. f. Sun, X. w. Liu, G. h. Zhang, Z. Qi and S. g. Wang, *Electrochimica Acta*, 2014, **132**, 496-503.
42. X. Lu, H. Dou, C. Yuan, S. Yang, L. Hao, F. Zhang, L. Shen, L. Zhang and X. Zhang, *Journal of Power Sources*, 2012, **197**, 319-324.
43. G. Wang, Q. Tang, H. Bao, X. Li and G. Wang, *Journal of Power Sources*, 2013, **241**, 231-238.
44. Q. Li, J. Liu, J. Zou, A. Chunder, Y. Chen and L. Zhai, *Journal of Power Sources*, 2011, **196**, 565-572.
45. P. Xiong, C. Hu, Y. Fan, W. Zhang, J. Zhu and X. Wang, *Journal of Power Sources*, 2014, **266**, 384-392.
46. S. B. Kulkarni, U. M. Patil, I. Shackery, J. S. Sohn, S. Lee, B. Park and S. Jun, *Journal of Materials Chemistry A*, 2014, **2**, 4989.
47. L.-J. Bian, J.-H. Zhang, J. Qi, X.-X. Liu, D. Dermot and K.-T. Lau, *Sensors and Actuators B: Chemical*, 2010, **147**, 73-77.
48. M. Bertotti and D. Pletcher, *Electroanalysis*, 1996, **8**, 1105-1111.
49. M. Jayalakshmi, M. M. Rao, N. Venugopal and K.-B. Kim, *Journal of Power Sources*, 2007, **166**, 578-583.
50. K. Wang, J. Huang and Z. Wei, *Journal Physical Chemistry C*, 2010, **114**, 8062-8067.
51. H. Su, T. Wang, S. Zhang, J. Song, C. Mao, H. Niu, B. Jin, J. Wu and Y. Tian, *Solid State Sciences*, 2012, **14**, 677-681.
52. T. Kuilla, S. Bhadra, D. Yao, N. H. Kim, S. Bose and J. H. Lee, *Progress in Polymer Science*, 2010, **35**, 1350-1375.
53. S. Sahoo, G. Karthikeyan, G. C. Nayak and C. K. Das, *Synthetic Metals*, 2011, **161**, 1713-1719.
54. Z. K. Abbas, Kingston University, 2009.
55. M. D. Stoller, S. Park, Y. Zhu, J. An and R. S. Ruoff, *Nano Letters*, 2008, **8**, 3498-3502.

56. M. D. Catedral, A. K. G. Tapia and R. V. Sarmago, *Science Diliman*, 2004, **16:2**, 41–46.
57. X. S. Du, M. Xiao and Y. Z. Meng, *European Polymer Journal*, 2004, **40**, 1489-1493.
58. Y. Liu, X. Zhou and Y. Guo, *Electrochimica Acta*, 2009, **54**, 3184-3190.
59. G. T.-K. Fey, C.-Z. Lu and T. P. Kumar, *Journal of Power Sources*, 2003, **115**, 332-345.
60. L. F. Jiao, H. T. Yuan, Y. C. Si, Y. J. Wang and Y. M. Wang, *Electrochemistry Communications*, 2006, **8**, 1041-1044.
61. Y. Shao, M. Engelhard and Y. Lin, *Electrochemistry Communications*, 2009, **11**, 2064-2067.
62. E. Casero, A. M. Parra-Alfambra, M. D. Petit-Domínguez, F. Pariente, E. Lorenzo and C. Alonso, *Electrochemistry Communications*, 2012, **20**, 63-66.
63. S. Wang, Q. Gao, Y. Zhang, J. Gao, X. Sun and Y. Tang, *Chemistry–A European Journal*, 2011, **17**, 1465-1472.
64. R. A. Friedel and G. L. Carlson, *The Journal of Physical Chemistry*, 1971, **75**, 1149-1151.
65. S. E. Bourdo and T. Viswanathan, *Carbon*, 2005, **43**, 2983-2988.
66. G. L. Chen, S. M. Shau, T. Y. Juang, R. H. Lee, C. P. Chen, S. Y. Suen and R. J. Jeng, *Langmuir*, 2011, **27**, 14563-14569.
67. D. K. Mahla, S. Bhandari, M. Rahaman and D. Khastgir, *Journal of Electrochemical Science and Engineering*, 2013, **3**, 157-166.
68. R. Bissessur, P. K. Y. Liu and S. F. Scully, *Synthetic Metals*, 2006, **156**, 1023-1027.
69. H. Mi, X. Zhang, S. An, X. Ye and S. Yang, *Electrochemistry Communications*, 2007, **9**, 2859-2862.
70. X. Feng, N. Chen, J. Zhou, Y. Li, Z. Huang, L. Zhang, Y. Ma, L. Wang and X. Yan, *New Journal of Chemistry*, 2015, **39**, 2261-2268.
71. T. L. A. Campos, D. F. Kersting and C. A. Ferreira, *Surface and Coatings Technology*, 1999, **122**, 3-5.
72. K. Pielichowski, *Solid State Ionics*, 1997, **104**, 123–132

73. P. Ghosh, S. K. Siddhanta, S. R. Haque and A. Chakrabarti, *Synthetic Metals*, 2001, **123**, 83-89.
74. Y.-N. Qi, F. Xu, H.-J. Ma, L.-X. Sun, J. Zhang and T. Jiang, *Journal of Thermal Analysis and Calorimetry* 2008, **91**, 219–223.
75. J. Yan, T. Wei, Z. Fan, W. Qian, M. Zhang, X. Shen and F. Wei, *Journal of Power Sources*, 2010, **195**, 3041-3045.

## **Chapter 7: Novel Battery Based on Zinc (anode electrode) and Polyaniline/Metal Oxide/Graphite Composite as a Cathode Electrode.**

### **Contents**

<b>7.1</b>	<b>Overview .....</b>	<b>223</b>
<b>7.2</b>	<b>Commercial Zinc Batteries .....</b>	<b>224</b>
<b>7.3</b>	<b>Zinc-Polymer Battery Concept.....</b>	<b>224</b>
<b>7.4</b>	<b>Objective .....</b>	<b>225</b>
<b>7.5</b>	<b>Results and discussion .....</b>	<b>226</b>
7.5.1	Effect of polymer composite .....	226
7.5.2	Effect of electrolyte composition .....	229
7.5.3	Effect of current density .....	230
7.5.4	Effect of electrolyte temperature .....	233
7.5.5	Specific energy and specific power .....	235
7.5.6	CR2025 Coin cell assembly .....	237
7.5.7	Conclusion.....	240
<b>7.6</b>	<b>References.....</b>	<b>242</b>

## 7.1 Overview

A considerable amount of the literature has been devoted to power generation sources to encourage the development of new materials and devices due to an increasing requirement for electrical energy storage, and high-power and recyclable batteries.<sup>1-4</sup> Recently, polyaniline, which is among the family of conducting polymers, has been utilised more widely in many important applications, in such areas as corrosion,<sup>5, 6</sup> supercapacitors,<sup>1</sup> electrodes and sensors,<sup>7</sup> separation and extraction,<sup>8</sup> and rechargeable batteries.<sup>9, 10</sup> In the previous chapter, considerable interest was shown to polyaniline incorporated with graphite and metal oxide particles as conducting organic materials in supercapacitance applications. In this chapter, our research will focus on the application of polyaniline in rechargeable batteries. In view of all studies, there are important factors that affect battery design such as safety, the efficiency of the charge and discharge process, and cost. Lithium-based battery technology is one well-known revolution in power sources, and is the most promising battery chemistry with polymer electrolytes.<sup>11</sup> It has provided a series of advantages regarding energy and power density, excellent cycle life, flexible design, and an Li anode can produce a high open-circuit voltage (OCV) of between 3.0 and 4.0 V in non-aqueous cells.<sup>12-14</sup>

Despite these favourable properties, Li electrodes also have a number of drawbacks in use because of their low charge and discharge efficiency, the possibility of metallic lithium plating and hence safety concerns, and the deleterious dendritic morphology of deposited Li. In addition, one must consider control over the temperature of cell to avoid temperature extremes.<sup>15, 16</sup> Several studies have reported attempts at employing polymer electrolytes with lithium metal (anode) that were not successfully developed due to interfacial stability problems. Further research has been undertaken to optimise Li electrodes, involving covering the Li with various surface protective films before/during cycling, some of which are transparent to Li ions. Hence, these films can protect the Li metal from contact with the electrolyte through an *in situ* reaction between Li and compounds such as HF<sup>17, 18</sup> AlCl<sub>3</sub> and SnI<sub>2</sub>.<sup>19, 20</sup> Due to the high cost of such fabrication processes, which are not suitable for commercial rechargeable Li batteries and the porous morphologies of Li surface, many of these *ex situ* films failed.

Zinc can be used as an alternative to lithium, despite the OCV of charged Zn/PANI in aqueous electrolyte being in the range 1.1 - 1.5 V, which gives a lower energy density

than the Li/PANI batteries in non-aqueous media.<sup>21, 22</sup> It has some advantages that play a vital role in improving its performance as an anode candidate due to its environmental acceptability, inexpensive cost and availability in large quantities, and it can be used with a water-based electrolyte.<sup>2, 23</sup> The following section will focus on the concept of zinc-polymer battery systems as regards the main aim of this project.

## **7.2 Commercial Zinc Batteries**

Recent developments in zinc-based batteries are attractive with regards to improving high energy storage in batteries. Ag-Zn battery is composed of an Ag<sub>2</sub>O cathode and a Zn anode. A high power density of 500 – 800 W kg<sup>-1</sup> and an energy density of 80 – 120 Wh kg<sup>-1</sup> were achieved with this battery with an OCV of 1.86 V. However, one of the limitations of this battery is that the technology is expensive because the use of Ag, hence its potential use is limited to use in specialist fields, for example, air and space travel, weapons technology and high-cost electronic goods.<sup>24-26</sup> Moreover, researchers have shown an increased interest in Zn-Air batteries due to high energy densities and very low manufacturing costs. They were first produced in the charged state as primary batteries with a highest energy density of 1086 Wh kg<sup>-1</sup> (including oxygen). Despite their high energy density, these batteries suffer from significant drawbacks such as the metal electrode and air catalyst. Another problem is that they produce hydrogen gas, which can react with zinc to cause a non-uniform zinc dissolution and deposition, and hence effect the lifetime of the battery itself; as a consequence, studies are continuing into the improvement of Zn-Air batteries.<sup>27</sup>

## **7.3 Zinc-Polymer Battery Concept**

Recently, most studies regarding rechargeable batteries have used polyaniline as the positive electrode (cathode) and zinc metal as the negative electrode (anode). The safety of zinc with a conducting polymer battery is dependent on the selection of a suitable electrolyte. One study has reported such a system using aqueous electrolytes, but the limitations found were the cut-off voltage and reduced stability, which are affected by hydrogen evolution and dendritic growth of metal during charge-discharge cycling.<sup>28, 29</sup> Therefore, the researchers increased the pH of the electrolytic solution in the battery using an electrolyte containing ZnCl<sub>2</sub> and NH<sub>4</sub>Cl at a pH of 4 or higher to prevent corrosion of the zinc because the zinc electrode can be easily corroded at lower pH.<sup>30-32</sup>

Due to PANI having a poor stability during the charge and discharge processes, which leads to degradation of the polymer by overoxidation,<sup>33</sup> the polymer is combined with other materials. Carbonaceous materials (e.g. activated carbon, carbon nanotubes, graphene) are attractive for this purpose because of their homogeneous interactions with conducting polymers (e.g. PANI).<sup>1</sup> Hence, high power density, long lifetime, good mechanical and electrochemical properties for polyaniline batteries can be obtained.

To the best of our knowledge, there have been no comparative studies on the use of graphite and MoO<sub>2</sub> as dopant particles in polyaniline deposited from DES (Oxaline) for applications involving batteries compared with the same polymer composition grown from acidic solution (sulphuric acid). DESs are mainly used to overcome the problems mentioned above. The benefits of this system within the battery are high current efficiency, low gassing and the elimination of zinc dendritic deposition owing to the absence of water. The objective of this research was to investigate the use of a DES as a non-toxic electrolyte for battery application. This is based on the use of polyaniline doped with graphite and MoO<sub>2</sub> as cathode and zinc metal as anode in aqueous/DES electrolytes. The graphite and MoO<sub>2</sub> particles were used to further enhance the connectivity of the polyaniline battery.

#### **7.4 Objective**

The concept of a Zn/PANI battery has been demonstrated in an electrolyte consisting of 0.3 M zinc-bis(trifluoromethyl-sulfonyl) imide Zn(TFSI)<sub>2</sub> dissolved in propylene carbonate in previous work;<sup>2</sup> here, we built this battery using a DES electrolyte instead of Zn(TFSI)<sub>2</sub>, which is less expensive. Therefore, the key objective of this study is to determine whether a Zn/PANI composite in a deep eutectic solvent can be shown to be a promising candidate in the application of energy and power density for battery technology. In addition, using DES for growth and/or as the battery electrolyte can overcome the limiting processes in molecular solvents (e.g. aqueous solution) mentioned above. Several parameters will be investigated regarding the behaviour of the Zn/PANI battery; for example, composition of PANI, dopants, electrolyte (aqueous/DES), current density and temperature of the electrolyte. Furthermore, fabrication of a Zn/PANI coin cell and a test of the electrochemical performance of such cells was undertaken to evaluate the performance of the battery system.

## 7.5 Results and discussion

### 7.5.1 Effect of polymer composite

Polyaniline composite electrodes grown from Oxaline (the growth of the polymer was followed using the same process reported in chapter 6 and growth charge shown in the **Table 7.1**) cycled in an Ethaline electrolyte (monomer free) had 0.35 M  $\text{NH}_4\text{Cl}$  and 0.15 M  $\text{ZnCl}_2$  added, and the potential window was swept between 1.0 and 2.3 V versus a Zn wire at a scan rate of  $5 \text{ mV s}^{-1}$ , as shown in **Figure 7.1a**. It is clear from the potential window that the reference potential is shifted compared to the previous case (i.e. in chapter 6) because we used Zn as the reference electrode rather than Ag wire.

**Figure 7.1b** shows the CV of PANI composite electrodes (deposited from 1 M sulphuric acid solution) cycled in a 0.5 M  $\text{NH}_4\text{Cl}$  and 0.2 M  $\text{ZnCl}_2$  aqueous solution (monomer free) in a potential range of 0.7 to 1.8 V versus Zn wire at a scan rate of  $5 \text{ mV s}^{-1}$ . The potential window of these polymers in aqueous solution using Zn wire as the reference electrode was also shifted by  $\sim 900 \text{ mV}$  toward the positive side compared to the potential window of these polymers in chapter 6 when using an Ag/AgCl electrode as the reference electrode. Nearly all curves show two pairs of well-defined redox reactions, associated with leucoemeraldine  $\leftrightarrow$  emeraldine and emeraldine  $\leftrightarrow$  pernigraniline, respectively, which occurred during the oxidation and reduction reactions.<sup>34</sup> Further, the polyaniline electrode with graphite and/or  $\text{MoO}_2$  particles has a considerably higher redox current than the pure PANI, due to a greater effective surface area from the structural composition of the polymer being accessible to the electrolytes. We discussed the reasons behind this in more detail in chapter 6.

**Table 7.1:** Growth charge for various polymer electrodes at scan rates of  $5 \text{ mV s}^{-1}$

Polymers grown from Oxaline	Scan no.	Growth Charge (C)	Polymers grown from aqueous soln.	Scan no.	Growth Charge (C)
PANI	15	0.034	PANI	5	0.124
PANI/ $\text{MoO}_2$	15	0.043	PANI/ $\text{MoO}_2$	5	0.119
PANI/GR	15	0.059	PANI/GR	5	0.265
PANI/ $\text{MoO}_2$ /GR	15	0.063	PANI/ $\text{MoO}_2$ /GR	5	0.343

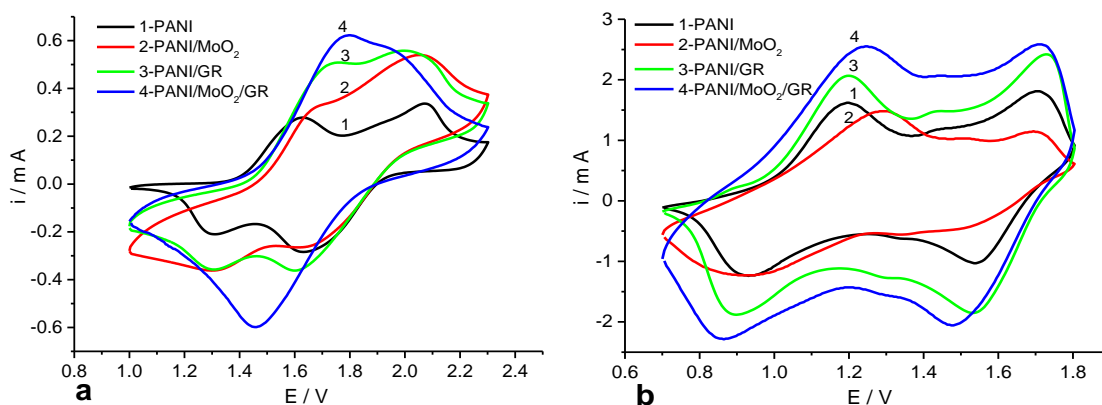


**Figure 7.1:** CV curves of the two types of PANI composite electrode grown in a) Oxaline and cycled in 0.35 M  $\text{NH}_4\text{Cl}$  + 0.15 M  $\text{ZnCl}_2$  Ethaline, and b) 1 M  $\text{H}_2\text{SO}_4/\text{H}_2\text{O}$  and cycled in 0.5 M  $\text{NH}_4\text{Cl}$  + 0.2 M  $\text{ZnCl}_2 \text{H}_2\text{O}$ , at scan rates of  $5 \text{ mV s}^{-1}$ . Numbers in the figure represent the PANI composite.

A test cell was constructed by assembling the cathode (PANI composite electrode on Pt) and anode (Zn metal) with electrolyte (aqueous solution/Ethaline) in a 25 ml beaker. **Figure 7.2** shows the charge and discharge behaviour of the PANI electrodes above in  $\text{NH}_4\text{Cl}$  and  $\text{ZnCl}_2$  (Ethaline/aqueous solutions) versus Zn at a current density of  $0.125 \text{ mA cm}^{-2}$  for the polymers used in **Figure 7.2a** and  $0.25 \text{ mA cm}^{-2}$  for the polymers used in **Figure 7.2b**. It can be seen that the charge/discharge characteristics of the cell are strongly affected by the structural composition of the polymer, which might be due to the limitation of anionic diffusion through the polymer morphology. For polymer electrodes deposited from Oxaline, the discharge and charge averages were 1.20 - 1.30 and 2.00 V, respectively, with an open circuit voltage of 1.83 V versus zinc, whereas, in the case of polymer electrodes deposited from aqueous solution, the discharge and charge averages were 0.74 and 1.65 V, respectively, with an open circuit potential of 1.60 - 1.61 V versus zinc.

From these data, it is observed that the decreasing voltage with time for PANI/MoO<sub>2</sub>, PANI/GR and PANI/MoO<sub>2</sub>/GR at the starting discharge is lower than for pure PANI. In other words, the lifetime for the pure PANI battery during the discharge process is shorter than for other polymers, which could be due to its lower energy density. Furthermore, this may be also because a lower internal resistance is obtained in the PANI battery that contained GR and/or MoO<sub>2</sub> particles compared to that of pure PANI due to the GR and/or MoO<sub>2</sub> particles increasing the porosity of the polyaniline electrode. As a result, there is an increase in the number of active sites on the surface of

the electrode, which results in the acceleration of the diffusion of the battery electrolyte into the cathodic electrodes. During charge and discharge processes for polymers grown from DES, the voltage–time behaviour of the proposed battery shows that the time periods for charge and discharge are not the same (not equal) compared to those polymers grown from aqueous solutions. This may indicate that the battery had a low charge–discharge efficiency, and thus less reversibility. Another reason could be the high viscosity of Ethaline at room temperature, which causes a reduction in the diffusion of ions into the cathode. The influence of temperature on the battery electrolyte will be discussed later, which gives the answer to the question: why are the charge and discharge times different for **Figure 7.2a**?

Generally, as the battery is charged, the voltage rises slowly and the reduced form of PANI composite is changed to its oxidized form. The cell voltage increases rapidly when PANI composite oxidation is completed and PANI is degraded to its electrochemical inactive form. There is a limit to the voltage change, and if it is exceeded, the corresponding overcharge leads to irreversible changes in the chemical composition of the polymer. Thus, charging is terminated when a cut-off voltage (COV) of 2.1V is reached (for example, **Figure 7.2a**). When the cell is discharged, the voltage decreases slowly until the PANI composite oxidized form is changed completely to its reduced form. Subsequently, the voltage decreases quickly. The discharge COV was between 1.40V and 1.30V (for example, **Figure 7.2a**).

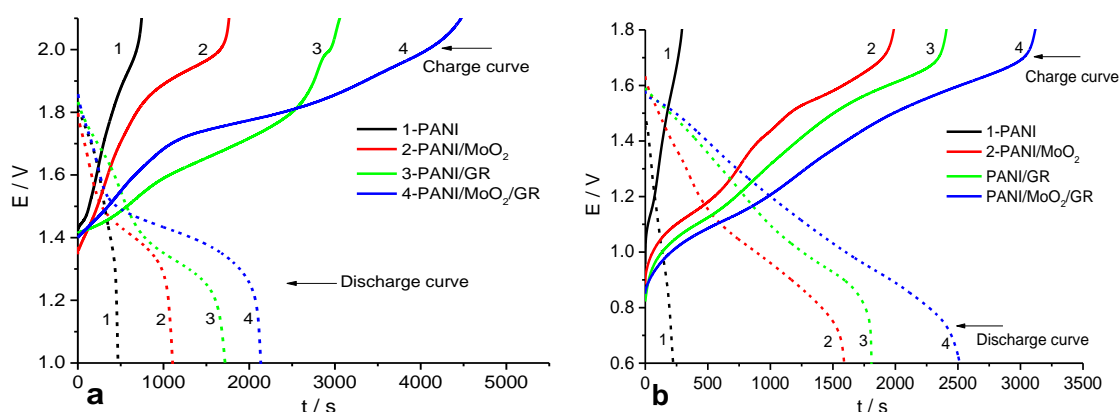


**Figure 7.2:** Charge and discharge curves of the PANI composite electrode in a) 0.35 M  $\text{NH}_4\text{Cl}$  + 0.15 M  $\text{ZnCl}_2$  in Ethaline electrolyte, at a current density of 0.125 mA  $\text{cm}^{-2}$ , and b) 0.5 M  $\text{NH}_4\text{Cl}$  + 0.2 M  $\text{ZnCl}_2$  in  $\text{H}_2\text{O}$  solution, at a current density of 0.25 mA  $\text{cm}^{-2}$ . The numbers in the figure represent the type of PANI composite. Note: the PANI composite electrode used in a) was grown from Oxaline and b) grown from aqueous solution.

### 7.5.2 Effect of electrolyte composition

As mentioned in previous studies, acid solutions (e.g. HCl) cannot be employed as the electrolyte in the polymer battery due to the key problem of corrosion of the zinc anode with these solutions,<sup>35</sup> so we avoided the use of such electrolytes in this study. Following the data in the previous section, the ternary polymer was selected for further investigation in different electrolytes using Ethaline/water as basic electrolytes containing ammonium salts and zinc salts (both have the same counter anion). **Figure 7.3** exhibits the charge/discharge curves of the PANI/MoO<sub>2</sub>/GR electrode in different electrolytes at current densities of 0.125 mA cm<sup>-2</sup> and 0.25 mA cm<sup>-2</sup> for polymer grown from Oxaline (**Figure 7.3a**) and from aqueous solution (**Figure 7.3b**), respectively. The curves showed that the charge/discharge data in all investigated electrolytes are different with regards to decreasing voltage with time. Hence, it is observed that charge/discharge characteristics are influenced by the size and the type of ions that are present in the electrolyte during the doping/dedoping reaction, as was observed in chapters 4 and 5. It can be concluded from **Figure 7.3** that the influence of an anionic electrolyte on the charge/discharge characteristic of the polymers is not, relatively, the same order (i.e. when the polymer is transferred in various electrolytes). For example, the charge and discharge rate of the electrode (**Figure 7.3a**, polymer grown from Oxaline) in Ethaline electrolytes follows the order ClO<sub>4</sub><sup>-</sup> > Cl<sup>-</sup> > NO<sub>3</sub><sup>-</sup> > SO<sub>4</sub><sup>2-</sup>, while electrodes (**Figure 7.3b** polymer grown from aqueous solution) in aqueous electrolytes follow this order ClO<sub>4</sub><sup>-</sup> > Cl<sup>-</sup> > SO<sub>4</sub><sup>2-</sup> > NO<sub>3</sub><sup>-</sup>.

The OCV for the PANI/MoO<sub>2</sub>/GR electrode (**Figure 7.3b**) is not similar in all characterised electrolytes, as it is in a voltage range between 1.20 - 1.51 V, indicating an unstable potential plateau. Thus, the range of discharge potential was between 0.74 and 0.87 V, while the range of charge potential occurred between 1.55 and 1.63 V. However, the OCV for the PANI/MoO<sub>2</sub>/GR electrode (**Figure 7.3a**) starts at 1.83 V in all characterised electrolytes, indicating that these polymers are at a more stable potential plateau. The discharge point occurs in the potential range between 1.20 and 1.30 V, while the charge point occurs at 2.00 V. From this observation, we concluded that the OCVs of all cells in DES systems are higher than in aqueous systems. Hence, selecting an electrolyte system can be of considerable significance to voltage range,

which in turn can affect charge and discharge rates due to the occurrence of variations in polymer morphology during the charge/discharge process.<sup>36</sup>

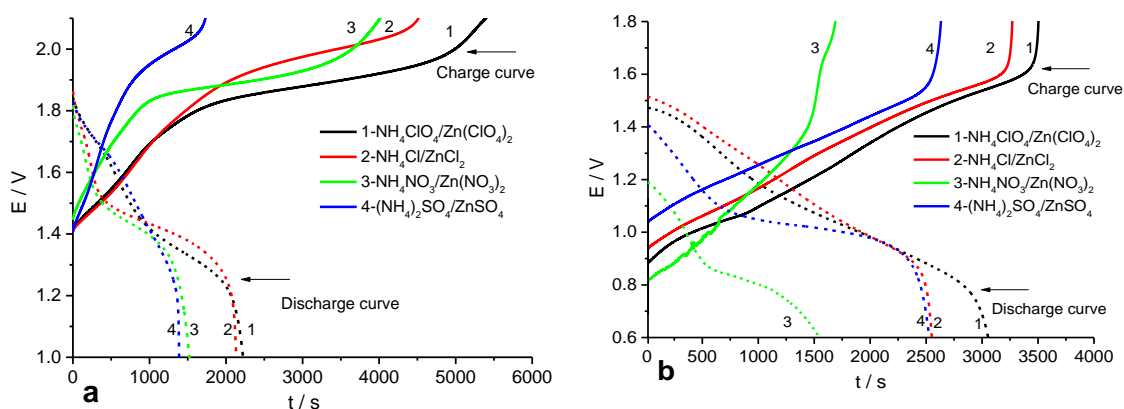


**Figure 7.3:** Charge and discharge curves of a PANI/MoO<sub>2</sub>/GR electrode grown in a) Oxaline and cycled in 0.35 M NH<sub>4</sub>X + 0.15 M ZnX<sub>2</sub> Ethaline electrolyte, at current density 0.125 mA cm<sup>-2</sup>, and b) 1 M H<sub>2</sub>SO<sub>4</sub>/H<sub>2</sub>O and cycled in 0.5 M NH<sub>4</sub>X + 0.2 M ZnX<sub>2</sub> in H<sub>2</sub>O solution, at current density 0.25 mA cm<sup>-2</sup>. Numbers in the figure represent the different electrolytes, where; X= 1) ClO<sub>4</sub><sup>-</sup>, 2) SO<sub>4</sub><sup>-2</sup>, 3) Cl<sup>-</sup> and 4) NO<sub>3</sub><sup>-</sup>.

### 7.5.3 Effect of current density

In this section, the influence of current density on the charge–discharge processes was studied, the results of which are shown in **Figure 7.4**. The electrolyte containing ammonium perchlorate and zinc perchlorate was selected for the PANI/MoO<sub>2</sub>/GR electrode from the comparative study of electrolytes in the previous section, which showed better performance of the cell with this electrolyte, and a high discharge capacitance for PANI/MoO<sub>2</sub>/GR active materials.

**Figure 7.4a** shows charge/discharge characteristics of the PANI/MoO<sub>2</sub>/GR electrode (grown from Oxaline) in 0.35 M NH<sub>4</sub>ClO<sub>4</sub> + 0.15 M Zn(ClO<sub>4</sub>)<sub>2</sub> in Ethaline at various current densities. As can be seen from **Figure 7.4a**, the charge and discharge times are increased when the current density is reduced. Similar to the findings shown in **Figure 7.4a**, the polymer electrode in **Figure 7.4b** (grown from aqueous) was also affected by applying various current densities during charge/discharge of the polymer electrode in 0.5 M NH<sub>4</sub>ClO<sub>4</sub> + 0.2 M Zn(ClO<sub>4</sub>)<sub>2</sub> aqueous solution. This may be due to two reasons; the first could be a high current density causing an increase in charge transfer resistance and diffusion over-potential. As a result, the capacity density of the PANI electrode will

be decreased at higher current densities due to electrode polarization.<sup>37</sup> The second reason may be the reduction of anion movement through polymer chains.<sup>35, 38</sup>

The rate (the C-rate is a rating for total discharge in 1 hour) of charge/discharge cells at different current densities are shown in **Tables 7.2** and **7.3**. The capacity of battery in mA h g<sup>-1</sup> with respect to the weight of polyaniline can be calculated from equation 7.1.<sup>28, 39</sup>

$$C = \frac{it}{w} \quad 7.1$$

where  $C$  is the capacity (mA h g<sup>-1</sup>),  $i$  the current (mA),  $t$  the time (h), and  $w$  the polyaniline weight (g).

**Table 7.2:** Charge/Discharge rate profiles of Zn/(PANI/MoO<sub>2</sub>/GR) cell (grown from Oxaline) cycled in 0.35 M NH<sub>4</sub>ClO<sub>4</sub> + 0.15 M Zn(ClO<sub>4</sub>)<sub>2</sub> Ethaline electrolyte at 25 ± 2°C under different current density ratings. The mass of polymer was 1.4 × 10<sup>-4</sup> g and the electrode area was 0.55 cm<sup>2</sup>

Current density (mA cm <sup>-2</sup> )	time (h)		C-rate (mC cm <sup>-2</sup> )		Capacity (mA h g <sup>-1</sup> )	
	Charge	Discharge	Charge	Discharge	Charge	Discharge
0.0625	2.01	1.02	0.13	0.06	494	250
0.125	1.32	0.65	0.17	0.08	648	319
0.25	0.65	0.32	0.16	0.08	638	314
0.35	0.47	0.19	0.16	0.07	646	261
0.50	0.21	0.08	0.11	0.04	413	157

**Table 7.3:** Charge/Discharge rate profiles for Zn/(PANI/MoO<sub>2</sub>/GR) cell (grown from aqueous solution) cycled in 0.5 M NH<sub>4</sub>ClO<sub>4</sub> + 0.2 M Zn(ClO<sub>4</sub>)<sub>2</sub> in H<sub>2</sub>O electrolyte at 25 ± 2°C under different current density ratings. Weight of polymer 6.8 × 10<sup>-4</sup> g and the electrode area was 0.55 cm<sup>2</sup>.

Current density (mA cm <sup>-2</sup> )	time (h)		C-rate (mC cm <sup>-2</sup> )		Capacity (mA h g <sup>-1</sup> )	
	Charge	Discharge	Charge	Discharge	Charge	Discharge
0.20	1.30	1.21	0.26	0.24	210	196
0.25	1.02	0.93	0.26	0.23	206	188
0.50	0.57	0.51	0.28	0.25	231	206
0.75	0.34	0.29	0.26	0.22	206	176
1.00	0.25	0.21	0.25	0.21	202	170

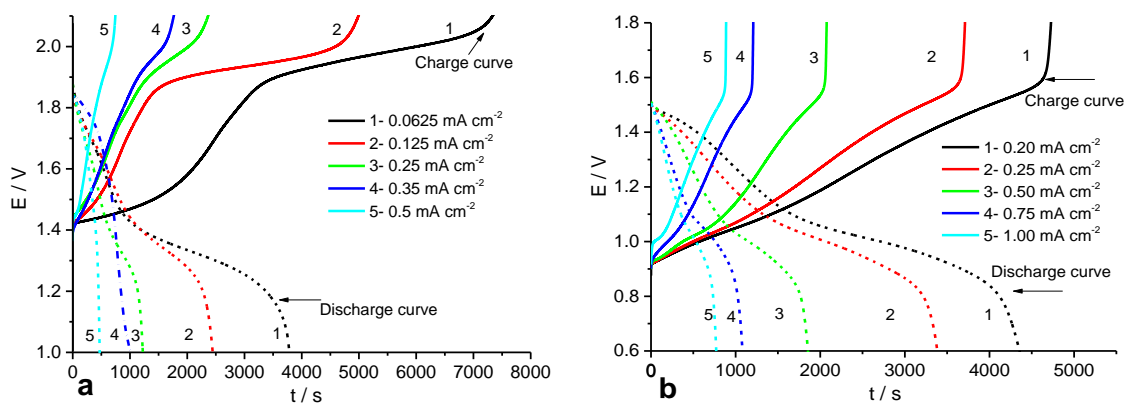


**Figure 7.4:** Charge and discharge curves of a PANI/MoO<sub>2</sub>/GR electrode grown in a) Oxaline and cycled in 0.35 M NH<sub>4</sub>ClO<sub>4</sub> + 0.15 M Zn(ClO<sub>4</sub>)<sub>2</sub> Ethaline electrolyte. b) 1 M H<sub>2</sub>SO<sub>4</sub>/H<sub>2</sub>O and cycled in 0.5 M NH<sub>4</sub>ClO<sub>4</sub> + 0.2 M Zn(ClO<sub>4</sub>)<sub>2</sub> in H<sub>2</sub>O electrolyte at various current density. Numbers in the figure represent the current density.

From **Figure 7.4**, the coulombic efficiency of charge/discharge was investigated, which is strongly based on the current density. The coulombic efficiency of the battery was calculated from equation 7.2:<sup>28</sup>

$$\text{Coulombic efficiency} = \frac{t_2}{t_1} \times 100 \quad 7.2$$

where  $t_1$  and  $t_2$  are the times taken to charge and discharge at constant current density, respectively. The results obtained from **Figure 7.5** show that the coulombic efficiency of both electrodes is decreased with increasing current density. In the case of the PANI/MoO<sub>2</sub>/GR electrode (grown from Oxaline), the coulombic efficiency was calculated as 51 % at a current density of 0.0625 mA cm<sup>-2</sup>, becoming 41 % at a current density of 0.5000 mA cm<sup>-2</sup>. With reference to the decline in coulombic efficiency with increasing current density, similar results were observed for the PANI/MoO<sub>2</sub>/GR electrode grown from aqueous solution. At a current density of 0.2000 mA cm<sup>-2</sup>, the coulombic efficiency was 93 %, which decreases to 84 % at a current density of 1.0000 mA cm<sup>-2</sup>. These data indicate that at low current densities, the battery can be worked for longer time with regards to the charge/discharge process due to the PANI electrode having sufficient time to oxidise and reduce, and the mass transport process being slower than charge transfer. As a consequence, the coulombic efficiency is boosted by a drop in current density. The results presented in this section (i.e. that charge/discharge is strongly dependent on the applied current density) are in agreement with the previous literature.<sup>31, 40</sup>

From this observation, it was found that the coulombic efficiency of the battery containing polymer 2 (i.e. polymer grown from aqueous solution) is greater than that of the battery containing polymer 1 (i.e. polymer grown from Oxaline), as shown in **Figure 7.5**. Indeed, this could be attributed to the hysteresis phenomena of structural changes in the polymer PANI/MoO<sub>2</sub>/GR (polymer1) caused by dopants and solvent during the oxidation and reduction process. Otherwise, the movement of the species and/or solvent (Ethaline) into/out of the polymer is very slow, which is expected due to the high viscosity of the solution. Therefore, it is essentially to perform this experiment at high temperature to reduce the viscosity of solvent and see whether this effect is related to the viscosity of solvent or the structural changes in the polymer. The following section will explain this experiment in detail.

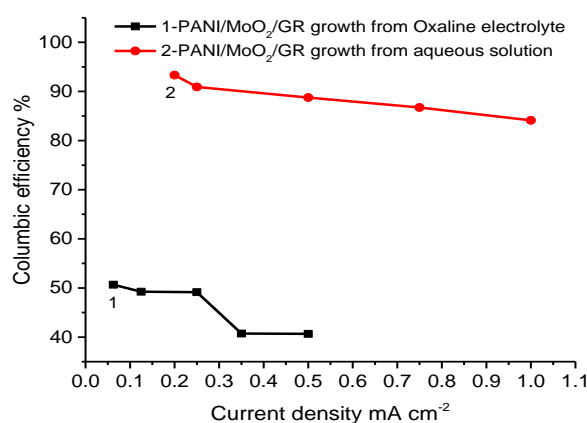


**Figure 7.5:** The influence of current density on the coulombic efficiency of the battery

#### 7.5.4 Effect of electrolyte temperature

The influence of electrolyte temperature on the current density during the charge–discharge processes was studied for the same film as in the previous section (polymer 1, grown from DES) in order to optimise the coulombic efficiency of the charge–discharge reaction. **Figure 7.6a** shows the charge/discharge profiles of the PANI/MoO<sub>2</sub>/GR electrode (grown from Oxaline) at various current densities from 0.0625 to 0.5000 mA cm<sup>-2</sup> in 0.35 M NH<sub>4</sub>ClO<sub>4</sub> + 0.15 M Zn (ClO<sub>4</sub>)<sub>2</sub>/Ethaline electrolyte at 50°C. As shown in **Figure 7.6a**, the time of discharge capacity for the PANI/MoO<sub>2</sub>/GR electrode in this work at 50°C is higher than that reported in the previous section at room temperature. For example, at 50°C, the time of discharge ( $t_2$ ) at a current density of 0.0625 mA cm<sup>-2</sup> was 4975 s, whereas for same film at 25°C, the time of discharge ( $t_2$ ) was 3671 s (**Figure 7.4a**). This is attributed to an increase in ion diffusion and charge transfer in the

electrolyte due to the decreasing viscosity of the solution at higher temperature. It is noticeable that the electrode charge-discharge curve is quite symmetric between the charge and discharge plateaus at high temperature in Ethaline compared to the same polymer electrode at room temperature (polymer 1 in **Figure 7.4a**), which shows a long charging period for the polymer when we applied low current density, and a short time for discharge. This implies that the reversibility of the charge-discharge process for the polymer in DES at high temperature (50°C) is better than that at room temperature, due to the decrease in the viscosity of electrolyte as the temperature was raised.

The coulombic efficiency of the electrode in an electrolyte at 50°C decreases gradually with increasing current densities, as shown in **Figure 7.6b**. At a current density of 0.0625 mA cm<sup>-2</sup>, the coulombic efficiency for the battery used at 50°C was 97 %, whereas at room temperature it was 51 %. This study found that the charge and discharge times for the polymer in DES used at high temperature has less hysteresis than at low temperature. This might be because of when charging the polymer (oxidising), the polymer chains take a long time to open, and to thus allow ingress of anions and solvent, and thus to swell. This is due to the fact that when discharging the polymer, it becomes more dense and compact as solvent (or possibly other ionic species) is lost during the discharge process. Therefore, when we try to charge the polymer again, through ingress of the solvent and other species it takes a long time to open and to thus also allow ingress of anions and solvent, and thus to swell. This is related to the kinetic phenomena of the polymer, which are dependent on of the rate of incorporation the species through polymeric chains. Therefore, the rate of species uptake was affected by the high viscosity of the electrolyte at lower temperature, as reported in chapters 4 and 5 when we studied the mass change of pure PANI during the redox process at high temperature and room temperature using EQCM. This tells us further information about the mass hysteresis during the redox process. Charge/discharge rates and capacities of the cell based on Zn/(PANI/MoO<sub>2</sub>/GR) (grown from Oxaline) cycled in electrolyte at 50°C under different current densities are shown in **Table 7.4**.

**Table 7.4:** Charge/Discharge rate profiles of Zn/(PANI/MoO<sub>2</sub>/GR) (grown from Oxaline) cell cycled in 0.35 M NH<sub>4</sub>ClO<sub>4</sub> + 0.15 M Zn(ClO<sub>4</sub>)<sub>2</sub> Ethaline electrolyte at 50°C under different current density rating. The mass of polymer was 1.4×10<sup>-4</sup> g and the electrode area was 0.55 cm<sup>2</sup>.

Current density (mA cm <sup>-2</sup> )	time (h)		C-rate (mC cm <sup>-2</sup> )		Capacity (mA h g <sup>-1</sup> )	
	Charge	Discharge	Charge	Discharge	Charge	Discharge
0.0625	1.42	1.40	0.09	0.09	349	344
0.125	1.02	0.92	0.13	0.12	501	452
0.25	0.48	0.42	0.12	0.11	471	413
0.35	0.31	0.27	0.11	0.09	426	371
0.50	0.17	0.14	0.09	0.07	334	275

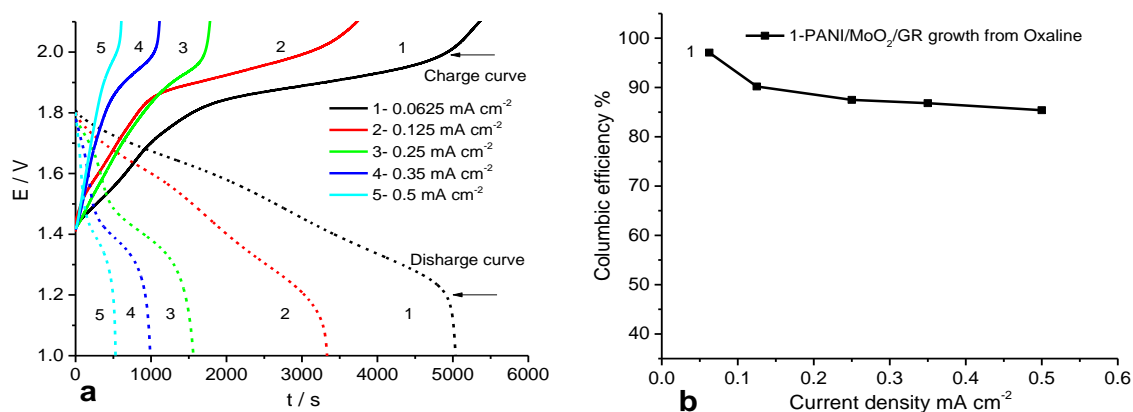


**Figure 7.6:** panel a) Charge and discharge curve of a PANI/MoO<sub>2</sub>/GR-electrode grown from Oxaline and cycled in 0.35 M NH<sub>4</sub>ClO<sub>4</sub> + 0.15 M Zn (ClO<sub>4</sub>)<sub>2</sub>/Ethaline electrolyte at 50°C, at different current densities. Panel b) influence of current density on the columbic efficiency of the battery with electrolyte at 50°C. Numbers in the figure represent the current density.

### 7.5.5 Specific energy and specific power

Specific energy and specific power are important factors in characterising the performance of energy storage devices. They can be calculated from galvanostatic discharge curves using equations 7.3 and 7.4:<sup>41, 42</sup>

$$E = \frac{1}{2} \times C_s V^2 \quad 7.3$$

$$P = \frac{E}{t} \quad 7.4$$

where  $E$  is the specific energy ( $Wh\ kg^{-1}$ ),  $C_s$  is the specific capacitance ( $F\ g^{-1}$ ) obtained from the discharge value of the last cycle for polymer growth using CV,  $V$  is the difference between the potential at the beginning and at the end of the discharge (cut-off potential) during the galvanostatic discharge process,  $t$  is the discharge time, and  $P$  is the specific power ( $W\ kg^{-1}$ ).

All specific power and specific energy of the PANI/MoO<sub>2</sub>/GR composite grown from (i) Oxaline ( $C_s = 575\ Fg^{-1}$ ) and cycled in Ethaline salt (at 50°C) and (ii) H<sub>2</sub>O ( $C_s = 662.67\ F\ g^{-1}$ ) and cycled in water salt at various currents, are shown in **Figure 7.7a** and **b**, respectively. The polymer-Oxaline, at the highest current density ( $0.5\ mA\ cm^{-2}$ ) showed a specific energy of  $87\ Wh\ kg^{-1}$  at a specific power of  $608\ W\ kg$ , whereas at the lowest current density ( $0.0625\ mA\ cm^{-2}$ ) it showed a specific energy of  $104\ Wh\ kg^{-1}$  at a specific power of  $75\ W\ kg$ . Similar to this, the high current response for the polymer grown from aqueous solution was also affected in terms of specific energy and specific power, where the specific energy at the highest current density ( $1\ mA\ cm^{-2}$ ) of  $135\ Wh\ kg^{-1}$  was obtained at a specific power of  $638\ W\ kg$ . It can be concluded that when current density is increased we observe a decrease in the specific energy and an increase in the specific power due to a decrease in the discharge/charge time as function of voltage.

**Figure 7.7d** shows the Ragone plot of our data compared to the standard Ragone plot of different energy storage devices, which is shown in **Figure 7.7c**. This type of battery could be nominally identified as a hybrid between a battery and a fuel cell. The high specific energy and specific power values are attributed to the synergistic effect of the combination of the PANI, MoO<sub>2</sub> and GR particles, which lead to an increase in porosity of the morphology of the film. As a result, the nanostructure of both PANI/GR and/or MoO<sub>2</sub> facilitates the diffusion of ions through the polymer net, and hence gives a higher capacitance. In addition, the optimised configuration can extend the operating potential window, thus enabling charge and discharge from various oxidation states.

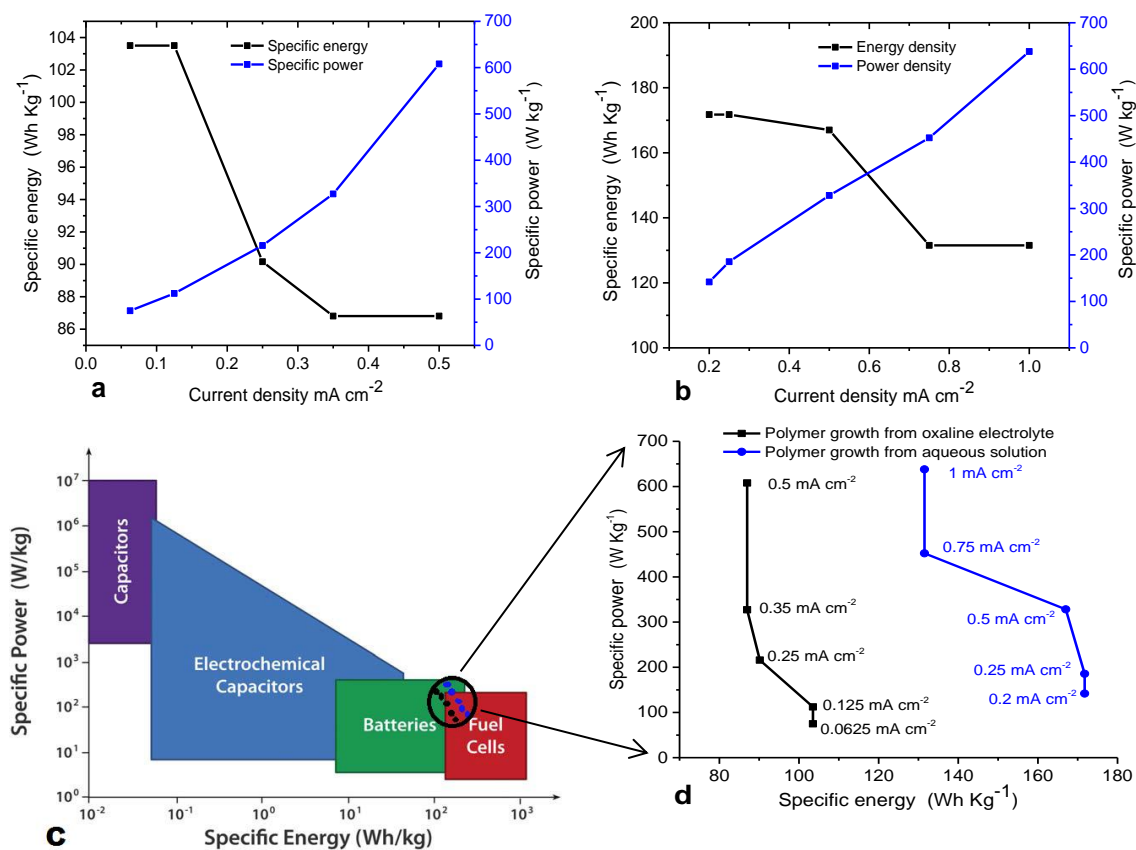


**Figure 7.7:** Variation of specific energy and specific power of a) polymer grown from Oxaline, b) polymer grown from aqueous solution at different discharge current densities, c) Ragone plot of different energy storage devices<sup>43</sup>, and d) PANI/MoO<sub>2</sub>/GR from both electrolytes compared with a Ragone plot.

### 7.5.6 CR2025 Coin cell assembly

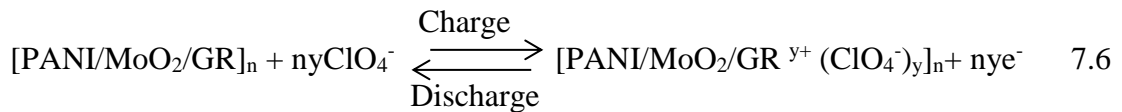
In order to demonstrate the applicability of the above data to devices, composite polymer batteries were prepared from two systems (DES and aqueous solution) as follows. The batteries were composed of (i) PANI/MoO<sub>2</sub>/GR composite deposited from Oxaline on a Pt substrate ( $A = 2.0096 \text{ cm}^2$ ) used as the cathode, Zn metal as the anode, and 0.35 M NH<sub>4</sub>ClO<sub>4</sub> + 0.15 M Zn(ClO<sub>4</sub>)<sub>2</sub> in Ethaline as the battery electrolyte, and (ii) PANI/MoO<sub>2</sub>/GR composite deposited from 1 M H<sub>2</sub>SO<sub>4</sub>/H<sub>2</sub>O on a Pt substrate used as the cathode, Zn metal as the anode, and 0.5 M NH<sub>4</sub>ClO<sub>4</sub> + 0.2 M Zn(ClO<sub>4</sub>)<sub>2</sub> in aqueous solution as the battery electrolyte. After growing the polymer using the CV method, the polymer was fabricated as a polymer battery employing a coin-type (CR2025) cell configuration, and the voltage of the battery was tested using a DT830b Digital Multimeter and an LED. **Figure 7.8** shows a) the materials used for the cell, b) the construction of the CR2025 coin cell, c) the hand-operated closing tool and d) the coin

cell voltage measurement, respectively. The mechanism of cell operation was as follows: during the charging process,  $Zn^{2+}$  cations are deposited on a zinc plate from the electrolytic solution and the PANI composite cathode is oxidised with  $ClO_4^-$  incorporated in the opposite cell. On the other hand, when the battery is discharged, metallic zinc is dissolved into the electrolytic solution and the PANI composite is reduced with the release  $ClO_4^-$ .<sup>2</sup> Therefore, the electrochemical system of the battery will be based on the following half-cell reactions:

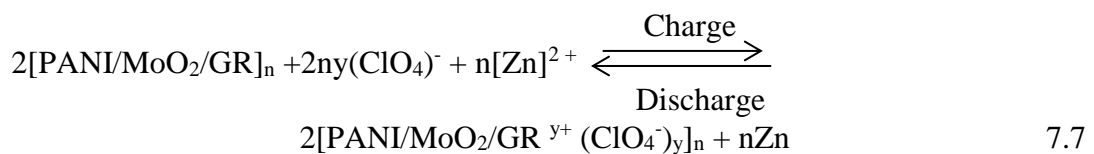
Negative electrode reaction:



Positive electrode reaction:



where  $y$  is doping degree, and the overall reaction of the battery during the charge and discharge of the cell will be as follows:



Due to the reversible reaction in the battery, the overall discharge reaction is the reverse of equation 7.7.

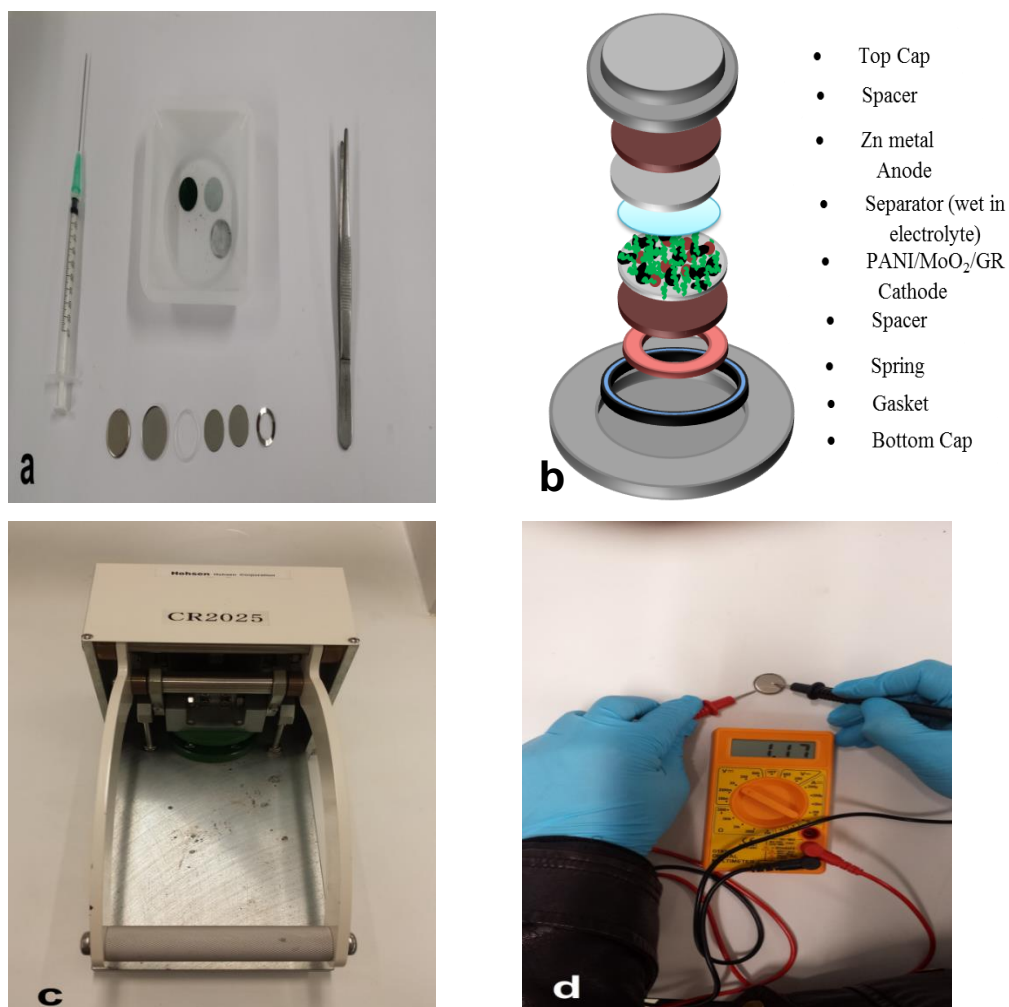


**Figure 7.8:** a) Materials used for battery, b) Construction of CR2025 coin cell, c) Hand-operated closing tool and d) Coin battery voltage measurement.

**Table 7.5:** The voltage measurements of all Zn/PANI coins battery during one week.

Polymer samples	Self-voltage discharge per unit time			
	First Voltage (V)	Voltage after 1 day	Voltage after 2 days	Voltage after 7 days
PANI-Oxaline	0.44	0.20	0.01	-
PANI-H <sub>2</sub> O	0.54	0.18	0.005	-
PANI/MoO <sub>2</sub> /GR-Oxaline	1.17	1.1	0.99	0.92
PANI/MoO <sub>2</sub> /GR-H <sub>2</sub> O	1.22	1.17	1.03	1.0

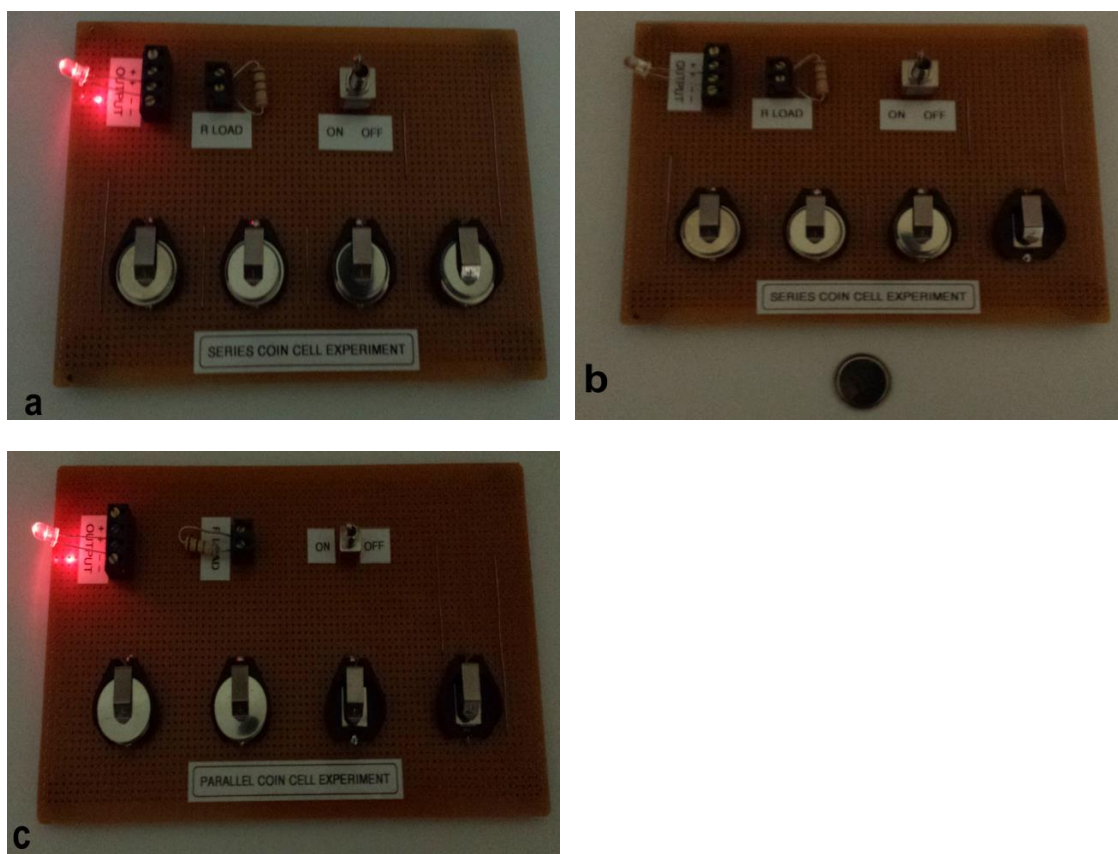


**Figure 7.9:** Images showing PANI/MoO<sub>2</sub>/GR-electrodes with Zn used as coin batteries to power the red LED bulb in series a) and b), and c) in parallel.

### 7.5.7 Conclusion

The main goal of of this work was to investigate whether a PANI composite could be successfully employed as a cathode, with Zn metal as an anode, in wet batteries. The experimental results showed that the capacitance and efficiency of the battery are improved by addition of GR and/or MoO<sub>2</sub> particles to polyaniline, as compared to pure PANI batteries. In addition, using perchlorate or chlorate anions as the dopant in the battery electrolyte increased the open-circuit voltage and the efficiency of battery, and is better than using either SO<sub>4</sub><sup>2-</sup> or NO<sub>3</sub><sup>-</sup> anions.

For PANI/MoO<sub>2</sub>/GR grown from and cycled in DES, the problem of coulombic efficiency was quite pronounced at room temperature, though at higher temperature was found to improve. We overcame this problem by changing the temperature of the battery electrolyte to 50°C. At 50°C and a current density of 0.0625 mA cm<sup>-2</sup>, the battery had an output and input capacity of 344 and 349 mA h g<sup>-1</sup>, respectively, with a coulombic efficiency of 97 %. The average discharge and charge potential were 1.20 and

2.00 V, respectively, with an OCV of 1.83 V versus zinc, whereas for the same sample and the same current density at room temperature, the battery had an output and input capacity of 250 and 494 mA h g<sup>-1</sup>, respectively, with a columbic efficiency of 51 %. Therefore, the effects of current densities on the charge and discharge times at high temperature show a lower mass hysteresis in comparison with at room temperature.

These observations suggest that for the Zn-Polymer battery device, it is preferable not to use water solvents or any organic solvent containing water for safety reasons, and to avoid the use of zinc from the point of view of avoiding corrosion and/or dendrite formation on the anode of the battery. Therefore, whilst DESs (especially Ethaline) are a more appropriate electrolyte for the battery device rather than those used in conventional systems, they were limited by the high viscosity of the electrolytes at room temperature. It would, then, clearly be advantageous for battery electrolyte applications to be able to operate efficiently at room temperature and, therefore, it would be interesting to trial ionic liquids electrolytes of lower viscosities and with higher ion mobilities, such as Ethaline 400 (type III). More research is needed with DESs to enhance the capacitance and cycle life of the Zn/PANI battery by improving the composition of the cathode material, battery electrolyte and battery configuration. As a result, it is possible that PANI and DES could be employed as an electrode material and electrolyte in practical rechargeable batteries.

## 7.6 References

1. M. R. Arcila-Velez, R. K. Emmett, M. Karakaya, R. Podila, K. P. Díaz-Orellana, A. M. Rao and M. E. Roberts, *Synthetic Metals*, 2016, **215**, 35-40.
2. A. Guerfi, J. Trottier, I. Boyano, I. De Meazza, J. A. Blazquez, S. Brewer, K. S. Ryder, A. Vijn and K. Zaghbi, *Journal of Power Sources*, 2014, **248**, 1099-1104.
3. M. H. Chakrabarti, F. S. Mjalli, I. M. AlNashef, M. A. Hashim, M. A. Hussain, L. Bahadori and C. T. J. Low, *Renewable and Sustainable Energy Reviews*, 2014, **30**, 254-270.
4. A. Ritchie and W. Howard, *Journal of Power Sources*, 2006, **162**, 809-812.
5. A. Mirmohseni and A. Oladegaragoze, *Synthetic Metals*, 2000, **114**, 105-108.
6. D. E. Tallman, G. Spinks, A. Dominis and G. G. Wallace, *Journal of Solid State Electrochemistry*, 2002, **6**, 73-84.
7. S. H. Hosseini and A. A. Entezami, *Polymers for Advanced Technologies*, 2001, **12**, 524-534.
8. H. Bagheri, M. Saraji, M. Chitsazan, S. R. Mousavi and M. Naderi, *Journal of Chromatography A*, 2000, **888**, 197-208.
9. M. S. Rahmanifara, M. F. Mousavia and M. Shamsipur, *Journal of Power Sources*, 2002, **110** 229–232.
10. C. Y. Wang, V. Mottaghitlab, C. O. Too, G. M. Spinks and G. G. Wallace, *Journal of Power Sources*, 2007, **163**, 1105-1109.
11. M. Z. A. Munshi and B. B. Owens, *Solid State Ionics*, 1988, **26** 41-46.
12. A. Taguchi and T. Tanaka, *Journal of Power Sources*, 1987, **20**, 249-252.
13. F. Goto, K. Abe, K. Ikabayashi, T. Yoshida and H. Morimoto, *Journal of Power Sources*, 1987, **20**, 243-248.
14. Y.-G. Lee, K. S. Ryu and S. H. Chang, *Journal of Power Sources*, 2003, **119-121**, 321-325.
15. S. Tobishima, M. Arakawa, H. Hirai and J. Yamaki, *Journal of Power Sources*, 1989, **26**, 449 - 454.
16. R. Rauh and S. Brummer, *Electrochimica Acta*, 1977, **22**, 75-83.
17. Z. i. Takehara, *Journal of Power Sources*, 1997 **68** 82-86.
18. K. Kanamura, S. Shiraishi and Z. i. Takehara, *Journal of the Electrochemical Society*, 1996, **143**, 2187-2197.

19. Y. Fung and H. Lai, *Journal of Applied Electrochemistry*, 1992, **22**, 255-261.
20. J. Besenhard, J. Yang and M. Winter, *Journal of Power Sources*, 1997, **68**, 87-90.
21. A. Mirmohseni and R. Solhjo, *European Polymer Journal*, 2003, **39** 219–223.
22. F. Trinidad, M. Montemayor and E. Fatas, *Journal of the Electrochemical Society*, 1991, **138**, 3186-3189.
23. B. Z. Jugović, T. L. Trišović, J. Stevanović, M. Maksimović and B. N. Grgur, *Journal of Power Sources*, 2006, **160**, 1447-1450.
24. P. Suresh, D. H. Nagaraju, A. K. Shukla and N. Munichandraiah, *Electrochimica Acta*, 2005, **50**, 3262-3272.
25. J. Huang and Z. Yang, *RSC Advances*, 2015, **5**, 33814-33817.
26. C. H. Hamann, A. Hamnett and W. Vielstich, *Electrochemistry*, Wiley, 2007.
27. Y. Li and H. Dai, *Chemical Society Reviews*, 2014, **43**, 5257-5275.
28. H. Karami, M. F. Mousavi and M. Shamsipur, *Journal of Power Sources*, 2003, **124**, 303-308.
29. R. Sivakumar and R. Saraswathi, *Journal of Power Sources*, 2002, **104**, 226-233.
30. W. Baochen, L. Gi, L. Changzhi and W. Fosong, *Journal of Power Sources*, 1988, **24**, 115 - 120.
31. H. Karami, M. F. Mousavi and M. Shamsipur, *Journal of Power Sources*, 2003, **117**, 255-259.
32. S. Li, G. Zhang, G. Jing and J. Kan, *Synthetic Metals*, 2008, **158**, 242-245.
33. P. R. Deshmukh, S. V. Patil, R. N. Bulakhe, S. N. Pusawale, J.-J. Shim and C. D. Lokhande, *RSC Advances*, 2015, **5**, 68939-68946.
34. E. M. Genies and C. Tsintavis, *Journal of Electroanalytical Chemistry*, 1985, **195**, 109-128.
35. B. N. Grgur, M. M. Gvozdrenović, J. Stevanović, B. Z. Jugović and V. M. Marinović, *Electrochimica Acta*, 2008, **53**, 4627-4632.
36. J. P. Ferraris, M. M. Eissa, I. D. Brotherston and D. C. Loveday, *Chemistry of Materials*, 1998, **10**, 3528-3535.
37. Y. Zhao, S. Si and C. Liao, *Journal of Power Sources*, 2013, **241**, 449-453.
38. B. C. Dalui, I. N. Basumallick and S. Ghosh, *Indian Journal of Chemical Technology*, 2008, **15**, 576-580.

39. H. Karami, M. F. Mousavi, M. Shamsipur and S. Riahi, *Journal of Power Sources*, 2006, **154**, 298-307.
40. M. Shaolin, Y. Jinhai and W. Yuhua, *Journal of Power Sources*, 1993, **45**, 153-159.
41. G. M. Zhou, D. W. Wang, F. Li, L. L. Zhang, Z. Weng and H. M. Cheng, *New Carbon Materials*, 2011, **26**, 180-186.
42. S. Sahoo, G. Karthikeyan, G. C. Nayak and C. K. Das, *Synthetic Metals*, 2011, **161**, 1713-1719.
43. N. Armaroli and V. Balzani, *Energy & Environmental Science*, 2011, **4**, 3193-3222.

## **Chapter 8: General Conclusions and Future Work**

### **Contents**

<b>8.1</b>	<b>General Conclusions .....</b>	<b>246</b>
<b>8.2</b>	<b>Future work.....</b>	<b>249</b>
<b>8.3</b>	<b>References.....</b>	<b>250</b>

## 8.1 General Conclusions

The mechanism of mass transport and charge transfer across the film/solution interface in conducting polymers is an important factor in any electrochemical energy storage system. These mechanisms are affected by many factors such as growth conditions, polymer composition, polymer thickness, the size and type of species present in the background electrolyte (i.e. the electrolytes used for electro-polymerisation or as monomer-free electrolytes during the redox process), morphologies of polymers, pH of the solution, the viscosity of electrolyte, and the electrolyte temperature.<sup>1-3</sup> Therefore, the growth mechanism of PANI-modified electrodes and their characterisation in various electrolytes (aqueous solutions and DESs) were extensively studied in this thesis. PANI electrodes grown from aqueous solutions result from an autocatalytic mechanism, whereas in DESs this is not the case. Therefore, it can be said that the mass increase in the polymer in DESs is related to the evolution of redox reactions with an increasing number of scans. The current peak of PANI films during deposition from aqueous solutions was much higher than PANI films grown from DESs due to the high viscosity of the latter, which affected the diffusion of species. The more compact and dense polyaniline (PANI) films were achieved in DESs, while the films produced from aqueous media exhibited open structures with higher porosity. PANI films grown from Oxaline and sulphuric acid were identified as the best model polymer for further studies using EQCM depending on the amount of the charge passed; rough surface topography (greater porosity), as well as the initial observations of the polymer film stability, looked very promising in terms of charge storage applications.

During the p-doping process, PANI films showed good electroactivity in DESs inducing to the conversion of leucoemeraldine salt to emeraldine salt and *vice versa* during undoping. The dynamics of the PANI reaction in DESs were affected by the type of HBD forming the electrolyte. Generally, the mass change of PANI electrodes (deposited from aqueous/DES) throughout all redox reactions was an anion-dominated reaction during the redox switching in an aqueous acidic medium (monomer free). However, the mass/charge behaviour of PANI electrodes (deposited from aqueous/DES) in DESs (ethaline and propaline) at 50°C was most associated with cation ( $\text{Ch}^+$ ) egress (i.e. mass decrease) during the oxidation reaction and anion ( $\text{EG}_2\text{Cl}^-$  /  $\text{PG}_2\text{Cl}^-$ ) ingress (i.e. mass increase) during the reduction reaction. The mass/charges

resulting from films in other DES at 50°C (Oxaline, Glyceline and Reline) during redox processes showed significantly lower mass changes and more fluctuation than in Ethaline and Propaline. As a result, PANI films have excellent mass change stabilities in Ethaline and Propaline. This is due to the lower viscosity and higher ionic character of these electrolytes, which effectively increase the stability of PANI. The viscosity and conductivity of DESs (type III), which are arguably the most important physical properties affecting electrolyte diffusion, were measured by rotational viscometry over a wide range of temperatures (25°C to 80°C). Ethaline was of lower viscosity and higher conductivity compared to other DESs. It has been found that the conductivities of these electrolytes at 50°C follow the order Ethaline > Oxaline > Propeline > Glyceline > Reline, while their viscosities follow the order Ethaline < Propeline < Oxaline < Glyceline < Reline, as reported in section 5.3.1. PANI films prepared from aqueous solution/Oxaline and cycled in DESs at 50°C, took only a short period to reach equilibrium from cation transfer dominated to anion transfer dominated compared to cycling in DESs at room temperature.

One of the major issues with PANI films is the poor electrochemical stability of the film during the charge and discharge process.<sup>4, 5</sup> Therefore, improvement in the charge storage capabilities of the polymer has become one of the most important issues as regards batteries and supercapacitor applications. Electrochemists are continuously trying to improve the capacitance and stability of charge transfer and mass transport in energy storage devices using various metal oxides and carbonaceous materials having large surface areas, resulting in an increase in power.<sup>6</sup> One suggestion is an increase in the porosity of polymer-modified electrodes by incorporating them with nanoscale electrodes.<sup>7</sup> As a consequence, a great species flux can ingress/egress into the bulk of the polymer-modified films, resulting in an increase in capacitance and electrochemical stability, which makes them suitable as energy and power sources for supercapacitor and battery applications.

Our studies were focussed on the growth of PANI electrodes (from 1 M H<sub>2</sub>SO<sub>4</sub>/H<sub>2</sub>O and Oxaline) with graphite and molybdenum dioxide as follows: PANI/MoO<sub>2</sub>, PANI/GR, PANI/MoO<sub>2</sub>/GR, with the results compared to pure PANI film. The results showed that the rate of polymerisation and capacitance increased with the addition of MoO<sub>2</sub>, GR particles, and both MoO<sub>2</sub> and GR, with the highest capacitance observed for

the PANI/MoO<sub>2</sub>/GR sample, as compared to the other samples. After growth, each modified electrode was transferred to various electrolytes; for example, PANI-modified electrodes grown from Oxaline were transferred into Ethaline, 0.5 M H<sub>2</sub>SO<sub>4</sub>, and Ethaline, respectively, for 100 cycles in each electrolyte, using a scan rate was 5 mV s<sup>-1</sup> in all processes. In these electrolytes, the highest capacitance retention values were found in the PANI/MoO<sub>2</sub>/GR 87 % and PANI/GR 83 %, while the lowest retention was found for PANI/MoO<sub>2</sub> 42 % and PANI 13 % over 300 cycles. The modified polymers were grown from aqueous solution and transferred to 0.5 M H<sub>2</sub>SO<sub>4</sub>, Ethaline, and 0.5 M H<sub>2</sub>SO<sub>4</sub>, respectively, for 100 cycles in each electrolyte, at a scan rate of 5 mV s<sup>-1</sup> in all processes. Their capacitance retention followed the order PANI/MoO<sub>2</sub>/GR > PANI/GR > PANI > PANI/MoO<sub>2</sub>, with associated values of 73 %, 70 %, 30 % and 9 %, respectively, relative to the initial specific capacitances. The capacitance of PANI-modified electrodes decreased with increasing scan rate, because ion transport from/to the film is faster than electron transfer with increasing the scan rate. This leads to insufficient time for species movement during the redox process, and hence the capacitance of the film decreases during the redox process at high scan rates ( $v > 5 \text{ mV s}^{-1}$ ).

Adding graphite and MoO<sub>2</sub> particles to PANI, improved properties such as the conductivity of the polymer, the porosity of the morphology, mechanical properties, and impedance behaviour. This study found that PANI/GR and PANI/MoO<sub>2</sub>/GR electrodes were not affected by chemical changes, and maintained their electroactivity when transferred between multiple electrolytes (e.g. DES, H<sub>2</sub>SO<sub>4</sub>/H<sub>2</sub>O and DES, respectively, or *vice versa*). However, pure PANI and PANI/MoO<sub>2</sub> showed there was a loss in electroactivity of the polymers when transferred between multiple electrolytes due to changes in polymer structure, which resulted in polymer degradation.

The PANI-modified electrodes (grown from aqueous and Oxaline electrolytes) were also investigated with regards to battery applications. In this study, PANI composites in aqueous/DES were used as a cathode and Zn used as an anode in wet rechargeable batteries. PANI/MoO<sub>2</sub>/GR-modified films were selected for further battery studies due to their more porous surface electrodes having higher electroactive areas. The results showed that the rate-limiting process does not only depend on the growth conditions of the films and the viscosity of the battery electrolyte, but also on other factors such as

the type and size of the species present in the solution, current densities, and the potential window used during charge and discharge processes, which led to various cycling responses that affected the performance of the resulting films. Ethaline is a good electrolyte for the battery device rather than those used in conventional systems for Zn-PANI battery, but it was limited by the high viscosity of the electrolytes at room temperature. Finally, coin cell assembly has been tested and the results were quite satisfied, but there are some limitations due to the fact that the subject for the first time studied. It can be concluded that in the energy storage devices, desirable features such as porous membranes, electrolytes having lower viscosities and metal anodes that do not corrode and/or suffer from dendrite formation in the battery are needed.

## **8.2 Future work**

Recently, PANI nanostructures have been of considerable interest in enhancing performance over a wide range of applications mentioned in this thesis. This research has showed that the energy capacitance behaviour and ion dynamics of PANI can yield significant improvements in DESs compared to aqueous solution, in some cases affecting rate-limiting processes such as the high viscosity of electrolytes and the composition of the polymer. This was seen when PANI films grown in DESs (type III) that were transferred to DESs at room temperature took a much longer time to reach equilibrium compared to high temperature DESs. Therefore, it is recommended that further research be undertaken in the following areas:

Growth of pure PANI films or PANI nanostructures (involving metal oxides and carbonaceous material) in ionic liquids (other types of DESs) have low viscosity values then transferred to low ionic viscosity electrolytes in order to characterise ion exchange dynamics and stability during redox cycling, as well as examination for energy storage devices. In addition, synthesis of other conducting polymers (i.e. polypyrrol, polythiophene), copolymer or copolymer nanostructures in DESs media and cycled in similar deposition solutions to study the mass change and charge transfer from/into film/solution during the redox reaction. The same strategy as presented in this thesis could be used with copolymer films. Novel cells for preparation of copolymer nanostructures could be designed, which could be used in battery applications with and without the presence of an electrolyte. Variations in the cell battery configurations may be considered.

### 8.3 References

1. J. Manuel, M. Kim, D. Fapyane, I. S. Chang, H.-J. Ahn and J.-H. Ahn, *Materials Research Bulletin*, 2014, **58**, 213-217.
2. G. Ćirić-Marjanović, *Synthetic Metals*, 2013, **177**, 1-47.
3. G. Inzelt, *Conducting Polymers: A New Era in Electrochemistry*, Springer-Verlag Berlin Heidelberg, 2008.
4. E. Frackowiak, V. Khomenko, K. Jurewicz, K. Lota and F. Béguin, *Journal of Power Sources*, 2006, **153**, 413-418.
5. M. Oh, S.-J. Park, Y. Jung and S. Kim, *Synthetic Metals*, 2012, **162**, 695-701.
6. P. V. Braun and R. G. Nuzzo, *Nature nanotechnology*, 2014, **9**, 962-963.
7. D. R. Rolison, J. W. Long, J. C. Lytle, A. E. Fischer, C. P. Rhodes, T. M. McEvoy, M. E. Bourg and A. M. Lubers, *Chemical Society Reviews*, 2009, **38**, 226-252.

## Chapter 9: Appendix

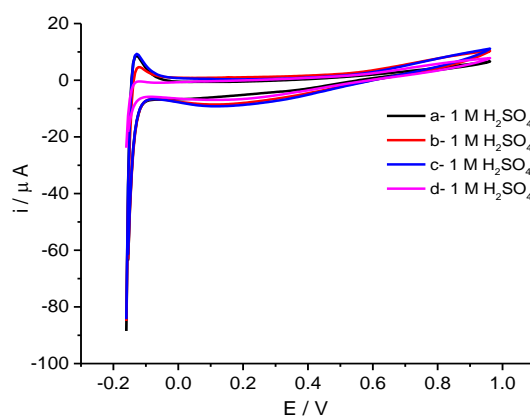


**Figure 9.1:** shows CVs of the background electrolytes without aniline monomer, using a Pt electrode (1 mm diameter) as working electrode; a)  $\text{H}_2\text{SO}_4$ , b)  $\text{HCl}$ , c)  $\text{HNO}_3$ , and d)  $\text{HClO}_4$  (-0.16 to 0.96 V;  $100 \text{ mV s}^{-1}$ ,  $10^{\text{th}}$  scan shown).

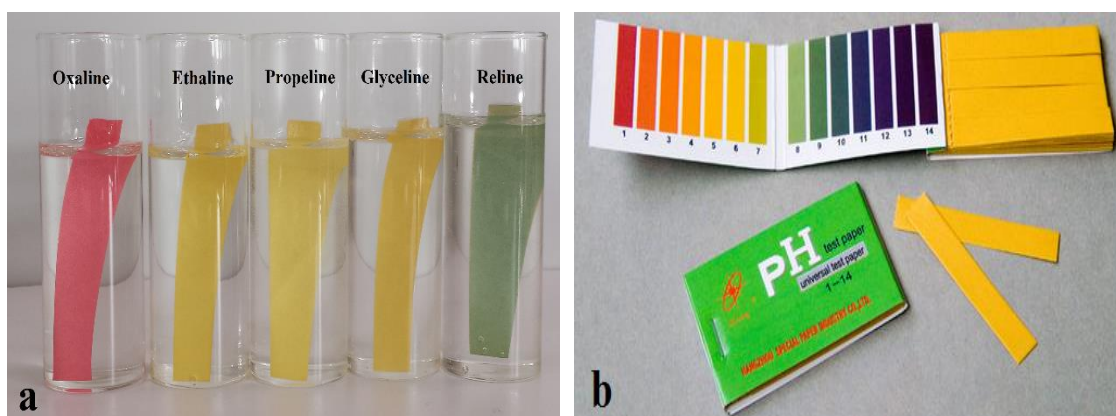


**Figure 9.2:** Panel a) show solutions of DESs and universal indicator paper as a pH indicator, while panel b) show a pH indicator.

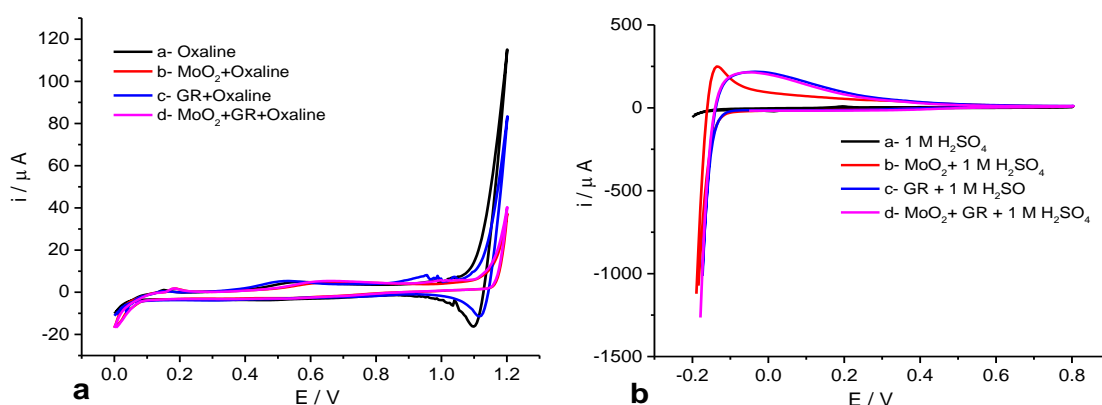


**Figure 9.3:** shows CVs of the background electrolytes without aniline monomer, using a Pt electrode (8 mm diameter) as working electrode; a) Oxaline, b)  $1 \text{ M H}_2\text{SO}_4/\text{H}_2\text{O}$  ( $5 \text{ mV s}^{-1}$ ,  $10^{\text{th}}$  scan shown).

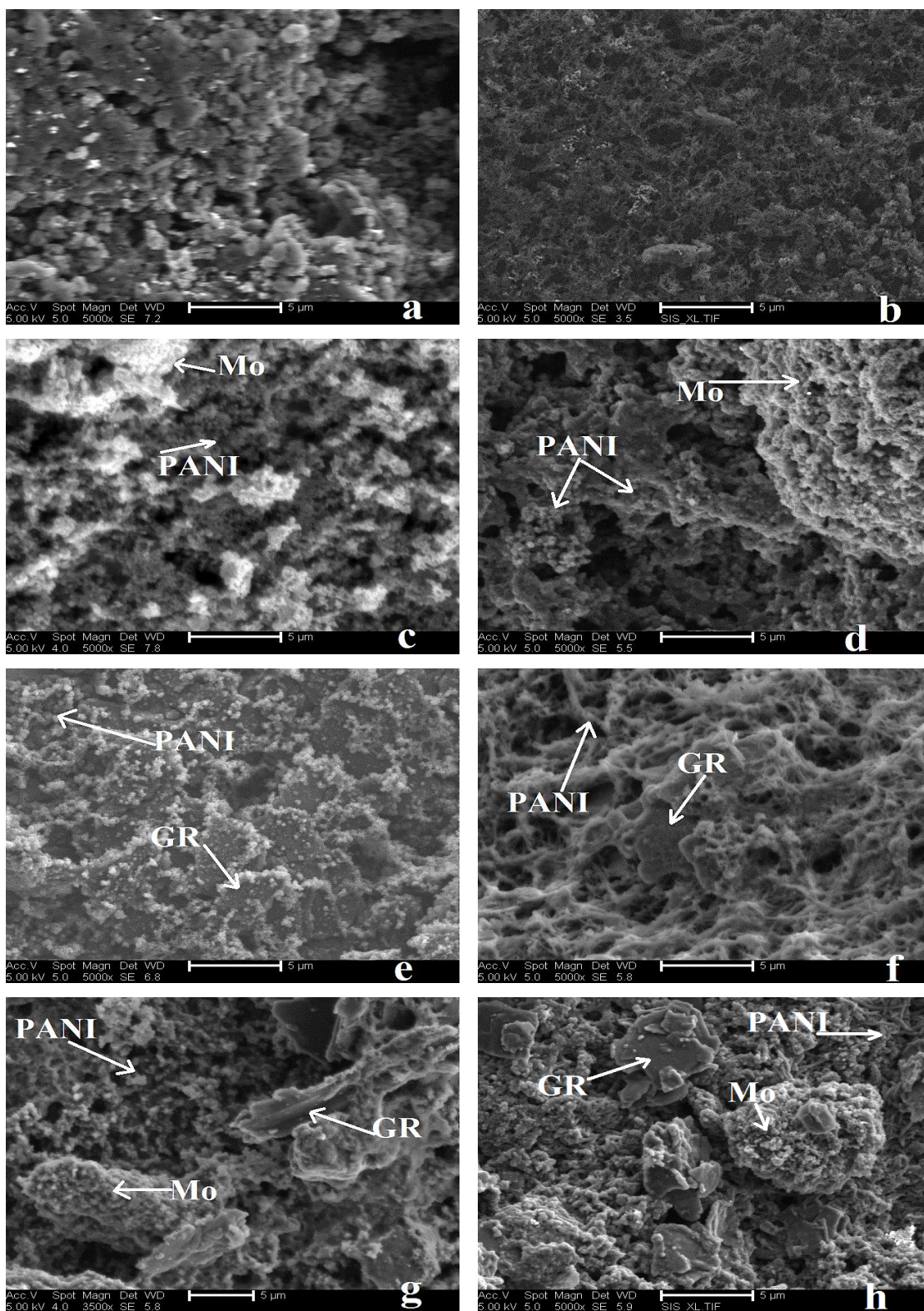


**Figure 9.4:** SEM images of PANI, PANI/MoO<sub>2</sub>, PANI/GR and PANI/MnO<sub>2</sub>/GR composite films after 300 cycles in electrolytes (monomer free) at 5 mV s<sup>-1</sup>. The left-hand images show samples prepared from an Oxaline electrolyte, while the right-hand images show samples prepared in an aqueous electrolyte.

**Viscosity of aqueous solution:** The kinematic viscosity ( $\nu$ ) is generally expressed as

$$\nu = Kt \quad 9.1$$

where K is the constant rate, determined from the reference liquid measurement such as water, t is the efflux time viscometer. The dynamic viscosity ( $\eta$ ) is defined as

$$\nu = \frac{\eta}{\rho} \quad 9.2$$

The common units for the dynamic viscosity of liquids are Centipoise (cP) which is 1/100 of a Poise and Poise is  $\text{g cm}^{-1} \cdot \text{s}^{-1}$ . The SI units are  $\text{N} \cdot \text{s m}^{-2}$  or Pa.s. The dynamic viscosity can be also calculated as

$$\eta_2 = \frac{\eta_1 \rho_2 t_2}{\rho_1 t_1} \quad 9.3$$

where  $\eta_2$ ,  $\rho_2$  and  $t_2$  are viscosity, liquid density and the efflux time viscometer of the material to be measured (unknown material) whereas  $\eta_1$ ,  $\rho_1$  and  $t_1$  are viscosity, liquid density and the efflux time viscometer of water.

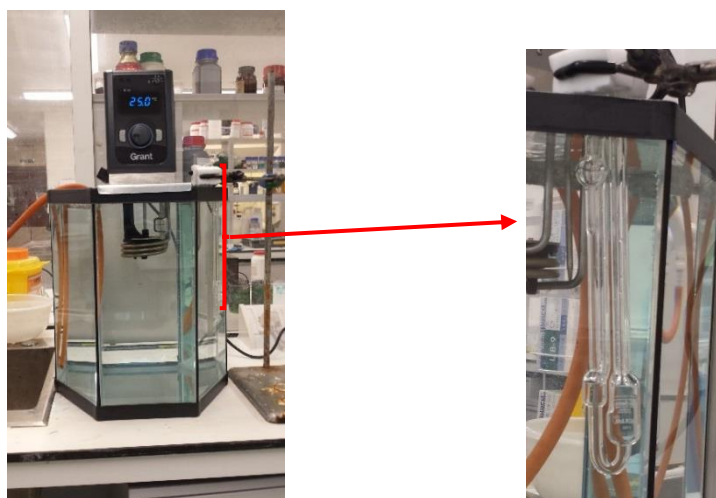


**Figure 9.5:** An Ostwald viscometer in the bath at 25°C to measure the viscosity of deionised water and its with acid.

**Table 9.1:** The absolute or dynamic viscosity of pure deionised water and its with acid at 25°C measured by Ostwald viscometer.

Sample	Viscosity in cP
Deionised water	0.89
0.5 M H <sub>2</sub> SO <sub>4</sub>	0.97
1 M H <sub>2</sub> SO <sub>4</sub>	1.1

**Table 9.2:** Specific capacitance values for PANI composite samples (growth from Oxaline) cycled in Ethaline, 0.5 M H<sub>2</sub>SO<sub>4</sub> and Ethaline, respectively at 5 mV s<sup>-1</sup>.

Polymer samples		Specific Capacitance (F/g) at cycle number											
		Cycle 1	Cycle 10	Cycle 20	Cycle 30	Cycle 40	Cycle 50	Cycle 60	Cycle 70	Cycle 80	Cycle 90	Cycle 100	% Capacitance Retention
PANI	Ethaline	543	551	541	502	484	480	480	472	472	464	461	<b>85</b>
	0.5 M H <sub>2</sub> SO <sub>4</sub>	586	598	583	554	541	513	497	465	413	389	358	<b>61</b>
	Ethaline	141	130	124	106	97	95	91	84	80	77	71	<b>50</b>
PANI/ MoO <sub>2</sub>	Ethaline	552	561	592	603	613	621	610	609	607	606	606	<b>110</b>
	0.5 M H <sub>2</sub> SO <sub>4</sub>	827	857	852	809	775	745	702	673	634	603	573	<b>69</b>
	Ethaline	275	275	279	276	266	261	251	245	239	232	233	<b>85</b>
PANI/GR	Ethaline	613	652	659	654	648	646	626	617	616	603	596	<b>97</b>
	0.5 M H <sub>2</sub> SO <sub>4</sub>	546	617	659	674	710	711	687	667	651	614	577	<b>106</b>
	Ethaline	555	555	559	561	557	547	538	532	516	509	508	<b>92</b>
PANI/GR/ MoO <sub>2</sub>	Ethaline	603	646	661	670	677	679	677	665	644	627	620	<b>103</b>
	0.5 M H <sub>2</sub> SO <sub>4</sub>	847	918	939	971	962	952	946	920	884	847	814	<b>96</b>
	Ethaline	509	553	587	588	588	580	569	550	541	531	522	<b>103</b>

**Table 9.3:** Specific capacitance values for PANI composite samples (growth from aqueous solution) cycled in 0.5 M H<sub>2</sub>SO<sub>4</sub>, Ethaline and 0.5 M H<sub>2</sub>SO<sub>4</sub>, respectively at 5 mV s<sup>-1</sup>.

Polymer samples		Specific Capacitance (F/g) at cycle number											
		Cycle 1	Cycle 10	Cycle 20	Cycle 30	Cycle 40	Cycle 50	Cycle 60	Cycle 70	Cycle 80	Cycle 90	Cycle 100	% Capacitance Retention
PANI	0.5 M H <sub>2</sub> SO <sub>4</sub>	627	638	644	641	620	607	592	575	555	529	498	<b>79</b>
	Ethaline	259	249	236	237	232	230	224	222	222	220	215	<b>83</b>
	0.5 M H <sub>2</sub> SO <sub>4</sub>	471	450	411	367	331	297	269	246	225	209	191	<b>41</b>
PANI/ MoO <sub>2</sub>	0.5M H <sub>2</sub> SO <sub>4</sub>	602	565	536	490	444	399	359	323	269	224	189	<b>31</b>
	Ethaline	134	117	116	114	111	109	108	102	99	95	99	<b>74</b>
	0.5M H <sub>2</sub> SO <sub>4</sub>	124	124	117	111	97	88	76	78	62	58	53	<b>43</b>
PANI/GR	0.5M H <sub>2</sub> SO <sub>4</sub>	799	791	783	780	763	745	745	741	740	720	711	<b>89</b>
	Ethaline	183	183	183	182	179	179	179	179	177	174	174	<b>95</b>
	0.5 M H <sub>2</sub> SO <sub>4</sub>	539	543	546	545	551	552	554	556	557	557	556	<b>103</b>
PANI/GR/ MoO <sub>2</sub>	0.5 M H <sub>2</sub> SO <sub>4</sub>	766	824	822	820	821	821	822	822	821	821	821	<b>107</b>
	Ethaline	195	194	195	194	192	192	191	190	186	185	185	<b>95</b>
	0.5 M H <sub>2</sub> SO <sub>4</sub>	543	541	544	547	570	581	580	577	571	570	560	<b>103</b>